Performance Analysis of Iterative Soft Interference Cancellation Algorithms and New Link Adaptation Strategies for Coded MIMO Systems.

Baozhu Ning

N° d'ordre : 2013-34-TH

SUPELEC

ECOLE DOCTORALE STITS

« Sciences et Technologies de l'Information des Télécommunications et des Systèmes »

THÈSE DE DOCTORAT

DOMAINE : STIC

SPECIALITE : Télécommunications

Soutenue le 16 Décembre 2013

par :

Baozhu NING

Analyse des performances des algorithmes itératifs par soustraction d'interférence et nouvelles stratégies d'adaptation de lien pour systèmes MIMO codés

Directeur de thèse :	Antoine Berthet	Professeur (SUPELEC)
Co-directeur de thèse :	Raphaël Visoz	Ingénieur de recherche (ORANGE)

Composition du jury :

Président du jury :	Michel KIEFFER	Professeur des Universités (UNIV. PARIS-SUD XI)
Rapporteurs :	Didier LE RUYET	Professeur des Universités (CNAM)
	Jean-Pierre CANCES	Professeur des Universités (ENSIL)
Examinateurs :	Floria KALTENSBERGER	Professeur assistant (EURECOM)

Acknowledgments

This dissertation is the result of a three years research project carried out at the departement of telecommunication, SUPELEC and the Radio Innovative DEsign (RIDE) team of french operator Orange. The study is under the supervision and guidance of Professor Antoine Berthet (SUPELEC) and Dr. Raphael Visoz (Orange).

I would like to thank my supervisors for their advice, guidance and patience during the three years of my doctorate. It has been an honor for me to work with you who are not only technically knowledgeable, but also very passionate. Both of you have contributed greatly to my doctorate and I have been able to learn a lot from both of you.

I would like to thank all the colleagues and secretaries of both SUPELEC and Orange. Thanks for your inspiring discussions, friendly assistance and collaboration.

I would like to thank my reviewers for the time they have dedicated for the reading of this PhD thesis and the development of their reports. I thank Professor Didier LE RUYET and Professor Jean-Pierre CANCES for having accepted this responsibility. I also thank them for their interests to my work and their availability.

The accomplishment of current work cannot be without the strong support and understanding from my parents, my brother Ning Zhaoxiang and his wife Liu Yefei and my lovely niece Ning Yangyang and nephew Ning Junqi. Thanks for your constant love and affection.

Baozhu NING

10/10/2013

Abstract

Current wireless communication systems evolve toward an enhanced reactivity of Radio Resource Management (RRM) and Fast Link Adaptation (FLA) protocols in order to jointly optimize the Media Access Control (MAC) and Physical (PHY) layers. In parallel, multiple antenna technology and advanced turbo receivers have a large potential to increase the spectral efficiency of future wireless communication system. These two trends, namely, cross layer optimization and turbo processing, call for the development of new PHY-layer abstractions (also called performance prediction method) that can capture the iterative receiver performance per iteration to enable the smooth introduction of such advanced receivers within FLA and RRM.

The PhD thesis first revisits in detail the architecture of the turbo receiver, more particularly, the class of iterative Linear Minimum Mean-Square Error (soft) Interference Cancellation (LMMSE-IC) algorithms. Then, a semi-analytical performance prediction method is proposed to analyze its evolution through the stochastic modeling of each of the components. Intrinsically, the performance prediction method is conditional on the available Channel State Information at Receiver (CSIR), the type of channel coding (convolutional code or turbo code), the number of codewords and the type of Log Likelihood Ratios (LLR) on coded bits fed back from the decoder for interference reconstruction and cancellation inside the iterative LMMSE-IC algorithms.

In the second part, closed-loop FLA in coded MIMO systems based on the proposed PHY-layer abstractions for iterative LMMSE-IC receiver have been tackled. The proposed link adaptation scheme relies on a low rate feedback and operates joint spatial precoder selection (e.g., antenna selection) and Modulation and Coding Scheme (MCS) selection so as to maximize the average rate subject to a target block error rate constraint. The cross antenna coding (the transmitter employs a Space-Time Bit-Interleaved Coded Modulation (STBICM)) and per antenna coding (Each antenna employs an independent Bit-Interleaved Coded Modulation(BICM)) cases are both considered.

Contents

List of Figures

List of Acronyms

Here is a list of main acronyms used in this document.

1G	First Generation
2G	Second Generation
3G	Third Generation
3GPP	Third Generation Partnership Project
4G	Forth Generation
5G	Fifth Generation
AMC	Adaptive Modulation and Coding
AMI	Average Mutual Information
AWGN	Additive White Gaussian Noise
BER	Bit-Error-Rate
BICM	Bit-Interleaved Coded Modulation
BLER	BLock Error Rate
BPSK	Binary Phase-Shift Keying
CAZAC	Constant Amplitude Zero AutoCorrelation
CDI	Channel Distribution Information
CDMA	Code- Division Multiple Access
CoMP	Coordinated MultiPoint
CQI	Channel Quality Indicator
CRC	Cyclic Redundancy Check
CSI	Channel State Information
CSIR	Channel State Information at the Receiver
CSIT	Channel State Information at the Transmitter
DE	Density Evolution
EDGE	Enhanced Data rates for GSM Evolution
EESM	Exponential Effective SNR Mapping
EXIT	EXtrinsic Information Transfer
FDD	Frequency-Division Duplexing
FDMA	Frequency-Division Multiple Access
FLA	Fast Link Adaptation
GSM	Global System for Mobile communications

HARQ	Hybrid Automatic Repeat Request
HSDPA	High Speed Downlink Packet Access
HSUPA	High Speed Uplink Packet Access
IA	Interference Alignment
IR	Incremental-Redundancy
ISI	Inter-Symbol Interference
ITU	International Telecommunication Union
ITU-R	International Telecommunication Union - Radiocommunication
LAPPR	Log A Posteriori Probability Ratios
LEXTPR	Log Extrinsic Probability Ratios
LLR	Log Likelihood Ratios
LMMSE	Linear Minimum Mean Square Error
LMMSE-IC	Linear Minimum Mean Square Error-Interference Cancellation
LTE	Long Term Evolution
LTE-A	Long Term Evolution - Advanced
LUT	Look Up Table
MAC	Media Access Control
MAP	Maximum A Posteriori
MCS	Modulation and Coding Scheme
MIESM	Mutual Information Effective SNR Mapping
MIMO	Multiple-Input Multiple-Output
MSE	Mean Square Error
MUD	MultiUser Detector
MU-MIMO	Multiple-User Multiple-Input Multiple-Output
NRNSC	Non-Recursive Non-Systematic Convolutional
OFDM	Orthogonal Frequency-Division Multiplexing
OFDMA	Orthogonal Frequency-Division Multiple Access
PARC	Per Antenna Rate Control
PAPR	Peak-to-Average Power Ratio
PDC	Personal Digital Communication
PHY	Physical
PMI	Precoding Matrix Indicator
QAM	Quadrature Amplitude Modulation
QPSK	Quadrature Phase-Shift Keying
RRM	Radio Resource Management
RI	Rank Indicator
RSC	Recursive Systematic Convolutional
RV	Random Variable

SC-FDMA	Single-Carrier Frequency-Division Multiple Access
SIC	Successive Interference Cancellation
SINR	Signal-to-Interference-plus-Noise Ratio
SLA	Slow Link Adaptation
SNR	Signal-to-Noise Ratio
STBICM	Space-Time Bit-Interleaved Coded Modulation
SU-MIMO	Single-User Multiple-Input Multiple-Output
TDD	Time- Division Duplexing
TDMA	Time- Division Multiple Access
TD-SCDMA	Time- Division Synchronous CDMA
UE	User Equipment
UMTS	Universal Mobile Telephone Service
WLAN	Wireless Local Area Networks
w.r.t.	with respect to

Notations

Here is a list of main operations and symbols used in this document.

$\mathbb{R}$	Set of reals
$\mathbb{C}$	Set of complex numbers
$\mathbf{x}$	A vector
$\|\mathbf{x}\|$	Euclidean norm of the vector $\mathbf{x}$
$\mathbf{X}$	A matrix
$x_{i;j,\ell}$ or $[\mathbf{X}_i]_{j,\ell}$	The entry (j, ℓ) of the matrix $\mathbf{X}_i$.
$\mathbf{x}_i$	The i^{th} column of the matrix $\mathbf{X}$.
$\mathbf{x}^j$	The j^{th} row of the matrix $\mathbf{X}$.
$\text{diag}(\mathbf{X})$	Diagonal operator on the square matrix $\mathbf{X}$. $\text{diag}(p_1, p_2, \cdots, p_n)$ is a diagonal matrix with the diagonal entries equal to $p_1, p_2, \cdots, p_n$.
$\mathbf{I}_n$	The n-square identity matrix
$\mathbf{0}_n$	n-tuples of zeros
$\mathbf{1}_n$	n-tuples of ones
$\mathbf{e}_n$	n-th unit vector
$\|\mathscr{X}\|$	Cardinality of the set $\mathscr{X}$
$\mathbf{x} \sim p(\mathbf{x})$	The random vector $\mathbf{x}$ follows the probability distribution function $p(\mathbf{x})$.
$x \sim P(x)$	The discrete random variable x has a probability mass function $P(x)$.
$\mathcal{N}_C(m, v)$	The circularly-symmetric complex Gaussian distribution with mean m and variance v.
$\mathcal{N}_C(\boldsymbol{\mu}, \boldsymbol{\Sigma})$	The circularly-symmetric complex Gaussian distribution with mean $\boldsymbol{\mu}$ and covariance matrix $\boldsymbol{\Sigma}$.
$(\cdot)^\top$	Transpose operator
$(\cdot)^\dagger$	Complex conjugate transpose / Hermitian operator
$(\cdot)^{-1}$	Inverse operator
$\exp(\cdot)$	Exponential function
$\log(\cdot)$	Logarithmic function
$\mathbb{E}\{\cdot\}$	Operator of expected value

Résumé détaillé

Selon les estimations de l'Union Internationale des Télécommunications (ITU) [1], le nombre d'abonnements mobiles cellulaires atteint 6,8 milliards en 2013, ce qui correspond à un taux de pénétration global de 96%. Aujourd'hui, les gens peuvent communiquer les uns avec les autres facilement que ce soit vocalement ou par SMS et disposent d'une connexion Internet dès lors qu'ils sont couverts par le réseau de communications mobile.

Les systèmes de première génération (1G) ont été développés dans les années 1980. Ces systèmes utilisaient la technologie analogique et ont été conçus uniquement pour le service vocal.

A partir de 1991, les systèmes de deuxième génération (2G) qui ont été développés commençaient à utiliser la technologie numérique, comme le Système Mondial de Communications mobiles (GSM) en Europe, la Communication Numérique Personnel (PDC) au Japon et IS- 95 aux Etats-Unis. Parmi ces systèmes, le GSM a été largement accepté et déployé dans la plupart des pays et est encore utilisé aujourd'hui. Les systèmes 2G ont été conçus pour fournir la voix et le SMS, et également plus tard un service de données avec GSM Evolution (EDGE). Parmi la famille des systèmes 2G, GSM et PDC ont été basés sur deux techniques différentes. La première est le Fréquence-Division Multiple Access (FDMA) [2] : toute la bande passante est divisée en de multiples canaux à bande étroite éloignées en fréquence et de multiples utilisateurs peuvent transmettre simultanément sur plusieurs canaux à bande étroite. La deuxième techniques est le Time Division Multiple Access (TDMA) [2] : plusieurs utilisateurs peuvent transmettre sur un canal à bande étroite à un instant différent. Système IS-95 était basé sur le Code-Division Multiple Access (CDMA) [2] : chaque utilisateur transmet ses signaux sur la totalité de la bande passante et chaque utilisateur est identifié par un code spécifique.

Les systèmes de troisième génération (3G) incluent deux familles de technologies : Universal Mobile Telecommunications System (UMTS), publié

par l'organisme de normalisation de la Third Generation Partnership Project (3GPP) en version R99 suivant GSM et CDMA2000 suivant IS-95. Le système UMTS a été largement déployé dans de nombreux pays alors que le système CDMA2000 est principalement déployé en Asie et en Amérique du Nord. Les systèmes 3G amènent une amélioration significative par rapport aux systèmes 2G et visent à fournir des débits de données plus élevés, à améliorer les services vocaux ainsi que les services de données et les applications. À la suite de l'effort mondial de normalisation, la famille des systèmes 3G a été uniformément basée sur la technologie CDMA. UMTS utilise le CDMA large bande (WCDMA) qui prend en charge des modes de duplex par séparation temporelle (TDD) et duplex par séparation fréquentielle (FDD). Une variante de l'UMTS TDD, nommée Time Division Synchronous CDMA (TD-SCDMA), a été également normalisé par le 3GPP, et est principalement déployée en Chine.

Par la suite, le UMTS a été renforcé par High Speed Downlink Packet Access (HSDPA) et High Speed Uplink Packet Access (HSUPA) dans le 3GPP. Des modulations d'ordre supérieur sont prises en charge : 16 Quadrature Amplitude Modulation (16QAM) est introduite dans la liaison descendante comme une amélioration de la Quadrature Phase Shift Keying (QPSK) de la version R99 et QPSK est introduite dans la liaison montante comme complémentaire de Binary Phase Shift Keying (BPSK) de la version R99. Le méchanisme Adaptatif de Modulation et Codage (AMC) est introduit afin d'adapter dynamiquement le taux de codage et l'ordre de modulation aux conditions radio instantanées et aux besoins des utilisateurs. Un nouveau mécanisme de rêquete automatique de répétition hybride (HARQ) est ajouté entre les utilisateurs et la station de base afin de réduire la latence du système en cas de perte de paquets.

L'évolution de HSPA, HSPA + (R7, R8) a été conçue pour améliorer le débit de données par l'introduction de nouvelles techniques. Les liaisons descendante et montante ont commencé à supporter 64QAM et 16QAM, respectivement. Les systèmes de Multiple-Input Multiple-Output(MIMO) [3], [4] sont également introduits. La technologie MIMO peut être utilisée pour augmenter le taux de données [3], [5], [6], [7] (gain de multiplexage spatial), pour augmenter la robustesse de transmission (gain de diversité spatiale) ou pour concentrer l'énergie de transmission dans une certaine direction (précodage ou de formation de faisceaux).

En tant que quatrième étape remarquable, le Long Term Evolution

(LTE), publié dans la version R8/9 et bientôt LTE-Advanced (LTE -A), publié dans la version R10/11, définis par le 3GPP sont largement reconnus comme les systèmes de quatrième génération (4G) qui ont été caractérisés par la technologie Orthogonal Frequency - Division Multiplexing (OFDM). Les avantages de l'OFDM [2] sont multiples, tels que la robustesse aux interférences inter-symboles (ISI) qui dégradent les performances du CDMA, la flexibilité de déploiement sur différents grande bande qui fait défaut au CDMA, l'adéquation de transmission MIMO, la gestion et la planification de large bande, la flexibilité de l'accès multiple, etc. Les sous-porteuses de la technologie OFDM se chevauchent mais restent orthogonales, ce qui donne à OFDM uen très grande efficacité spectrale [8]. LTE-A a choisi pour la liaison descendante un système Orthogonal Frequency - Division Multiple Access (OFDMA) [9] et pour la liaison montante un système Single Carrier Frequency - Division Multiple Access (SC-FDMA) [10] . Le choix différent pour la liaison descendante et montante vient du ratio puissance crête à puissance moyenne (PAPR) [11] relativement élevé d'un signal OFDM qui n'est pas tolérable pour l'UE.

LTE-A prend en charge la modulation 64QAM à la fois pour la liaison montante et descendante. Sur la couche physique (PHY), turbo code [12] est utilisé pour protéger les données. La coordination simple d'interférence inter-cellule (ICIC) dans la version R10, transmission/réception MultiPoint coordonnée (COMP) dans la version R11, ainsi que l'agrégation des porteuses sont des techniques importantes qui peuvent encore accroître l'efficacité spectrale. Afin de réaliser l'adaptation de liaison, l'UE remonte régulièrement une information d'état du canal (CSI) à la station de base. Celles-ci comprennent : un indicateur de la qualité du canal (CQI), un indicateur de la Matrice de Précodage préférée (PMI), un Indicator de rang (RI) (= nombre de flux spatiaux pris en charge). Certains paramètres sont importants comme le retard de rétroaction, la période de rétroaction et éventuellement le filtrage de CQI.

Il existe d'autres types de système sans fil autres que cellulaire, tels que les réseaux locaux sans fil (WLAN) [2]. Ceux-ci sont conçus pour des débits beaucoup plus élevés que les systèmes cellulaires, mais sont similaires à une seule cellule d'un système cellulaire. Ils sont principalement conçus pour fournir en couverture à large bande. Les principales normes de réseau local sans fil sont la famille IEEE 802.11 et le terme Wi-Fi est utilisé comme synonyme pour le WLAN. Le Wi-Fi prend en charge les modulations d'ordre

élevé (64QAM et même 256QAM), MIMO et l'adaptation de liaison. La couche PHY emploie le code convolutif afin de protéger les données.

Dans l'effort mondial de recherche en cours sur les futurs systèmes de communications sans fil, l'allocation adaptative des ressources, tels que l'heure, le code, l'espace et la fréquence, basée sur le CSI et les besoins des utilisateurs, est largement reconnue comme un élément clé pour approcher la capacité des canaux MIMO à large bande sélectifs en fréquence [13] , [14], [15], [16], [17], [18], [19], [20], [21], [22] , [23]. La gestion de resource radio (RRM) traditionnelle et l'adaptation lente de liaison (SLA) ont été construites sur une interface lien à système, dénommée interface à valeur moyenne [24], dans laquelle la performance individuelle de liaison radio est évaluée par des simulations Monte-Carlo moyennant sur les statistiques de l'évanouissement rapide. Pour que cette approche soit valable, le délai de RRM et LA doit être grand par rapport à la dynamique de l'évanouissement rapide. A l'inverse, les systèmes sans fil actuels évoluent vers une meilleure réactivité des protocoles de RRM et adaptation rapide de liaison (FLA) afin d'optimiser conjointement la couche de contrôle d'accès de média (MAC) et la couche PHY. Un nouveau type d'interface lien à système, appelé interface de valeur réelle [24], a vu le jour dans lequel RRM avancée et les mécanismes de la FLA sont conçus et optimisés afin d'exploiter les rétroactions de métriques représentant les performances individuelles instantanées de la liaison radio basée sur des abstractions de la couche PHY (également appelées méthodes de prédiction de performance).

Les interférences dans les réseaux cellulaires peuvent être gérées par des techniques d'évitement des interférences côté de l'émetteur tel que l'ordonnancement intelligent [25], [chapitre 6, [2]] , canal de diffusion, codage de papier sale, précodage sous-optimal ZF, l'alignement d'interférence MIMO (IA) [26], etc. Cette stratégie d'évitement des interférences a été suivie par WP1 du projet européen ARTIST4G intitulé "*interference avoidance*". De cette manière, un récepteur linéaire d'une faible complexité peut être suffisant. Cependant, ces techniques d'évitement des interférences exigent des CSI parfaites et instantanées à l'émetteur (CSIT) qui n'est pas disponible dans la pratique. Trop de rétroactions de CSIT diminuent l'efficacité spectrale du système et rendent le système peu robustesse. Enfin, l'interférence ne peut être évitée qu'à un certain niveau. Par conséquent, les techniques d'annulation des interférences côté récepteur basées sur certains traitements du signal avancés complexes sont des complémentaires importants aux tech-

niques d'évitement des interférences précédentes. Par rapport aux CSIT, le CSI à récepteur (CSIR) est toujours disponible en communications mono-utilisateur MIMO (SU-MIMO) et pour la liaison montante (canaux d'accès multiple). Pour la liaison descendante, la conversion du canal de diffusion dans un canal à accès multiple avec les informations de côté (fourni par le réseau) au niveau de chaque récepteur est actuellement à l'étude par l'industrie [27]. Cette dernière stratégie semble plus robuste aux informations de côté imparfaite que la première. En fait, l'idée d'abandonner le synchronisme et l'orthogonalité dans les systèmes sans fil de demain, admettant ainsi des interférences, et de contrôler ces troubles par une structure d'émetteur-récepteur adaptée était au coeur de la ARTISTE4G WP2 intitulé "*interférences exploitation* " et est maintenant annoncée par plusieurs projets européens comme un concept de construction pour la cinquième génération (5G) au niveau des couches PHY/MAC.

En parallèle, le succès des turbo codes [12] et le principe du turbo [28] ont inspiré de nouvelle modulations codées qui pouraient potentiellement atteindre la capacité. De nouvelles architectures de multiplexage spatial et techniques d'accès multiple non-orthogonales basées sur des codages puissants ont été proposées pour atteindre une efficacité spectrale très élevée, dont la pertinence est toutefois subordonnée à un traitement itératif au niveau du récepteur. Ces deux tendances, à savoir, l'optimisation inter couche et le traitement turbo, demanede le développement de nouvelles abstractions de la couche PHY qui peuvent capturer les performances du récepteur itératif par itération conditionnelle sur le CSIR disponible qui permet une introduction en douceur de ces récepteurs avancés dans FLA et RRM.

Au sujet de la prédiction de la convergence et/ou l'analyse de la performance de décodage itératif, nous avons d'abord distingué les approches déterministes et les approches stochastiques [29]. Les approches déterministes traitent le décodage comme un processus déterministe et tentent de caractériser le comportement du décodeur pour chaque instance du signal reçu. Par exemple, [30] est en mesure de révéler un certain nombre de comportements dynamiques de turbo-décodage, tels que l'existence de points fixes ainsi que des conditions d'unicité et de stabilité pour les points fixes. Cependant, la connaissance de l'existence d'un point fixe ne suffit pas, comme plusieurs points fixes ou même des cycles limités peuvent exister. En outre, les conditions de l'unicité et de la stabilité sont spécifiques à chaque bloc de décodage et sont difficiles à calculer, ce qui signifie qu'ils ne sont pas utiles

pour prédire les performances d'un turbo-décodeur donné. Basé sur l'hypothèse d'une grande longueur de mots de code (ou de manière équivalente grande taille d'entrelacement), les approches stochastiques, elles voient les signaux d'entrée et de sortie circulant dans le décodeur itératif des processus aléatoires ergodiques [29] dont les statistiques sont calculables à l'aide de réalisations (ou instances). En Traitant les rapports de vraisemblance logarithmique (LLR) de messages binaires comme des variables aléatoires (RV), l'évolution de la densité (DE) [31, 32] est proposée pour analyser la performance du décodage somme-produit [33] de code Low-Density Parity-Check (LDPC) [34] sur des canaux d'entrée et de sortie symétriques binaires simples. Cependant, la rigueur mathématique de DE introduit une complexité élevée parce que cette méthode estime effectivement l'évolution de leurs distributions de probabilité (exprimée en forme fermée) par le biais de simulations numériques.

D'autres approches stochastiques simples existent, elles ont toutes en commun d'utiliser un paramètre statistique unique (par opposition à une distribution complète de probabilité) pour caractériser les signaux d'entrée et de sortie concernés par le processus itératif. Les graphiques du transfert d'information extrinsèque (EXIT) ont été lancés par ten Brink, qui le premier les a présentés dans le cadre du choix d'un mappeur approprié et d'une constellation convenable, dans un schéma de demapping et décodage itératif [35], et ensuite les a appliqués pour analyser les turbo codes [36, 37]. Ils constituent un outil puissant pour analyser les comportements itératifs, basé sur le suivi des paramètres statistiques. L'évolution de l'information mutuelle moyenne (AMI) entre les bits d'information (ou codés) et les LLR de sortie post-décodage BCJR [38] est observée à la place de l'évolution des densités réelles. Une approximation gaussienne unidimensionnelle simple de l'évolution de la densité a été également suggérée par Chung et al. dans [39,40] pour les codes LDPC. Des idées connexes ont été proposées indépendamment pour analyser les turbo codes [41, 42] et la détection multi-utilisateurs et le décodage itératif [43, 44]. Ces approximations gaussiennes se distinguent par le choix du paramètre unidimensionnel qui est choisi pour caractériser une densité, par exemple, Rapport Signal sur Bruit (SNR) [41, 42] ou moyenne [39, 40] sous condition de symétrie et de la propriété de cohérence. Cependant, les expériences ont montré que l'AMI utilisée dans les EXIT est le paramètre statistique le plus robuste par rapport aux variations des distributions de probabilité de LLR [45].

L'utilisation du graphique EXIT pour prédire la performance des récepteurs turbo sur un système multi-utilisateurs et canal MIMO (non-ergodique) avec évanouissement par bloc et sélectivité fréquentielle révèle plusieurs questions. Si chaque utilisateur utilise un schéma de modulation codée, les récepteurs turbo sont caractérisés par la circulation itérative de messages entre d'une part, le détecteur multi-utilisateur (MUD) (en utilisant l'information a priori sur des bits codés générés par le décodeur), et d'autre part, la banque des décodeurs du canal d'entré-souple et de sortie-souple.

La première question concerne la contrainte forte de temps qui ne nous permet pas d'obtenir l'AMI extrinsèque au niveau du bit codé pour n'importe quelle réalisation du canal donnée en exécutant une longue simulation. En conséquence, l'AMI extrinsèque de MUD doit être calculée analytiquement ou au moins semi-analytiquement. Il existe une classe de MUD simplifiée (sub-optimale), dénommée détection linéaire par minimisation d'erreur quadratique moyenne avec annulation d'interférence (LMMSE -IC), pour laquelle le calcul des sorties de MUD peut être réalisé en deux étapes : une étape de calcul purement analytique du signal sur interférence plus bruit (SINR), consacré à la détection IC et LMMSE des symboles transmis, et une autre étape asseuée par le démappeur. Cette étude de doctorat met l'accent sur cette classe de détection LMMSE -IC [46–49], car c'est une tâche difficille pour une détection (optimale localement) d'être dérivée comme une application stricte des règles somme-produits sur le sous-graphe correspondant [33]. Cette ligne de pensée est suivie et développée dans [50–57] (voir aussi [44, 58] pour des solutions alternatives).

Un deuxième problème réside dans le fait que les bits codés sont répartis sur des symboles qui connaissent différents canaux. C'est la cas pour le modèle du canal MIMO d'évanouissement par bloc [59]. Les caractéristiques des sorties de MUD doivent être calculées pour chacun de ces états de canaux qui servent en tant qu'information a priori pour le calcul des caractéristiques de sortie des décodeurs du canal. Nous devons compresser ces multiples sorties extrinsèques de MUD (un par état de canal) en une seule afin d'éviter d'utiliser une Look-Up-Table (LUT) multidimensionnelle pour caractériser les sorties extrinsèques du décodeur dont le stockage ne serait pas abordable. Le problème est résolu dans [50–52] en faisant la moyenne de l'AMI, entre la sortie extrinsèque de MUD et les bits codés liés, sur tous les états de canaux existants.

Fait intéressant, ce second problème a également été rencontré dans

un autre domaine de recherche traitant de l'évaluation adaptative de modulation/codage au niveau du système, dénommé techniques de compression [60–63]. Les techniques de compression visent à ramener de multiples SNR instantanés représentant différents états de canal en un seul SNR effectif. Les deux techniques le plus étudiées sont la compression de SNR effectif via fonction exponentielle (EESM) [64] et la compression de SNR effectif via information mutuelle (MIESM) [61] où dans le premier une fonction exponentielle est utilisée comme une mesure de l'information basée sur la borne de Chernoff alors que dans le second une capacité normalisée du shéma Bit-Interleaved Coded modulation (BICM) [65] est utilisée comme une mesure de l'information. EESM nécessite généralement des facteurs d'ajustement pour atteindre une bonne précision pour une MCS donnée. MIESM est beaucoup moins sensible à des facteurs d'ajustement et sa supériorité a été rapporté dans un certain nombre de contributions passées [61]. Cette déclaration semble en ligne avec [49]. Il convient de noter que l'idée de compression a été redécouverte et formalisée par Yuan et al . dans [56, Assomption V].

Dans [66], une étude est mise en place sur les méthodes semi-analytiques rapides et précises pour prédire le taux d'erreur de block (BLER)/taux d'erreur binaire (BER) par utilisateur et par itération dans un système multiple -utilisateurs où chaque utilisateur emploie un Space-time Bit- Interleaved Coded modulation (STBICM) construit à partir de code convolutif et où LMMSE -IC conjoint décodage itératif (en bref LMMSE -IC itératif) est réalisée au récepteur. Par LMMSE -IC conjoint décodage, on parle de la détection LMMSE utilisant une information a priori à partir du décodeur [67] avec l'hypothèse inconditionnelle [48, 49]. L'hypothèse inconditionnelle consiste à moyenner des statistiques au second ordre au cours du temps, pour rendre le filtre LMMSE indépendant du temps (donc facile à mettre en oeuvre). Fait intéressant, cette hypothèse n'est la plupart du temps pas préjudiciable en termes de performances finales [49]. Les abstractions de la couche PHY décrites dans [66] reposent sur la technique de MIESM au niveau bit ou symbole. Dans la première méthode, les sorties extrinsèques de MUD jusqu'aux décodeurs de canal, voyant la détection LMMSE -IC et demapping comme un processus conjoint, sont calculées analytiquement. Cette méthode suit le cadre classique de graphique EXIT et suit l'évolution de l'AMI définie au niveau du bit codé circulant entre le MUD et la banque de décodeurs de canal extérieures [65, Section III], [68, Section V], [69], [70, Section III.B]. Ensuite, avec le déplacement de point de vue, la deuxième

méthode voit le demapping et décodage comme un processus conjoint, et permet de suivre l'évolution de l'AMI définie au niveau du symbole modulé circulant entre l'interface LMMSE -IC et la banque de démappeur conjoints les décodeurs de canal [71] est proposée. Ceci permet d'éviter la question cruciale de paramétrage du demapping . Les deux méthodes donnent des résultats comparables pour les modulations non-linéaires d'ordre faible. Au contraire, la second méthode, qui comprend le démappeur à l'intérieur des LUT se révèle plus robuste pour les modulations non linéaires d'ordre élevé, ce qui démontre sa supériorité .

Cependant, dans la classe de récepteurs de turbo basés sur LMMSE - IC, on fait souvent la distinction souvent entre l'algorithme basé sur les ratios logarithmiques de probabilité extrinsèque (LEXTPR) ou les ratios logarithmiques de probabilité a posteriori (LAPPR). Les deux algorithmes diffèrent par le type d'information probabiliste réinjecté par le décodeur pour la régénération d'interférence et d'annulation souple, à savoir LEXTPR ou LAPPR sur les bits codés. Les expérimentations empiriques révèlent que l'algorithme itératif basé sur LAPPR peut surpasser de façon significative son homologue LEXTPR pour les systèmes à antennes multiples ou multi-utilisateurs très chargés. Dans de tels scénarios en effet, utiliser LAPPR à la place de LEXTPR conduit à des estimations de symboles MMSE plus fiables. Cela est dû à l'information supplémentaire glanée dans le processus d'égalisation/détection, ce qui permet d'annuler plus d'interférences à chaque itération. Les analyses dans [66] sont correctes pour l'algorithme itératif basé sur LEXTPR étant donné une taille d'entrelaceur suffisante grande, mais [66, Hypothèses A1 à A4] ne tiennent pas même avec une taille d'entrelacement infinie pour l'algorithme itératif basé sur LAPPR. En raison d'inexactitudes d'hypothèses négligées, la méthode proposée au niveau du symbole se révèle trop optimiste pour l'algorithme itératif basé sur LAPPR. Ce phénomène est d'autant plus évident pour les MCS avec une modulation d'ordre élevé et un taux de codage élevé. Par conséquent, un examen attentif des hypothèses fondamentales sous-jacentes à cette famille de récepteur est nécessaire afin de proposer une amélioration de l'abstraction de la couche PHY pour l'algorithme basé sur LAPPR, qui est le point de départ du travail.

Sinon, l'adaptation du lien en boucle fermée dans LTE (LTE-A) implique une famille de MCS construite à partir de turbo codes. Le turbo-décodeur contient deux décodeurs BCJR [38] qui échangent l'information probabiliste

(log domaine). En raison de leur structure particulière, les turbo codes ne peuvent pas être décodés de manière optimale à l'exception d'une longueur de bloc très limitée. Dans la pratique, un décodage itératif est appliqué, où l'information probabiliste est échangée entre les décodeurs constitutifs. Le premier décodeur BCJR calcule les LAPPRs sur ses propres bits codés (bits d'information et parité) en tenant compte de l'information a priori disponible sur les bits d'information systématiques stockée à partir d'une activation plus tôt (c'est à dire, les plus récents LEXTPRs sur les bits d'information systématiques fournis par le deuxième décodeur BCJR). Ensuite, le second décodeur BCJR est activé et calcule les LAPPRs sur ses propres bits codés (bits d'information et parité), en tenant compte de l'information a priori disponible transmise par le premier décodeur BCJR.

LMMSE-IC itératif mixte d'un turbo-décodage donne naissance à une structure de récepteur complexe avec au moins deux processus itératifs imbriqués. Certaines similitudes peuvent être trouvées dans les travaux antérieurs sur plusieurs codes concaténés et l'analyse de la convergence de leur décodage itératif [72] [49] [73] [74]. Par conséquent, l'introduction en douceur des récepteurs de turbo basés sur LMMSE -IC en LTE appelle à de nouvelles abstractions de la couche PHY à cette situation non trivial.

Lorsque l'hypothèse de CSIR parfaite est enlevée, les abstractions de la couche PHY doivent être dérivées sous CSIR imparfaite et sous une estimation du canal erronée. Si le nombre de symboles de pilote est suffisant pour assurer une estimation proche de la perfection, il suffit d'adopter l'hypothèse dite mismatch [75–77] qui postule simplement que l'estimation du canal assistée de symboles de pilote est parfaite. Dans ce cas, les abstractions de la couche PHY dérivées sous l'hypothèse de CSIR parfaite peuvent être utilisées dans la pratique. Toutefois, si le nombre de symboles de pilote est réduit grace à un système avancé d'estimation du canal semi-aveugle côté du récepteur, l'hypothèse mismatch n'est plus valide. En effet, il est assez connu que faire la détection et l'estimation du canal dans une même itération (en utilisant a priori d'un décodage du canal) permet de réduire considérablement le nombre de signaux de référence pour une performance donnée [78–81]. Il y a une richesse de la littérature sur le sujet de l'analyse de performance d'estimation du canal semi-aveugle, [75–77, 80, 82–84]. Par exemple, [80] est assez exhaustive en découlant et en comparant différents MSE d'estimation du canal semi-aveugle, mais seulement se réfère à des schémas de détection mismatch itératives sans analyse. Alors que, d'autre

part, [77] considère la détection maximum a posteriori (MAP) itérative avec l'estimation du canal utilisant seulement les symboles de pilote. Cependant, la combinaison de la détection LMMSE -IC (en tenant compte des erreurs d'estimation du canal) et de l'estimation du canal LMMSE semi-aveugle, n'a jamais été abordée en tant que telle, que ce soit d'une évaluation de la performance pure ou d'une prédiction.

Une fois les abstractions de la couche PHY sont dérivées avec les récepteurs de turbo, le pont entre les couches PHY et MAC est construit. La tâche suivante est de réaliser l'optimisation inter-couches PHY et MAC, parfois appelée "l'allocation des ressources en coopération", qui est actuellement l'un des sujets de recherche les plus passionnants dans la conception de systèmes MU-MIMO. Les contributions actuelles limitent souvent leur étude à des récepteurs linéaires simples (voir, par exemple, [85] et [86]) ou , s'ils manipulent des structures non-linéaires plus sophistiquées, par exemple, l'annulation d'interférence successive (SIC) [87], idéalisent certaines parties du processus de décodage, en supposant généralement des canaux d'entrée continue avec dictionnaires gaussiens à zéro erreur, et en négligeant la propagation d'erreur, ce qui conduit à un débit prédit inexact (c'est à dire, trop optimiste). Les systèmes réels traitent les chaînes d'entrée discrètes et MCS non-idéal de longueur finie. Le sujet de cette thèse de doctorat est de mesurer l'impact réel des récepteurs de turbo sur la performance au niveau du lien/système.

Les travaux de cette thèse peuvent être principalement divisés en deux parties : les abstractions de la couche PHY pour la classe de récepteur LMMSE-IC itératif, d'une part, et la nouvelle adaptation du lien en présence d'un tel récepteur évolué, d'autre part.

Dans la première partie, cette thèse a été en mesure de proposer des abstractions de la couche PHY semi-analytiques précises, robustes et pratiques pour les systèmes MIMO avec le récepteur LMMSE-IC itératif. Les abstractions de la couche PHY dépendent des hypothèses fondamentales de la couche PHY et la structure du récepteur, comme la disposition de la CSIR, le MCS adopté et le type d'information probabiliste sur les bits codés réinjectée par le décodeur pour la reconstruction d'interférence dans l'algorithme LMMSE-IC itératif. Ces travaux ouvrent la voie à l'optimisation inter-couches en présence d'un tel récepteur itératif avancé et pourraient être utilisés comme une étape importante pour concevoir de nouveaux moteurs d'annulation d'interférences pour les réseaux sans fil de prochaine

génération.

- Chapter 2

  Ce chapitre se concentre sur la clarification des hypothèses sous-jacentes nécessaires pour dériver LMMSE -IC (itératif), la compréhension des similitudes et des différences entre algorithme itératif basé sur LEXPTR et LAPPR afin de proposer une abstraction de la couche PHY pour l'algorithme itératif basé sur LAPPR sous CSIR parfaite. Le MCS est construit à partir de codes convolutifs. L'abstraction de la couche PHY pour l'algorithme basé sur LAPPR est plus sophistiquée. Une procédure de calibration simple, mais efficace, a été proposée, dont le principe est d'ajuster la variance du symbole (une seule variance est utilisée pour mesurer la fiabilité des interférences reconstruites basé sur l'hypothèse inconditionnelle) avec un facteur multiplicatif de valeur réelle supérieure à un, ce qui a pour effet de réduire artificiellement les SINR qui sont utilisés dans le procédé de prédiction de performance. Le facteur de calibration optimale par MCS est recherché en minimisant la distance entre les BLERs (ou BERs) simulés et prédits calibrés sur un grand nombre de réalisations de canal à chaque itération. Simulations exhaustives révèlent que le facteur de calibration dépend du MCS, mais ne varie pas de façon significative par rapport au nombre d'antennes de transmission et de réception ainsi que les caractéristiques du canal. Les résultats ont été publiés dans :

  – B. Ning, R. Visoz, A.O. Berthet, *Extrinsic versus a posteriori probability based iterative LMMSE-IC algorithms for coded MIMO communications : Performance and analysis*, Proc. IEEE ISWCS, Paris, France, Aug. 2012.

- Chapter 3

  Ce chapitre étudie les abstractions de la couche PHY sous CSIR imparfaite. Le MCS est construit à partir de codes convolutifs. L'accent est mis sur la situation lorsque le nombre de symboles de pilote est réduit et l'hypothèse mismatch n'est plus valide. De nouvelles abstractions de la couche PHY sont dérivées subordonné à la disposition d'information a priori seulement, c'est à dire, l'hypothèse match [75–77], qui sont l'estimation du canal utilisant seulement les symboles de pilote

et la distribution des canaux à long terme (CDI). Les résultats sur ce sujet ont été ou seront publiés dans :

- B. Ning, R. Visoz, A.O. Berthet, *Semi-Analytical Performance Prediction Method for Iterative MMSE-IC Detection and Semi-blind Channel Estimation*, Proc. IEEE VTC Spring, Hungrary, Budapest, May 2011.
- B. Ning, R. Visoz, A.O. Berthet, *Performance analysis of LMMSE-IC based turbo equalization and semi-blind channel estimation*, in preparation for IEEE Trans. Sig. Proc.

- Chapter 4

  Ce chapitre présente les abstractions de la couche PHY compte tenu de la combinaison de turbo codes et algorithme LMMSE-IC itératif. On constate que, même dans le cas simplifié de mapping Gray, trois LUT à deux entrées sont nécessaires pour caractériser l'évolution du démapper joint turbo décodeur. Ceci est en contraste avec [71] [66] où le code convolutif est examiné et une LUT univariée est suffisante. Les résultats à ce sujet ont été publiés dans :

  - S. Martinez Lopez, F. Diehm, R. Visoz, B. Ning, *Measurement and Prediction of Turbo-SIC Receiver Performance for LTE*, Proc. IEEE VTC Fall, Québec City, Canada, Sept. 2012.
  - un brevet français, déposé en février 2013.
  - Contribution à la normalisation 3GPP : *Physical layer abstraction for turbo-CWIC receivers*, R4-134328, Aug. 2013.
  - Contribution à la normalisation 3GPP : *Physical layer abstraction for turbo-CWIC receivers*, R1-134672, Nov. 2013.
  - B. Ning, R. Visoz, A.O. Berthet, *Physical Layer Abstraction of LMMSE-IC based Turbo Receivers for LTE evolution*, IEEE GLOBECOM, Atlanta, US, Dec. 2013.

- Chapter 5

  Dans ce chapitre, les abstractions de la couche PHY pour un système MIMO générique turbo codé par antenne utilisant LMMSE-IC itératif sont introduites. Comparée au troisième sujet de cette partie, un nouveau degré de liberté est l'ordre de décodage. La performance globale

du récepteur de turbo dépend de l'ordre de décodage qui doit être pris en compte dans les abstractions de la couche PHY.

Dans la deuxième partie, l'adaptation du lien en boucle fermée dans les systèmes MIMO a été abordée en utilisant des abstractions de la couche PHY proposées pour le récepteur LMMSE-IC itérative. CSI partielle est prise en charge à l'émetteur en vertu des rétroactions limitées provenants des abstractions de la couche PHY et CSI parfaite est supposé au niveau du récepteur. Les performances prédites et simulées sont comparées dans de différents scénarios de communication pour mesurer l'impact réel apporté par les récepteurs de turbo.

- Chapter 6

  Ce chapitre aborde la FLA dans le système MIMO codé en boucle fermée utilisant le récepteur LMMSE-IC itératif basé sur LAPPR. Les systèmes MIMO avec MCS construits à partir de turbo code ou code convolutif sont considérés. Les LUTs univariés et les facteurs de calibration optimaux pour tous les MCS construits à partir de codes convolutifs sont obtenus hors ligne. De même, les LUTs bivariés et les facteurs de calibration optimaux pour tous les MCS construits à partir de turbo codes sont obtenus hors ligne. L'adaptation du lien en boucle fermée effectue une sélection de précodage spatial et de MCS en fonction des rétroactions limitées. Elle vise à maximiser le débit moyen soumis à une contrainte d'un BLER cible en supposant le récepteur LMMSE-IC itératif basé sur LAPPR est utilisé à la destination. Les résultats à ce sujet ont été publiés dans :

  - B. Ning, R. Visoz, A.O. Berthet, *Link Adaptation in Closed-Loop MIMO Systems of LTE with LMMSE-IC based Turbo Receivers*, Proc. IEEE WIMOB, Lyon, France, Oct. 2013.
  - B. Ning, R. Visoz, A.O. Berthet, *Link Adaptation in Closed-Loop Coded MIMO Systems with LMMSE-IC based Turbo Receivers*, Proc. IEEE ICNC, Honolulu, Hawaii, US, Feb. 2014.
  - B. Ning, R. Visoz, A.O. Berthet, *Link adaptation in closed-loop coded MIMO systems with LMMSE-IC based turbo receivers*, in preparation for IEEE Trans. Wireless Commun.

- Chapter 7

Ce chapitre aborde le controle de débit par antenne (PARC) en boucle fermée pour le système MIMO turbo codé indépendemment par antenne avec le récepteur LMMSE-IC itératif basé sur LAPPR. Ayant en main les LUT bivariés et facteurs de calibration optimaux pour tous les MCS construits à partir de turbo codes, l'algorithme effectue une sélection conjointe des précodeurs spatials, de l'ordre de décodage et de la combinaison de MCS. Le but est de maximiser le débit moyen soumis à une contrainte d'un BLER cible. Les résultats à ce sujet seront publiés dans un article de conférence en préparation.

- Chapter 8

  Dans ce chapitre, les conclusions et les suggestions pour la poursuite des travaux sont données.

Les futurs sujets de recherche comprennent plusieurs volets principaux :

- Récepteur itératif plus performant :

  Il existe toujours un écart entre les performances des algorithmes LMMSE-IC itératifs et l'annulation d'interférence parfaite lié à des scénarios de communication SU-MIMO. La poursuite de l'amélioration de l'efficacité spectrale s'appuie sur un récepteur plus puissant tel que le récepteur MAP itératif. Nous aimerions proposer une abstraction de la couche PHY semi-analytique précise, robuste et pratique pour le récepteur MAP itératif, mais il n'y a pas de SINR à calculer. Inspiré par l'introduction d'un facteur supérieure à un de calibration sur la variance pour compenser les inexactitudes des hypothèses pour l'algorithme LMMSE-IC itératif basé sur LAPPR, l'algorithme MAP itératif peut être approché par un algorithme LMMSE-IC itératif virtuel basé sur LEXTPR compensé par un facteur inférieur à un de calibration sur la variance. Si cette idée est validée, nous sommes en mesure de proposer un cadre d'abstractions de la couche PHY pour les récepteurs de turbo.

- Calibration plus agressives en collaboration avec IR-HARQ :

  Les facteurs de calibration introduits sont obtenus par la minimisation de la somme de la distance entre les BLERs simulés et prédits calibrés sur un grand nombre de réalisations de canal tirées d'un

modèle de canal générique. Du coup, les facteurs de calibration obtenus fonctionnent bien pour la plupart des réalisations de canaux. En évitant d'affecter des débits de données trop optimistes pour des conditions radio mauvaises, causant un grand nombre de retransmissions, l'utilisation des facteurs de calibration sacrifie inévitablement des débits de données sur de bonnes conditions radio. Si nous voulons adopter des facteurs de calibration plus agressifs (plus petits) pour allouer des débits plus élevés sur de bonnes conditions radio, il devrait exister des mécanismes pour compenser les attributions possibles des débits de données trop optimistes sur des conditions radio mauvaises. Dans cette ligne de pensée, il est nécessaire d'employer IR-HARQ [88], [89], [90], [91], [92], [93] dans la transmission.

- Adaptation du lien en boucle ouverte :

  La partie traitant la FLA dans cette étude de doctorat est basée sur une rétroaction instantanée et parfaite, et toutes les rétroactions instantanées peuvent être traitées par la couche MAC immédiatement. Toutefois, ces hypothèses ne peuvent pas être réalistes dans la pratique. Par exemple, les rétroactions ne sont plus fiables lorsque l'UE se déplace trop rapidement, ou bien une station de base sous la charge lourde n'est pas en mesure de suivre les rétroactions de chaque UE. Dans de telles situations, la meilleure stratégie consiste à effectuer une adaptation du lien en boucle ouverte quelle que soit la rétroaction instantanée. Avec le passage de boucle fermée en boucle ouverte, le gain apporté par le récepteur itératif comparé à un récepteur linéaire classique va augmenter. Par conséquent, il est intéressant de comparer les performances de différents types de récepteurs dans le contexte d'adaptation de liaison en boucle ouverte.

- Modèle de canal plus générique :

  L'optimisation inter-couches a été abordée principalement sur les systèmes SU-MIMO. Les futurs sujets comprennent l'évaluation de la performance au niveau du système pour la liaison montante/descendante, ainsi qu'une extension de ce travail à multicellulaire MIMO. Cependant, nous avons observé que l'optimisation inter-couches commence à introduire une complexité de calcul très élevée à la recherche de la solution optimale quand le degré de libertés augmente considérablement. En raison de la contrainte de complexité, le PARC sélectif est limité

à la transmission de double mots de code sur un modèle de canal 2x2 MIMO d'évanouissement par bloc dans cette étude de doctorat. L'étape suivante doit être PARC sélectif pour la transmission de double mots de code sur un modèle de canal 4x4 MIMO d'évanouissement par bloc. En outre, une exploration intelligente de l'espace de recherche est nécessaire pour réduire la complexité de l'optimisation de tous les degrés de libertés : mode, antenne, précodage, débit et ordre de décodage. Nous croyons que les récepteurs itératifs, avec ces mécanismes de LA et RRM avancés, vont augmenter sensiblement les débits du système.

Chapter 1

Introduction

The purpose of the first chapter is to give an overview of the whole PhD study. In section 1.1, the evolution and technical preliminaries of wireless communication systems are described. In section 1.2, the motivations of the PhD thesis are introduced. In section 1.3, state of the art is presented. In section 1.4, the contributions of the PhD study and the thesis outline are listed.

1.1 Evolution of wireless communication systems

As per the estimates of the International Telecommunication Union (ITU) [1], the number of mobile-cellular subscriptions reaches 6.8 billion in 2013, corresponding to a global penetration of 96%. Today, people can communicate with each other conveniently by voice, text message and have Internet connection wherever is covered by the mobile communication network.

The First Generation (1G) systems were developed in the 1980s. These systems used analogue technology and were designed only for voice service.

From 1991, the Second Generation (2G) systems were developed which started to use digital technology, such as Global System for Mobile communications (GSM) in Europe, the Personal Digital Communication (PDC) in Japan and IS-95 in the USA. Among these systems, the GSM were widely accepted and deployed in most of countries and are still being used today. The 2G systems were designed to provide voice and text message, and later also data service by Enhanced Data rates for GSM Evolution (EDGE). Among the family of 2G systems, GSM and PDC were based on Frequency-Division Multiple Access (FDMA) [2], i.e., the whole bandwidth is divided

into multiple narrow-band channel far apart in frequency and multiple users can transmit simultaneously over different narrow-band channels, and Time-Division Multiple Access (TDMA) [2], i.e., multiple users can transmit over one narrow-band channel at different time. IS-95 system was based on Code-Division Multiple Access (CDMA) [2], i.e., each user transmits its signals over the entire bandwidth and each user is identified by a specific code.

The Third Generation (3G) systems included two families of technology: Universal Mobile Telephone Service (UMTS), published by the standardization organization of the Third Generation Partnership Project (3GPP) in Release 99 following GSM, and CDMA2000 following IS-95. The UMTS system was widely deployed in many countries while CDMA2000 system was mainly deployed in Asia and North America. 3G systems were a significant improvement over 2G systems and aimed to provide higher data rates, improved voice capacity as well as data services and applications. As a result of global standardization effort, the family of 3G systems were uniformly based on CDMA. UMTS employs the Wideband CDMA (WCDMA) which supports both Time-Division Duplexing (TDD) and Frequency-Division Duplexing (FDD) modes. One variate of TDD UMTS, named Time-Division Synchronous CDMA (TD-SCDMA), is also normalized by 3GPP which is mainly deployed in China.

The UMTS was further enhanced by High Speed Downlink Packet Access (HSDPA) and High Speed Uplink Packet Access (HSUPA) in 3GPP. Higher-order modulation are supported: 16 Quadrature Amplitude Modulation (16QAM) is introduced to the downlink as an enhancement of Quadrature Phase Shift Keying (QPSK) of Release 99 and QPSK is introduced to the uplink as a complementary of Binary Phase Shift Keying (BPSK) of Release 99. Adaptive Modulation and Coding (AMC) is introduced to adapt dynamically the modulation order and channel coding rate to the instantaneous radio conditions and user's requirements. A new retransmission scheme Hybrid Automatic Repeat reQuest (HARQ) is added between the users and the base-station to reduce system latency in case of packet loss.

The HSPA evolutions HSPA+ (Release 7, 8) have been designed to further improve the data rate by the introductions of new techniques. The downlink and uplink started to support 64QAM and 16QAM, respectively. The Multiple-Input Multiple-Output (MIMO) [3], [4] antenna systems are also introduced. MIMO technology can be used to increase data rate [3], [5], [6], [7] (spatial multiplexing gain) , to increase the robustness of trans-

mission (spatial diversity gain) and to concentrate the transmission energy to a certain direction (precoding or beamforming).

As the forth remarkable step, the Long Term Evolution (LTE) published in Release 8/9 and soon LTE-Advanced (LTE -A) published in Release 10/11 defined by 3GPP are recognized widely as the Forth Generation (4G) systems which were characterized by Orthogonal Frequency-Division Multiplexing (OFDM) technology. The advantages of OFDM [2] are multiples, such as the robustness to Inter-Symbol Interference (ISI) from which CDMA suffers, flexibility of deployment over different large band to which CDMA is limited, the adequacy to MIMO transmission, management and scheduling of wide band, flexibility to multiple access, etc. The subcarriers of OFDM technology are overlapping but orthogonal which make OFDM highly spectrally efficient [8]. LTE-A has chosen for the downlink the scheme of Orthogonal Frequency-Division Multiple Access (OFDMA) [9] and for the uplink the scheme of Single-Carrier Frequency-Division Multiple Access (SC-FDMA) [10]. The different choice for downlink and uplink comes from the relatively high Peak-to-Average Power Ratio (PAPR) [11] of an OFDM signal which is not tolerable for the UE.

LTE-A supports 64QAM at both uplink and downlink. At the Physical (PHY) layer, turbo code [12] is employed to protect the data. Enhanced Inter-Cell Interference Coordination (ICIC) in Release 10, Coordinated MultiPoint (CoMP) transmission/reception in Release 11 as well as Carrier Aggregation are some important techniques that can further increase spectral efficiency. In order to perform link adaptation, the UE regularly reports a Channel State Information (CSI) to the base station. These CSI comprise of: Channel Quality Indicator (CQI), preferred Precoding Matrix Indicator (PMI), Rank Indicator (RI) (= number of spatial streams supported). Some important parameters are the reporting delay, the reporting period and possibly CQI filtering.

There are other kinds of wireless system other than cellular, such as Wireless Local Area Networks (WLAN) [2]. These are designed for much higher data rates than cellular systems, but are similar to a single cell of a cellular system. These are mainly designed to provide in-building broadband coverage. The major standards for WLAN are the IEEE 802.11 family and the term Wi-Fi is used as a synonym for WLAN. Wi-Fi supports high-order modulation (64QAM and even 256QAM), MIMO and link adaptation. The PHY layer employs convolutional code to protect the data.

1.2 Motivations of the PhD thesis

Within the ongoing global research effort on future wireless communications systems, adaptive allocation of time, code, space and frequency resources based on CSI and users' requirements is widely recognized as a key feature to approach the capacity of MIMO broadband frequency-selective channels [13], [14], [15], [16], [17], [18], [19], [20], [21], [22], [23]. The traditional Radio Resource Management (RRM) and Slow Link Adaptation (SLA) have been built on a link-to-system interface, referred to as average value interface [24], in which the individual radio link performance is evaluated through Monte-Carlo simulations averaged over the fast fading statistics. For this approach to be valid the RRM and LA timescales must be large compared to the fast fading dynamics. On the opposite, current wireless systems evolve toward an enhanced reactivity of RRM and Fast Link Adaptation (FLA) protocols in order to jointly optimize the Media Access Control (MAC) and PHY layers. A new type of link-to-system interface, referred to as actual value interface [24], has emerged in which advanced RRM and FLA mechanisms are designed and optimized so as to exploit feedback metrics representative of the instantaneous individual radio link performance based on PHY-layer abstractions (also called performance prediction methods).

Interference in cellular networks can be managed by interference avoidance techniques at the transmitter side such as clever scheduling [25], [chapter 6, [2]], broadcast channel, dirty paper coding, suboptimal ZF precoding, MIMO Interference Alignment (IA) [26], etc. This strategy was followed by WP1 of the European project ARTIST4G entitled "*Interference Avoidance*". In this way, low complexity linear receiver can be sufficient. However, these interference avoidance techniques require perfect and instantaneous CSI at the Transmitter (CSIT) which, in practice, is not available. Too much CSIT feedbacks will sacrifice the system spectral efficiency and make the system lack of robustness. Finally, the interference can be avoided only to a certain level. Therefore, the interference cancellation techniques at the receiver side based on some complex advanced signal processing are important complementary to the previous interference avoidance techniques. Compared to the CSIT, the Channel State Information at Receiver (CSIR) is always available in Single-User MIMO (SU-MIMO) communications and uplink communications (multiple access channel). For downlink, converting the broadcast channel into some multiple access channel with side information (provided

by the network) at the level of each receiver is currently under investigation by the industry [27]. This latter strategy seems more robust to imperfect side information than the former. In fact, the idea to abandon synchronism and orthogonality in future wireless systems, thereby admitting some interference, and to control these impairments by a suitable transceiver structure was at the core of ARTIST 4G WP2 entitled "*Interference Exploitation*" and is now advertised by several European projects as a building concept for the Fifth Generation (5G) at the PHY/MAC layers.

In parallel, the success of turbo codes [12] and turbo principle [28] has inspired new potentially capacity achieving coded modulations. New spatial multiplexing architectures and non-orthogonal multiple-access techniques based on powerful coding schemes have been proposed to achieve very high spectral efficiency, whose relevance is, however, conditional upon iterative processing at the receiver. These two trends, namely, cross layer optimization and turbo processing, call for the development of new PHY-layer abstractions that can capture the iterative receiver performance per iteration conditional on the available CSIR that enables the smooth introduction of such advanced receivers within FLA and RRM.

1.3 State of the art

On the subject of predicting the convergence and/or analysing the performance of iterative decoding, we first distinguish between deterministic approaches and stochastic ones [29]. Deterministic approaches treat decoding as a deterministic process and try to characterise the behavior of the decoder for each instance of the received signal. For example, [30] is able to reveal a number of dynamic behaviors of turbo decoding, such as the existence of fixed points as well as some conditions for the uniqueness and stability of fixed points. However, knowing the existence of a fixed point is not sufficient, as multiple fixed points or even limit cycles may exist. Moreover, the conditions for the uniqueness and stability are specific to each decoding block and difficult to compute, meaning that they are not useful in predicting the performance of a given turbo decoder.

Based on the assumption of large codeword lengths (or equivalently large interleaver size), the stochastic approaches, on the other hand, view the input and output signals circulating within the iterative decoder as ergodic random processes [29] whose statistics are computable using realizations (or

instances). Treating Log Likelihood Ratios (LLRs) of exchanged binary messages as Random Variables (RVs), the Density Evolution (DE) [31, 32] is proposed for analysing the performance of the sum-product decoding [33] of Low-Density Parity-Check (LDPC) codes [34] over simple binary-input output-symmetric channels. However, the mathematical rigorousness of DE introduces intrinsic high complexity as this method actually estimates the evolution of their probability distributions (expressed in closed-form) by means of numerical simulations.

Other simpler stochastic approaches exist which all have in common to employ a single statistical parameter (as opposed to a complete probability distribution) to characterise the input and output signals involved in the iterative process. EXtrinsic Information Transfer (EXIT) charts, pioneered by ten Brink who first introduced them in the context of choosing a suitable mapper and a suitable constellation in an iterative demapping and decoding scheme [35] and soon thereafter applied them to analyze turbo codes [36, 37], is a powerful tool to analyze iterative behaviors, based on single statistical parameter tracking. The evolution of the Average Mutual Information (AMI) between the information (or coded) bits and the corresponding output LLRs after BCJR decoding [38] is observed instead of the evolution of the true densities. A simple one-dimensional Gaussian approximation to the density evolution has also been suggested by Chung et al. in [39, 40] for LDPC codes. Related ideas have been independently proposed for analysing turbo codes [41, 42] and iterative multiuser detection and decoding [43, 44]. These Gaussian approximations differ in the choice of the one-dimensional parameter which is chosen to characterise a density, e.g., Signal-to-Noise Ratio (SNR) [41, 42] or mean [39, 40] under symmetry condition and consistency property. However, experiments have shown that the AMI used in EXIT charts is the most robust statistical parameter w.r.t. the variations of the LLRs probability distributions and consequently the most faithful one [45].

Introducing EXIT charts to predict the performance of turbo receivers over a multiuser systems and (non-ergodic) MIMO block fading frequency selective channel reveals several issues. If each user employs a coded modulation scheme, the turbo receivers are characterized by iterative message circulations between the MultiUser Detector (MUD) (using a priori information on users' coded bits generated by the decoder) and the bank of soft-in soft-out channel decoders.

The first issue consists in the strong time constraint which does not allow us to obtain the MUD's extrinsic AMI at coded bit level for any given channel realization by running a long simulation. As a consequence, the MUD's extrinsic AMI must be computed analytically or at least semi-analytically. Some simplified (suboptimal) class of MUD, named as Linear Minimum Mean Square Error Interference Cancellation (LMMSE-IC) MUD exit for which the calculation can be performed in two steps: one step, purely analytical computation of Signal-to-Interference-plus-Noise Ratio (SINR), devoted to IC and LMMSE detection of users' transmitted symbols and the other step to demapping. This PhD study focus on this class of LMMSE-IC detection scheme [46–49], since it is a challenging, if not impossible, task for a (locally optimum) detection derived as a strict application of the sum-product rules on the corresponding subgraph [33]. This line of thought is followed and developed in [50–57] (see also [44, 58] for alternatives).

A second issue consists in the fact that the coded bits are spread over symbols that experience different channel fading states. This situation is behind the MIMO block fading channel model [59]. The MUD's EXIT characteristics should be computed for each of such channel states which serve as a priori input for the computation of EXIT characteristics of the user's channel decoders. We have to compress (map) these multiple MUD's extrinsic outputs (one per channel state) to a single one to avoid using a multidimensional Look-Up-Tables (LUTs) to characterize the decoder's extrinsic outputs whose storage would not be affordable. The problem is solved in [50–52] by averaging the AMI, between the MUD's extrinsic output and the related coded bits, over all existing channel states.

Interestingly, this second problem was also encountered in another research community dealing with adaptive modulation/coding and system-level evaluation referred to as compression techniques [60–63]. Compression techniques aim at bringing back the multiple instantaneous SNRs representative of the different channel states that coded bits may experience into a single effective SNR. The two most studied compression techniques are Exponential Effective SNR Mapping (EESM) [64] and Mutual Information Effective SNR Mapping (MIESM) [61] where in the former an exponential function is used as an information measure based on Chernoff bound and in the latter an normalized Bit-Interleaved Coded Modulation(BICM) [65] constrained capacity is used as an information measure. EESM usually requires fine-tuned adjusting factors to reach good accuracy for a given MCS

while MIESM is much less sensitive to adjustment factors and its superiority has been reported in a number of past contributions [61]. This statement seems in line with [49]. It is worth noticing that the idea of compression has been rediscovered and formalised by Yuan et al. in [56, Assumption V].

In [66], a study is set up on fast and accurate semi-analytical methods to predict the Block-Error-Rate (BLER)/Bit-Error-Rate (BER) performance per user and per iteration in a Multiple-User (MIMO) MU-MIMO system where each user employs a Space-Time Bit-Interleaved Coded Modulation (STBICM) constructed out of convolutional code and where iterative LMMSE-IC joint decoding (in short iterative LMMSE-IC) is performed at the receiver. By LMMSE-IC joint decoding it is meant LMMSE detection using a priori information from the decoder [67] together with the unconditional assumption [48,49]. The unconditional assumption consists of averaging the symbol second order statistics over time, to render the LMMSE filter time-independent (thus easy to implement). Interestingly, this assumption is most of the time not detrimental in terms of final performance [49]. The PHY-layer abstractions described in [66] rely on the MIESM technique at bit or symbol level. In the first method, the MUD's extrinsic outputs up to the users' channel decoders, seeing LMMSE-IC detection and demapping as a joint process, are analytically computed. This method follows the classical framework of EXIT charts and tracks the evolution of the AMI defined at coded bit level circulating between the MUD and the bank of outer channel decoders [65, Section III], [68, Section V], [69], [70, Section III.B]. Then, shifting in viewpoint and considering user demapping and decoding as a joint process, an alternative method which tracks the evolution of the AMI defined at coded modulated symbol level and circulating between the LMMSE-IC interface and the bank of joint demappers and outer channel decoders [71] is proposed. This allows to avoid the critical issue of parameterising the demapping. The two methods give comparable results for low-order non-linear mapping. On the contrary, the second method, which includes the demapping inside the LUTs reveals more robust to high-order non-linear mapping, demonstrating its superiority.

However, within the class of LMMSE-IC based turbo receivers, we often distinguish between Log Extrinsic Probability Ratios (LEXTPR) based and Log A Posteriori Probability Ratios (LAPPR) based iterative LMMSE-IC algorithms. The two algorithms differ by the type of probabilistic information fed back by the decoder for soft interference regeneration and cancella-

tion, namely LEXTPR or LAPPR on coded bits. Empirical evidence reveals that the LAPPR-based iterative algorithm can significantly outperform its LEXTPR-based counterpart for highly loaded multiantenna or multiuser systems. In such scenarios indeed, using LAPPR instead of LEXTPR leads to more reliable MMSE symbol estimates. This is due to the extra information gleaned from the equalization/detection process, which allows to cancel out more interference at each iteration. The analysis in [66] are correct for LEXTPR-based iterative algorithm given sufficient large interleaver size while [66, Assumption A1 and A4] never hold even with infinite interleaver size for LAPPR-based iterative algorithm. Due to the neglected inaccuracies of assumptions, the symbol-wise method based predicted performance reveal too optimist compare to simulated performance of LAPPR-based iterative algorithm. This phenomena is all more evident for MCS with high-order mapping and high coding rate. Therefore, a careful examination of underlying fundamental assumptions for this family of receiver is necessary so as to propose an improved PHY-layer abstraction for LAPPR-based algorithm, which is the point of start of this PhD study.

Otherwise, closed-loop link adaptation in LTE (LTE-A) involves a family of MCS constructed out of powerful turbo codes. The turbo decoder is made of *two* BCJR decoders [38] exchanging probabilistic information (log domain). Due to their particular structure, turbo codes cannot be optimally decoded except for very limited block length. In practice, a suboptimal iterative decoding is applied, where probabilistic soft information is exchanged between the constituent decoders. The first BCJR decoder computes the LAPPRs on its own coded bits (information and parity bits) taking into account the available a priori information on systematic information bits stored from an earlier activation (i.e., the most recent LEXTPRs on systematic information bits delivered by the second BCJR decoder). Then the second BCJR decoder is activated and computes the LAPPRs on its own coded bits (information and parity bits) taking into account the available a priori information transmitted by the first BCJR decoder. Joint iterative LMMSE-IC and turbo decoding gives rise to a complicated receiver structure with at least two interwoven iterative processes. Some similarities can be found in earlier works dealing with multiple concatenated codes and the convergence analysis of their iterative decoding, see e.g., [72] [49] [73] [74]. Hence, the smooth introduction of LMMSE-IC based turbo equalization receivers in LTE calls for new PHY-layer abstractions to this non-trivial

situation.

When the perfect CSIR assumption is removed, the PHY-layer abstractions should be derived under imperfect CSIR and channel estimation error. If the number of pilot symbols is sufficient to ensure close to perfect CSI, then it is sufficient to adopt the so-called mismatched assumption [75–77] which simply postulates that the initial pilot assisted channel estimate is noiseless. In that case, PHY-layer abstractions derived under the assumption of perfect CSIR can be used in practice. However, if the number of pilot symbols are reduced conditional on some advanced semi-blind channel estimation scheme at the receiver side, the mismatched assumption is not valid anymore. Indeed, it is quite known that performing detection and channel estimation within a same iteration (using channel decoding a priori) allows reducing drastically the number of reference signals for a given performance, see, e.g., [78–81]. There is a wealth of literature on the subject of analyzing semi-blind channel estimation performance, e.g., [**?**, 75–77, 80, 82, 84]. For instance, [80] is rather exhaustive in deriving and comparing different semi-blind channel estimate MSEs, but only refer to iterative mismatched detection schemes without analysis. While, on the other hand, [77] considers iterative matched Maximum A Posteriori (MAP) detection with pilot assisted only channel estimation. However, the combination of the matched LMMSE-IC (taking into account the channel estimation errors) detection and LMMSE semi-blind channel estimation was never tackled as such either from a pure performance evaluation or prediction perspective.

Once the PHY-layer abstractions are derived with turbo receiver, the brigades between PHY and MAC layers are built. The following task is to realize cross optimization between PHY and MAC layers, sometimes referred to as cooperative resource allocation which is currently one of the most exciting research topics in the design of MU-MIMO systems. The existing contributions often restrict their study to simple linear receivers (see e.g., [85] and [86]) or, if dealing with more sophisticated non-linear receiver structures, e.g., Successive Interference Cancellation (SIC) [87], idealize some parts of the decoding process, typically assuming continuous-input channels with zero-error Gaussian codebooks, and neglecting error propagation, which leads to inaccurate (i.e., too optimistic) predicted throughputs. Real systems though deal with discrete-input channels and non-ideal finite-length MCS. The subject of this PhD study is to measure the true impact of turbo receivers on the link/system level performance.

1.4 Thesis outline

The work of this PhD study can be mainly divided into two parts: PHY-layer abstractions for the class of iterative LMMSE-IC receiver and new link adaptation in presence of such advanced receiver.

1.4.1 Part I: PHY-layer abstractions

In the first part, this PhD study has been able to propose accurate, robust and practical semi-analytical PHY-layer abstractions for MIMO systems employing iterative LMMSE-IC receiver. The PHY-layer abstractions depend on PHY layer fundamental assumptions and the receiver structure, such as the available CSIR, the MCS adopted and the type of LLR on coded bits fed back from the decoder for interference reconstruction and cancellation in the iterative LMMSE-IC algorithms. These work pave the way for cross layer optimization in presence of such advanced iterative receiver and could be used as a milestone to design new interference cancellation engines for next-generation wireless networks.

- Chapter 2 This chapter focus the clarification of the underlying assumptions needed for deriving (iterative) LMMSE-IC, the understanding of the similarities and differences between the LEXPTR and LAPPR based iterative algorithm and finally the proposition of an improved PHY-layer abstraction for LAPPR based iterative algorithm under perfect CSIR. The MCS is constructed of convolutional code. The PHY-layer abstraction for LAPPR-based algorithm is more sophisticated. A simple, yet effective, calibration procedure has been proposed whose principle is to adjust the soft symbol variance (a single variance is used to measure the reliability of re-constructed interference based on the unconditional assumption) with a real-valued multiplicative factor greater than one which has the effect to artificially reduce the SINRs that are used in the performance prediction method. The optimal calibration factor per MCS is searched by minimizing the error between the simulated BLER (or BER) and the calibrated predicted BLER (or BER) over a large number of channel outcomes at each iteration for the BLER range of interest. Exhaustive simulations revealed that the calibration factor depends on the MCS but does not vary significantly w.r.t. the number of transmit and receive antennas as well

as the channel characteristics. The results have been published in:

  - B. Ning, R. Visoz, A.O. Berthet, *Extrinsic versus a posteriori probability based iterative LMMSE-IC algorithms for coded MIMO communications: Performance and analysis*, Proc. IEEE ISWCS, Paris, France, Aug. 2012.

- Chapter 3 This chapter investigates the PHY-layer abstractions under imperfect CSIR. The MCS is constructed of convolutional code. The emphasis is put on the situation when the number of pilot symbols are reduced and the mismatched assumption is not valid anymore. New PHY-layer abstractions are derived conditional on the available a priori information only, i.e., the so-called matched assumption [75–77], which are the initial pilot assisted channel estimate and the long-term Channel Distribution Information (CDI), (such as the channel and noise probability distribution functions). The results on this subject have been or will be published in:

  - B. Ning, R. Visoz, A.O. Berthet, *Semi-Analytical Performance Prediction Method for Iterative MMSE-IC Detection and Semi-blind Channel Estimation*, Proc. IEEE VTC Spring, Hungrary, Budapest, May 2011.
  - B. Ning, R. Visoz, A.O. Berthet, *Performance analysis of LMMSE-IC based turbo equalization and semi-blind channel estimation*, in preparation for IEEE Trans. Sig. Proc.

- Chapter 4 This chapter presents the PHY-layer abstractions considering the combination of turbo code and iterative LMMSE-IC algorithm. It is found that, even in the simplified case of Gray mapping, a bivariate LUT is needed to characterize the evolution of the joint demapper and turbo decoder embedded within the LMMSE-IC based turbo equalization. This is in contrast with [71] [66] where simple convolutional codes were considered and univariate LUT sufficient. The results on this subject have been published in:

  - S. Martinez Lopez, F. Diehm, R. Visoz, B. Ning, *Measurement and Prediction of Turbo-SIC Receiver Performance for LTE*, Proc. IEEE VTC Fall, Québec City, Canada, Sept. 2012.

  - One french patent, filed date: February 2013.
  - Contribution to 3GPP standardization: *Physical layer abstraction for turbo-CWIC receivers*, R4-134328, Aug. 2013.
  - Contribution to 3GPP standardization: *Physical layer abstraction for turbo-CWIC receivers*, R1-134672, Nov. 2013.
  - B. Ning, R. Visoz, A.O. Berthet, *Physical Layer Abstraction of LMMSE-IC based Turbo Receivers for LTE evolution*, IEEE GLOBECOM, Atlanta, US, Dec. 2013.

- Chapter 5

  In this chapter, PHY-layer abstractions for a generic per-antenna turbo coded MIMO system employing iterative LMMSE-IC in is introduced. Compare to the third topic of this part, a new degree of freedom is the decode ordering. The global turbo receiver performance depends on the decode ordering which should be taken into account in the PHY-layer abstractions.

1.4.2 Part II: Link adaptation

In the second part, closed-loop link adaptations in MIMO systems based on the proposed PHY-layer abstractions for iterative LMMSE-IC receiver have been tackled. Partial CSI is assumed at the transmitter under limited feedback derived by the PHY-layer abstractions and perfect CSI is assumed at the receiver. Link level predicted and simulated performance are compared in different communication scenarios to measure the true impact on the performance brought by turbo receiver.

- Chapter 6

  This chapter tackles FLA in closed-loop coded MIMO systems employing LAPPR-based iterative LMMSE-IC receiver. Both convolutionally and turbo coded MIMO systems are considered. Univariate LUTs and associated optimal calibration factors per MCS constructed out of convolutional code are obtained off-line. Bivariate LUTs and associated optimal calibration factor per MCS constructed out of turbo code are obtained off-line. Closed-loop link adaptation performs joint spatial precoder selection and MCS selection based on limited feedback. It aims to maximize the average rate subject to a target BLER constraint

assuming LAPPR-based iterative LMMSE-IC at the destination. The results on this subject have been published in:

  - B. Ning, R. Visoz, A.O. Berthet, *Link Adaptation in Closed-Loop MIMO Systems of LTE with LMMSE-IC based Turbo Receivers*, Proc. IEEE WIMOB, Lyon, France, Oct. 2013.
  - B. Ning, R. Visoz, A.O. Berthet, *Link Adaptation in Closed-Loop Coded MIMO Systems with LMMSE-IC based Turbo Receivers*, Proc. IEEE ICNC, Honolulu, Hawaii, US, Feb. 2014.
  - B. Ning, R. Visoz, A.O. Berthet, *Link adaptation in closed-loop coded MIMO systems with LMMSE-IC based turbo receivers*, in preparation for IEEE Trans. Wireless Commun.

- Chapter 7

  The chapter tackles selective Per Antenna Rate Control (PARC) in closed-loop independent per-antenna turbo coded MIMO systems with LAPPR-based iterative LMMSE-IC receiver. Having in hand the off-line obtained bivariate LUTs and optimal calibration factors for each MCS constructed out of turbo code, the algorithm performs joint selection of spatial precoder, decode ordering and MCS combination so as to maximize the average rate subject to a target BLER constraint. The results on this subject will be published in a conference paper in preparation.

1.4.3 Conclusions

- Chapter 8

  In this chapter, conclusions and suggestions for further work are given.

Part I

PHY-layer abstraction algorithms

Chapter 2

PHY-layer abstractions for convolutionally coded MIMO systems with iterative LMMSE-IC

2.1 Introduction

Since more than a decade, iterative detection and decoding algorithms have received much attention in the literature. Prominent amongst them is the class of iterative LMMSE-IC algorithms. Within the class of LMMSE-IC based turbo receivers, we often distinguish between LEXTPR-based and LAPPR-based iterative LMMSE-IC algorithms. The two algorithms differ by the type of probabilistic information fed back by the decoder for soft interference regeneration and cancellation, namely LEXTPR or LAPPR on coded bits. Empirical evidence reveals that the LAPPR-based iterative LMMSE-IC algorithm can significantly outperform its LEXTPR-based counterpart for highly loaded multiantenna or multiuser systems. In such scenarios indeed, using LAPPR instead of LEXTPR leads to more reliable MMSE symbol estimates. This is due to the extra information gleaned from the equalization/detection process, which allows to cancel out more interference at each iteration [94, Section 4, Fig. 4]. While LMMSE-IC algorithms can

This chapter is partially presented in the paper accepted to IEEE VTC Spring'2012 and the journal paper submitted to the journal IEEE Signal Processing

be rigorously analysed in terms of the SINR evolution when they are based on LEXTPRs, this is not the case for LAPPRs. Therefore, the underlying assumptions needed for the derivation of (iterative) LMMSE-IC algorithm and its associated SINRs should be emphasized for both LEXTPR-based and LAPPR-based algorithm.

In parallel, current wireless systems evolve toward an enhanced reactivity of RRM and FLA in order to jointly optimize the MAC and PHY layers. Hence, a new type of link-to-system interface, referred to as actual value interface, has emerged in which advanced mechanisms, based on performance prediction methods [61], are designed so as to improve the feedback metrics representative of the instantaneous individual radio link performance. These two trends, namely, turbo processing and cross-layer optimization, call for the development of new PHY-layer abstractions that can capture the evolution of iterative receivers (seen as complex dynamical systems). This chapter focus on PHY-layer abstractions for such receivers assuming perfect CSIR in convolutional coded MIMO systems.

2.2 System model

Single-user transmission occurs over a MIMO block Rayleigh fading multipath Additive White Gaussian Noise (AWGN) channel with n_b fading block, n_t transmit antennas and n_r receiver antennas. Perfect channel state information is assumed at the receiver. A STBICM, indexed by ν, is used at the transmitter, specified by a linear binary convolutional code $\mathscr{C}_\nu$ of rate r_ν, a complex constellation $\mathscr{X}_\nu \subset \mathbb{C}$ of cardinality 2^{q_ν} and a memoryless labeling rule μ_ν. We define the rate of the MCS as $\rho_\nu = r_\nu q_\nu$ (bits/complex dimension). The encoding process for MCS is detailed. The vector of binary data (or information bits) $\mathbf{u}$ enters an encoder φ_ν whose output is the codeword $\mathbf{c} \in \mathscr{C}_\nu$ of length $n_{\nu,c} = n_s n_t q_\nu$. The codeword bits are interleaved by a random space time interleaver π_ν and reshaped as a integer matrice $\{\mathbf{D}_b\}_{b=1}^{n_b}$ with $\mathbf{D}_b \in \mathbb{Z}_{2^{q_\nu}}^{n_t \times L}$. Each integer entry can be decomposed into a sequence of q_ν bits. A Gray mapping μ_ν transforms each matrix $\mathbf{D}_b$ into a complex matrix $\mathbf{S}_b \in \mathscr{X}_\nu^{n_t \times L}$. $\mathscr{X}_{\nu,j}^{(0)}$ and $\mathscr{X}_{\nu,j}^{(1)}$ denote the subsets of points in $\mathscr{X}_\nu$ whose labels have a 0 or a 1 at position j. With a slight abuse of notation, let $\{d_{b;t,l,j}\}_{j=1}^{q_\nu}$ denote the set of bits labeling the symbol $s_{b;t,l} \in \mathscr{X}_\nu$. Let also $\mu_{\nu,j}^{-1}(s)$ be the value of the j-th bit in the labeling of any point $s \in \mathscr{X}_\nu$. The STBICM is described in Fig. 2.1.

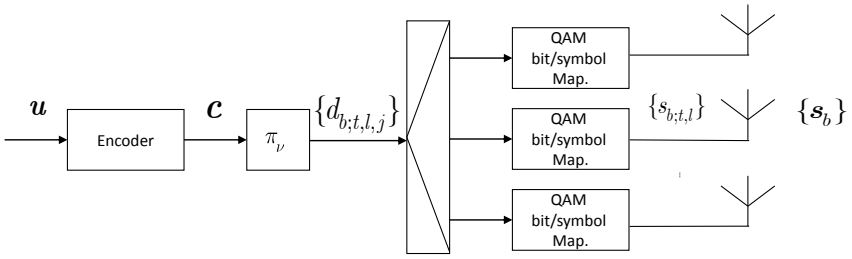

Figure 2.1: Transmitter model (STBICM)

For the b-th fading block, the $n_\tau+1$ finite-length impulse response (FIR) describes the small-scale multipath fading

$$\mathbf{H}_b(l) = \sum_{\tau=0}^{n_\tau} \mathbf{H}_{b;\tau}\delta(l-\tau). \tag{2.1}$$

Each tap gain $\mathbf{H}_{b;\tau}$ is an $n_r \times n_t$ random matrix whose entries are modeled as i.i.d. circularly-symmetric complex Gaussian random variables with zero-mean and variance $\sigma^2_{b;\tau}$ under the constraint $\sum_{\tau=0}^{n_\tau}\sigma^2_{b;\tau} = 1$. The discrete-time vector $\mathbf{y}_{b;l} \in \mathbb{C}^{n_r}$ received by the destination at b-th fading block and time $l = 1, \ldots, L$, is expressed as

$$\mathbf{y}_{b;l} = \sum_{\tau=0}^{n_\tau} \mathbf{H}_{b;\tau}\mathbf{s}_{b;l-\tau} + \mathbf{w}_{b;l} \tag{2.2}$$

with proper boundary conditions. In (2.2), the vectors $\mathbf{s}_{b;l} \in \mathscr{X}_\nu^{n_t}$ are i.i.d. random vectors (uniform distribution) with $\mathbb{E}[\mathbf{s}_{b;l}] = \mathbf{0}_{n_t}$ and $\mathbb{E}[\mathbf{s}_{b;l}\mathbf{s}^\dagger_{b;l}] = \mathbf{I}_{n_t}$, and the vectors $\mathbf{w}_{b;l} \in \mathbb{C}^{n_r}$ are i.i.d. random vectors, circularly-symmetric Gaussian, with zero-mean and covariance matrix $\sigma^2_w\mathbf{I}_{n_r}$.

Based on (2.2), the discrete-time baseband equivalent sliding-window model used for detecting $s_{b;t,l}$ in $\mathbf{S}_b$ is given by

$$\underline{\mathbf{y}}_{b;l} = \underline{\mathbf{H}}_b\underline{\mathbf{s}}_{b;l} + \underline{\mathbf{w}}_{b;l} \tag{2.3}$$

where

- $L_{SW} = L_1 + L_2 + 1$
- $\underline{\mathbf{y}}_{b;l} = [\mathbf{y}^\top_{b;l-L_1}, \ldots, \mathbf{y}^\top_{b;l+L_2}]^\top$

- $\underline{\mathbf{s}}_{b;l} = [\mathbf{s}_{b;l-L_1-n_\tau}^\top, \ldots, \mathbf{s}_{b;l+L_2}^\top]^\top$
- $\underline{\mathbf{w}}_{b;l} = [\mathbf{w}_{b;l-L_1}^\top, \ldots, \mathbf{w}_{b;l+L_2}^\top]^\top$
- $\underline{\mathbf{H}}_b$ is the suitable Sylvester matrix of dimension $L_{SW}n_r \times (L_{SW}+n_\tau)n_t$.

For a fixed l, index l' which serves to point a component in the vectors varies from $l - L_1 - n_\tau$ to $l + L_2$. The 2-tuple (t', l') of indices differs from the 2-tuple of indices (t, l) as soon as any of the indices is different. Let $\underline{\mathbf{e}}_t$ denote the unit vector of dimension $(L_{SW} + n_\tau)n_t$ with a 1 at position $(L_1 + n_\tau)n_t + t$.

In LEXTPR-based LMMSE-IC, the set of LEXTPRs $\{\Lambda_{E,DEC}^E(c_n)\}$ on coded bits are used as a priori information. Let $\{\Lambda_{A,LE}\}_{s_{b;t,l}}$ and $\{\Lambda_{A,LE}\}_{\underline{\mathbf{s}}_{b;l}}$ be the set of all LEXTPRs on coded bits involved in the labeling of $s_{b;t,l}$ and $\underline{\mathbf{s}}_{b;l}$, respectively. Let also $\{\Lambda_{A,LE}\}_{\underline{\mathbf{s}}_{b;l} \setminus s_{b;t,l}}$ be the set of all LEXTPRs on coded bits involved in the labeling of $\underline{\mathbf{s}}_{b;l}$ *except* the coded bits involved in the labeling of $s_{b;t,l}$. In LAPPR-based LMMSE-IC, the set of LAPPRs $\{\Lambda_{D,DEC}^D(c_n)\}$ on coded bits are used as "a priori" information. In the sequel, $\Lambda_{D,LE}$ is used to denote the interleaved LAPPRs (as opposed to the notation $\Lambda_{A,LE}$).

2.3 Iterative LMMSE-IC

2.3.1 LEXTPR-based LMMSE-IC

2.3.1.1 Interference regeneration and cancellation

Prior to LMMSE estimation of the symbol $s_{b;t,l}$, we compute the conditional MMSE estimate of the interference, defined as

$$\underline{\breve{\mathbf{y}}}_{b;l\setminus t}^E = \mathbb{E}[\underline{\mathbf{y}}_{b;l} | \{\Lambda_{A,LE}\}_{\underline{\mathbf{s}}_{b;l} \setminus s_{b;t,l}}] \tag{2.4}$$

This computation is tractable by making two symplifying assumptions.

A1-a The pdf $p_{\underline{\mathbf{s}}_{b;l},\underline{\mathbf{w}}_{b;l}|\{\Lambda_{A,LE}\}_{\underline{\mathbf{s}}_{b;l}\setminus s_{b;t,l}}}\left(\underline{\mathbf{s}}_{b;l},\underline{\mathbf{w}}_{b;l}\right)$ factorizes as

$$\begin{array}{l} p_{\underline{\mathbf{s}}_{b;l},\underline{\mathbf{w}}_{b;l}|\{\Lambda_{A,LE}\}_{\underline{\mathbf{s}}_{b;l}\setminus s_{b;t,l}}}\left(\underline{\mathbf{s}}_{b;l},\underline{\mathbf{w}}_{b;l}\right) = \\ P(s_{b;t,l})p_{\underline{\mathbf{w}}_{b;l}}(\underline{\mathbf{w}}_{b;l})\prod_{(t',l')\neq(t,l)}P(s_{b;t',l'}|\{\Lambda_{A,LE}\}_{s_{b;t',l'}}). \end{array} \tag{2.5}$$

A2-a The pmf $P(s_{b;t',l'}|\{\Lambda_{A,LE}\}_{s_{b;t',l'}})$ in (2.5) is given by

$$P(s_{b;t',l'}|\{\Lambda_{A,LE}\}_{s_{b;t',l'}}) \propto e^{\sum_j \mu_{\nu,j}^{-1}(s_{b;t',l'})\Lambda_{A,LE}(d_{b;t',l',j})}.$$

As a matter of fact, the assumptions (A1-a) and (A2-a) hold for an interleaver with sufficient large size. Under (A1-a), the MMSE estimate of the interference affecting the symbol $s_{b;t,l}$ is given by

$$\underline{\tilde{\mathbf{y}}}^E_{b;l\setminus t} = \underline{\mathbf{H}}_b(\mathbf{I}_{(L_{SW}+n_\tau)n_t} - \underline{\mathbf{e}}_t\underline{\mathbf{e}}_t^\dagger)\underline{\mathbf{m}}^E_{b;l} \tag{2.6}$$

where $\underline{\mathbf{m}}^E_{b;l}$ is the vector made of all estimates $m^E_{b;t',l'} = \mathbb{E}\left[s_{b;t',l'}|\{\Lambda_{A,LE}\}_{s_{b;t',l'}}\right]$ evaluated under (A2-a). After IC, the new observed vector is $\underline{\mathbf{y}}_{b;l} - \underline{\tilde{\mathbf{y}}}^E_{b;l\setminus t}$.

2.3.1.2 LMMSE estimation – unconditional case

The optimization problem to solve can be formulated as follows: Find $\breve{s}^E_{b;t,l} = \underline{\breve{\mathbf{f}}}^{E^\dagger}_{b;t}(\underline{\mathbf{y}}_{b;l} - \underline{\breve{\mathbf{y}}}^E_{b;l\setminus t})$ minimizing the *unconditional* Mean Square Error (MSE) $\mathbb{E}\left[|\breve{s}^E_{b;t,l} - s_{b;t,l}|^2\right]$ defined as

$$\mathbb{E}\left[\mathbb{E}\left[|\breve{s}^E_{b;t,l} - s_{b;t,l}|^2|\{\Lambda_{A,LE}\}_{\underline{\mathbf{s}}_{b;l}\setminus s_{b;t,l}}\right]\right]. \tag{2.7}$$

The outer expectation in (2.7) renders the (biased) LMMSE filter time-invariant given by $\underline{\breve{\mathbf{f}}}^E_{b;t} = \underline{\breve{\mathbf{\Xi}}}^{E^{-1}}_{b;t}\,\underline{\breve{\boldsymbol{\xi}}}^E_{b;t}$ where $\underline{\breve{\boldsymbol{\xi}}}^E_{b;t} = \mathbb{E}\left[\underline{\breve{\boldsymbol{\xi}}}^E_{b;t,l}\right]$ with

$$\underline{\breve{\boldsymbol{\xi}}}^E_{b;t,l} = \mathbb{E}\left[(\underline{\mathbf{y}}_{b;l} - \underline{\breve{\mathbf{y}}}^E_{b;l\setminus t})s^*_{b;t,l}|\{\Lambda_{A,LE}\}_{\underline{\mathbf{s}}_{b;l}\setminus s_{b;t,l}}\right]$$

and where $\breve{\underline{\Xi}}_{b;t}^{E} = \mathbb{E}\left[\breve{\underline{\Xi}}_{b;t,l}^{E}\right]$ with

$$\breve{\underline{\Xi}}_{b;t,l}^{E} = \mathbb{E}\left[(\underline{\mathbf{y}}_{b;l} - \breve{\underline{\mathbf{y}}}_{b;l\backslash t}^{E})(\underline{\mathbf{y}}_{b;l} - \breve{\underline{\mathbf{y}}}_{b;l\backslash t}^{E})^{\dagger} | \{\Lambda_{A,LE}\}_{\underline{\mathbf{s}}_{b;l}\backslash s_{b;t,l}}\right].$$

The computation of $\breve{\underline{\mathbf{f}}}_{b;t}^{E}$ is again intractable. However, under (A1-a), $\breve{\underline{\boldsymbol{\xi}}}_{b;t}^{E}$ and $\breve{\underline{\Xi}}_{b;t}^{E}$ become $\underline{\boldsymbol{\xi}}_{b;t}^{E} = \underline{\mathbf{h}}_{b;t} = \underline{\mathbf{H}}_{b}\underline{\mathbf{e}}_{t}$ and $\underline{\Xi}_{b;t}^{E} = \underline{\mathbf{H}}_{b}\underline{\mathbf{V}}_{b;\backslash t}^{E}\underline{\mathbf{H}}_{b}^{\dagger} + \sigma_{w}^{2}\mathbf{I}_{L_{SW}n_{r}}$ where $\underline{\mathbf{V}}_{b;\backslash t}^{E}$ is the *unconditional* symbol covariance matrix defined as

$$\underline{\mathbf{V}}_{b;\backslash t}^{E} = \mathbf{I}_{(L_{SW}+n_{\tau})} \otimes \mathrm{diag}\{v_{b;1}^{E}, \ldots, v_{b;t-1}^{E}, 1, v_{b;t+1}^{E}, \ldots, v_{b;n_{t}}^{E}\}$$

where $\forall t' \neq t$, $v_{b;t'}^{E} = \mathbb{E}\left[v_{b;t',l}^{E}\right]$ with $v_{b;t',l}^{E} = \mathbb{E}\left[|s_{b;t',l} - m_{b;t',l}^{E}|^{2} | \{\Lambda_{A,LE}\}_{s_{b;t',l}}\right]$ evaluated under (A2-a). Using the matrix inversion lemma, we obtain the filter

$$\underline{\mathbf{f}}_{b;t}^{E} = \frac{1}{1 + \eta_{b;t}^{E}(1 - v_{b;t}^{E})}\underline{\boldsymbol{\Sigma}}_{b}^{E^{-1}}\underline{\mathbf{h}}_{b;t} \tag{2.8}$$

where $\underline{\boldsymbol{\Sigma}}_{b}^{E} = \underline{\mathbf{H}}_{b}\underline{\mathbf{V}}_{b}^{E}\underline{\mathbf{H}}_{b}^{\dagger} + \sigma_{w}^{2}\mathbf{I}_{L_{SW}n_{r}}$ and $\eta_{b;t}^{E} = \underline{\mathbf{h}}_{b;t}^{\dagger}\underline{\boldsymbol{\Sigma}}_{b}^{E^{-1}}\underline{\mathbf{h}}_{b;t}$ with

$$\underline{\mathbf{V}}_{b}^{E} = \underline{\mathbf{V}}_{b;\backslash t}^{E} - (1 - v_{b;t}^{E})\underline{\mathbf{e}}_{t}\underline{\mathbf{e}}_{t}^{\dagger} \tag{2.9}$$

where $v_{b;t}^{E} = \mathbb{E}\left[v_{b;t,l}^{E}\right]$ with $v_{b;t,l}^{E} = \mathbb{E}\left[|s_{b;t,l} - m_{b;t,l}^{E}|^{2} | \{\Lambda_{A,LE}\}_{s_{b;t,l}}\right]$ evaluated under (A2-a). The corresponding estimate $\hat{s}_{b;t,l}^{E}$ of $s_{b;t,l}$ can be expressed as

$$\hat{s}_{b;t,l}^{E} = \underline{\mathbf{f}}_{b;t}^{E^{\dagger}}(\underline{\mathbf{y}}_{b;l} - \underline{\tilde{\mathbf{y}}}_{b;l\backslash t}^{E}) = g_{b;t}^{E}s_{b;t,l} + \zeta_{b;t,l}^{E} \tag{2.10}$$

where $g_{b;t}^{E} = \underline{\mathbf{f}}_{b;t}^{E^{\dagger}}\underline{\mathbf{h}}_{b;t}$ and $\zeta_{b;t,l}^{E}$ is the residual interference plus noise term. Clearly, $\zeta_{b;t,l}^{E}$ in (2.10) is zero-mean and uncorrelated with the useful signal $s_{b;t,l}$ under (A1-a), i.e., $\mathbb{E}[s_{b;t,l}\zeta_{b;t,l}^{E^{*}}] = 0$. Under (A1-a) and (A2-a) the variance of $\zeta_{b;t,l}^{E}$ is $\varsigma_{b;t}^{E} = g_{b;t}^{E}(1 - g_{b;t}^{E})$ which allows us to define the *unconditional* SINR as

$$\gamma_{b;t}^{E} = \frac{g_{b;t}^{E}}{1 - g_{b;t}^{E}} = \frac{\eta_{b;t}^{E}}{1 - \eta_{b;t}^{E}v_{b;t}^{E}}. \tag{2.11}$$

A3-a Due to the particular structure of the MCS, the so-called *equal vari-*

ance assumption holds, which states that

$$\underline{\mathbf{V}}_b^E = v^E \mathbf{I}_{(L_{SW}+n_\tau)n_t}, \forall b. \tag{2.12}$$

so that

$$\gamma_{b;t}^E = \frac{\eta_{b;t}^E}{1 - \eta_{b;t}^E v^E}. \tag{2.13}$$

The assumption (A3-a) holds for an interleaver of sufficient large size L, but forcing it induces no performance degradation.

A4-a Assuming sufficiently large values of L, v^E can be replaced by its empirical mean $\bar{v}^E$ given by

$$\bar{v}^E = \frac{1}{n_b n_t L} \sum_{b=1}^{n_b} \sum_{t=1}^{n_t} \sum_{l=1}^{L} v_{b;t,l}^E. \tag{2.14}$$

As a matter of fact, the assumption (A4-a) is part of the baseline assumptions of EXIT charts (ergodic regime) [37].

2.3.1.3 Demapping and decoding

The estimate $\hat{s}_{b;t,l}^E$ is used as a *decision statistic* to compute the LEXTPR on the q_ν bits involved in the labeling of $s_{b;t,l}$.

A5-a In (2.10), the conditional pdf $p_{\hat{s}_{b;t,l}^E|s_{b;t,l}}(\hat{s}_{b;t,l}^E)$ is circularly-symmetric complex Gaussian distributed.
Under (A1-a),(A2-a) and (A5-a) the conditional pdf $p_{\hat{s}_{b;t,l}^E|s_{b;t,l}}(\hat{s}_{b;t,l}^E)$ is $\mathcal{N}_{\mathbb{C}}(g_{b;t}^E s_{b;t,l}, \varsigma_{b;t}^E)$. As a result, under (A1-a),(A2-a) and (A5-a), for the *special case* of Gray labeling, the LEXTPR $\Lambda_{E,DEM}^E(d_{b;t,l,j})$ on labeling bit $d_{b;t,l,j}$ is expressed as

$$\Lambda_{E,DEM}^E(d_{b;t,l,j}) = \frac{\sum_{s \in \mathscr{X}_{\nu,j}^{(1)}} e^{-|\hat{s}_{b;t,l}^E - g_{b;t}^E s|^2/\varsigma_{b;t}^E}}{\sum_{s \in \mathscr{X}_{\nu,j}^{(0)}} e^{-|\hat{s}_{b;t,l}^E - g_{b;t}^E s|^2/\varsigma_{b;t}^E}} \tag{2.15}$$

The set $\mathbf{\Lambda}_{E,DEM}^E$ of all LEXTPR on labeling bits becomes after deinterleav-

ing the set $\mathbf{\Lambda}^E_{I,DEC}$ of all log intrinsic probability ratios on coded bits used as input for the decoder.

A6-a The pdf $p_{\mathbf{\Lambda}^E_{I,DEC}|\mathbf{c}}(\mathbf{\Lambda}^E_{I,DEC})$ factorizes as

$$p_{\mathbf{\Lambda}^E_{I,DEC}|\mathbf{c}}(\mathbf{\Lambda}^E_{I,DEC}) = \prod_{n=1}^{n_c} p_{\Lambda^E_{I,DEC}(c_n)|c_n}(\Lambda^E_{I,DEC}(c_n))$$

where $\Lambda^E_{I,DEC}(c_n)$ is the log intrinsic probability ratio on coded bit c_n. The assumption (A6-a) allows to simplify the decoding task. It is rightfully confirmed for an interleaver of finite, but large enough, depth. Under (A6-a), the decoder computes the LAPPR $\Lambda^E_{D,DEC}(c_n)$ on coded bit c_n as

$$\Lambda^E_{D,DEC}(c_n) = \frac{\sum_{\mathbf{c}\in\mathscr{C}:c_n=1} \prod_{n=1}^{n_c} p_{\Lambda^E_{I,DEC}(c_n)|c_n}(\Lambda^E_{I,DEC}(c_n))}{\sum_{\mathbf{c}\in\mathscr{C}:c_n=0} \prod_{n=1}^{n_c} p_{\Lambda^E_{I,DEC}(c_n)|c_n}(\Lambda^E_{I,DEC}(c_n))}. \tag{2.16}$$

Finally the LEXTPR on coded bit c_n can be computed as

$$\Lambda^E_{E,DEC}(c_n) = \Lambda^E_{D,DEC}(c_n) - \Lambda^E_{I,DEC}(c_n) \tag{2.17}$$

This completes one iteration. The different steps are for LEXTPR based iterative LMMSE-IC are described in Fig. 2.2.

2.3.2 LAPPR-based LMMSE-IC

For the sake of simplicity, some notation used in this section are similar to those of the previous section, but refer to different mathematical objects.

2.3.2.1 Interference regeneration and cancellation

Prior to LMMSE estimation of the symbol $s_{b;t,l}$, we compute the *conditional* MMSE estimate of the interference, defined as $\breve{\underline{\mathbf{y}}}^D_{b;l\setminus t} = \mathbb{E}\left[\underline{\mathbf{y}}_{b;l}|\{\Lambda_{D,LE}\}_{\underline{\mathbf{s}}_{b;l}\setminus s_{b;t,l}}\right]$. This computation is tractable by making two symplifying assumptions.

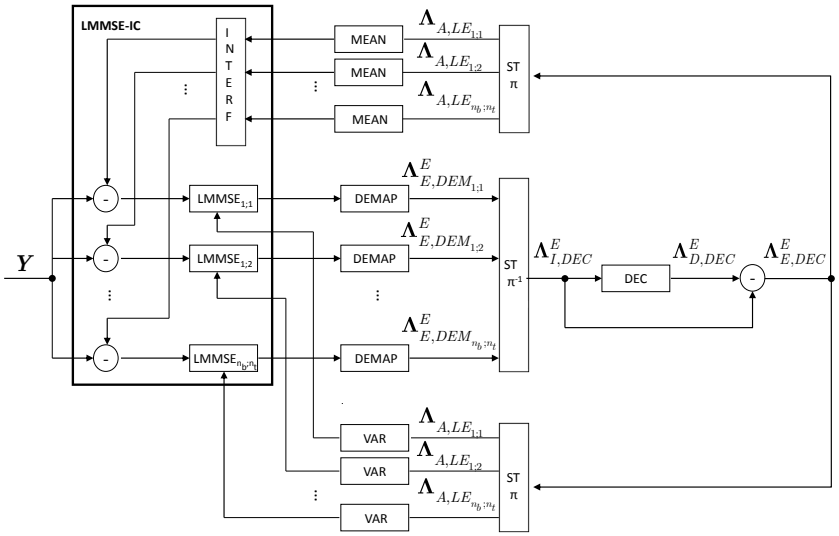

Figure 2.2: LEXTPR-based iterative LMMSE-IC (adapted to STBICM with convolutional code and Gray labeling)

A1-b The pdf $p_{\underline{\mathbf{s}}_{b;l},\underline{\mathbf{w}}_{b;l}|\{\Lambda_{D,LE}\}_{\underline{\mathbf{s}}_{b;l}\setminus s_{b;t,l}}}\left(\underline{\mathbf{s}}_{b;l},\underline{\mathbf{w}}_{b;l}\right)$ factorizes as

$$\begin{aligned} &p_{\underline{\mathbf{s}}_{b;l},\underline{\mathbf{w}}_{b;l}|\{\Lambda_{D,LE}\}_{\underline{\mathbf{s}}_{b;l}\setminus s_{b;t,l}}}\left(\underline{\mathbf{s}}_{b;l},\underline{\mathbf{w}}_{b;l}\right) = \\ &P(s_{b;t,l})p_{\underline{\mathbf{w}}_{b;l}}(\underline{\mathbf{w}}_{b;l})\prod_{(t',l')\neq(t,l)}P(s_{b;t',l'}|\{\Lambda_{D,LE}\}_{s_{b;t',l'}}). \end{aligned} \tag{2.18}$$

A2-b The pmf $P(s_{b;t',l'}|\{\Lambda_{D,LE}\}_{s_{b;t',l'}})$ in (2.18) is given by

$$P(s_{b;t',l'}|\{\Lambda_{D,LE}\}_{s_{b;t',l'}}) \propto e^{\sum_j \mu_{\nu,j}^{-1}(s_{b;t',l'})\Lambda_{D,LE}(d_{b;t',l',j})}.$$

As a matter of fact, the assumptions (A1-b) and (A2-b) never hold even for an ideal interleaver of infinite depth. But we can still force them in all subsequent derivations. Under (A1-b), the MMSE estimate of the interference affecting the symbol $s_{b;t,l}$ is given by

$$\underline{\tilde{\mathbf{y}}}^D_{b;l\setminus t} = \underline{\mathbf{H}}_b(\mathbf{I}_{(L_{SW}+n_\tau)n_t} - \underline{\mathbf{e}}_t\underline{\mathbf{e}}_t^\dagger)\underline{\mathbf{m}}^D_{b;l} \tag{2.19}$$

where $\underline{\mathbf{m}}^D_{b;l}$ is the vector made of all estimates $m^D_{b;t',l'} = \mathbb{E}\left[s_{b;t',l'}|\{\Lambda_{D,LE}\}_{s_{b;t',l'}}\right]$

evaluated under (A2-b). After IC, the new observed vector is $\underline{\mathbf{y}}_{b;l} - \underline{\tilde{\mathbf{y}}}^{D}_{b;l\backslash t}$.

2.3.2.2 LMMSE estimation – unconditional case

The optimization problem to solve can be formulated as follows: Find $\breve{s}^{D}_{b;t,l} = \underline{\breve{\mathbf{f}}}^{D^{\dagger}}_{b;t}(\underline{\mathbf{y}}_{b;l} - \underline{\breve{\mathbf{y}}}^{D}_{b;l\backslash t})$ minimizing the *unconditional* MSE $\mathbb{E}\left[|\breve{s}^{D}_{b;t,l} - s_{b;t,l}|^2\right]$ defined as

$$\mathbb{E}\left[\mathbb{D}\left[|\breve{s}^{D}_{b;t,l} - s_{b;t,l}|^2 | \{\Lambda_{D,LE}\}_{\underline{\mathbf{s}}_{b;l}\backslash s_{b;t,l}}\right]\right]. \tag{2.20}$$

The outer expectation in (2.20) renders the (biased) LMMSE filter time-invariant given by $\underline{\breve{\mathbf{f}}}^{D}_{b;t} = \underline{\breve{\mathbf{\Xi}}}^{D^{-1}}_{b;t}\underline{\breve{\boldsymbol{\xi}}}^{D}_{b;t}$ where $\underline{\breve{\boldsymbol{\xi}}}^{D}_{b;t} = \mathbb{E}\left[\underline{\breve{\boldsymbol{\xi}}}^{D}_{b;t,l}\right]$ with

$$\underline{\breve{\boldsymbol{\xi}}}^{D}_{b;t,l} = \mathbb{E}\left[(\underline{\mathbf{y}}_{b;l} - \underline{\breve{\mathbf{y}}}^{D}_{b;l\backslash t})s^{*}_{b;t,l} | \{\Lambda_{D,LE}\}_{\underline{\mathbf{s}}_{b;l}\backslash s_{b;t,l}}\right]$$

and where $\underline{\breve{\mathbf{\Xi}}}^{D}_{b;t} = \mathbb{E}\left[\underline{\breve{\mathbf{\Xi}}}^{D}_{b;t,l}\right]$ with

$$\underline{\breve{\mathbf{\Xi}}}^{D}_{b;t,l} = \mathbb{E}\left[(\underline{\mathbf{y}}_{b;l} - \underline{\breve{\mathbf{y}}}^{D}_{b;l\backslash t})(\underline{\mathbf{y}}_{b;l} - \underline{\breve{\mathbf{y}}}^{D}_{b;l\backslash t})^{\dagger} | \{\Lambda_{D,LE}\}_{\underline{\mathbf{s}}_{b;l}\backslash s_{b;t,l}}\right].$$

The computation of $\underline{\breve{\mathbf{f}}}^{D}_{b;t}$ is again intractable. However, under (A1-b), $\underline{\breve{\boldsymbol{\xi}}}^{D}_{b;t}$ and $\underline{\breve{\mathbf{\Xi}}}^{D}_{b;t}$ become $\underline{\boldsymbol{\xi}}^{D}_{b;t} = \underline{\mathbf{h}}_{b;t} = \underline{\mathbf{H}}_{b}\underline{\mathbf{e}}_{t}$ and $\underline{\mathbf{\Xi}}^{D}_{b;t} = \underline{\mathbf{H}}_{b}\underline{\mathbf{V}}^{D}_{b;\backslash t}\underline{\mathbf{H}}^{\dagger}_{b} + \sigma^2_w\mathbf{I}_{L_{SW}n_r}$ where $\underline{\mathbf{V}}^{D}_{b;\backslash t}$ is the *unconditional* symbol covariance matrix defined as

$$\underline{\mathbf{V}}^{D}_{b;\backslash t} = \mathbf{I}_{(L_{SW}+n_\tau)} \otimes \mathrm{diag}\{v^{D}_{b;1}, \ldots, v^{D}_{b;t-1}, 1, v^{D}_{b;t+1}, \ldots, v^{D}_{b;n_t}\}$$

where $\forall t' \neq t$, $v^{D}_{b;t'} = \mathbb{E}\left[v^{D}_{b;t',l}\right]$ with $v^{D}_{b;t',l} = \mathbb{E}\left[|s_{b;t',l} - m^{D}_{b;t',l}|^2 | \{\Lambda_{D,LE}\}_{s_{b;t',l}}\right]$ evaluated under (A2-b). Using the matrix inversion lemma, we obtain the filter

$$\underline{\mathbf{f}}^{D}_{b;t} = \frac{1}{1 + \eta^{D}_{b;t}(1 - v^{D}_{b;t})}\underline{\mathbf{\Sigma}}^{D^{-1}}_{b}\underline{\mathbf{h}}_{b;t} \tag{2.21}$$

where $\underline{\mathbf{\Sigma}}^{D}_{b} = \underline{\mathbf{H}}_{b}\underline{\mathbf{V}}^{D}_{b}\underline{\mathbf{H}}^{\dagger}_{b} + \sigma^2_w\mathbf{I}_{L_{SW}n_r}$ and $\eta^{D}_{b;t} = \underline{\mathbf{h}}^{\dagger}_{b;t}\underline{\mathbf{\Sigma}}^{D^{-1}}_{b}\underline{\mathbf{h}}_{b;t}$ with

$$\underline{\mathbf{V}}^{D}_{b} = \underline{\mathbf{V}}^{D}_{b;\backslash t} - (1 - v^{D}_{b;t})\underline{\mathbf{e}}_{t}\underline{\mathbf{e}}^{\dagger}_{t} \tag{2.22}$$

where $v_{b;t}^D = \mathbb{E}\left[v_{b;t,l}^D\right]$ with $v_{b;t,l}^D = \mathbb{E}\left[|s_{b;t,l} - m_{b;t,l}^D|^2 | \{\Lambda_{D,LE}\}_{s_{b;t,l}}\right]$ evaluated under (A2-b). The corresponding estimate $\hat{s}_{b;t,l}^D$ of $s_{b;t,l}$ can be expressed as

$$\hat{s}_{b;t,l}^D = \underline{\mathbf{f}}_{b;t}^{D\dagger}(\underline{\mathbf{y}}_{b;l} - \underline{\tilde{\mathbf{y}}}_{b;l\backslash t}^D) = g_{b;t}^D s_{b;t,l} + \zeta_{b;t,l}^D \tag{2.23}$$

where $g_{b;t}^D = \underline{\mathbf{f}}_{b;t}^{D\dagger}\underline{\mathbf{h}}_{b;t}$ and $\zeta_{b;t,l}^D$ is the residual interference plus noise term. Clearly, $\zeta_{b;t,l}^D$ in (2.23) is zero-mean and uncorrelated with the useful signal $s_{b;t,l}$ under (A1-b), i.e., $\mathbb{E}[s_{b;t,l}\zeta_{b;t,l}^{D^*}] = 0$. Under (A1-b) and (A2-b) the variance of $\zeta_{b;t,l}^D$ is $\varsigma_{b;t}^D = g_{b;t}^D(1 - g_{b;t}^D)$ which allows us to define the *unconditional* SINR as

$$\gamma_{b;t}^D = \frac{g_{b;t}^D}{1 - g_{b;t}^D} = \frac{\eta_{b;t}^D}{1 - \eta_{b;t}^D v_{b;t}^D}. \tag{2.24}$$

A3-b Due to the particular structure of the MCS, the so-called *equal variance assumption* holds, which states that

$$\underline{\mathbf{V}}_b^D = v^D \mathbf{I}_{(L_{SW}+n_\tau)n_t}, \forall b. \tag{2.25}$$

so that

$$\gamma_{b;t}^D = \frac{\eta_{b;t}^D}{1 - \eta_{b;t}^D v^D}. \tag{2.26}$$

The assumption (A3-b) never holds even for an ideal interleaver of infinite depth, but forcing it induces no performance degradation.

A4-b Assuming sufficiently large values of L, v^D can be replaced by its empirical mean $\bar{v}^D$ given by

$$\bar{v}^D = \frac{1}{n_b n_t L} \sum_{b=1}^{n_b} \sum_{t=1}^{n_t} \sum_{l=1}^{L} v_{b;t,l}^D. \tag{2.27}$$

As a matter of fact, the assumption (A4-b) is part of the baseline assumptions of EXIT charts (ergodic regime) [37].

2.3.2.3 Demapping and decoding

The estimate $\hat{s}^D_{b;t,l}$ is used as a *decision statistic* to compute the LEXTPR on the q_ν bits involved in the labeling of $s_{b;t,l}$.

A5-b In (2.23), the conditional pdf $p_{\hat{s}^D_{b;t,l}|s_{b;t,l}}(\hat{s}^D_{b;t,l})$ is circularly-symmetric complex Gaussian distributed.
Under (A1-b),(A2-b) and (A5-b) the conditional pdf $p_{\hat{s}^D_{b;t,l}|s_{b;t,l}}(\hat{s}^D_{b;t,l})$ is $\mathcal{N}_{\mathbb{C}}(g^D_{b;t}s_{b;t,l}, \varsigma^D_{b;t})$. As a result, under (A1-b),(A2-b) and (A5-b), for the *special case* of Gray labeling, the LEXTPR $\Lambda^D_{E,DEM}(d_{b;t,l,j})$ on labeling bit $d_{b;t,l,j}$ is expressed as

$$\Lambda^D_{E,DEM}(d_{b;t,l,j}) = \frac{\sum_{s\in\mathscr{X}^{(1)}_{\nu,j}} e^{-|\hat{s}^D_{b;t,l}-g^D_{b;t}s|^2/\varsigma^D_{b;t}}}{\sum_{s\in\mathscr{X}^{(0)}_{\nu,j}} e^{-|\hat{s}^D_{b;t,l}-g^D_{b;t}s|^2/\varsigma^D_{b;t}}} \tag{2.28}$$

The set $\mathbf{\Lambda}^D_{E,DEM}$ of all LEXTPR on labeling bits becomes after deinterleaving the set $\mathbf{\Lambda}^D_{I,DEC}$ of all log intrinsic probability ratios on coded bits used as input for the decoder.

A6-b The pdf $p_{\mathbf{\Lambda}^D_{I,DEC}|\mathbf{c}}(\mathbf{\Lambda}^D_{I,DEC})$ factorizes as

$$p_{\mathbf{\Lambda}^D_{I,DEC}|\mathbf{c}}(\mathbf{\Lambda}^D_{I,DEC}) = \prod_{n=1}^{n_c} p_{\Lambda^D_{I,DEC}(c_n)|c_n}(\Lambda^D_{I,DEC}(c_n))$$

where $\Lambda^D_{I,DEC}(c_n)$ is the log intrinsic probability ratio on coded bit c_n. The assumption (A6-b) allows to simplify the decoding task. It is rightfully confirmed for an interleaver of finite, but large enough, depth. Under (A6-b), the decoder computes the LAPPR $\Lambda^D_{D,DEC}(c_n)$ on coded bit c_n as

$$\Lambda^D_{D,DEC}(c_n) = \frac{\sum_{\mathbf{c}\in\mathscr{C}:c_n=1}\prod_{n=1}^{n_c} p_{\Lambda^D_{I,DEC}(c_n)|c_n}(\Lambda^D_{I,DEC}(c_n))}{\sum_{\mathbf{c}\in\mathscr{C}:c_n=0}\prod_{n=1}^{n_c} p_{\Lambda^D_{I,DEC}(c_n)|c_n}(\Lambda^D_{I,DEC}(c_n))}. \tag{2.29}$$

Finally the LEXTPR on coded bit c_n can be computed as

$$\Lambda^D_{E,DEC}(c_n) = \Lambda^D_{D,DEC}(c_n) - \Lambda^D_{I,DEC}(c_n) \tag{2.30}$$

This completes one iteration. The different steps are for LAPPR based iterative LMMSE-IC are described in Fig. 2.3

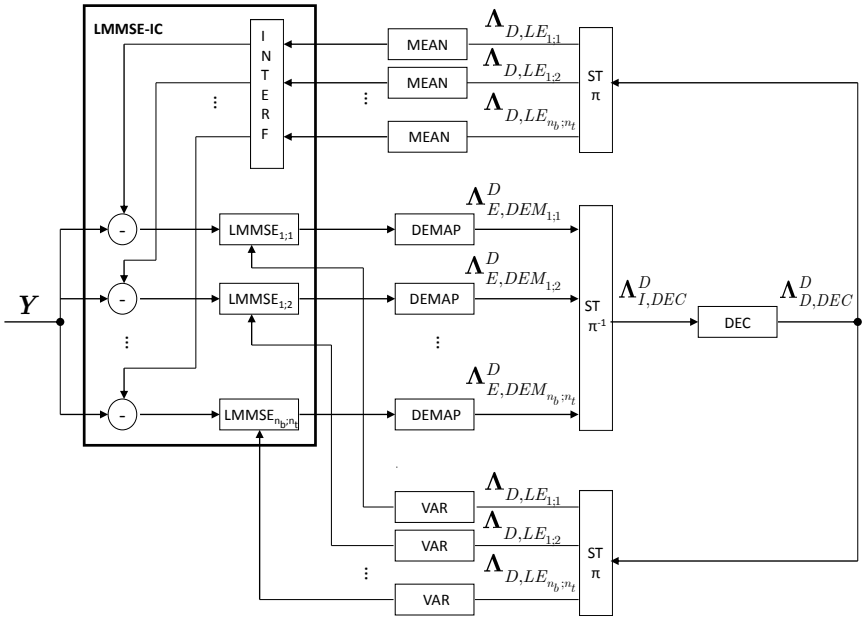

Figure 2.3: LAPPR-based iterative LMMSE-IC (adapted to STBICM with convolutional code and Gray labeling)

2.4 PHY-layer abstractions

2.4.1 LEXTPR-based iterative LMMSE-IC

An LMMSE-IC based turbo receiver turns out to be a complicated non-linear dynamical system. Our objective is to analyze its evolution as iterations progress. The proposed performance prediction method is semi-analytical and relies on ten Brink's stochastic approach of EXIT charts [37] particularly useful in understanding and measuring the dynamics of turbo processing.

2.4.1.1 Transfer characteristics of LMMSE-IC

The LMMSE-IC part of the receiver ends up with $n_b \times n_t$ independent *parallel channels* under (A6-a). Each of them is modeled as a discrete-input AWGN

channel under (A5-a) whose SNR, given by

$$\gamma_{b;t}^{E} = \frac{\eta_{b;t}^{E}}{1 - \eta_{b;t}^{E}\bar{v}^{E}} \tag{2.31}$$

under (A1-a)-(A4-a), turns out to be a function ϕ_t of b, t, $\mathbf{H}_b$, σ_w^2 and the input variance $\bar{v}^E$. For each such channel, we can compute the average mutual information (AMI) $I_{LE_{b;t}}^{E}$ between the discrete input $s_{b;t,l} \in \mathscr{X}_\nu$ and the output $\tilde{s}_{b;t,l}^{E} = s_{b;t,l} + \epsilon_{b;t,l}^{E}$ with $\epsilon_{b;t,l}^{E} \sim \mathcal{NC}(0, 1/\gamma_{b;t}^{E})$. The value of $I_{LE_{b;t}}^{E}$ depends on the single parameter $\gamma_{b;t}^{E}$. Let $\bar{I}_{LE}^{E}$ be the arithmetic mean of the values $\{I_{LE_{b;t}}^{E}\}$, i.e.,

$$\bar{I}_{LE}^{E} = \frac{1}{n_b n_t} \sum_{b=1}^{n_b} \sum_{t=1}^{n_t} I_{LE_{b;t}}^{E}. \tag{2.32}$$

The AMI $I_{LE_{b;t}}^{E} = \psi(\gamma_{b;t}^{E})$ is a monotone increasing, thus invertible, function of the SNR, and depends on the MCS. It is simulated off-line and stored in a LUT.

2.4.1.2 Transfer characteristics of joint demapping and decoding

The functional module is MCS-dependent and comprises the following steps: demapping, deinterleaving, *BCJR decoder*, reinterleaving, and computation of the mean and variance of transmitted symbols based on LEXTPR on coded bits (as described before). The generated observed symbols are the output of a virtual AWGN channel with discrete input in $\mathscr{X}_\nu$ and SNR γ. For an arbitrary labeling rule, bivariate transfer function is required to stochastically characterize the joint demapper and decoder. With Gray labeling however, log a priori probability ratios on labeling bits do not intervene in the computation of the LEXTPR on the labeling bits (see (2.15)) and, hence, need not be taken into account in the stochastic modeling of the demapper. Therefore, simpler univariate transfer function is sufficient to stochastically characterize the joint demapper and BCJR decoder. These functions are the measured BLER $P_e = F_{JDD_\nu}(\gamma)$, the variance $\bar{v}^E = G_{JDD_\nu}^{E}(\gamma)$. They are computed off-line and stored in separate LUTs. It is necessary to emphasize that the LUTs are generated with channel use number fixed to n_s, thus are independent with the number of fading block. The algorithm used to generate the different LUTs is summarized in Algorithm 1. Note that the

Algorithm 1

Inputs ν, n_t, n_s
for $\gamma = \gamma_{min}$ to γ_{max} **do**
  for $bk = 1$ to n_{bk} **do**
    Channel interleaver random generation: π
    Codeword generation: $\mathbf{u} \rightarrow \mathbf{c} \rightarrow \mathbf{D} \rightarrow \mathbf{S}$
    Virtual AWGN Channel: Generate $\tilde{\mathbf{S}}$ s.t. $\tilde{s}_{1;t,l} \sim \mathcal{N}_{\mathbb{C}}(s_{1;t,l}, 1/\gamma)$
    Demapping: Compute $\{\Lambda^E_{E,DEM}(d_{1;t,l,j})\}$ as (2.15) with $\hat{s}^E_{1;t,l} = \tilde{s}_{1;t,l}$ and $g^E_{1;t} = 1$
    Deinterleaving: $\mathbf{\Lambda}^E_{E,DEM} \rightarrow \mathbf{\Lambda}^E_{I,DEC}$
    BCJR decoding: Compute $\{\Lambda^E_{D,DEC}(c_n)\}$ and $\Lambda^E_{E,DEC}(c_n)\}$ based on $\{\Lambda^E_{I,DEC}(c_n)\}$
    Update counter block errors
    Interleaving: $\mathbf{\Lambda}^E_{E,DEC} \rightarrow \mathbf{\Lambda}_{A,LE}$
    Compute $\{v^E_{1;t,l}\}$ using $\{\{\Lambda_{A,LE}\}_{s_{1;t,l}}\} \rightarrow \{\bar{v}^E_{bk}\}$ as (2.14)
  end for
  Compute P_e and $\bar{v}^E = \frac{1}{n_{bk}} \sum_{bk=1}^{n_{bk}} \bar{v}^E_{bk}$
end for
Outputs $P_e = F_{JDD_\nu}(\gamma)$, $\bar{v}^E = G^E_{JDD_\nu}(\gamma)$

LUTs for BER can be generated in the same way.

2.4.1.3 Evolution analysis

It remains to relate the output $\bar{I}^E_{LE}$ of the first transfer function (LMMSE-IC) and the input SNR of the second transfer function (joint demapping and decoding) at any iteration. This is done by assuming that $\bar{I}^E_{LE}$ which measures the information content of knowledge on coded modulated symbols $\{s_{b;t,l}\}$, averaged over all parallel AWGN channels, is equal to the information content of knowledge on coded modulated symbols transmitted over a *single* virtual discrete-input (with values in $\mathscr{X}_\nu$) AWGN channel with effective SNR $\bar{\gamma}^E_{LE}$ given by

$$\bar{\gamma}^E_{LE} = \psi^{-1}(\bar{I}^E_{LE}) = \psi^{-1}\left(\frac{1}{n_b n_t}\sum_{b=1}^{n_b}\sum_{t=1}^{n_t} I^E_{LE_{b;t}}\right). \tag{2.33}$$

This technique inherited from EXIT charts is widely used in practice and often referred to as MIESM [61]. In our framework, it relies on all the defined assumptions (A1-a)-(A6-a) or, equivalently, on (A5-a) and (A6-a)

for the first iteration. The variance $\bar{v} = G^E_{JDD_\nu}(\bar{\gamma}^E_{LE})$ is used in (2.12) under (A4-a) for next iteration. Hence, the evolution of LEXTPR-based iterative LMMSE-IC can be tracked through the single scalar parameter $\bar{v}^E$. The different steps of PHY-layer abstraction for LEXTPR-based iterative LMMSE-IC are described in Fig. 2.4

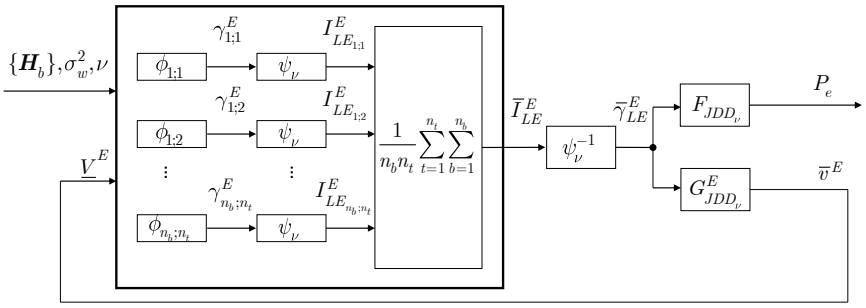

Figure 2.4: PHY-layer abstraction for LEXTPR-based iterative LMMSE-IC

2.4.2 LAPPR-based iterative LMMSE-IC

To make things even more complicated, some assumptions are not valid when it is based on LAPPR on coded bits. Our objective is to analyze its evolution as iterations progress.

2.4.2.1 Transfer characteristics of LMMSE-IC

The LMMSE-IC part of the receiver ends up with $n_b \times n_t$ independent *parallel channels* under (A6-b). Each of them is modeled as a discrete-input AWGN channel under (A5-b) whose SNR, given by

$$\gamma^D_{b;t} = \frac{\eta^D_{b;t}}{1 - \eta^D_{b;t}\bar{v}^D} \tag{2.34}$$

under (A1-b)-(A4-b), turns out to be a function ϕ_t of b, t, $\mathbf{H}_b$, σ_w^2 and the input variance $\bar{v}^D$. For each such channel, we can compute the average mutual information (AMI) $I^D_{LE_{b;t}}$ between the discrete input $s_{b;t,l} \in \mathscr{X}_\nu$ and the output $\tilde{s}^D_{b;t,l} = s_{b;t,l} + \epsilon^D_{b;t,l}$ with $\epsilon^D_{b;t,l} \sim \mathcal{N}_{\mathbb{C}}(0, 1/\gamma^D_{b;t})$. The value of $I^D_{LE_{b;t}}$ depends on the single parameter $\gamma^D_{b;t}$. Let $\bar{I}^D_{LE}$ be the arithmetic mean of the

values $\{I^D_{LE_{b;t}}\}$, i.e.,

$$\bar{I}^D_{LE} = \frac{1}{n_b n_t} \sum_{b=1}^{n_b} \sum_{t=1}^{n_t} I^D_{LE_{b;t}}. \tag{2.35}$$

The AMI $I^D_{LE_{b;t}} = \psi(\gamma^D_{b;t})$ is a monotone increasing, thus invertible, function of the SNR, and depends on the MCS. It is simulated off-line and stored in a LUT.

2.4.2.2 Transfer characteristics of joint demapping and decoding

The functional module is MCS-dependent and comprises the following steps: demapping, deinterleaving, *BCJR decoder*, reinterleaving, and computation of the mean and variance of transmitted symbols based on LAPPR on coded bits(as described before). The generated observed symbols are the output of a virtual AWGN channel with discrete input in $\mathscr{X}_\nu$ and SNR γ. For an arbitrary labeling rule, trivariate transfer function is required to stochastically characterize the joint demapper and decoder. With Gray labeling however, log a priori probability ratios on labeling bits do not intervene in the computation of the LEXTPR on the labeling bits (see (2.28)) and, hence, need not be taken into account in the stochastic modeling of the demapper. Therefore, simpler univariate transfer function is sufficient to stochastically characterize the joint demapper and BCJR decoder. These functions are the measured BLER $P_e = F_{JDD_\nu}(\gamma)$, the variance $\bar{v}^D = G^D_{JDD_\nu}(\gamma)$. They are computed off-line and stored in separate LUTs. It is necessary to emphasize that the LUTs are generated with channel use number fixed to n_s, thus are independent with the number of fading block. The algorithm used to generate the different LUTs is summarized in Algorithm 2. Note that the LUTs for BER can be generated in the same way.

2.4.2.3 Evolution analysis

It remains to relate the output $\bar{I}^D_{LE}$ of the first transfer function (LMMSE-IC) and the input SNR of the second transfer function (joint demapping and decoding) at any iteration. This is done by assuming that $\bar{I}^D_{LE}$ which measures the information content of knowledge on coded modulated symbols $\{s_{b;t,l}\}$, averaged over all parallel AWGN channels, is equal to the information content of knowledge on coded modulated symbols transmitted over a *single* virtual discrete-input (with values in $\mathscr{X}_\nu$) AWGN channel with effec-

Algorithm 2

Inputs ν, n_t, n_s
for $\gamma = \gamma_{min}$ to γ_{max} **do**
  for $bk = 1$ to n_{bk} **do**
    Channel interleaver random generation: π
    Codeword generation: $\mathbf{u} \rightarrow \mathbf{c} \rightarrow \mathbf{D} \rightarrow \mathbf{S}$
    Virtual AWGN Channel: Generate $\tilde{\mathbf{S}}$ s.t. $\tilde{s}_{1;t,l} \sim \mathcal{N}_{\mathbb{C}}(s_{1;t,l}, 1/\gamma)$
    Demapping: Compute $\{\Lambda^D_{E,DEM}(d_{1;t,l,j})\}$ as (2.15) with $\hat{s}^D_{1;t,l} = \tilde{s}_{1;t,l}$ and $g^D_{1;t} = 1$
    Deinterleaving: $\mathbf{\Lambda}^D_{E,DEM} \rightarrow \mathbf{\Lambda}^D_{I,DEC}$
    BCJR decoding: Compute $\{\Lambda^D_{D,DEC}(c_n)\}$ and $\Lambda^D_{E,DEC}(c_n)\}$ based on $\{\Lambda^D_{I,DEC}(c_n)\}$
    Update counter block errors
    Interleaving: $\mathbf{\Lambda}^D_{E,DEC} \rightarrow \mathbf{\Lambda}_{D,LE}$
    Compute $\{v^D_{1;t,l}\}$ using $\{\{\Lambda_{D,LE}\}_{s_{1;t,l}}\} \rightarrow \{\bar{v}^D_{bk}\}$ as (2.27)
  end for
  Compute P_e and $\bar{v}^D = \frac{1}{n_{bk}} \sum_{bk=1}^{n_{bk}} \bar{v}^D_{bk}$
end for
Outputs $P_e = F_{JDD_\nu}(\gamma)$, $\bar{v}^D = G^D_{JDD_\nu}(\gamma)$

tive SNR $\bar{\gamma}^D_{LE}$ given by

$$\bar{\gamma}^D_{LE} = \psi^{-1}(\bar{I}^D_{LE}) = \psi^{-1}\left(\frac{1}{n_b n_t}\sum_{b=1}^{n_b}\sum_{t=1}^{n_t} I^D_{LE_{b;t}}\right). \tag{2.36}$$

This technique inherited from EXIT charts is widely used in practice and often referred to as MIESM [61]. In our framework, it relies on all the defined assumptions (A1-b)-(A6-b) or, equivalently, on (A5-b) and (A6-b) for the first iteration. The variance $\bar{v} = G^D_{JDD_\nu}(\bar{\gamma}^D_{LE})$ is used in (2.25) under (A4-b) for next iteration. Hence, the evolution of LAPPR-based iterative LMMSE-IC can be tracked through the single scalar parameter $\bar{v}^D$.

2.4.2.4 Calibration

A major drawback of the performance prediction method for LAPPR-based iterative LMMSE-IC is that the assumptions (A1-b), (A2-b) and (A3-b) do not hold for LAPPR-based iterative LMMSE-IC. As a consequence, not only the filters $\{\mathbf{f}^D_{b;t}\}$ but also the SINRs $\{\gamma^D_{b;t}\}$ given by (2.24) are approximated. The true SINRs, if we could have to access to them, would be smaller. This

fact explains why the prediction performance method expounded in [66] yields too optimistic results compared to the true simulated performance. To solve this problem, we proposed a simple, yet effective, calibration procedure whose principle is to adjust $\bar{v}$ with a real-valued factor $\beta_\nu \geq 1$. More specifically, $\bar{v}$ is replaced by $C_\nu(\bar{v}) = \min(\beta_\nu \bar{v}, 1)$, which has the effect to artificially reduce the SINRs that are used in the performance prediction method. We searched the optimal β_ν minimizing the error between the simulated BLER (or BER) and the calibrated predicted BLER (or BER)over a large number of channel outcomes at each iteration $i > 1$ for the BLER range of interest $[0.9, 0.01]$. The algorithm for generating the link level simulations for calibration is summarized in Algorithm 3.

Algorithm 3 Algorithm for generating the link level simulations for calibration

Inputs ν, n_t, n_r, n_b, n_τ n_s, $\Delta\gamma$, n_{it}
for $ch = 1$ to n_{ch} **do**
  Generate $\{\mathbf{H}_{b;\tau}\}_{ch}$
  for $\gamma = \gamma_{min}$ to γ_{max} **do**
    for $bk = 1$ to n_{bk} **do**
      Channel interleaver random generation
      Codeword random generation
      AWGN random generation
      Transmission
      for $i = 1$ to n_{it} **do**
        Perform LAPPR-based iterative LMMSE-IC receiver
        update counter block errors
      end for
    end for
    Compute $BLER_{simu}(\{\mathbf{H}_{b;\tau}\}_{ch}, \gamma, i, \nu), \forall i = 1, \ldots, n_{it}$
    $\gamma = \gamma + \Delta\gamma$
  end for
  Store $\{\mathbf{H}_{b;\tau}\}_{ch}$, γ and $\{BLER_{simu}(\{\mathbf{H}_{b;\tau}\}_{ch}, \gamma, i, \nu)\}, \forall i = 1, \ldots, n_{it}$
end for

Then the instantaneous predicted BLER are obtained with calibration, i.e., $\{BLER_{pred}(\{\mathbf{H}_{b;\tau}\}_{ch}, \gamma, i, \nu, \beta)\}, \forall i = 1, \ldots, n_{it}, \forall \beta = \beta_{min}, \ldots, \beta_{max}$. A recapitulative diagram of the performance prediction method with calibration is depicted in Fig. 2.5.

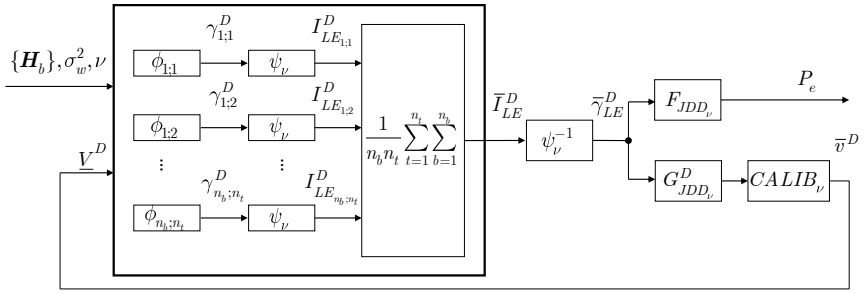

Figure 2.5: PHY-layer abstraction for LAPPR-based iterative LMMSE-IC

The optimal β denoted β_ν is found as follows:

$$\beta_\nu = \arg\min_{\beta} \sum_{ch=1}^{n_{ch}} \sum_{\gamma=\gamma_{min}}^{\gamma_{max}} \sum_{i=2}^{n_{it}} D\left(BLER_{simu}(\{\mathbf{H}_{b;\tau}\}_{ch},\gamma,i,\nu), BLER_{pred}(\{\mathbf{H}_{b;\tau}\}_{ch},\gamma,i,\nu,\beta)\right) \tag{2.37}$$

where n_{it} is the number of iterations and $D(x,y) = |\log_{10}(x) - \log_{10}(y)|^2$.

Exhaustive simulations revealed that β_ν depends on the MCS but does not vary significantly w.r.t. the number of transmit and receive antennas as well as the channel characteristics.

2.5 Numerical results

We consider an STBICM with the following parameters: rate-1/2 non-recursive non-systematic binary convolutional encoder as mother code with generator polynomials $(171, 133)_8$ and Quadrature Amplitude Modulation (QAM) constellation with Gray labeling. The number of channel use $n_s = 288$.

2.5.1 LMMSE receiver

The mismatches between predicted and simulated performance will accumulate following iterations. Accurate prediction at one iteration help obtain accurate prediction for the next iteration. In [61], the MIESM is shown to be the most robust and accurate amongst all candidate techniques. The simulation results in [61] are done for LMMSE receiver with interleaver re-drawn randomly and alters from block to block. However, pure random interleaver is not optimal for a STBICM transmission. The optimal interleaver should

be designed to be diagonal-random: $n_b n_t q_\nu$ nearby coded bits are separated into $n_b n_t q_\nu$ parallel virtual streams, which exploits all the diversity. The first questions comes: whether MIESM technique is sensible to the change of interleaver structure?

For this purpose, we evaluate the instantaneous predicted and simulated BER/BLER over 200 channel outcomes. For each channel outcome, the Monte Carlo simulation is stopped after 100 block errors (a block error is declared when at least one bit is wrongly detected). Pure-random or diagonal-random interleaver is drawn and alters from block to block. A 4×4 1-block fading channel is chosen for the test. Fig. 2.6 and Fig. 2.7 present the MIESM technique based instantaneous predicted vs. simulated instantaneous BER/BLER under diagonal structured or pure random interleaver with Quadrature Phase-Shift Keying (QPSK) - 1/2 and 16QAM-1/2, respectively. These two figures show that MIESM technique based predicted performance match very well the simulated performance when pure random interleaver is used (as in [61]), however are, in most of the cases, pessimist when diagonal random interleaver is used. The solution to help MIESM predict well the performance with diagonal-random interleaver seems not exist thus pure random interleaver will be kept in what follows.

2.5.2 Iterative LMMSE-IC

In what follows, the number of iterations is $n_{it} = 4$. We consider an STBICM with the following parameters: rate-1/2 non-recursive non-systematic binary convolutional encoder with generator polynomials $(171, 133)_8$ and 16QAM constellation with Gray labeling. Coded bits are mapped to 1152 symbols. For each iteration, the instantaneous simulated BER vs. the predicted effective SINR over almost 200 channel outcomes is plotted in Fig. 2.8, Fig. 2.10 and Fig. 2.12 (scatter diagrams) for a 4×4 MIMO 1-block fading Rayleigh fading channel. The pure random interleaver is altered randomly from block to block. For the sake of readability, we only plot the channel outcomes that reach the BLER region of interest (between 1 and 10^{-2}) at the fourth iteration. For each channel outcome, convergence of Monte-Carlo simulations is obtained for 100 block errors. To validate the proposed performance prediction methods, we also check that the averaged simulated BLER (over the joint statistics of the MIMO block fading channel and the AWGN) on a 4×4 MIMO 2-block Rayleigh fading channel, is well captured. We

stop the Monte-Carlo simulations after 800 block errors. The Genie-Aided (GA) lower bound corresponds to the BLER performance when all sources of interference are perfectly canceled.

Firstly, we investigate the LEXTPR-based iterative LMMSE-IC algorithm. Fig. 2.8 presents the instantaneous simulated BER vs. the predicted effective SNR *without calibration*. The plotted plain-line curve represents the predicted BER (which is actually the BER LUT). Obvisouly, the performance prediction method does not need calibration. Indeed, the approximations (A1-a) - (A6-a) are perfectly relevant and valid in this case (i.e., even for finite $N = 4608$). Fig. 2.9 confirms that the predicted averaged BLER performance without calibration matches exactly the simulated BLER performance.

We then move to LAPPR-based itarative LMMSE-IC, whose averaged BLER performance is 1.5 dB better than its LEXTPR-based counterpart at BLER 10^{-2} (see. Fig 2.13). Fig. 2.10 depicts the instantaneous simulated BER vs. the predicted effective SNR *without calibration*. Clearly, the predicted BER is too optimistic for most of the channel outcomes. Calibration is needed. For this specific MCS, we found $\beta_{opt} = 2.6$ as shown in Fig. 2.11. Fig. 2.12 plots the instantaneous simulated BER vs. the predicted effective SNR *with calibration*. The accuracy of the performance prediction is greatly improved. This is also visible on Fig. 2.13.

2.6 Conclusion

In this part, An effort is made to analyze the SINR evolution of LEXTPR-based LMMSE-IC and LAPPR-based LMMSE-IC algorithms under perfect CSIR in convolutionally coded MIMO systems. It has been numerically demonstrated that the performance prediction method described in [71] [66] is more accurate for LEXTPR-based LMMSE-IC than for LAPPR-based LMMSE-IC. Indeed, while the underlying assumptions made in the first case hold in practice, some of them prove to be approximate (and optimistic) in the second case. To solve this issue, an improved performance prediction method has been proposed for LAPPR-based LMMSE-IC, based on a simple calibration procedure whose efficiency has been validated by Monte-Carlo simulations.

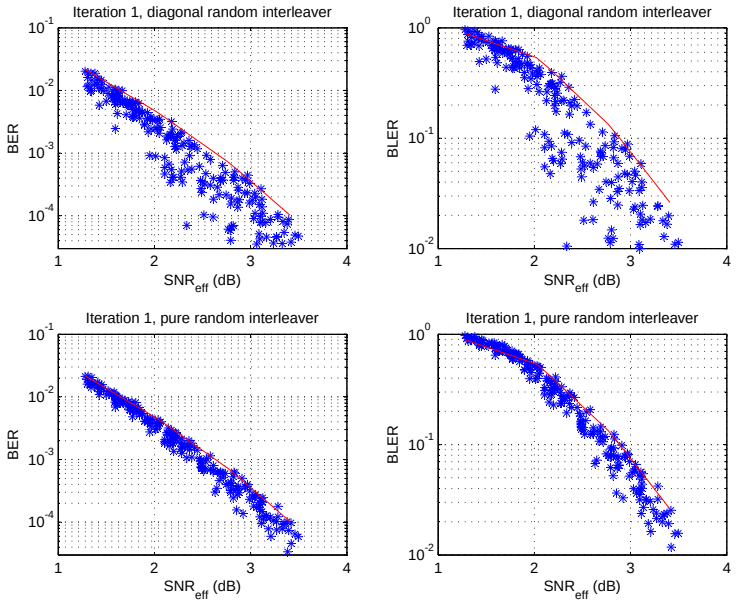

Figure 2.6: Diagonal random interleaver vs. pure random interleaver: instantaneous MIESM based predicted vs. simulated BER/BLER over 4×4 1-block fading channel with QPSK-1/2

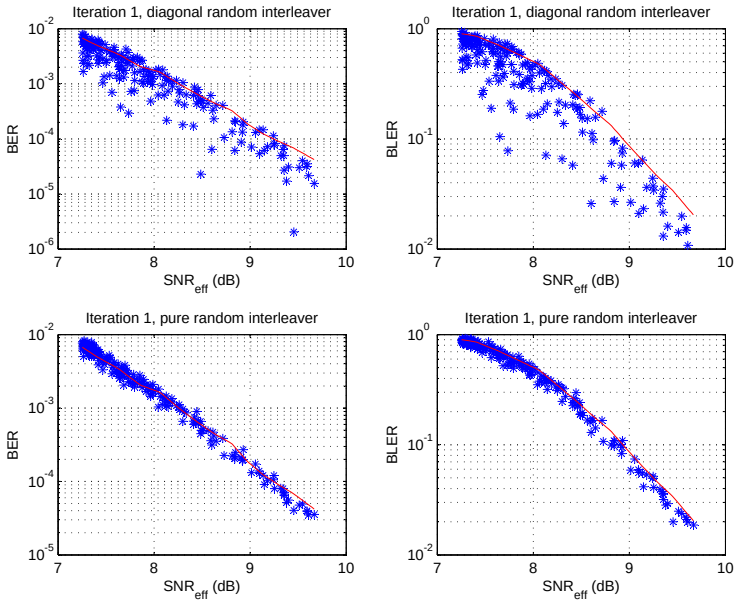

Figure 2.7: Diagonal random interleaver vs. pure random interleaver: instantaneous MIESM based predicted vs. simulated BER/BLER over 4×4 1-block fading channel with 16QAM-1/2

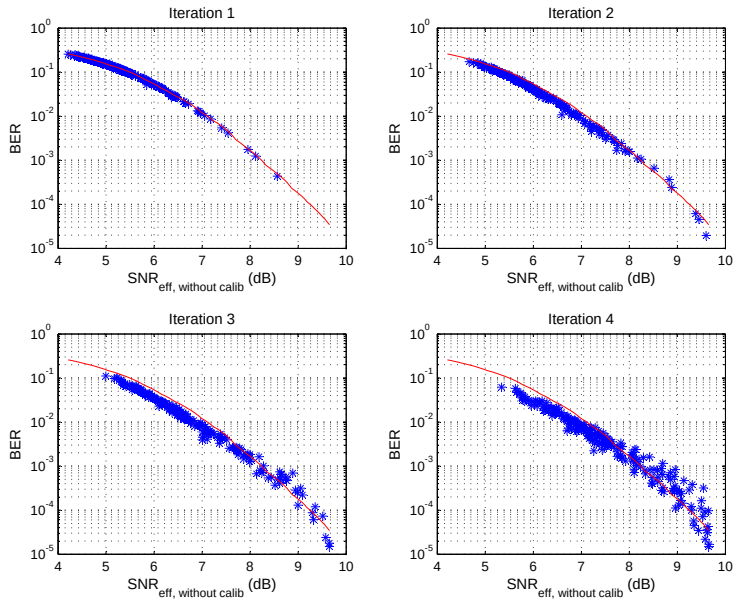

Figure 2.8: Instantaneous simulated BER vs. predicted effective SNR without calibration for LEXTPR-based iterative LMMSE-IC algorithm and 16QAM-1/2

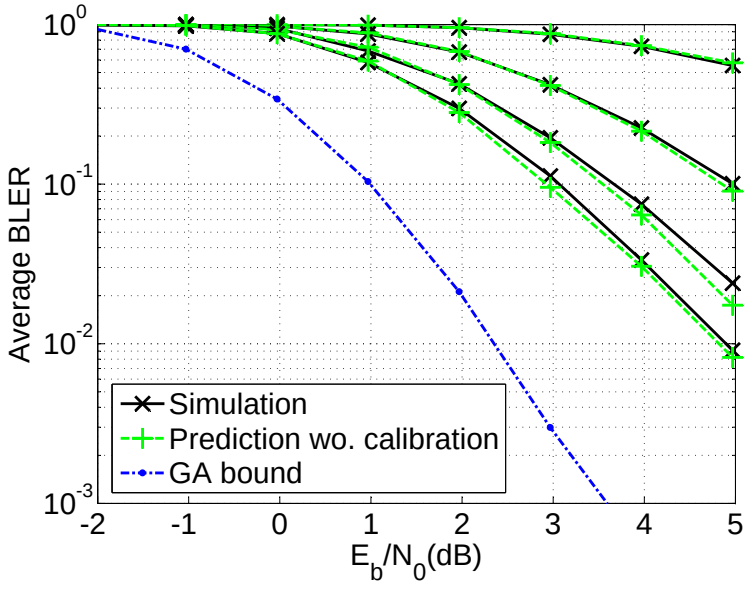

Figure 2.9: Averaged simulated BLER vs. predicted BLER without calibration for LEXTPR-based iterative LMMSE-IC algorithm and 16QAM-1/2

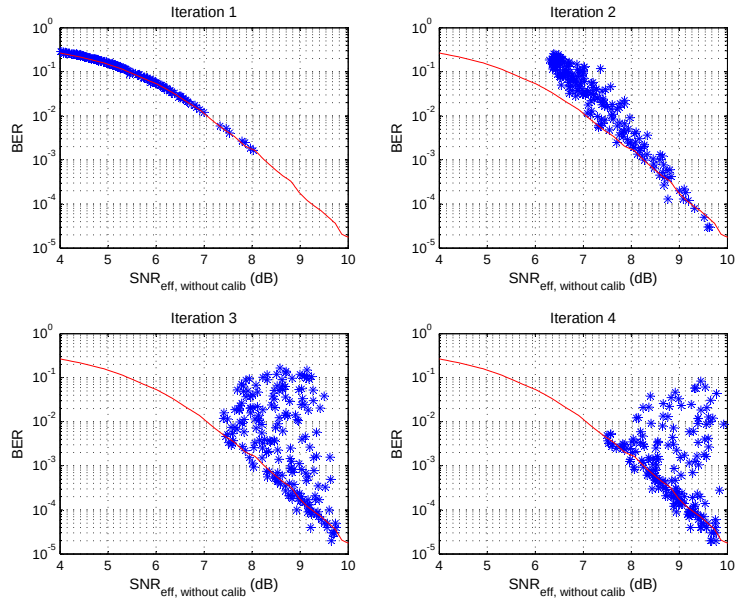

Figure 2.10: Instantaneous simulated BER vs. predicted effective SNR without calibration for LAPPR-based iterative LMMSE-IC algorithm and 16QAM-1/2

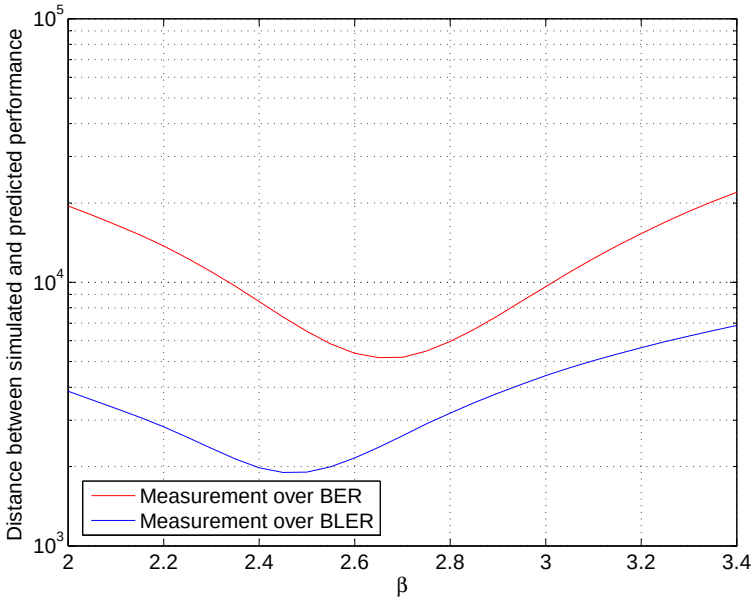

Figure 2.11: Calibration results for LAPPR-based iterative LMMSE-IC with 16QAM-1/2

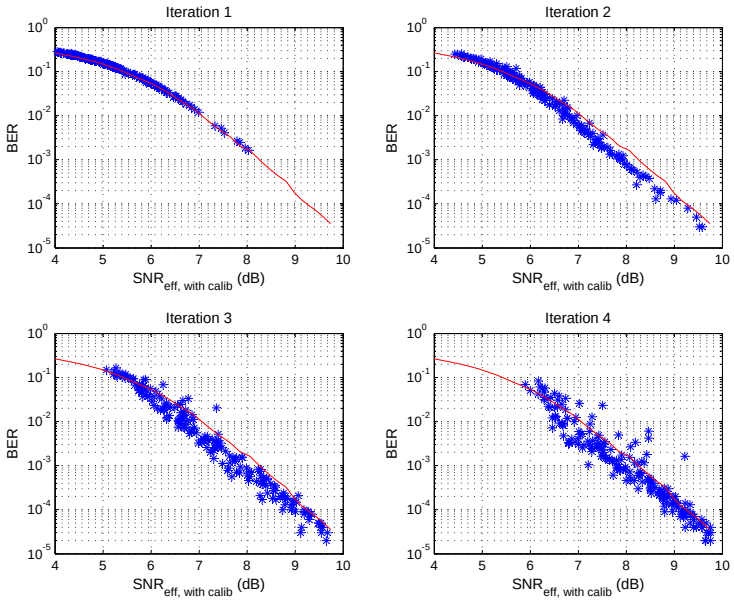

Figure 2.12: Instantaneous simulated BER vs. predicted effective SNR with calibration for LAPPR-based iterative LMMSE-IC algorithm and 16QAM-1/2

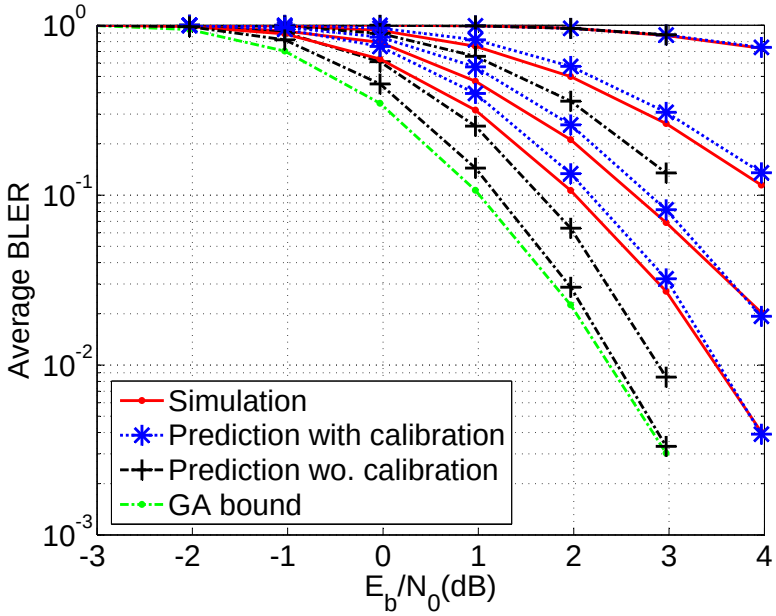

Figure 2.13: Averaged simulated BLER vs. predicted BLER with/without calibration for LAPPR-based iterative LMMSE-IC algorithm and 16QAM-1/2

Chapter 3

Extension to imperfect CSIR and iterative semi-blind channel estimation

3.1 Introduction

The PHY-ayer abstractions for iterative LMMSE-IC receivers under imperfect CSIR in convolutionally coded MIMO systems is the topic of this chapter. It is important to stress that adopting LEXTPR on coded bits at the output of soft-in soft-out decoder as a priori information for channel re-estimation, soft symbol-to-bit demapping and soft interference generation/cancellation is part of the receiver design basic assumption. Therefore, the notations are largely simplified. The generalization to LAPPR on coded bits based case is quite straightforward.

Under imperfect CSIR, if the number of pilot symbols is sufficient to ensure close to perfect CSI, then it is sufficient to adopt the so-called mismatched assumption which simply postulates that the initial pilot assisted channel estimate is noiseless [75–77]. In that case, performance prediction methods derived under the assumption of perfect CSIR can be used in practice. However, if the number of pilot symbols are reduced conditional on some advanced semi-blind channel estimation scheme at the receiver side, the mismatched assumption is not valid anymore. Indeed, it is quite known

This chapter is partially presented in the paper accepted to IEEE VTC Spring'2012 and the journal paper in preparation for IEEE Signal Processing

that performing detection and channel estimation within a same iteration (using channel decoding a priori) allows reducing drastically the number of reference signals for a given performance, see, e.g., [78–81]. Therefore, new prediction methods should be derived conditional on the available a priori information only, i.e., the so-called matched assumption [75–77], which are the initial pilot assisted channel estimate and the long-term CDI, (such as the channel and noise probability distribution functions).

The scope of application of this method in terms of semi-blind channel estimation algorithms as well as communication context is extremely large [66]. As a result, for the sake of simplicity and as a first step, only SU-MIMO frequency selective transmission is considered, modelled by a MIMO block fading AWGN channel, and semi-blind LMMSE channel re-estimation. The space time modulation and coding scheme is chosen as a STBICM without loss of generality. Indeed, the proposed double loop receiver architecture could be applied to any Space Time Codes provided that they rely on a bit or symbol interleaver and can be easily extended to a MU-MIMO context [66].

3.2 System model

The transmission occurs on a MIMO block Rayleigh fading AWGN channel with n_t transmit antenna, n_r receive antenna and n_b independent fading blocks. The total number n_s of channel use for transmission is constant. Thus each fading block is experienced by $L_{ds} = n_s/n_b$ channel uses. A STBICM, indexed by ν, is used at the transmitter, specified by a linear binary convolutional $\mathscr{C}_\nu$ of rate r_ν, a complex constellation $\mathscr{X}_\nu \subset \mathbb{C}$ of cardinality 2^{q_ν} with energy equal to σ_{ds}^2 and a memoryless labeling rule μ_ν. We define the rate of the MCS as $\rho_\nu = r_\nu q_\nu$ (bits/complex dimension). The encoding process for MCS is detailed. The vector of binary data (or information bits) $\mathbf{u}$ enters an encoder φ_ν whose output is the codeword $\mathbf{c} \in \mathscr{C}_\nu$ of length $n_{\nu,c} = n_s n_t q_\nu$. The codeword bits are interleaved by a random space time interleaver π_ν and reshaped as a integer matrice $\{\mathbf{D}_b\}_{b=1}^{n_b}$ with $\mathbf{D}_b \in \mathbb{Z}_{2^{q_\nu}}^{n_t \times L_{ds}}$. Each integer entry can be decomposed into a sequence of q_ν bits. A Gray mapping μ_ν transforms each matrix $\mathbf{D}_b$ into a complex matrix $\mathbf{S}_b \in \mathscr{X}_\nu^{n_t \times L_{ds}}$. $\mathscr{X}_{\nu,j}^{(0)}$ and $\mathscr{X}_{\nu,j}^{(1)}$ denote the subsets of points in $\mathscr{X}_\nu$ whose labels have a 0 or a 1 at position j. With a slight abuse of notation, let $\{d_{b;t,l,j}\}_{j=1}^{q_\nu}$ denote the set of bits labeling the symbol $s_{b;t,l} \in \mathscr{X}_\nu$. Let also $\mu_{\nu,j}^{-1}(s)$ be the value of the j-th bit in the labeling of any point $s \in \mathscr{X}_\nu$.

Pilot symbols are transmitted before the data symbols whose matrix form is given as $\mathbf{A}_b^{ps} \in \{-\sigma_{ps}, \sigma_{ps}\}^{n_t \times L_{ps}}$. The matrix $\mathbf{A}_b^{ps}$ is the same for each fading block and is built from a Constant Amplitude Zero AutoCorrelation (CAZAC) sequence $\mathbf{u} \in \{0,1\}^{1 \times L_{ps}}$ [95] such that $\mathbf{a}^t = \sigma_{ps}\left(2\mathbf{T}_{(t-1)}(\mathbf{u}) - \mathbf{1}\right)$ where $\mathbf{T}_i(.)$ denotes the right circular shift operator of i elements. The transmitter described above is depicted in Fig. 3.1.

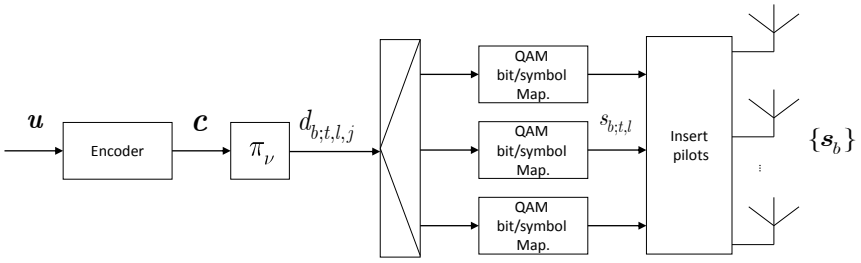

Figure 3.1: Transmitter model (STBICM with pilot symbol insertion)

It yields the receive base-band model :

$$\begin{cases} \mathbf{Y}_b^{ps} = \mathbf{H}_b \mathbf{A}_b^{ps} + \mathbf{W}_b^{ps} \\ \mathbf{Y}_b = \mathbf{H}_b \mathbf{S}_b + \mathbf{W}_b \end{cases} \tag{3.1}$$

where

- $\mathbf{Y}_b^{ps} = \left[\mathbf{y}_{b;1}^{ps}, \cdots, \mathbf{y}_{b;L_{ps}}^{ps}\right] \in \mathbb{C}^{n_r \times L_{ps}}$ with $\mathbf{y}_{b;l}^{ps} = [y_{b;1,l}^{ps}, \cdots, y_{b;n_r,l}^{ps}]^\top$ are the receive samples related to the pilot symbols
- $\mathbf{Y}_b = [\mathbf{y}_{b;1}, \cdots, \mathbf{y}_{b;L_{ds}}] \in \mathbb{C}^{n_r \times L_{ds}}$ with $\mathbf{y}_{b;l} = [y_{b;1,l}, \cdots, y_{b;n_r,l}]^\top$ are the receive samples related to the data symbols
- $\mathbf{W}_b^{ps} = \left[\mathbf{w}_{b;1}^{ps}, \cdots, \mathbf{w}_{b;L_{ps}}^{ps}\right] \in \mathbb{C}^{n_r \times L_{ps}}$ with $\mathbf{w}_{b;l}^{ps} = [w_{b;1,l}^{ps}, \cdots, w_{b;n_r,l}^{ps}]^\top$ are the noise samples associated to the pilot symbols
- $\mathbf{W}_b = [\mathbf{w}_{b;1}, \cdots, \mathbf{w}_{b;L_{ds}}] \in \mathbb{C}^{n_r \times L_{ds}}$ with $\mathbf{w}_{b;l} = [w_{b;1,l}, \cdots, w_{b;n_r,l}]^\top$ are the noise samples associated to the data symbols
- The b-th fading block channel gain $\mathbf{H}_b \in \mathbb{C}^{n_r \times n_t}$

A1 The entries of $\{\mathbf{w}_{b;l}\}$ are i.i.d and follows the pdf $\mathcal{N}_{\mathbb{C}}(0, N_0)$. The entries of the channel gain $\{\mathbf{H}_b\}$ are i.i.d and follows the pdf $\mathcal{N}_{\mathbb{C}}(0, \sigma_h^2)$.

3.3 Double loop receiver architecture

The proposed double loop receiver architecture is described in Fig. 3.2.

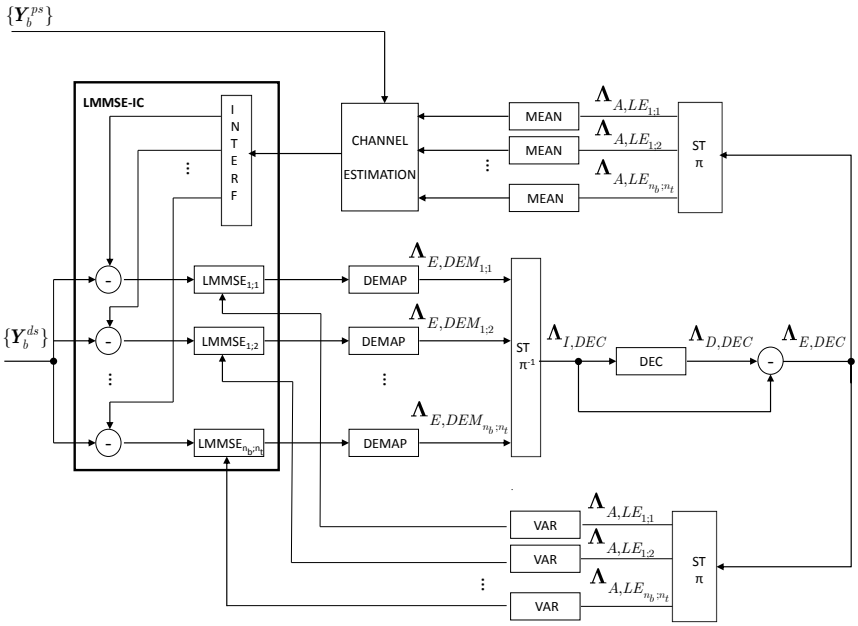

Figure 3.2: LEXTPR-based double loop receiver architecture with semi-blind channel estimation (adapted to STBICM with convolutional code and Gray labeling)

Let $\widehat{\mathbf{H}}_b^{(0)}$ denote the initial pilot assisted channel estimate. The fundamentals of iterative LMMSE-IC detection and LMMSE channel (re)estimation are recalled considering iteration $i \geq 1$ in progress. Based on the statistics soft symbol mean $\{m_{b;t',l}^{(i-1)} = \mathbb{E}\left[s_{b;t',l}|P(s_{b;t',l})\right]\}$, symbol variance $\{v_{b;t',l}^{(i-1)} = \mathbb{E}\left[|s_{b;t',l} - m_{b;t',l}|^2|P(s_{b;t',l})\right]\}$ (see Section 3.4) and previous channel estimation $\{\widehat{\mathbf{H}}_b^{(i-1)}\}$ (see Section 3.5) computed at iteration $i-1$, an estimate $\tilde{\mathbf{y}}_{b;l\backslash t}^{(i)}$ of the interference on symbol $s_{b;t,l}$ is first derived (see Section 3.6) and is subtracted to $\mathbf{y}_{b;l}$. A unconditional linear estimate $\hat{s}_{b;t,l}^{(i)} = \mathbf{f}_{b;t}^{\dagger}(\mathbf{y}_{b;l} - \tilde{\mathbf{y}}_{b;l\backslash t}^{(i)})$ is obtained based on the linear filtering by $\mathbf{f}_{b;t}$. Finally, soft symbol-to-bit demapping, deinterleaving, soft-in soft-out decoding, interleaving and soft bit-to-symbol mapping are performed to obtain new estimated $\{m_{b;t',l}^{(i)}\}$, $\{v_{b;t',l}^{(i)}\}$ which are used subsequently to derive $\widehat{\mathbf{H}}_b^{(i)}$ for next iteration. This concludes one iteration.

3.4 Soft bit-to-symbol mapping

Let $\mathbf{\Lambda}_{E,DEC}^{(i-1)} = \{\Lambda_{E,DEC}^{(i-1)}(c_{\nu,n})\}$ denote the set of all LEXTPR on coded bits generated by soft-in soft-out decoder which is interleaved to become the set $\mathbf{\Lambda}_{A,LE}^{(i-1)} = \{\Lambda_{A,LE}^{(i-1)}(d_{b;t',l,j})\}$ of all log "a priori" probability ratios on labeling bits used for soft symbol mean and variance computation. For $i = 1$, since no a priori information exist at the first iteration of detection, we set $\{\Lambda_{E,DEC}^{(0)}(c_n) = 0\}$, $\{\Lambda_{A,LE}^{(0)}(d_{b;t',l,j}) = 0\}$ and $\{m_{b;t',l}^{(0)} = 0\}$, $\{v_{b;t',l}^{(0)} = \sigma_{ds}^2\}$. Let $\{\Lambda_{A,LE}^{(i-1)}\}_{s_{b;t,l}}$ and $\{\Lambda_{A,LE}^{(i-1)}\}_{\mathbf{s}_{b;l}}$ be the set of all LEXTPR on coded bits involved in the labeling of $s_{b;t,l}$ and $\mathbf{s}_{b;l}$, respectively. Let also $\{\Lambda_{A,LE}^{(i-1)}\}_{\mathbf{s}_{b;l}\setminus s_{b;t,l}}$ be the set of all LEXTPR on coded bits involved in the labeling of $\mathbf{s}_{b;l}$ *except* the coded bits involved in the labeling of $s_{b;t,l}$.

Prior to LMMSE estimation of the symbol $s_{b;t,l}$, we compute the *conditional* MMSE estimate of the interference, defined as $\check{\mathbf{y}}_{b;l\setminus t} = \mathbb{E}\left[\mathbf{y}_{b;l}|\{\Lambda_{D,LE}\}_{\mathbf{s}_{b;l}\setminus s_{b;t,l}}\right]$. These computations are tractable based on two basic assumptions.

A2 The pdf $p_{\mathbf{s}_{b;l},\mathbf{w}_{b;l}|\{\Lambda_{A,LE}^{(i-1)}\}_{\mathbf{s}_{b;l}\setminus s_{b;t,l}}}(\mathbf{s}_{b;l},\mathbf{w}_{b;l})$ factorizes as

$$p_{\mathbf{s}_{b;l},\mathbf{w}_{b;l}|\{\Lambda_{A,LE}^{(i-1)}\}_{\mathbf{s}_{b;l}\setminus s_{b;t,l}}}(\mathbf{s}_{b;l},\mathbf{w}_{b;l}) = p_{\mathbf{w}_{b;l}}(\mathbf{w}_{b;l})P(s_{b;t,l})\prod_{t'\neq t}P(s_{b;t',l}|\{\Lambda_{A,LE}^{(i-1)}\}_{s_{b;t',l}}) \tag{3.2}$$

A3 The pmf $P(s_{b;t',l}|\{\Lambda_{A,LE}^{(i-1)}\}_{s_{b;t',l}})$ in (4.2) is given by

$$P(s_{b;t',l}|\{\Lambda_{A,LE}^{(i-1)}\}_{s_{b;t',l}}) \propto e^{\sum_j \mu_{\nu,j}^{-1}(s_{b;t',l})\Lambda_{A,LE}^{(i-1)}(d_{b;t',l,j})} \tag{3.3}$$

As a matter of fact, assumptions (A2) and (A3) hold with a sufficient large interleave length in practice for LEXTPR on coded bits. Based on these two assumptions, we can compute the $\forall t' = 1,\ldots,n_t$

$$\begin{cases} m_{b;t',l}^{(i-1)} = \mathbb{E}\left[s_{b;t',l}|\{\Lambda_{A,LE}^{(i-1)}\}_{s_{b;t',l}}\right] \\ v_{b;t',l}^{(i-1)} = \mathbb{E}\left[|m_{b;t',l} - s_{b;t',l}|^2|\{\Lambda_{A,LE}^{(i-1)}\}_{s_{b;t',l}}\right] \end{cases}$$

In order to reduce the complexity, matrix inversion at each time l can be avoided by adopting the unconditional detection approach which is based on a unconditional covariance matrix given as

$$\mathbf{V}_b^{(i-1)} = \mathrm{diag}\{v_{b;1}^{(i-1)},\ldots,v_{b;n_t}^{(i-1)}\}$$

where $v_{b;t'}^{(i-1)} = \mathbb{E}\left[v_{b;t',l}^{(i-1)}\right]$.

A4 Due to the particular structure of the MCS, the so-called *equal variance assumption* holds, which states that each variance $v_{b;t'}^{(i-1)}$ is equal to $v^{(i-1)}$ defiened as

$$\mathbf{V}_b^{(i-1)} = v^{(i-1)}\mathbf{I}_{n_t}, \forall b. \tag{3.4}$$

The assumption (A4) holds given an interleaver of sufficient large depth, and forcing it induces no performance degration.

A5 Furthermore, assuming sufficiently large interleaver size, we can replace $v^{(i-1)}$ by its empirical mean $\tilde{v}^{(i-1)}$ defined as

$$\tilde{v}^{(i-1)} = \frac{1}{L_{ds} n_b n_t} \sum_{l=1}^{L_{ds}} \sum_{b=1}^{n_b} \sum_{t'=1}^{n_t} v_{b;t',l}^{(i-1)} \tag{3.5}$$

This yields the final simplified symbol covariance matrix $\tilde{\mathbf{V}}^{(i-1)}$ given as

$$\tilde{\mathbf{V}}^{(i-1)} = \tilde{v}^{(i-1)}\mathbf{I}_{n_t} \tag{3.6}$$

As a matter of fact, the assumption (A5) is part of the baseline assumptions of EXIT charts (ergodic regime) [35]. For the sake of simplicity, we drop the index b when it is convenient because the derivation is the same for each fading block b. In a slight abuse of notation, $\mathbf{H}$ and $\hat{\mathbf{H}}$ stand either for the channel state for a given block b or for the set of channel states for all blocks $b = 1, \cdots, n_b$ depending on the context.

3.5 Channel estimation and a posteriori CDI

3.5.1 Initial pilot assisted channel estimation

The initial pilot assisted channel estimate $\widehat{\mathbf{H}}^{(0)}$ corresponds to the Maximum Likelihood (or Least Square) unbiased channel estimate

$$\widehat{\mathbf{H}}^{(0)} = \mathbf{Y}_{ps}\mathbf{A}^{\dagger}(\mathbf{A}\mathbf{A}^{\dagger})^{-1} \tag{3.7}$$

which yields the error model

$$\widehat{\mathbf{H}}^{(0)} = g^{(0)}\mathbf{H} + \mathbf{\Psi}^{(0)} \tag{3.8}$$

with $g^{(0)} = 1$. By choosing a CAZAC sequence of length $L_{ps} \geq 2n_t$, it yields $\mathbf{A}\mathbf{A}^{\dagger} = L_{ps}\sigma_{ps}^2\mathbf{I}_{n_t}$ (see [95]). Thus, it comes that the entries of $\mathbf{\Psi}^{(0)}$ are i.i.d, circularly-symmetric Gaussian, with zero mean and variance $\sigma^2_{\psi^{(0)}} = \frac{N_0}{L_{ps}\sigma_{ps}^2}$.

3.5.2 Joint pilot and data assisted channel estimation

Conditional on the knowledge of the soft estimates $\tilde{\mathbf{s}}_l^{(i-1)}$ at disposal at the end of the previous iteration ($i \geq 2$, see Fig. 3.2)

$$\begin{cases} \mathbf{Y}^{ps} = \mathbf{H}\mathbf{A}^{ps} + \mathbf{W}^{ps} \\ \mathbf{Y} = \mathbf{H}\tilde{\mathbf{S}}^{(i-1)} + \triangle\tilde{\mathbf{W}}^{(i-1)} \end{cases} \tag{3.9}$$

where $\triangle\tilde{\mathbf{W}}^{(i-1)} = [\triangle\mathbf{w}_1^{(i-1)}, \cdots, \triangle\mathbf{w}_{L_{ds}}^{(i-1)}]$ and $\tilde{\mathbf{S}}^{(i-1)} = [\tilde{\mathbf{m}}_1^{(i-1)}, \cdots, \tilde{\mathbf{m}}_{L_{ds}}^{(i-1)}]$. Note that

$$\triangle\mathbf{w}_l^{(i-1)} = \mathbf{H}(\mathbf{s}_l - \tilde{\mathbf{m}}_l^{(i-1)}) + \mathbf{w}_l. \tag{3.10}$$

The covariance matrix of $\triangle\mathbf{w}_l^{(i-1)}$ conditional on $\tilde{v}^{(i-1)}$ is

$$\mathbb{E}_{\mathbf{H},\mathbf{\Lambda}_{A,LE}^{(i-1)},\mathbf{w}|\tilde{v}^{(i-1)}}\left\{\triangle\mathbf{w}_l^{(i-1)}\triangle\mathbf{w}_l^{(i-1)^{\dagger}}\right\} = (n_t\sigma_h^2\tilde{v}^{(i-1)}+N_0)\mathbf{I}_{n_r} = (\triangle N_0^{(i-1)}+N_0)\mathbf{I}_{n_r} \tag{3.11}$$

where $\triangle N_0^{(i-1)} = n_t\sigma_h^2\tilde{v}^{(i-1)}$. By stacking the receive samples associated to data and pilot symbols, we further extend the matrix model to

$$\overline{\mathbf{Y}} = \mathbf{H}\overline{\mathbf{S}}^{(i-1)} + \overline{\mathbf{W}}^{(i-1)} \tag{3.12}$$

where $\overline{\mathbf{Y}} = [\mathbf{Y}^{ps}, \mathbf{Y}]$, $\overline{\mathbf{S}}^{(i-1)} = \left[\mathbf{A}^{ps}, \tilde{\mathbf{S}}^{(i-1)}\right]$ and $\overline{\mathbf{W}}^{(i-1)} = \left[\mathbf{W}^{ps}, \triangle\tilde{\mathbf{W}}^{(i-1)}\right]$. Since the rows of $\overline{\mathbf{Y}}$ are uncorrelated, the LMMSE channel estimation can be carried out independently on each row $\mathbf{h}^r$. The LMMSE filter $\mathbf{F}^{(i-1)} \in \mathbb{C}^{(L_{ps}+L_{ds})\times n_t}$ that aims at minimizing $\mathbb{E}_{\overline{\mathbf{h}}^r,\overline{\mathbf{w}}}\{||\overline{\mathbf{y}}^r\mathbf{F}^{(i-1)} - \mathbf{h}^r||^2\}$ is given by

$$\mathbf{F}^{(i-1)} = \mathbb{E}_{\overline{\mathbf{h}}^r,\overline{\mathbf{w}}}\{\overline{\mathbf{y}}^{r^{\dagger}}\overline{\mathbf{y}}^r\}^{-1}\mathbb{E}_{\overline{\mathbf{h}}^r,\overline{\mathbf{w}}}\{\overline{\mathbf{y}}^{r^{\dagger}}\mathbf{h}^r\} \tag{3.13}$$

or, equivalently, $\mathbf{F}^{(i-1)} = \mathbb{E}_{\mathbf{H},\overline{\mathbf{w}}}\{\overline{\mathbf{Y}}^{\dagger}\overline{\mathbf{Y}}\}^{-1}\mathbb{E}_{\mathbf{H},\overline{\mathbf{w}}}\{\overline{\mathbf{Y}}^{\dagger}\mathbf{H}\}$. Averaging over the channel statistics and applying the Matrix Inversion Lemma, we obtain

$$\mathbf{F}^{(i-1)} = (n_r\sigma_h^2)\boldsymbol{\Sigma}_{\overline{w}}^{(i-1)^{-1}}\overline{\mathbf{S}}^{(i-1)^{\dagger}}\left(\overline{\mathbf{S}}^{(i-1)}(n_r\sigma_h^2)\boldsymbol{\Sigma}_{\overline{w}}^{(i-1)^{-1}}\overline{\mathbf{S}}^{(i-1)^{\dagger}} + \mathbf{I}_{n_t}\right)^{-1} \quad (3.14)$$

where

$$\boldsymbol{\Sigma}_{\overline{w}}^{(i-1)} = \mathbb{E}\{\overline{\mathbf{W}}^{(i-1)^{\dagger}}\overline{\mathbf{W}}^{(i-1)}\} = \text{diag}\left(n_rN_0\mathbf{I}_{L_{ps}}, n_r(N_0 + \triangle N_0^{(i-1)})\mathbf{I}_{L_{ds}}\right). \quad (3.15)$$

After some lengthy derivation given in Appendix A, the resulting (biased) LMMSE channel estimation error model can be expressed as

$$\widehat{\mathbf{H}}^{(i-1)} = g^{(i-1)}\mathbf{H} + \boldsymbol{\Psi}^{(i-1)} \quad (3.16)$$

where

$$g^{(i-1)} = \frac{L_{ps}\sigma_{ps}^2 + L_{ds}(\sigma_{ds}^2 - \tilde{v}^{(i-1)})\frac{N_0}{\triangle N_0^{(i-1)}+N_0}}{L_{ps}\sigma_{ps}^2 + L_{ds}(\sigma_{ds}^2 - \tilde{v}^{(i-1)})\frac{N_0}{\triangle N_0^{(i-1)}+N_0} + \frac{N_0}{\sigma_h^2}} \quad (3.17)$$

and the entries of $\boldsymbol{\Psi}^{(i-1)}$ has zero mean and variance $\sigma^2_{\psi^{(i-1)}}$ given as

$$\sigma^2_{\psi^{(i-1)}} = N_0\frac{L_{ps}\sigma_{ps}^2 + L_{ds}(\sigma_{ds}^2 - \tilde{v}^{(i-1)})\frac{N_0}{\triangle N_0^{(i-1)}+N_0}}{\left(L_{ps}\sigma_{ps}^2 + L_{ds}(\sigma_{ds}^2 - \tilde{v}^{(i-1)})\frac{N_0}{\triangle N_0^{(i-1)}+N_0} + \frac{N_0}{\sigma_h^2}\right)^2}. \quad (3.18)$$

A6 In (3.16), The entries of $\boldsymbol{\Psi}^{(i-1)}$ are i.i.d and follows the pdf $\mathcal{N}_{\mathbb{C}}(0, \sigma^2_{\psi^{(i-1)}})$ with $\sigma^2_{\psi^{(i-1)}}$ given in (3.18).

Assumption A6 over $\boldsymbol{\Psi}^{(i-1)}$ contains two aspects: Firstly, single $\sigma^2_{\psi^{(i-1)}}$ can evaluate its variance which comes from assumption A2, A3 A4 and A5. Secondly, its Gaussian distribution is more valid when the soft symbol estimates are reliable such that the variance $\triangle N_0^{(i-1)} = n_t\sigma_h^2\tilde{v}^{(i-1)} < N_0$ or equivalently, $\tilde{v}^{(i-1)} < N_0/n_t\sigma_h^2$. Clearly, the MSE for each channel component is

$$\mathbb{E}\{|h_{r,t} - \hat{h}_{r,t}^{(i-1)}|^2\} = \frac{N_0}{L_{ps}\sigma_{ps}^2 + L_{ds}(\sigma_{ds}^2 - \tilde{v}^{(i-1)})\frac{N_0}{\triangle N_0^{(i-1)}+N_0} + \frac{N_0}{\sigma_h^2}}. \quad (3.19)$$

Note that this derivation is new. The closest state of the art can be found in [80], however, its MSE analyses are always based on an a posteriori combining of the pilot assisted channel estimate and data aided estimate [80, eq. (12)] while eq. (3.12) allows a joint pilot and data semi-blind LMMSE approach.

3.5.3 A posteriori CDI

From Assumption A1 and Assumption A6, it is clear that $\mathbf{H}$ and $\widehat{\mathbf{H}}^{(i-1)}$ are jointly Gaussian conditional on $\tilde{v}^{(i-1)}$. Therefore, the distribution $p(\mathbf{H}|\widehat{\mathbf{H}}^{(i-1)})$ can be easily obtained [75] [76]. It yields, $\forall i \geq 1$,

$$\mathbf{H} = \alpha^{(i-1)}\widehat{\mathbf{H}}^{(i-1)} + \triangle\mathbf{H}^{(i-1)} \tag{3.20}$$

where

$$\alpha^{(i-1)} = \frac{g^{(i-1)}\sigma_h^2}{g^{(i-1)^2}\sigma_h^2 + \sigma^2_{\psi^{(i-1)}}} \tag{3.21}$$

and the entries of $\triangle\mathbf{H}^{(i-1)}$ are i.i.d, circularly-symmetric Gaussian, with zero mean and variance $\sigma^2_{\triangle H^{(i-1)}}$ given as

$$\sigma^2_{\triangle H^{(i-1)}} = \frac{\sigma_h^2\sigma^2_{\psi^{(i-1)}}}{g^{(i-1)^2}\sigma_h^2 + \sigma^2_{\psi^{(i-1)}}}. \tag{3.22}$$

3.6 Linear IC and data detection

After the channel estimation step, available CSI are: channel estimate (3.8), (3.16) and a posteriori CDI (3.20). The fact that the real channel is never known and the receiver needs to detect symbols implies that we should see the channel observations as the output of a feasible base-band model other than non-feasible base-band model (3.1). Depending on using how much available CSI, two choices exist: a matched receiver base-band model using both channel estimate and conditional channel distribution or a mismatched receiver base-band model using only channel estimate.

3.6.1 Receive base-band model conditional on channel estimation

3.6.1.1 Matched receive base-band model

If we use both channel estimate and conditional CDI, an interesting matched receive base-band model can be obtained $\forall i \geq 1$, as [75–77]

$$\begin{aligned} \mathbf{y}_l &= \mathbf{H}\mathbf{s}_l + \mathbf{w}_l \\ &= \alpha^{(i-1)}\widehat{\mathbf{H}}^{(i-1)}\mathbf{s}_l + \triangle\mathbf{H}^{(i-1)}\mathbf{s}_l + \mathbf{w}_l \\ &= \widetilde{\mathbf{H}}^{(i-1)}\mathbf{s}_l + \boldsymbol{\zeta}_l^{(i-1)} \end{aligned} \tag{3.23}$$

where $\widetilde{\mathbf{H}}^{(i-1)} = \alpha^{(i-1)}\widehat{\mathbf{H}}^{(i-1)}$, $\boldsymbol{\zeta}_l^{(i-1)} = \triangle\mathbf{H}^{(i-1)}\mathbf{s}_l + \mathbf{w}_l$. The covariance matrix of $\boldsymbol{\zeta}_l^{(i-1)}$ is

$$\boldsymbol{\Sigma}_{\boldsymbol{\zeta}}^{(i-1)} = \mathbb{E}_{\mathbf{H}|\widehat{\mathbf{H}}^{(i-1)}}\left\{\boldsymbol{\zeta}_l^{(i-1)}\boldsymbol{\zeta}_l^{(i-1)^\dagger}\right\} = N_0(1+\varepsilon^{(i-1)})\mathbf{I}_{n_r} \tag{3.24}$$

with, using (3.17), (3.18) and (3.22),

$$\varepsilon^{(i-1)} = \frac{n_t\sigma_{ds}^2}{L_{ps}\sigma_{ps}^2 + L_{ds}(\sigma_{ds}^2 - \tilde{v}^{(i-1)})\frac{N_0}{n_t\sigma_h^2\tilde{v}^{(i-1)}+N_0} + \frac{N_0}{\sigma_h^2}}. \tag{3.25}$$

Note that in [75, Appendix I] an alternative derivation is proposed relying on the joint Gaussianity of $\mathbf{y}_{ds,l}$ and $\widehat{\mathbf{H}}^{(i-1)}$. From (3.23), IC make sense now without the knowledge of $\mathbf{H}$ and the interference $\widetilde{\mathbf{y}}_{l\backslash t}^{(i)}$ over $s_{t,l}$ with matched receive base-band model is generated as

$$\widetilde{\mathbf{y}}_{l\backslash t}^{(i)} = \widetilde{\mathbf{H}}^{(i-1)}(\tilde{\mathbf{m}}_l^{(i-1)} - m_{t,l}^{(i-1)}\mathbf{e}_t) \tag{3.26}$$

with $\mathbf{e}_t = [0, \cdots, 1 \cdots, 0]^\top$ which has a 1 in position t.

3.6.1.2 Mismatched receive base-band model

A further simplified mismatched receive base-band model uses only channel estimate by assuming $\hat{\mathbf{H}}^{(i-1)} = \mathbf{H}$ [**?**] which yields

$$\mathbf{y}_l = \widehat{\mathbf{H}}^{(i-1)}\mathbf{s}_l + \mathbf{w}_l \tag{3.27}$$

From (3.27), the interference $\widetilde{\mathbf{y}}_{l\backslash t}^{(i)}$ over $s_{t,l}$ with mismatched receive base-band model is generated as

$$\widetilde{\mathbf{y}}_{l\backslash t}^{(i)} = \widehat{\mathbf{H}}^{(i-1)}(\tilde{\mathbf{m}}_l^{(i-1)} - m_{t,l}^{(i-1)}\mathbf{e}_t) \tag{3.28}$$

3.6.2 Linear-IC detection error model

IC and linear filtering by $\mathbf{f}_t^{(i)} \in \mathbb{C}^{n_r \times 1}$ make sense now without the knowledge of $\mathbf{H}$. Indeed, it yields the symbol estimates

$$\hat{s}_{t,l}^{(i)} = \mathbf{f}_t^{(i)\dagger}(\mathbf{y}_l - \widetilde{\mathbf{y}}_{l\backslash t}^{(i)}) \tag{3.29}$$

Working with matched receive base-band model (3.23) yields matched SINR model and working with feasible mismatched receive base-band model (3.27) yields mismatched SINR model.

3.6.2.1 Matched SINR model

Working with feasible model (3.23), (3.29) becomes

$$\widehat{s}_{t,l}^{(i)} = \mathbf{f}_t^{(i)\dagger}\widetilde{\mathbf{h}}_t^{(i-1)}s_{t,l} + \tilde{n}_{t,l}^{(i)}. \tag{3.30}$$

where $\tilde{n}_{t,l}^{(i)} = \mathbf{f}_t^{(i)\dagger}[\widetilde{\mathbf{H}}_{\backslash t}^{(i-1)}(\mathbf{s}_l - \tilde{\mathbf{m}}_l^{(i-1)}) + \boldsymbol{\zeta}_{ds,l}^{(i-1)}]$ with $\widetilde{\mathbf{H}}_{\backslash t}^{(i-1)} = \widetilde{\mathbf{H}}^{(i-1)}(\mathbf{I} - \mathbf{e}_t\mathbf{e}_t^{\dagger})$. We define the matched SINR $\tilde{\gamma}_t^{(i)}(\mathbf{f}_t^{(i)})$ as follows

$$\tilde{\gamma}_t^{(i)}(\mathbf{f}_t^{(i)}) = \frac{\left|\mathbf{f}_t^{(i)\dagger}\widetilde{\mathbf{h}}_t^{(i-1)}\right|^2 \sigma_{ds}^2}{\mathbb{E}_{\mathbf{H},s,\mathbf{w}|\widetilde{\mathbf{H}}^{(i-1)},\widetilde{\boldsymbol{v}}^{(i-1)}}\left\{|\tilde{n}_{t,l}^{(i)}|^2\right\}} = \frac{\left|\mathbf{f}_t^{(i)\dagger}\widetilde{\mathbf{h}}_t^{(i-1)}\right|^2 \sigma_{ds}^2}{\sigma_{\tilde{n}_{t,l}^{(i)}}^2}. \tag{3.31}$$

The denominator is now averaged over $\mathbf{H}$ conditional on $\widetilde{\mathbf{H}}^{(i-1)}$ and is given by

$$\sigma^2_{\tilde{n}^{(i)}_{t,l}} = \mathbf{f}_t^{(i)^\dagger} \left\{ \tilde{v}^{(i-1)} \widetilde{\mathbf{H}}^{(i-1)}_{\backslash t} \widetilde{\mathbf{H}}^{(i-1)^\dagger}_{\backslash t} + \mathbf{\Sigma}^{(i-1)}_{\boldsymbol{\zeta}} \right\} \mathbf{f}_t^{(i)} \tag{3.32}$$

where $\mathbf{\Sigma}^{(i-1)}_{\boldsymbol{\zeta}}$ is given in (3.24).

3.6.2.2 Mismatched SINR model

Working with feasible model (3.27), (3.29) becomes

$$\widehat{s}^{(i)}_{t,l} = \mathbf{f}_t^{(i)^\dagger} \widehat{\mathbf{h}}^{(i-1)}_t s_{t,l} + \hat{n}^{(i)}_{t,l}. \tag{3.33}$$

where $\hat{n}^{(i)}_{t,l} = \mathbf{f}_t^{(i)^\dagger}[\widehat{\mathbf{H}}^{(i-1)}_{\backslash t}(\mathbf{s}_l - \tilde{\mathbf{m}}^{(i-1)}_l) + \mathbf{w}_l]$, $\widehat{\mathbf{H}}^{(i-1)}_{\backslash t} = \widehat{\mathbf{H}}^{(i-1)}(\mathbf{I} - \mathbf{e}_t \mathbf{e}_t^\dagger)$. The mismatched SINR $\hat{\gamma}^{(i)}_t(\mathbf{f}^{(i)}_t)$ is given as

$$\hat{\gamma}^{(i)}_t(\mathbf{f}^{(i)}_t) = \frac{\left| \mathbf{f}_t^{(i)^\dagger} \widehat{\mathbf{h}}^{(i-1)}_t \right|^2 \sigma^2_{ds}}{\mathbb{E}_{s,\mathbf{w}|\widehat{\mathbf{H}}^{(i-1)},\tilde{v}^{(i-1)}} \left\{ |\hat{n}^{(i)}_{t,l}|^2 \right\}} = \frac{\left| \mathbf{f}_t^{(i)^\dagger} \widehat{\mathbf{h}}^{(i-1)}_t \right|^2 \sigma^2_{ds}}{\sigma^2_{\hat{n}^{(i)}_{t,l}}}. \tag{3.34}$$

The denominator is now given by

$$\sigma^2_{\hat{n}^{(i)}_{t,l}} = \mathbf{f}_t^{(i)^\dagger} \left\{ \tilde{v}^{(i-1)} \widehat{\mathbf{H}}^{(i-1)}_{\backslash t} \widehat{\mathbf{H}}^{(i-1)^\dagger}_{\backslash t} + N_0 \mathbf{I}_{n_r} \right\} \mathbf{f}_t^{(i)} \tag{3.35}$$

3.6.2.3 Exact SINR model

Note that both matched (3.31) and mismatched (3.34) SINR model developed above are feasible (approximated) SINR model in practice without perfect knowledge of channel $\mathbf{H}$. Clearly, the exact SINR model depends on $\mathbf{H}$. From (3.23), (3.29) and assuming perfect knowledge of $\mathbf{H}$, we can compute the exact SINR in matched receive base-band model

$$\widehat{s}^{(i)}_{t,l} = \mathbf{f}_t^{(i)^\dagger}[\mathbf{h}_t s_{t,l} + \mathbf{H}_{\backslash t}\mathbf{s}_l - \widetilde{\mathbf{H}}^{(i-1)}_{\backslash t} \tilde{\mathbf{m}}^{(i-1)}_l + \mathbf{w}_l] = \mathbf{f}_t^{(i)^\dagger} \mathbf{h}_t s_{t,l} + n^{(i)}_{t,l}. \tag{3.36}$$

where $\mathbf{H}_{\backslash t} = \mathbf{H}(\mathbf{I}_{n_t} - \mathbf{e}_t\mathbf{e}_t^\dagger)$, $n_{t,l}^{(i)}$ models the residual interference and noise. The exact SINR of (3.36) is equal to

$$\gamma_t^{(i)}(\mathbf{f}_t^{(i)}) = \frac{\left|\mathbf{f}_t^{(i)^\dagger}\mathbf{h}_t\right|^2 \sigma_{ds}^2}{\sigma^2_{n_{t,l}^{(i)}}}. \tag{3.37}$$

where,

$$\begin{aligned}\sigma^2_{n_{t,l}^{(i)}} &= \mathbf{f}_t^{(i)^\dagger}\Big[\sigma_{ds}^2\mathbf{H}_{\backslash t}\mathbf{H}_{\backslash t}^\dagger + \widetilde{\mathbf{H}}_{\backslash t}^{(i-1)}(\sigma_{ds}^2 - v^{(i-1)})\widetilde{\mathbf{H}}_{\backslash t}^{(i-1)^\dagger} \\ &\quad -\mathbf{H}_{\backslash t}(\sigma_{ds}^2 - v^{(i-1)})\widetilde{\mathbf{H}}_{\backslash t}^{(i-1)^\dagger} - \widetilde{\mathbf{H}}_{\backslash t}^{(i-1)}(\sigma_{ds}^2 - v^{(i-1)})\mathbf{H}_{\backslash t}^\dagger\Big]\mathbf{f}_t^{(i)} \\ &\quad +\mathbf{f}_t^{(i)^\dagger}N_0\mathbf{f}_t^{(i)}. \end{aligned} \tag{3.38}$$

Note that this exact SINR model (3.37) in matched receive base-band model exploits all available CSI before data transmission for feasible receive base-band model and also unavailable CSI for SINR computation, thus it presents the upper bound. For this reason, the exact SINR model in mismatched receive base-band model is less interesting. However, this exact SINR model (3.36), (3.37) and (3.38) can not be exploited to compute the filter $\mathbf{f}_t$. Again, we need resort to the matched SINR (3.30), (3.31) and (3.32) or mismatched SINR (3.33), (3.34) and (3.35) to compute the filter.

3.6.3 LMMSE-IC key equations

3.6.3.1 Matched LMMSE

The matched LMMSE filter $\tilde{\mathbf{f}}_t^{(i)}$ aims at maximizing the matched SINR $\tilde{\gamma}_t^{(i)}$ (3.31) which yields, using the the Matrix Inversion Lemma,

$$\widetilde{\mathbf{f}}_t^{(i)^\dagger} = \eta^{(i)}\widetilde{\mathbf{h}}_t^{(i-1)^\dagger}\left(\tilde{v}^{(i-1)}\widetilde{\mathbf{H}}^{(i-1)}\widetilde{\mathbf{H}}^{(i-1)^\dagger} + \mathbf{\Sigma}_{\boldsymbol{\zeta}}^{(i-1)}\right)^{-1} \tag{3.39}$$

where

$$\eta^{(i)} = \frac{\sigma_{ds}^2}{1 + \widetilde{\beta}_t^{(i)}\left(\sigma_{ds}^2 - \tilde{v}^{(i-1)}\right)} \tag{3.40}$$

and

$$\widetilde{\beta}_t^{(i)} = \widetilde{\mathbf{h}}_t^{(i-1)^\dagger} \left(\tilde{v}^{(i-1)} \widetilde{\mathbf{H}}^{(i-1)} \widetilde{\mathbf{H}}^{(i-1)^\dagger} + \mathbf{\Sigma}_{\boldsymbol{\zeta}}^{(i-1)} \right)^{-1} \widetilde{\mathbf{h}}_t^{(i-1)}.$$

From (3.30), (3.31) and (3.32), the matched SINR based on matched LMMSE becomes

$$\tilde{\gamma}_t^{(i)}(\tilde{\mathbf{f}}_t^{(i)}) = \frac{\tilde{\mathbf{f}}_t^{(i)^\dagger} \widetilde{\mathbf{h}}_t^{(i-1)}}{1 - \tilde{\mathbf{f}}_t^{(i)^\dagger} \widetilde{\mathbf{h}}_t^{(i-1)}}. \tag{3.41}$$

Remark that the exact SINR based on matched LMMSE filter can be obtained by adopting $\tilde{\mathbf{f}}_t^{(i)}$ in (3.36), (3.37) and (3.38).

3.6.3.2 Mismatched LMMSE

The mismatched LMMSE filter $\hat{\mathbf{f}}_t^{(i)}$ aims at maximizing the mismatched SINR $\hat{\gamma}_t^{(i)}$ (3.34). We do not give the mathematical formulas of $\hat{\mathbf{f}}_t^{(i)}$ since it can be obtained from $\tilde{\mathbf{f}}_t^{(i)}$ by forcing $\sigma^2_{\Psi^{(i-1)}} = 0$ and $g^{(i-1)} = 1$. From (3.33), (3.34) and (3.35), the mismatched SINR based on mismatched LMMSE filter becomes

$$\hat{\gamma}_t^{(i)}(\hat{\mathbf{f}}_t^{(i)}) = \frac{\hat{\mathbf{f}}_t^{(i)^\dagger} \widehat{\mathbf{h}}_t^{(i-1)}}{1 - \hat{\mathbf{f}}_t^{(i)^\dagger} \widehat{\mathbf{h}}_t^{(i-1)}}. \tag{3.42}$$

3.7 Soft symbol-to-bit demapping and decoding

3.7.1 Soft symbol-to-bit demapping

The estimate $\hat{s}_{t,l}^{(i)}$ is used as a *decision statistic* to compute the LEXTPR on the q_ν bits involved in the labeling of $s_{t,l}$. It is explained for any linear filter $\mathbf{f}_t^{(i)^\dagger}$ and do not precise it to be the matchel LMMSE filter (3.39) or mismatched LMMSE filter.

A7 Given any linear filter $\mathbf{f}_t^{(i)^\dagger}$,

- the pdf $p_{\hat{s}_{t,l}^{(i)}|s_{t,l}}(\hat{s}_{t,l}^{(i)}) = \mathcal{N}_{\mathbb{C}}(\mathbf{f}_t^{(i)^\dagger} \widetilde{\mathbf{h}}_t^{(i-1)} s_{t,l}, \sigma^2_{\tilde{n}_{t,l}^{(i)}})$ in (3.30)
- the pdf $p_{\hat{s}_{t,l}^{(i)}|s_{t,l}}(\hat{s}_{t,l}^{(i)}) = \mathcal{N}_{\mathbb{C}}(\mathbf{f}_t^{(i)^\dagger} \widehat{\mathbf{h}}_t^{(i-1)} s_{t,l}, \sigma^2_{\hat{n}_{t,l}^{(i)}})$ in (3.33)
- and the pdf $p_{\hat{s}_{t,l}^{(i)}|s_{t,l}}(\hat{s}_{t,l}^{(i)}) = \mathcal{N}_{\mathbb{C}}(\mathbf{f}_t^{(i)^\dagger} \mathbf{h}_t s_{t,l}, \sigma^2_{n_{t,l}^{(i)}})$ in (3.36).

Soft symbol-to-bit demapping is performed based on Assumption A7. Adopting the matched SINR model, the log extrinsic probability ratio for

each digit $\Lambda_{E,DEM}^{(i)}(x_{t,l,q})$ after soft demapping is computed as

$$\Lambda_{E,DEM}^{(i)}(d_{t,l,j}) = \ln \frac{\sum_{s\in\mathscr{X}_\nu:\mu_{\nu,j}^{-1}(s)=1} \exp\left\{-\tilde{\gamma}_t^{(i)}(\mathbf{f}_t^{(i)})|\frac{1}{\mathbf{f}_t^{(i)\dagger}\widetilde{\mathbf{h}}_t^{(i-1)}}\widehat{s}_{t,l}^{(i)} - s|^2 + \sum_{j'\neq j}\mu_{\nu,j'}^{-1}(s)\Lambda_{A,LE}^{(i-1)}(d_{t,l,j'})\right\}}{\sum_{s\in\mathscr{X}_\nu:\mu_{\nu,j}^{-1}(s)=0} \exp\left\{-\tilde{\gamma}_t^{(i)}(\mathbf{f}_t^{(i)})|\frac{1}{\mathbf{f}_t^{(i)\dagger}\widetilde{\mathbf{h}}_t^{(i-1)}}\widehat{s}_{t,l}^{(i)} - s|^2 + \sum_{j'\neq j}\mu_{\nu,j'}^{-1}(s)\Lambda_{A,LE}^{(i-1)}(d_{t,l,j'})\right\}} \tag{3.43}$$

For the special case of Gray labeling, the $\{\Lambda_{A,LE}^{(i-1)}(d_{t,l,j'})\}_{j'\neq j}$ have little impact on the value of $\Lambda_{E,DEM}^{(i)}(x_{t,l,q})$ and can be neglected which yields

$$\Lambda_{E,DEM}^{(i)}(d_{t,l,q}) = \ln \frac{\sum_{s\in\mathscr{X}_\nu:\mu_{\nu,j}^{-1}(s)=1} \exp\left\{-\tilde{\gamma}_t^{(i)}(\mathbf{f}_t^{(i)})|\frac{1}{\mathbf{f}_t^{(i)\dagger}\widetilde{\mathbf{h}}_t^{(i-1)}}\widehat{s}_{t,l}^{(i)} - s|^2\right\}}{\sum_{s\in\mathscr{X}_\nu:\mu_{\nu,j}^{-1}(s)=0} \exp\left\{-\tilde{\gamma}_t^{(i)}(\mathbf{f}_t^{(i)})|\frac{1}{\mathbf{f}_t^{(i)\dagger}\widetilde{\mathbf{h}}_t^{(i-1)}}\widehat{s}_{t,l}^{(i)} - s|^2\right\}} \tag{3.44}$$

The soft symbol-to-bit demapping adopting the mismatched SINR model or exact SINR model follows the same principle, we just need to replace $\tilde{\gamma}_t^{(i)}(\mathbf{f}_t^{(i)})$, $\widetilde{\mathbf{h}}_t^{(i-1)}$ in (3.43), (3.44) by $\hat{\gamma}_t^{(i)}(\mathbf{f}_t^{(i)})$, $\widehat{\mathbf{h}}_t^{(i-1)}$ and $\gamma_t^{(i)}(\mathbf{f}_t^{(i)})$, $\mathbf{h}_t$, respectively.

3.7.2 Decoding

The set $\mathbf{\Lambda}_{E,DEM}^{(i)}$ of all LEXTPR on labeling bits after demapping becomes after deinterleaving the set $\mathbf{\Lambda}_{I,DEC}^{(i)}$ of all log intrinsic probability ratios on coded bits used as input for the decoder.

A8 The pdf $p_{\mathbf{\Lambda}_{I,DEC}^{(i)}|\mathbf{c}}(\mathbf{\Lambda}_{I,DEC}^{(i)})$ factorizes as

$$p_{\mathbf{\Lambda}_{I,DEC}^{(i)}|\mathbf{c}}(\mathbf{\Lambda}_{I,DEC}^{(i)}) = \prod_{n=1}^{n_{\nu,c}} p_{\Lambda_{I,DEC}^{(i)}(c_n)|c_n}(\Lambda_{I,DEC}^{(i)}(c_n))$$

where $\Lambda_{I,DEC}^{(i)}(c_n)$ is the log intrinsic probability ratio on coded bit c_n. The assumption (A8) allows to simplify the decoding task. It is rightfully confirmed for an interleaver of finite, but large enough, depth. Under (A8), the

decoder computes the LAPPR $\Lambda^{(i)}_{D,DEC}(c_n)$ on coded bit c_n as

$$\Lambda^{(i)}_{D,DEC}(c_n) = \frac{\sum_{\mathbf{c}\in\mathscr{C}:c_n=1}\prod_{n=1}^{n_{\nu,c}} p_{\Lambda^{(i)}_{I,DEC}(c_n)|c_n}(\Lambda^{(i)}_{I,DEC}(c_n))}{\sum_{\mathbf{c}\in\mathscr{C}:c_n=0}\prod_{n=1}^{n_{\nu,c}} p_{\Lambda^{(i)}_{I,DEC}(c_n)|c_n}(\Lambda^{(i)}_{I,DEC}(c_n))} \tag{3.45}$$

Finally the LEXTPR on coded bit c_n can be computed as

$$\Lambda^{(i)}_{E,DEC}(c_n) = \Lambda^{(i)}_{D,DEC}(c_n) - \Lambda^{(i)}_{I,DEC}(c_n) \tag{3.46}$$

3.8 PHY-layer abstraction

As a FLA metric (or conditional BLER given the initial channel estimate), we are interested in computing

$$\begin{aligned}
&\overline{\mathrm{BLER}}^{(i)}(\widehat{\mathbf{H}}^{(0)}) = \mathbb{E}_{\mathbf{H},\widehat{\mathbf{H}}^{(i-1)}|\widehat{\mathbf{H}}^{(0)}}\{\mathrm{BLER}^{(i)}(\mathbf{H},\widehat{\mathbf{H}}^{(i-1)})\}\\
&= \mathbb{E}_{\widehat{\mathbf{H}}^{(i-1)}|\widehat{\mathbf{H}}^{(0)}}\{\mathbb{E}_{\mathbf{H}|\widehat{\mathbf{H}}^{(i-1)},\widehat{\mathbf{H}}^{(0)}}\{\mathrm{BLER}^{(i)}(\mathbf{H},\widehat{\mathbf{H}}^{(i-1)})\}\}\\
&= \mathbb{E}_{\widehat{\mathbf{H}}^{(i-1)}|\widehat{\mathbf{H}}^{(0)}}\{\mathbb{E}_{\mathbf{H}|\widehat{\mathbf{H}}^{(0)}}\{\mathrm{BLER}^{(i)}(\mathbf{H},\widehat{\mathbf{H}}^{(i-1)})\}\}
\end{aligned}$$

with respect to the chosen MCS and average SNR. Clearly, the $\mathrm{BLER}^{(i)}(\mathbf{H},\widehat{\mathbf{H}}^{(i-1)})$ need to be predicted per iteration i based on the $n_b \times n_t$ exact SINRs $\gamma_t^{(i)}(\mathbf{f}_t^{(i)})$. As a result, we adopt the prediction method described in [66] which is built on the MIESM compression of the $n_b \times n_t$ multiple parallel SINRs to a single effective SNR or equivalently AMI. The correspondence between SNR and AMI is usually stored in a LUT $\Gamma(.)$. This effective SNR (respectively AMI) is then used to read pre-simulated MCS dependent LUTs that outputs the $\tilde{v}^{(i)}$ (for the next iteration) and the BLER (these LUTs are denoted in the following by $G_{JDD}(.)$ and $F_{JDD}(.)$, respectively).

3.8.1 Proposed algorithm

In this Section, we describe (in the context of FLA and for a given MCS) the proposed semi-analytical performance prediction method for iterative LMMSE-IC detection and semi-blind channel estimation algorithm. As mentioned above, it is partly built on the MIESM prediction method described in [66]. However, the obtained predicted BLER per iteration must

be averaged on the conditional pdfs $p(\mathbf{H}|\widehat{\mathbf{H}}^{(0)})$ and $p(\widehat{\mathbf{H}}^{(i-1)}|\mathbf{H}^{(0)})$. Since we were able to derive their closed-form expression in Section 3.5, it is possible to performed the averaging by an intertwined Monte Carlo approach as detailed in Algorithm 4. Note that ACC(i) is simply an intermediate variable to average the BLER on N_H channel outcomes at iteration i.

Algorithm 4 Algorithm of performance prediction in the context of FLA for a given $\widehat{\mathbf{H}}^{(0)}$

for SNRs **do**
  Init $\tilde{v}^{(0)} = \sigma_{ds}^2$, $\text{ACC}(i) = 0$ for $i = 1 \cdots n_{it}$
  for $n = 1$ to N_H **do**
    Draw $\mathbf{H}$ from $p\left(\mathbf{H}|\widehat{\mathbf{H}}^{(0)}\right)$
    for $i = 1$ to n_{it} iterations **do**
      Step 1 Compute the $n_b \times n_t$ SINRs according to $\tilde{v}^{(i-1)}$, $\widehat{\mathbf{H}}^{(i-1)}$, $\mathbf{H}$
      Step 2 Read from the AMI LUT the associated $n_b \times n_t$ AMIs
      Step 3 Compress the AMI: $I_{in}^{(i)} = \frac{1}{n_b n_t} \sum_b \sum_t I_{p,t}^{(i)}$
      Step 4 Read from the LUTs the $\text{BLER}^{(i)}$ and the symbol variance $\tilde{v}^{(i)}$: $\text{BLER}^{(i)} = F_{JDD}(I_{in}^{(i)})$ and $\tilde{v}^{(i)} = G_{JDD}(I_{in}^{(i)})$
      Step 5 Draw $\widehat{\mathbf{H}}^{(i)}$ from $p\left(\widehat{\mathbf{H}}^{(i)}|\mathbf{H}, \tilde{v}^{(i)}\right)$
      Step 6 Update $\text{ACC}(i) = \text{ACC}(i) + \text{BLER}^{(i)}$
    end for
  end for
  $\overline{\text{BLER}}^{(i)}\left(\text{SNR}, \widehat{\mathbf{H}}^{(0)}\right) = \frac{\text{ACC}(i)}{N_H}$
end for

Based on the proposed Algorithm 4, the SLA metric or average BLER comes naturally as

$$\overline{\overline{\text{BLER}}}^{(i)} = \mathbb{E}_{\widehat{\mathbf{H}}^{(0)}}\{\overline{\text{BLER}}^{(i)}(\widehat{\mathbf{H}}^{(0)})\}$$

with respect to the distribution of $\widehat{\mathbf{H}}^{(0)}$ whoses entries are i.i.d and follows the pdf $\mathcal{N}_{\mathbb{C}}(0, 1 + \sigma_{\psi(0)}^2)$.

3.8.2 Corrected SINR issue

The accuracy of the prediction strategy under imperfect CSIR for LEXTPR based iterative LMMSE-IC detection joint semi-blind channel estimation can be impacted by channel estimation error. The fact that the performance prediction method uses Matched LMMSE with exact SINR while the receiver uses Matched LMMSE with matched SINR (or mismatched SINR) can yield discrepancy between predicted and simulated performance depending on

the channel estimate error. When the channel estimation is good enough, the prediction method should work accurately since the difference between exact SINR and matched SINR model is relatively small. When the channel estimation is not good enough, the prediction method will be optimist to a certain level since the difference between exact SINR model and matched SINR model becomes relatively high. The solution, arbitrary but efficient, is to make the the exact SINR smaller in the prediction method. The corrected SINR $\gamma_t^{'(i)}(\mathbf{f}_t^{(i)})$ based on (3.36) is given as

$$\gamma_t^{'(i)}(\mathbf{f}_t^{(i)}) = \frac{\left|\mathbf{f}_t^{(i)\dagger}\mathbf{h}_t\right|^2 \sigma_{ds}^2}{\sigma^2_{n_{t,l}^{(i)}} + \sigma^2_{n_{t,l}^{'(i)}}}. \tag{3.47}$$

with

$$\sigma^2_{n_{t,l}^{'(i)}} = \sigma_{ds}^2 \mathbf{f}_t^{(i)\dagger}(\mathbf{h}_t - \widetilde{\mathbf{h}}_t^{(i-1)})(\mathbf{h}_t - \widetilde{\mathbf{h}}_t^{(i-1)})^\dagger \mathbf{f}_t^{(i)} \tag{3.48}$$

Note that $\sigma^2_{n_{t,l}^{'(i)}}$ represents the channel estimation error. When channel estimate $\widetilde{\mathbf{h}}_t^{(i-1)}$ is close the real channel $\mathbf{h}_t$, $\sigma^2_{n_{t,l}^{'(i)}}$ can be neglected.

3.9 Numerical results

Let us consider a STBICM with the following parameters: Rate-$\frac{1}{2}$ binary Non-Recursive Non-Systematic Convolutional (NRNSC) code with generator polynomials $(133, 171)_8$, pseudo-random interleaver and QPSK or 16QAM constellation with Gray labeling. A 1-Block ($n_b = 1$) 4×4 MIMO memoryless flat Rayleigh channel is selected for all simulations. We fix $\sigma_h^2 = 1$ and $\sigma_{ds}^2 = 1$. The total number of channel use L_{ds} is fixed to 288 which implies that each codeword will always be mapped to 1152 symbols. Thus, when using QPSK constellation, each codeword contains $n_c = 2048$ coded bits. When using 16QAM constellation, each codeword contains $n_c = 4096$ coded bits. The CAZAC sequence $\mathbf{u}$ is given in hexadecimal form as $68195E$ with length $L_{ps} = 24$ (here, $L_{ps} > 2n_t$ ensuring that $\mathbf{A}\mathbf{A}^\dagger = L_{ps}\sigma_{ps}^2\mathbf{I}_{n_t}$). The number of iteration of the double loop receiver is limited to five, i.e., $n_{it} = 5$ (which ensures convergence in practice) and the number of channel realizations is set to $N_H = 5000$ for the prediction of SLA metrics, or average BLER.

Firstly, we investigate pure simulation performance for Matched LMMSE with exact SINR, Matched LMMSE with matched SINR and Mismatched LMMSE with mismatched SINR. Obviously, the gain brought by the Matched

LMMSE filter compare to its mismatched counterpart is all the more important when

$$\epsilon^{(0)} = \frac{n_t}{L_{ps}\sigma_{ps}^2 + N_0}$$

is larger. That is why, we assign a very low power $\sigma_{ps}^2 = 0.1$ and a normal power $\sigma_{ps}^2 = 1$ for comparison. Fig. 3.3 presents the simulation performance with $\sigma_{ps}^2 = 0.1$ under QPSK (from $\epsilon^{(0)} = 0.7191$ at $E_b/N_0 = -5dB$ to $\epsilon^{(0)} = 1.3712$ at $E_b/N_0 = 3dB$) from which we can observe that, at BLER=0.01, iteration 5, Matched LMMSE with matched SINR outperforms always Mismatched LMMSE with mismatched SINR with a gain about 2.5dB and it is only about 0.7dB away from the optimal matched LMMSE with exact SINR. Fig. 3.4 shows the simulation performance with $\sigma_{ps}^2 = 0.1$ under 16QAM (from $\epsilon^{(0)} = 1.3204$ at $E_b/N_0 = -1dB$ to $\epsilon^{(0)} = 1.6327$ at $E_b/N_0 = 10dB$) from which we can observe that, at BLER=0.01, iteration 5, Matched LMMSE with matched SINR outperforms Mismatched LMMSE with mismatched SINR with a gain about 3dB and it is only about 0.7dB away from the optimal matched LMMSE with exact SINR. Fig. 3.5 and Fig. 3.6 show the simulation performance with $\sigma_{ps}^2 = 1$ under QPSK (from $\epsilon^{(0)} = 0.1473$ at $E_b/N_0 = -5dB$ to $\epsilon^{(0)} = 0.1613$ at $E_b/N_0 = 1dB$) and 16QAM (from $\epsilon^{(0)} = 0.1624$ at $E_b/N_0 = -5dB$ to $\epsilon^{(0)} = 0.1660$ at $E_b/N_0 = 7dB$) respectively from which we can see that there are nearly no difference in terms of performance for the three approaches because the channel estimates are good enough ($\epsilon^{(0)} << 1$). Thus we can conclude that matched LMMSE with matched SINR approach outperforms always the mismatched LMMSE with mismatched SINR approach and keeps always a good approximation for the matched LMMSE with exact SINR. Thus, we focus on the performance prediction method for double loop receiver adopting Matched LMMSE with matched SINR approach in what follows.

Secondly, we evaluate the proposed performance prediction methods using Matched LMMSE with exact SINR or corrected SINR. Fig. 3.7 and Fig. 3.8 present the simulated performance vs. predicted performance using exact SINR and corrected SINR with $\sigma_{ps}^2 = 0.1$ for QPSK and 16QAM respectively. No surprisingly, we can see that the predicted performance with exact SINR is somehow optimist compare to the simulated performance with matched SINR at this case because the channel estimation is not very good. And this effect can be compensated by predicting with corrected SINR. Fig. 3.9 and Fig. 3.10 show the simulated performance vs. predicted performance using exact SINR and corrected SINR with $\sigma_{ps}^2 = 1$ for QPSK and

16QAM respectively. Since the channel estimation becomes good enough, both the predicted performance with exact SINR and corrected SINR match extremely well the simulated performance with matched SINR.

The previous approach shows the result for different $\epsilon^{(0)}$ by fixing σ_{ps}^2 while changing SNR (N_0). We can also generate different $\epsilon^{(0)}$ by fixing SNR (N_0) while changing σ_{ps}^2, and we can compare the simulated performance and predicted performance in this way in the next step. Fig. 3.11 / Fig. 3.12 show the simulated MSE/BLER (Matched LMMSE with exact SINR and Matched LMMSE with matched SINR) vs. the predicted MSE/BLER (Matched LMMSE with exact SINR) for QPSK, $E_b/N_0 = -1dB$. From these two figures, we can see that 1), again, Matched LMMSE with exact SINR outperforms always Matched LMMSE with matched SINR for all simulated $\epsilon^{(0)}$. 2), the predicted performance (matched LMMSE with exact SINR) becomes even optimist for simulated performance with matched LMMSE with exact SINR when $\epsilon^{(0)} > 2$ which implies that the Gaussian Approximation A6 becomes less valid. Furthermore, Fig. 3.13 / Fig. 3.14 show the simulated MSE/BLER (matched LMMSE with matched SINR) and the predicted MSE/BLER (Matched LMMSE with exact SINR and Matched LMMSE with corrected SINR) under QPSK, $E_b/N_0 = -1dB$ and $\epsilon^{(0)} \leq 2$ (A6 is more valid) from which we can see that the corrected SINR can give satisfied predicted results.

We move to 16QAM. Fig. 3.15 / Fig. 3.16 show the simulated MSE/BLER (Matched LMMSE with exact SINR and Matched LMMSE with matched SINR) and the predicted MSE/BLER (Matched LMMSE with exact SINR) for 16QAM, $E_b/N_0 = 3dB$. From these two figures, we can see that 1), the matched LMMSE with exact SINR outperforms always matched LMMSE with matched SINR for all simulated $\epsilon^{(0)}$. 2), Interestingly, when $\epsilon^{(0)} > 2$ which implies that the Gaussian Approximation A6 becomes less valid, the predicted performance (matched LMMSE with exact SINR) becomes just slightly optimist compare to the simulated performance (matched LMMSE with exact SINR) even $\epsilon^{(0)}$ increases to 30. Thus, Fig. 3.17 / Fig. 3.18 show the simulated MSE/BLER (Matched LMMSE with matched SINR) and the predicted MSE/BLER (Matched LMMSE with exact SINR and Matched LMMSE with corrected SINR) under 16QAM, $E_b/N_0 = 3dB$ and $\epsilon^{(0)} \leq 30$ from which we can see that the corrected SINR can give satisfied predicted results.

3.10 Conclusion

In this part, a novel semi-analytical performance prediction method is proposed for LEXTPR-based iterative LMMSE-IC detection and semi-blind channel estimation in convolutionally coded MIMO systems. The proposed method extends existing MIESM link-to-system approach to the context of imperfect channel state information and semi-blind channel estimation at the receiver side. It allows computing the average BLER conditional on an initial pilot assisted channel estimation and long term channel distribution information. It heavily relies on Gaussian approximation on the LMMSE-IC and channel estimation error models whose second order statistics are governed by the SINRs and the channel estimate MSE, respectively. Simulation in the context of SU-MIMO frequency selective transmission, modelled by a discrete input MIMO memoryless block fading Rayleigh channel, demonstrates the validity of the proposed approach.

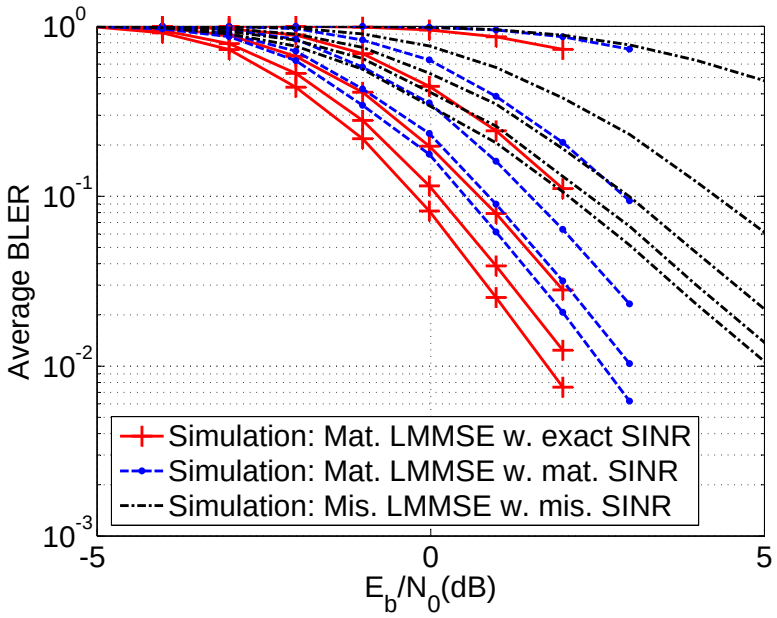

Figure 3.3: Simulated BLER comparison between Matched LMMSE with exact SINR, matched LMMSE with matched SINR and mismatched LMMSE with mismatched SINR, QPSK-1/2, $\sigma_{ps}^2 = 0.1$

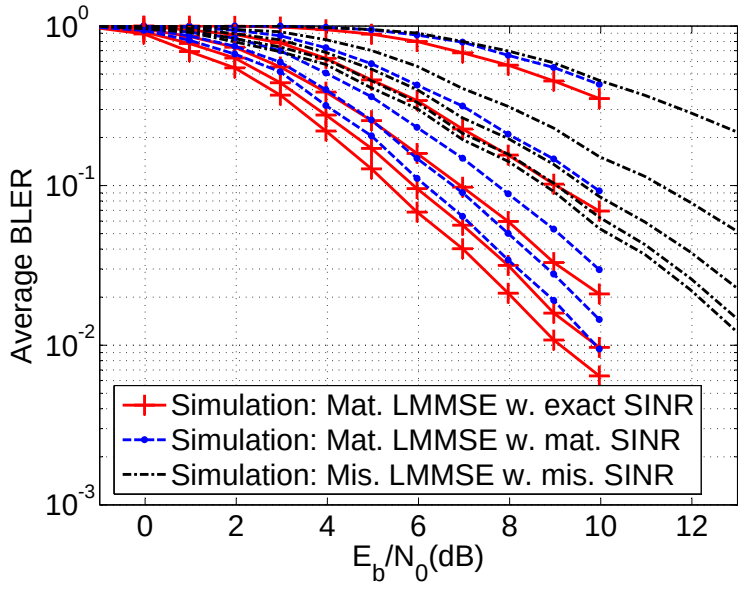

Figure 3.4: Simulated BLER comparison between Matched LMMSE with exact SINR, Matched LMMSE with matched SINR and Mismatched LMMSE with mismatched SINR, 16QAM-1/2, $\sigma_{ps}^2 = 0.1$

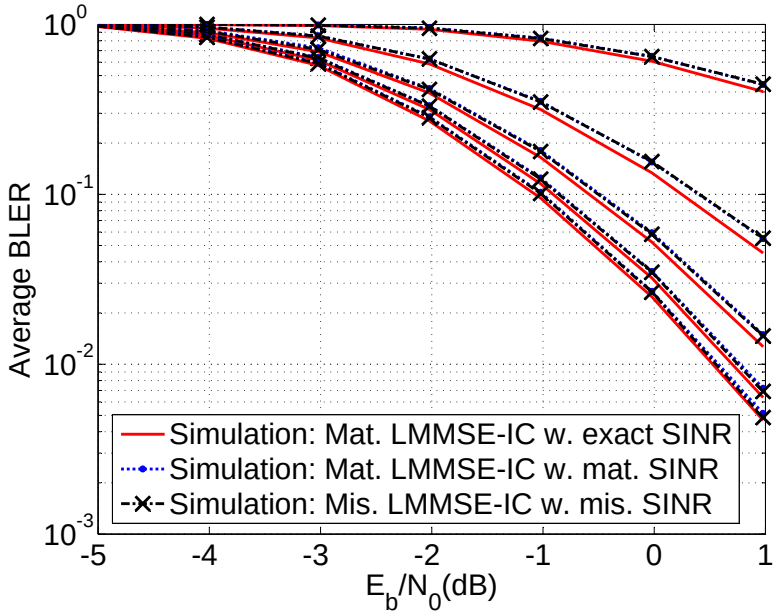

Figure 3.5: Simulated BLER comparison between Matched LMMSE with exact SINR, Matched LMMSE with matched SINR and Mismatched LMMSE with mismatched SINR, QPSK-1/2, $\sigma_{ps}^2 = 1$

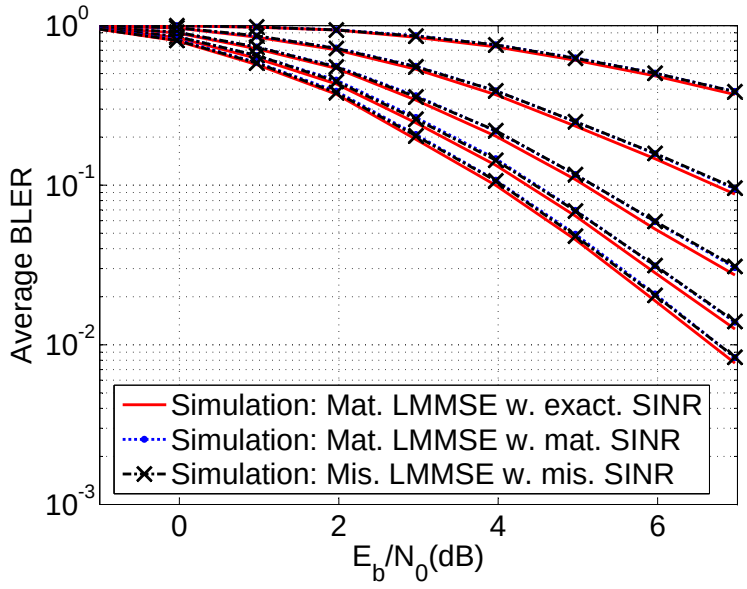

Figure 3.6: Simulated BLER comparison between Matched LMMSE with exact SINR, Matched LMMSE with matched SINR and Mismatched LMMSE with mismatched SINR, 16QAM-1/2, $\sigma_{ps}^2 = 1$

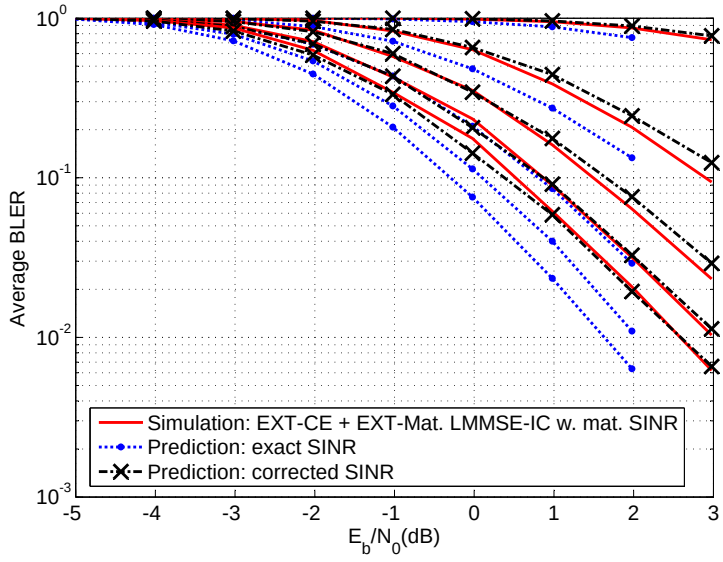

Figure 3.7: Simulated BLER (Matched LMMSE with matched SINR) vs. predicted BLER (Matched LMMSE with exact SINR and Matched LMMSE with corrected SINR), QPSK-1/2, $\sigma_{ps}^2 = 0.1$

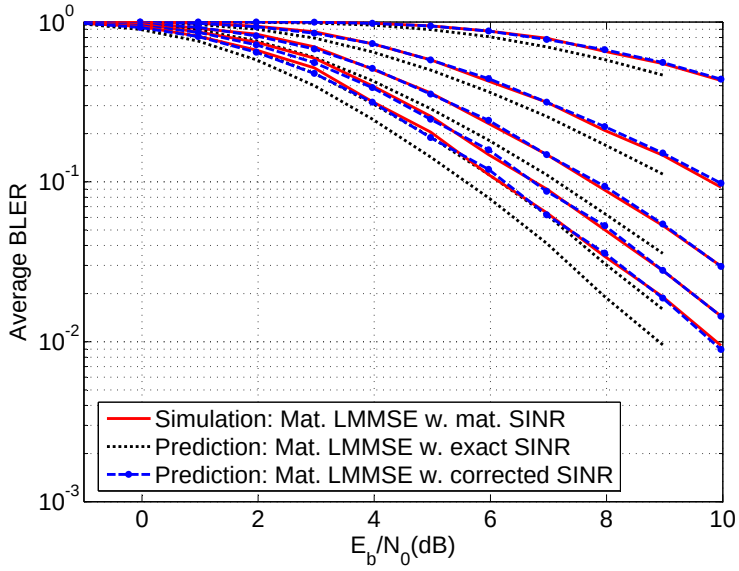

Figure 3.8: Simulated BLER (Matched LMMSE filter with matched SINR) vs. predicted BLER (Matched LMMSE with exact SINR and Matched LMMSE with corrected SINR), 16QAM-1/2, $\sigma_{ps}^2 = 0.1$

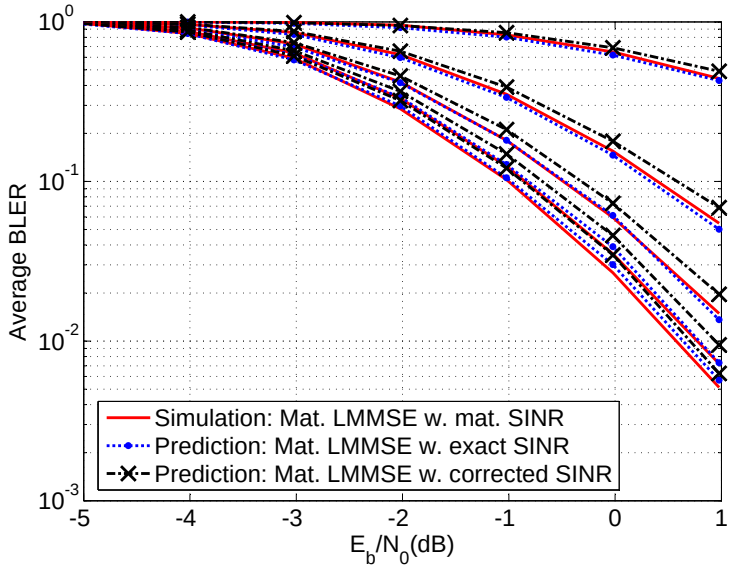

Figure 3.9: Simulated BLER (Matched LMMSE with matched SINR) vs. predicted BLER (Matched LMMSE with exact SINR and Matched LMMSE with corrected SINR), QPSK-1/2, $\sigma_{ps}^2 = 1$

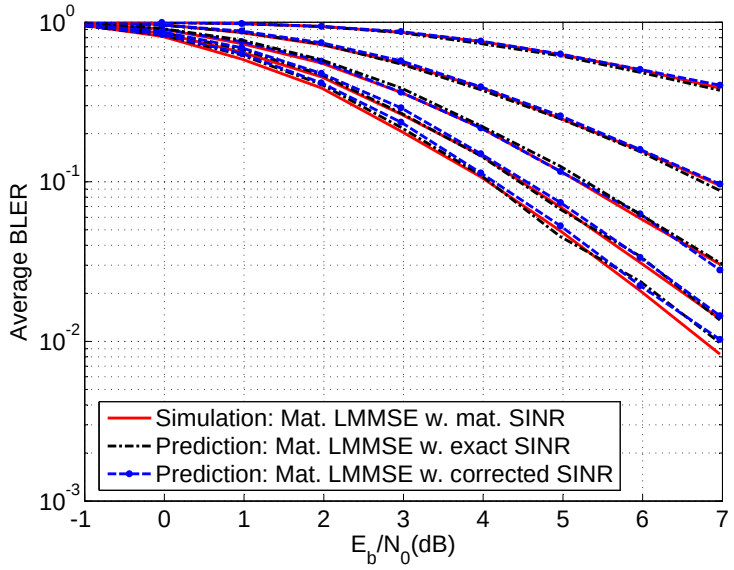

Figure 3.10: Simulated BLER (Matched LMMSE with matched SINR) vs. predicted BLER (Matched LMMSE with exact SINR and Matched LMMSE with corrected SINR), 16QAM-1/2, $\sigma_{ps}^2 = 1$

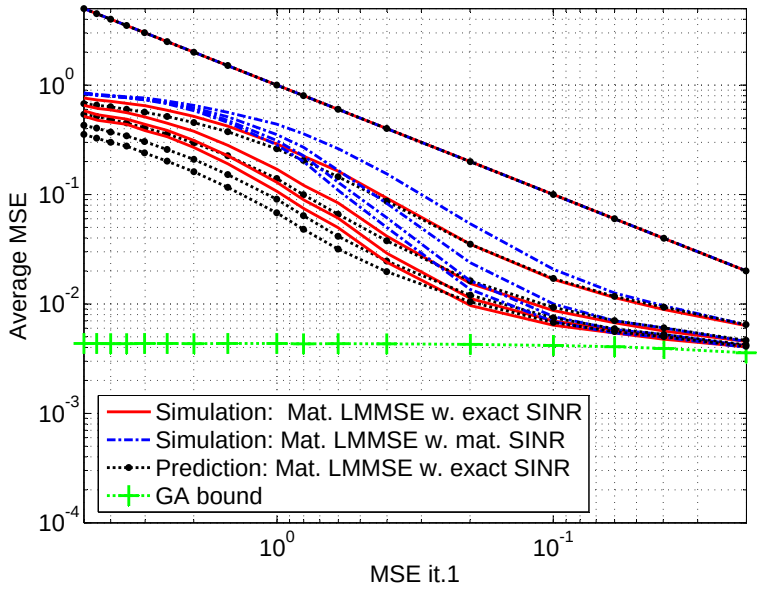

Figure 3.11: Simulated MSE(Matched LMMSE with exact SINR, Matched LMMSE with matched SINR) vs. predicted MSE (Matched LMMSE with exact SINR) conditional on initial $\epsilon^{(0)}$, QPSK-1/2, $E_b/N_0 = -1dB$

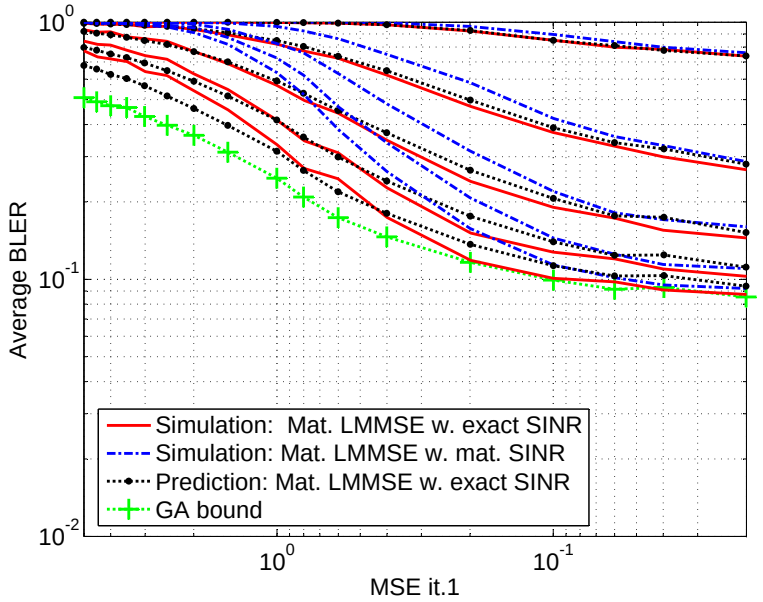

Figure 3.12: Simulated BLER(Matched LMMSE with matched SINR) vs. predicted BLER (Matched LMMSE with exact SINR and Matched LMMSE with corrected SINR) conditional on initial $\epsilon^{(0)}$, QPSK-1/2, $E_b/N_0 = -1dB$

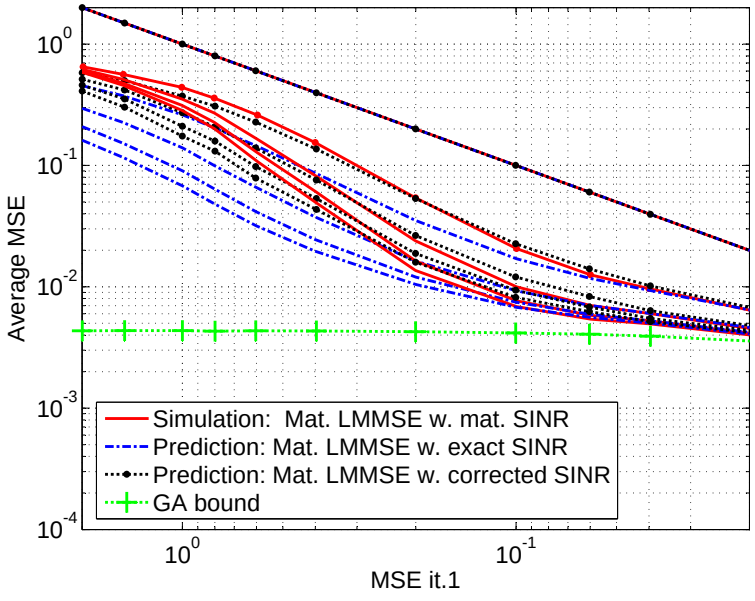

Figure 3.13: Simulated MSE(Matched LMMSE with matched SINR) vs. predicted MSE (Matched LMMSE with exact SINR and Matched LMMSE with corrected SINR) conditional on initial $\epsilon^{(0)}$, QPSK-1/2, $E_b/N_0 = -1dB$

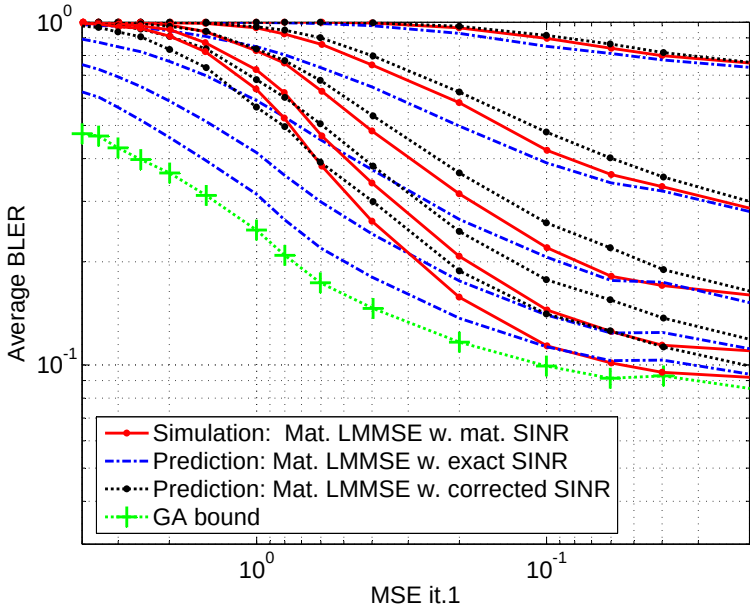

Figure 3.14: Simulated BLER(Matched LMMSE with matched SINR) vs. predicted BLER (Matched LMMSE with exact SINR and Matched LMMSE with corrected SINR) conditional on initial $\epsilon^{(0)}$, QPSK-1/2, $E_b/N_0 = -1dB$

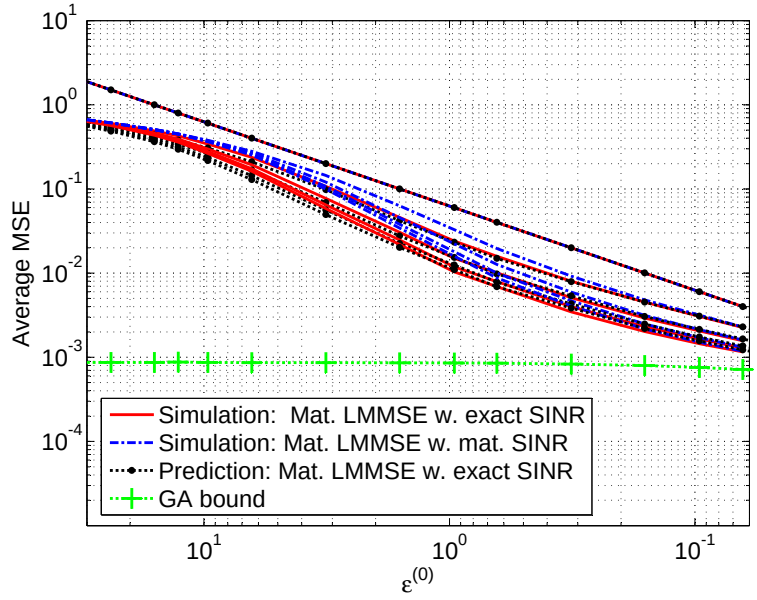

Figure 3.15: Simulated MSE(Matched LMMSE with exact SINR, Matched LMMSE with matched SINR) vs. predicted MSE (Matched LMMSE with exact SINR) conditional on initial $\epsilon^{(0)}$, 16QAM-1/2, $E_b/N_0 = 3dB$

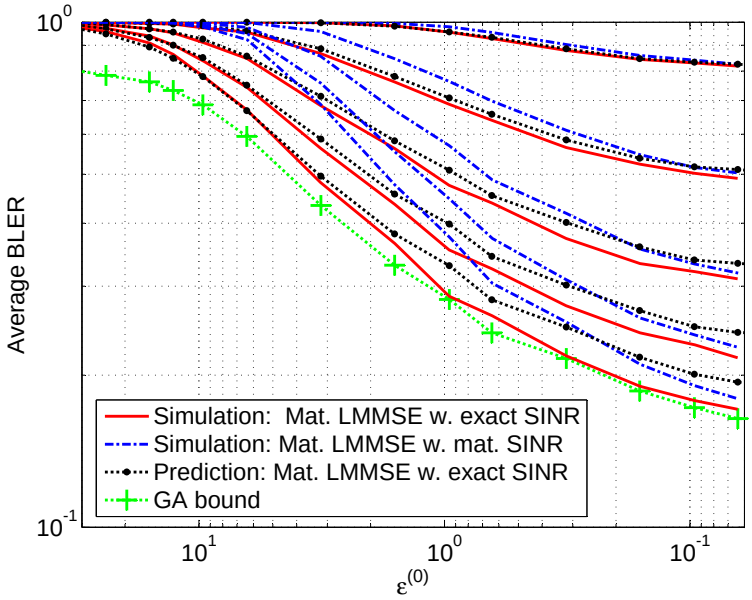

Figure 3.16: Simulated BLER(Matched LMMSE with exact SINR, Matched LMMSE with matched SINR) vs. predicted BLER (Matched LMMSE with exact SINR) conditional on initial $\epsilon^{(0)}$, 16QAM-1/2, $E_b/N_0 = 3dB$

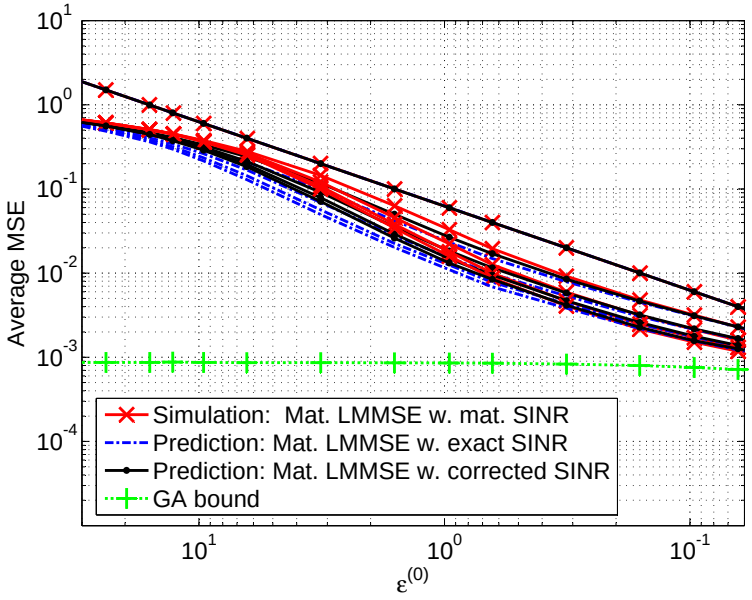

Figure 3.17: Simulated MSE(Matched LMMSE with matched SINR) vs. predicted MSE (Matched LMMSE with exact SINR and Matched LMMSE with corrected SINR) conditional on initial $\epsilon^{(0)}$, 16QAM-1/2, $E_b/N_0 = 3dB$

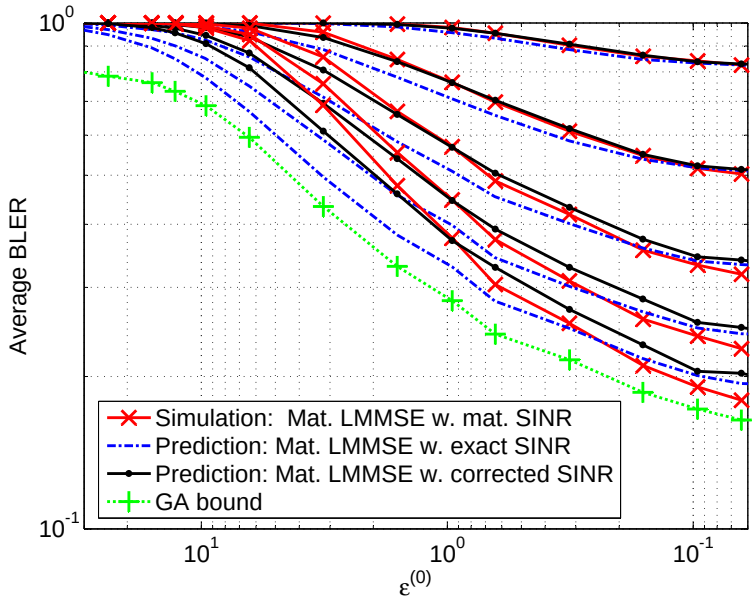

Figure 3.18: Simulated BLER(Matched LMMSE with matched SINR) vs. predicted BLER (Matched LMMSE with exact SINR and Matched LMMSE with corrected SINR) conditional on initial $\epsilon^{(0)}$, 16QAM-1/2, $E_b/N_0 = 3dB$

Chapter 4

Extension to turbo coded MIMO systems

4.1 Introduction

To make things even more complicated, closed-loop link adaptation in LTE-A involves a family of MCS constructed out of powerful turbo codes. In practice, a suboptimal iterative decoding is applied. Hence, the smooth introduction of LMMSE-IC based turbo equalization receivers in LTE calls for a new PHY-layer abstraction to this non-trivial situation. Progress in this research area is of uttermost importance for the design and real capability evaluation of next generation wireless systems in presence of advanced turbo receiver.

A novel stochastic modeling of the whole turbo receiver will be proposed using EXIT charts (and variants) [37] in this chapter. The approach is inspired from earlier works dealing with multiple concatenated codes and the convergence analysis of their iterative decoding (see e.g., [72] [49] [73] [74]). As the core of the contribution, it is found that, even in the simplified case of Gray mapping, a bivariate information transfer function is needed to characterize the evolution of the joint demapper and turbo decoder embedded within the LMMSE-IC based turbo equalization. This is in contrast with [71] [66] where simple convolutional codes were considered and univari-

This chapter is partially presented in the paper accepted to IEEE GLOBECOM'2013, one patent and two contributions of 3GPP

ate information transfer functions sufficient.

4.2 System model

We consider a single-user transmission over a MIMO block Rayleigh fading AWGN channel with n_b fading blocks, n_t transmit and n_r receive antennas. Perfect channel state information is assumed at the receiver. The total number n_s of channel uses available for transmission is fixed and the number of channel uses per fading block is given as $L = n_s/n_b$.

4.2.1 Coding strategy

A STBICM is used at the transmitter, specified by a linear binary *turbo code* $\mathscr{C}_\nu$ of rate r_ν, a complex constellation $\mathscr{X}_\nu \subset \mathbb{C}$ of cardinality 2^{q_ν} and a memoryless labeling rule μ_ν. We define the rate of the MCS ν as $\rho_\nu = r_\nu q_\nu$ (bits/complex dimension). The encoding process for MCS ν is detailed. The vector of binary data (or information bits) $\mathbf{u}$ enters a turbo encoder φ_ν whose output is the codeword $\mathbf{c} \in \mathscr{C}_\nu$ of length $n_{c,\nu} = n_s n_t q_\nu$. The codeword bits are interleaved by a random space time interleaver π_ν and reshaped as a integer matrice $\{\mathbf{D}_b\}_{b=1}^{n_b}$ with $\mathbf{D}_b \in \mathbb{Z}_{2^{q_\nu}}^{n_t \times L}$. Each integer entry can be decomposed into a sequence of q_ν bits. A Gray mapping μ_ν transforms each matrix $\mathbf{D}_b$ into a complex matrix $\mathbf{S}_b \in \mathscr{X}_\nu^{n_t \times L}$. $\mathscr{X}_{\nu,j}^{(0)}$ and $\mathscr{X}_{\nu,j}^{(1)}$ denote the subsets of points in $\mathscr{X}_\nu$ whose labels have a 0 or a 1 at position j. With a slight abuse of notation, let $\{d_{b;t,l,j}\}_{j=1}^{q_\nu}$ denote the set of bits labeling the symbol $s_{b;t,l} \in \mathscr{X}_\nu$. Let also $\mu_{\nu,j}^{-1}(s)$ be the value of the j-th bit in the labeling of any point $s \in \mathscr{X}_\nu$.

4.2.2 Received signal model

Let $\mathbf{H}_b \in \mathbb{C}^{n_r \times n_t}$ denotes the channel for the b-th fading block. The discrete-time vector $\mathbf{y}_{b;l} \in \mathbb{C}^{n_r}$ received at the destination for the b-th fading block and time $l = 1, \ldots, L$ is expressed as

$$\mathbf{y}_{b;l} = \mathbf{H}_b \mathbf{s}_{b;l} + \mathbf{w}_{b;l} \tag{4.1}$$

In (4.1), the vectors $\mathbf{s}_{b;l} \in \mathscr{X}_\nu^{n_t}$ are i.i.d. random vectors with $\mathbb{E}[\mathbf{s}_{b;l}] = \mathbf{0}_{n_t}$ and $\mathbb{E}[\mathbf{s}_{b;l}\mathbf{s}_{b;l}^\dagger] = \mathbf{I}_{n_t}$, and the vectors $\mathbf{w}_{b;l} \in \mathbb{C}^{n_r}$ are i.i.d. random vec-

tors, circularly-symmetric Gaussian, with zero-mean and covariance matrix $\sigma_w^2 \mathbf{I}_{n_r}$.

4.3 LMMSE-IC based turbo receivers

We focus on the LAPPR-based iterative LMMSE-IC algorithms for the mathematical derivation part. In LAPPR-based iterative LMMSE-IC, the set $\mathbf{\Lambda}_{D,DEC}$ of all LAPPR on coded bits becomes after interleaving the set $\mathbf{\Lambda}_{D,LE}$ of all log "a priori" probability ratios on labeling bits used for (soft) interference regeneration and cancellation, although LAPPR contain "observation". Let $\{\Lambda_{D,LE}\}_{s_{b;t,l}}$ and $\{\Lambda_{D,LE}\}_{\mathbf{s}_{b;l}}$ be the set of all LAPPR on coded bits involved in the labeling of $s_{b;t,l}$ and $\mathbf{s}_{b;l}$, respectively. Let also $\{\Lambda_{D,LE}\}_{\mathbf{s}_{b;l}\setminus s_{b;t,l}}$ be the set of all LAPPR on coded bits involved in the labeling of $\mathbf{s}_{b;l}$ *except* the coded bits involved in the labeling of $s_{b;t,l}$. Since the different steps described hereinafter are identical for each iteration of the receiver, the iteration index is dropped.

4.3.1 Interference regeneration and cancellation

Prior to LMMSE estimation of the symbol $s_{b;t,l}$, we compute the *conditional* MMSE estimate of the interference, defined as $\breve{\mathbf{y}}_{b;l\setminus t} = \mathbb{E}\left[\mathbf{y}_{b;l}|\{\Lambda_{D,LE}\}_{\mathbf{s}_{b;l}\setminus s_{b;t,l}}\right]$. This computation is intractable for useful signal components and noise samples are of course no more independent conditional on $\{\Lambda_{D,LE}\}_{\mathbf{s}_{b;l}\setminus s_{b;t,l}}$. To solve this issue, we make two symplifying assumptions.
A1 The pdf $p_{\mathbf{s}_{b;l},\mathbf{w}_{b;l}|\{\Lambda_{D,LE}\}_{\mathbf{s}_{b;l}\setminus s_{b;t,l}}}(\mathbf{s}_{b;l},\mathbf{w}_{b;l})$ factorizes as

$$\begin{aligned} &p_{\mathbf{s}_{b;l},\mathbf{w}_{b;l}|\{\Lambda_{D,LE}\}_{\mathbf{s}_{b;l}\setminus s_{b;t,l}}}(\mathbf{s}_{b;l},\mathbf{w}_{b;l}) = \\ &P(s_{b;t,l})p_{\mathbf{w}_{b;l}}(\mathbf{w}_{b;l})\prod_{t'\neq t}P(s_{b;t',l}|\{\Lambda_{D,LE}\}_{s_{b;t',l}}). \end{aligned} \tag{4.2}$$

A2 The pmf $P(s_{b;t',l}|\{\Lambda_{D,LE}\}_{s_{b;t',l}})$ in (4.2) is given by

$$P(s_{b;t',l}|\{\Lambda_{D,LE}\}_{s_{b;t',l}}) \propto e^{\sum_j \mu_{\nu,j}^{-1}(s_{b;t',l})\Lambda_{D,LE}(d_{b;t',l,j})}.$$

As a matter of fact, the assumptions (A1) and (A2) never hold even for an ideal interleaver of infinite depth. But we can still force them in all subsequent derivations. Under (A1), the MMSE estimate of the interference

affecting the symbol $s_{b;t,l}$ is given by

$$\tilde{\mathbf{y}}_{b;l\backslash t} = \mathbf{H}_b(\mathbf{I}_{n_t} - \mathbf{e}_t\mathbf{e}_t^\dagger)\mathbf{m}_{b;l} \tag{4.3}$$

where $\mathbf{m}_{b;l}$ is the vector made of all estimates $m_{b;t',l} = \mathbb{E}\left[s_{b;t',l}|\{\Lambda_{D,LE}\}_{s_{b;t',l}}\right]$ evaluated under (A2). After IC, the new observed vector is $\mathbf{y}_{b;l} - \tilde{\mathbf{y}}_{b;l\backslash t}$.

4.3.2 LMMSE estimation – unconditional case

The optimization problem to solve can be formulated as follows: Find $\breve{s}_{b;t,l} = \breve{\mathbf{f}}_{b;t}^\dagger(\mathbf{y}_{b;l} - \breve{\mathbf{y}}_{b;l\backslash t})$ minimizing the *unconditional* mean square error (MSE) $\mathbb{E}\left[|\breve{s}_{b;t,l} - s_{b;t,l}|^2\right]$ defined as

$$\mathbb{E}\left[\mathbb{E}\left[|\breve{s}_{b;t,l} - s_{b;t,l}|^2|\{\Lambda_{D,LE}\}_{\mathbf{s}_{b;l}\backslash s_{b;t,l}}\right]\right]. \tag{4.4}$$

The outer expectation in (4.4) renders the (biased) LMMSE filter time-invariant given by $\breve{\mathbf{f}}_{b;t} = \breve{\mathbf{\Xi}}_{b;t}^{-1}\breve{\boldsymbol{\xi}}_{b;t}$ where $\breve{\boldsymbol{\xi}}_{b;t} = \mathbb{E}\left[\breve{\boldsymbol{\xi}}_{b;t,l}\right]$ with

$$\breve{\boldsymbol{\xi}}_{b;t,l} = \mathbb{E}\left[(\mathbf{y}_{b;l} - \breve{\mathbf{y}}_{b;l\backslash t})s_{b;t,l}^*|\{\Lambda_{D,LE}\}_{\mathbf{s}_{b;l}\backslash s_{b;t,l}}\right]$$

and where $\breve{\mathbf{\Xi}}_{b;t} = \mathbb{E}\left[\breve{\mathbf{\Xi}}_{b;t,l}\right]$ with

$$\breve{\mathbf{\Xi}}_{b;t,l} = \mathbb{E}\left[(\mathbf{y}_{b;l} - \breve{\mathbf{y}}_{b;l\backslash t})(\mathbf{y}_{b;l} - \breve{\mathbf{y}}_{b;l\backslash t})^\dagger|\{\Lambda_{D,LE}\}_{\mathbf{s}_{b;l}\backslash s_{b;t,l}}\right].$$

The computation of $\breve{\mathbf{f}}_{b;t}$ is again intractable. However, under (A1), $\breve{\boldsymbol{\xi}}_{b;t}$ and $\breve{\mathbf{\Xi}}_{b;t}$ become $\boldsymbol{\xi}_{b;t} = \mathbf{h}_{b;t} = \mathbf{H}_b\mathbf{e}_t$ and $\mathbf{\Xi}_{b;t} = \mathbf{H}_b\mathbf{V}_{b;\backslash t}\mathbf{H}_b^\dagger + \sigma_w^2\mathbf{I}_{n_r}$ where $\mathbf{V}_{b;\backslash t}$ is the *unconditional* symbol covariance matrix defined as

$$\mathbf{V}_{b;\backslash t} = \mathrm{diag}\{v_{b;1}, \ldots, v_{b;t-1}, 1, v_{b;t+1}, \ldots, v_{b;n_t}\}$$

where $\forall t' \neq t$, $v_{b;t'} = \mathbb{E}\left[v_{b;t',l}\right]$ with $v_{b;t',l} = \mathbb{E}\left[|s_{b;t',l} - m_{b;t',l}|^2|\{\Lambda_{D,LE}\}_{s_{b;t',l}}\right]$ evaluated under (A2). Using the matrix inversion lemma, we obtain the filter

$$\mathbf{f}_{b;t} = \frac{1}{1 + \eta_{b;t}(1 - v_{b;t})}\mathbf{\Sigma}_b^{-1}\mathbf{h}_{b;t} \tag{4.5}$$

where $\mathbf{\Sigma}_b = \mathbf{H}_b\mathbf{V}_b\mathbf{H}_b^\dagger + \sigma_w^2\mathbf{I}_{n_r}$ and $\eta_{b;t} = \mathbf{h}_{b;t}^\dagger\mathbf{\Sigma}_b^{-1}\mathbf{h}_{b;t}$ with

$$\mathbf{V}_b = \mathbf{V}_{b;\setminus t} - (1 - v_{b;t})\mathbf{e}_t\mathbf{e}_t^\dagger \tag{4.6}$$

where $v_{b;t} = \mathbb{E}\left[v_{b;t,l}\right]$ with $v_{b;t,l} = \mathbb{E}\left[|s_{b;t,l} - m_{b;t,l}|^2|\{\Lambda_{D,LE}\}_{s_{b;t,l}}\right]$ evaluated under (A2). The corresponding estimate $\hat{s}_{b;t,l}$ of $s_{b;t,l}$ can be expressed as

$$\hat{s}_{b;t,l} = \mathbf{f}_{b;t}^\dagger(\mathbf{y}_{b;l} - \tilde{\mathbf{y}}_{b;l\setminus t}) = g_{b;t}s_{b;t,l} + \zeta_{b;t,l} \tag{4.7}$$

where $g_{b;t} = \mathbf{f}_{b;t}^\dagger\mathbf{h}_{b;t}$ and $\zeta_{b;t,l}$ is the residual interference plus noise term. Clearly, $\zeta_{b;t,l}$ in (4.7) is zero-mean and uncorrelated with the useful signal $s_{b;t,l}$ under (A1), i.e., $\mathbb{E}[s_{b;t,l}\zeta_{b;t,l}^*] = 0$. Under (A1) and (A2) the variance of $\zeta_{b;t,l}$ is $\varsigma_{b;t} = g_{b;t}(1 - g_{b;t})$. Thus, we can define the *unconditional* SINR under (A1) and (A2) as

$$\gamma_{b;t} = \frac{g_{b;t}}{1 - g_{b;t}} = \frac{\eta_{b;t}}{1 - \eta_{b;t}v_{b;t}}. \tag{4.8}$$

In practical implementation, we make several assumptions over the covariance matrices $\mathbf{V}_b$.

A3 Due to the particular structure of the MCS, the so-called *equal variance assumption* holds, which states that

$$\mathbf{V}_b = v\mathbf{I}_{n_t}\forall b. \tag{4.9}$$

A4 v can be replaced by its empirical mean $\bar{v}$

$$\bar{v} = \frac{1}{n_b n_t L}\sum_{b=1}^{n_b}\sum_{t=1}^{n_t}\sum_{l=1}^{L} v_{b;t,l}. \tag{4.10}$$

assuming sufficiently large L. Actually, the ergodic regime assumption (A4) is part of the baseline assumptions of EXIT charts [37]. The assumption (A3) never holds even for an ideal interleaver of infinite depth, but forcing it induces no performance degradation.

4.3.3 Demapping and decoding

The estimate $\hat{s}_{b;t,l}$ is used as a *decision statistic* to compute the LEXTPR on the q_ν bits involved in the labeling of $s_{b;t,l}$.
A5 In (4.7), the conditional pdf $p_{\hat{s}_{b;t,l}|s_{b;t,l}}(\hat{s}_{b;t,l})$ is circularly-symmetric complex Gaussian distributed.
Under (A1), (A2) and (A5) the conditional pdf $p_{\hat{s}_{b;t,l}|s_{b;t,l}}(\hat{s}_{b;t,l})$ is $\mathcal{N}_{\mathbb{C}}(g_{b;t}s_{b;t,l}, \varsigma_{b;t})$. As a result, under (A1),(A2), and (A5), for the *special case* of Gray labeling, the LEXTPR $\Lambda_{E,DEM}(d_{b;t,l,j})$ on labeling bit $d_{b;t,l,j}$ is expressed as

$$\Lambda_{E,DEM}(d_{b;t,l,j}) = \frac{\sum_{s \in \mathscr{X}_{\nu,j}^{(1)}} e^{-|\hat{s}_{b;t,l} - g_{b;t}s|^2/\varsigma_{b;t}}}{\sum_{s \in \mathscr{X}_{\nu,j}^{(0)}} e^{-|\hat{s}_{b;t,l} - g_{b;t}s|^2/\varsigma_{b;t}}} \tag{4.11}$$

4.3.4 Message-passing schedule for turbo decoding

The set $\mathbf{\Lambda}_{E,DEM}$ of all LEXTPR on labeling bits becomes after deinterleaving the set $\mathbf{\Lambda}_{I,DEC}$ of all log intrinsic probability ratios on coded bits used as input for the decoder.
A6 The pdf $p_{\mathbf{\Lambda}_{I,DEC}|\mathbf{c}}(\mathbf{\Lambda}_{I,DEC})$ factorizes as

$$p_{\mathbf{\Lambda}_{I,DEC}|\mathbf{c}}(\mathbf{\Lambda}_{I,DEC}) = \prod_{n=1}^{n_{c,\nu}} p_{\Lambda_{I,DEC}(c_n)|c_n}(\Lambda_{I,DEC}(c_n))$$

where $\Lambda_{I,DEC}(c_n)$ is the log intrinsic probability ratio on coded bit c_n. The assumption (A6) allows to simplify the decoding task. It is rightfully confirmed for an interleaver of finite, but large enough, depth. The turbo decoder is made of *two* BCJR decoders [38] exchanging probabilistic information (log domain). The first BCJR decoder computes the LAPPRs on its own coded bits (information and parity bits) taking into account the available a priori information $\mathbf{\Lambda}_{A,DEC} = \{\Lambda_{A,DEC}(u_n)\}$ on systematic information bits stored from an earlier activation (i.e., the most recent LEXTPRs on systematic information bits delivered by the second BCJR decoder). Then the second BCJR decoder is activated and computes the LAPPRs on its own coded bits (information and parity bits) taking into account the available a priori information transmitted by the first BCJR decoder. The best schedule we have found is the following: one pass of equalizer followed by one

pass of first BCJR decoder followed by one pass of second BCJR decoder. This completes one global iteration of the turbo receiver. Such a message-passing schedule provides much better results than the conventional one, i.e., a single pass of equalizer followed by an arbitrary number of turbo decoder iterations. The performance degradation which comes from *not* using the extrinsic information available from the second BCJR decoder as an input of the first BCJR decoder as in [96] might be *substantial*, especially for low rate MCS, or slightly modified message-passing schedules with several internal iterations within the turbo decoder per global iteration. The different steps of the algorithm are summarized in Fig. 4.1 for the 1-block fading case.

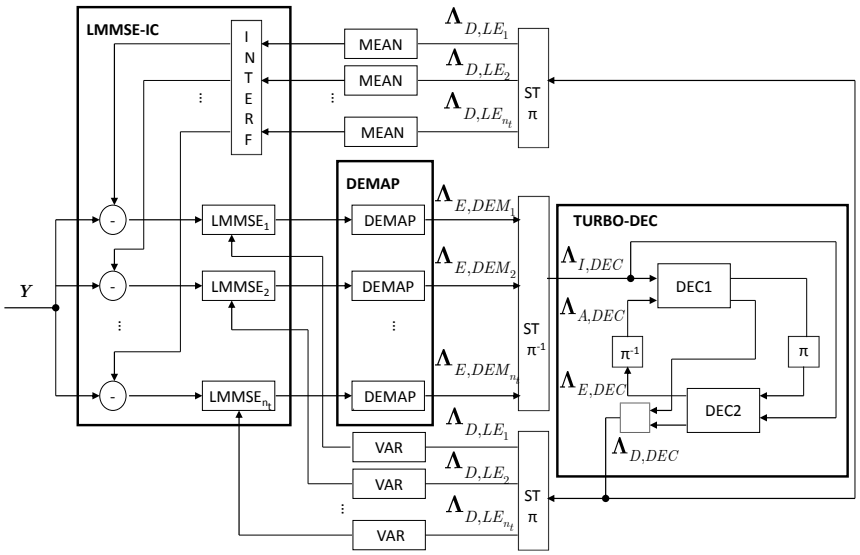

Figure 4.1: LAPPR-based iterative LMMSE receiver structure (adapted to STBICM with turbo code and Gray labeling)

4.4 PHY-layer abstraction

The proposed performance prediction method is semi-analytical and relies on ten Brink's stochastic approach of EXIT charts [37] particularly useful in understanding and measuring the dynamics of turbo processing.

4.4.1 Transfer characteristics of LMMSE-IC

The LMMSE-IC part of the receiver ends up with $n_b \times n_t$ independent parallel channels under (A6). Each of them is modeled as a discrete-input AWGN channel under (A5) whose SNR, given by

$$\gamma_{b;t} = \frac{\eta_{b;t}}{1 - \eta_{b;t}\bar{v}} \tag{4.12}$$

under (A1)-(A4), turns out to be a function ϕ_t of b, t, $\mathbf{H}_b$, σ_w^2 and the input variance $\bar{v}$. For each such channel, we can compute the AMI $I_{LE_{b;t}}$ between the discrete input $s_{b;t,l} \in \mathscr{X}_\nu$ and the output $\tilde{s}_{b;t,l} = s_{b;t,l} + \epsilon_{b;t,l}$ with $\epsilon_{b;t,l} \sim \mathcal{N}_{\mathbb{C}}(0, 1/\gamma_{b;t})$. The value of $I_{LE_{b;t}}$ depends on the single parameter $\gamma_{b;t}$. Let $\bar{I}_{LE}$ be the arithmetic mean of the values $\{I_{LE_{b;t}}\}$, i.e.,

$$\bar{I}_{LE} = \frac{1}{n_b n_t} \sum_{b=1}^{n_b} \sum_{t=1}^{n_t} I_{LE_{b;t}}. \tag{4.13}$$

The AMI $I_{LE_{b;t}} = \psi_\nu(\gamma_{b;t})$ is a monotone increasing, thus invertible, function of the SNR, and depends on the MCS index ν. It is simulated off-line and stored in a LUT.

4.4.2 Transfer characteristics of joint demapping and decoding

The functional module is MCS-dependent and comprises the following steps: demapping, deinterleaving, turbo decoding (one pass of the first *BCJR decoder* followed by one pass of the second *BCJR decoder*), reinterleaving, and computation of the mean and variance of transmitted symbols from LAPPR on coded bits(as described before). The generated observed symbols are the output of a virtual AWGN channel with discrete input in $\mathscr{X}_\nu$ and SNR γ. Let $\psi_{BPSK}(\gamma)$ be the Binary Phase-Shift Keying (BPSK) mutual information for a (real) AWGN channel whose associated SNR is γ. The a priori information $\{\Lambda_{A,DEC}(u_n)\}$, measured by mutual information I_A, are generated as $\Lambda_{A,DEC}(u_n) = \mathcal{N}((2u_n - 1)m_A, \sigma_A^2)$ where $\sigma_A^2 = 4\psi_{BPSK}^{-1}(I_A)$, $m_A = \sigma_A^2/2$ [37]. For an arbitrary labeling rule, trivariate transfer function is required to stochastically characterize the joint demapper and turbo decoder. With Gray labeling however, log a priori probability ratios on

labeling bits do not intervene in the computation of the LEXTPR on the labeling bits (see (4.11)) and, hence, need not be taken into account in the stochastic modeling of the demapper. Therefore, simpler bivariate transfer function is sufficient to stochastically characterize the joint demapper and turbo decoder for the latter proceeds iteratively. This is the major difference with previous work. These functions are the measured BLER $P_e = F_{JDD_\nu}(\gamma, I_A)$, the variance $\bar{v} = G_{JDD_\nu}(\gamma, I_A)$, and the mutual information $I_E = T_{JDD_\nu}(\gamma, I_A)$. They are computed off-line and stored in separate LUTs. It is necessary to emphasize that the LUTs are generated with channel use number fixed to n_s, thus are independent with the number of fading block. The algorithm used to generate the different LUTs is summarized in Algorithm 5.

Algorithm 5

Inputs ν, n_t, n_s
for $\gamma = \gamma_{min}$ to γ_{max} **do**
  for $I_A = 0$ to 1 **do**
    $\sigma_A^2 = 4\psi_{BPSK}^{-1}(I_A)$, $m_A = \sigma_A^2/2$
    for $bk = 1$ to n_{bk} **do**
      Channel interleaver random generation: π_ν
      Codeword generation: $\mathbf{u} \rightarrow \mathbf{c} \rightarrow \mathbf{D} \rightarrow \mathbf{S}$
      Virtual AWGN Channel: Generate $\tilde{\mathbf{S}}$ s.t. $\tilde{s}_{1;t,l} \sim \mathcal{N}_{\mathbb{C}}(s_{1;t,l}, 1/\gamma)$
      Demapping: Compute $\{\Lambda_{E,DEM}(d_{1;t,l,j})\}$ as (4.11) with $\hat{s}_{1;t,l} = \tilde{s}_{1;t,l}$ and $g_{1;t} = 1$
      Deinterleaving: $\mathbf{\Lambda}_{E,DEM} \rightarrow \mathbf{\Lambda}_{I,DEC}$
      Generate $\{\Lambda_{A,DEC}(u_n)\}$ with $\Lambda_{A,DEC}(u_n) = \mathcal{N}((2u_n - 1)m_A, \sigma_A^2)$
      Turbo decoding: Compute $\{\Lambda_{D,DEC}(c_n)\}$ and $\Lambda_{E,DEC}(u_n)\}$ based on $\{\Lambda_{I,DEC}(c_n)\}$ and $\{\Lambda_{A,DEC}(u_n)\}$
      Update counter block errors
      Interleaving: $\mathbf{\Lambda}_{D,DEC} \rightarrow \mathbf{\Lambda}_{D,LE}$
      Update histograms $H_{\Lambda_E|0}$ and $H_{\Lambda_E|1}$
      Compute $\{v_{1;t,l}\}$ using $\{\{\Lambda_{D,LE}\}_{s_{1;t,l}}\} \rightarrow \{\bar{v}_{bk}\}$ as (4.10)
    end for
    Compute P_e, $\bar{v} = \frac{1}{n_{bk}} \sum_{bk=1}^{n_{bk}} \bar{v}_{bk}$ and I_E using pdfs $p_{\Lambda_E|0}$ and $p_{\Lambda_E|1}$
  end for
end for
Outputs $P_e = F_{JDD_\nu}(\gamma, I_A)$, $\bar{v} = G_{JDD_\nu}(\gamma, I_A)$, and $I_E = T_{JDD_\nu}(\gamma, I_A)$

4.4.3 Evolution analysis

It remains to relate the output $\bar{I}_{LE}$ of the first transfer function (LMMSE-IC) and the input SNR of the second transfer function (joint demapping and decoding) at any iteration. This is done by assuming that $\bar{I}_{LE}$ which measures the information content of knowledge on coded modulated symbols $\{s_{b;t,l}\}$, averaged over all parallel AWGN channels, is equal to the information content of knowledge on coded modulated symbols transmitted over a *single* virtual discrete-input (with values in $\mathscr{X}_\nu$) AWGN channel with effective SNR $\bar{\gamma}_{LE}$ given by

$$\bar{\gamma}_{LE} = \psi_\nu^{-1}(\bar{I}_{LE}) = \psi_\nu^{-1}\left(\frac{1}{n_b n_t}\sum_{b=1}^{n_b}\sum_{t=1}^{n_t} I_{LE_{b;t}}\right). \tag{4.14}$$

This technique inherited from EXIT charts is widely used in practice and often referred to as MIESM [61]. In our framework, it relies on all the defined assumptions (A1)-(A6) or, equivalently, on (A5) and (A6) for the first iteration. The variance $\bar{v} = G_{JDD_\nu}(\bar{\gamma}_{LE}, I_A)$ is used in (4.9) under (A4) for next iteration. Hence, the evolution of LAPPR-based iterative LMMSE-IC can be tracked through the single scalar parameter $\bar{v}$.

4.4.4 Calibration

A major drawback of this performance prediction method is that the assumptions (A1), (A2) and (A3) do not hold for LAPPR-based iterative LMMSE-IC. As a consequence, not only the filters $\{\mathbf{f}_{b;t}\}$ but also the SINRs $\{\gamma_{b;t}\}$ given by (4.8) are approximated. The true SINRs, if we could have to access to them, would be smaller. This fact explains why the prediction performance method expounded in [66] yields too optimistic results compared to the true simulated performance. To solve this problem, we proposed in [97] a simple, yet effective, calibration procedure whose principle is to adjust $\bar{v}$ with a real-valued factor $\beta_\nu \geq 1$. More specifically, $\bar{v}$ is replaced by $C_\nu(\bar{v}) = \min(\beta_\nu \bar{v}, 1)$, which has the effect to artificially reduce the SINRs that are used in the performance prediction method. We searched the optimal β_ν minimizing the average relative error between the simulated BLER and the calibrated predicted BLER over a large number of channel outcomes at each iteration $i > 1$ for the BLER range of interest $[0.9, 0.01]$. In order to ensure that the calibration factor cope with a large distribution of channel

outcomes (or SINR distribution per block), we draw each channel outcome from a 4x4 MIMO 4-block Rayleigh fading AWGN channel. Exhaustive simulations revealed that β_ν depends on the MCS but does not vary significantly w.r.t. the number of transmit and receive antennas as well as the channel characteristics. The calibration procedures can be found in Section 2.4.2.4. A recapitulative diagram of the method is depicted in Fig. 4.2 for the 1-block fading case.

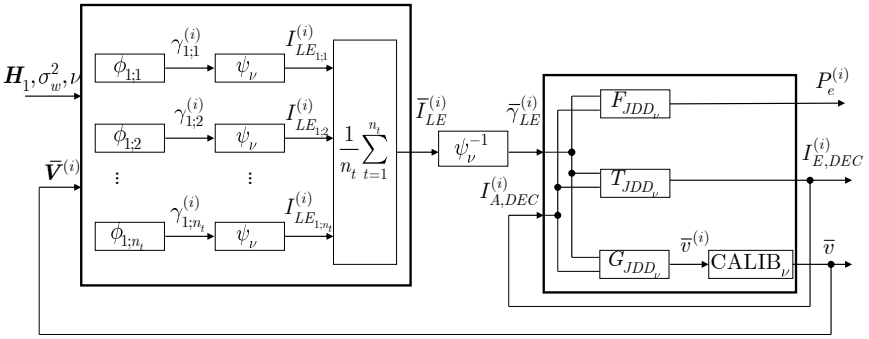

Figure 4.2: PHY-layer abstraction for LAPPR-based iterative LMMSE-IC (with calibration)

4.5 Numerical results

The proposed PHY-layer abstraction is tested over two types of channels: 4×4 MIMO flat channel (i.e., $n_b = 1$) and 2×2 MIMO 4-block fading channel (i.e., $n_b = 4$), referred to as CH1 and CH2, respectively. The MCS are built from turbo code based on two 8-state rate-1/2 Recursive Systematic Convolutional (RSC) encoders with generator matrix $\mathbf{G} = [1, \mathbf{g}_0/\mathbf{g}_1]$ where $\mathbf{g}_0 = [1011]$ and $\mathbf{g}_1 = [1101]$ and QAM modulation (with Gray labeling). When LEXTPR-based iterative LMMSE-IC is performed at the destination, no calibration is needed because assumptions (A1)–(A6) are rigorously valid. When LAPPR-based iterative LMMSE-IC is performed at the destination, a channel-independent calibration factor is introduced to compensate for assumption inaccuracies. The optimal calibration factors for QPSK-1/2 and 16QAM-1/2 are 1.7 and 3.3, respectively. The total number of channel uses available for transmission is $n_s = 2040$. Generally, 5 iterations are enough to ensure the convergence in practice. Fig. 4.3 depicts the 2D-LUT

$P_e = F_{JDD}(\gamma, I_A)$ for the 16QAM-1/2.

4.5.1 Average predicted vs. simulated BLER

First, average simulated and predicted BLER are compared over several SNR. For each SNR, we evaluated the average simulated BLER by Monte Carlo simulation which is stopped after 800 block errors. The predicted BLER is evaluated over 10000 channel outcomes. The genie-aided interference cancellation (Genie-Aided IC) curve is used as a lower bound on BLER. From Fig. 4.4, we observe that the simulated and predicted BLER of LEXTPR-based iterative LMMSE-IC coincide perfectly for 16QAM-1/2 over CH1. Furthermore, the performance degradation coming from no using the extrinsic information available from the second BCJR decoder is aroud 3dB at BLER=0.1 of the 5-th iteration. From Fig. 4.5, we observe that the simulated and predicted (with calibration) BLER of LAPPR-based iterative LMMSE-IC reveal a very good match for 16QAM-1/2 over CH1 which confirms the robustness and effectiveness of the proposed calibration procedure. The superiority of LAPPR-based iterative LMMSE-IC over LEXTPR-based iterative LMMSE-IC is obvious from these two curves, and is even more apparent for higher spectral efficiencies. The simulated and predicted results for QPSK - 1/2 and 16QAM - 1/2 over CH2 of LAPPR-based iterative LMMSE-IC are shown in Fig. 4.6 and Fig. 4.7, respectively. Again, we observe that the average predicted BLER match exactly the average simulated ones at every iterations.

4.5.2 Instantaneous predicted vs. simulated BLER

The instantaneous (conditional on a given channel outcome) simulated and predicted BLER for a large number of channel outcomes gives further insights into the accuracy of our prediction method. We generate randomly 200 channels over several SNR. For each channel outcome, the simulation is activated only if its instantaneous predicted BLER is between 0.9 and 0.01 at the considered iteration. This helps to capture the region of interest [0.9, 0.01] for all iterations. For each channel outcome, Monte Carlo simulation is stopped after 100 block errors. Then the predicted and simulated instantaneous BLER of this channel are plotted versus the effective SINR of the first iteration in the same figure. The results of iteration 1,2 and 5

for QPSK - 1/2 and 16QAM - 1/2 over CH2 are shown in Fig. 4.8 and Fig. 4.9, respectively. We observe that the instantaneous predicted BLER match quite exactly the instantaneous simulated ones at all iterations.

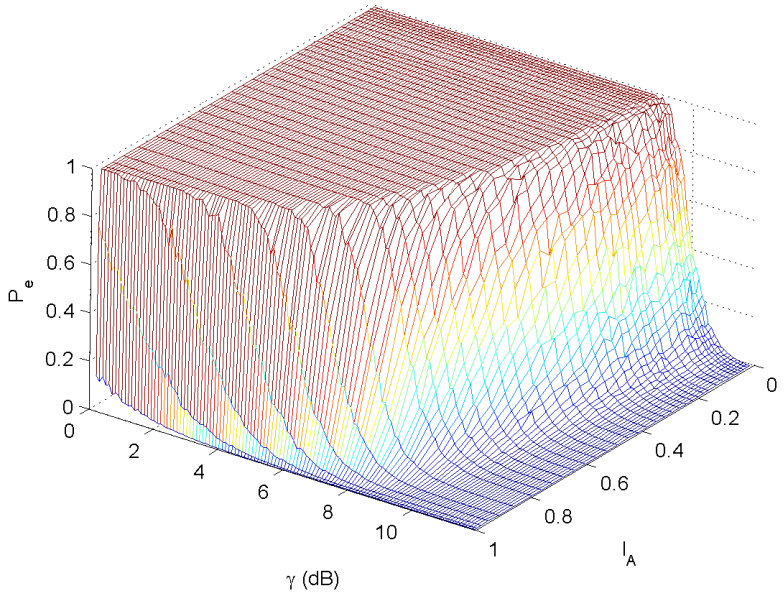

Figure 4.3: 2D-LUT for F_{JDD} of chosen MCS 16QAM-1/2

4.6 Conclusion

This chapter has addressed the issue of abstracting LMMSE-IC based turbo receivers assuming powerful turbo coded modulations at the transmitter. A stochastic modeling of the whole turbo receiver based on EXIT charts (and variants) has been proposed. Its effectiveness has been demonstrated through Monte Carlo simulations in a variety of transmission scenarios. The approach can be easily extended to other types of compound codes (e.g., serially concatenated codes, LDPC codes) and channel models (e.g., MIMO block fading) or used to predict convergence thresholds for a given channel outcome. More importantly, the approach may constitute the core of advanced link adaptation and RRM procedures in closed-loop coded MIMO systems employing LMMSE-IC based turbo receivers.

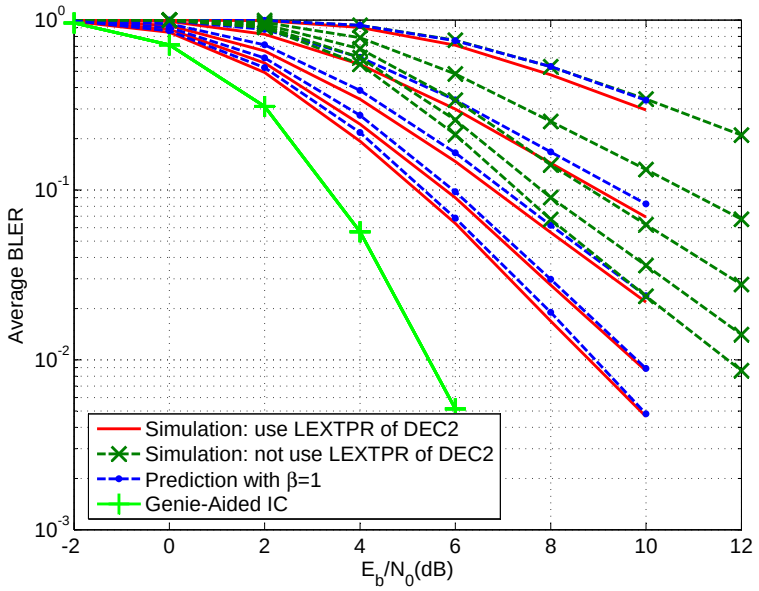

Figure 4.4: Average predicted and simulated BLER vs. SNR (dB) of proposed LEXTPR-based iterative LMMSE-IC with 16QAM-1/2 over CH1, simulated BLER of modified LEXTPR-based scheduling neglecting a priori extrinsic information from the second BCJR decoder.

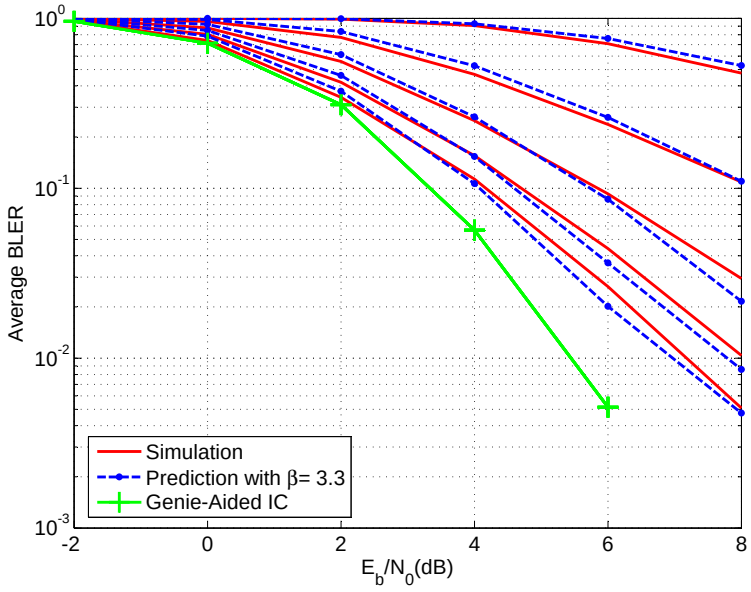

Figure 4.5: Average predicted and simulated BLER vs. SNR (dB) of LAPPR based iterative LMMSE-IC with 16QAM-1/2 over CH1

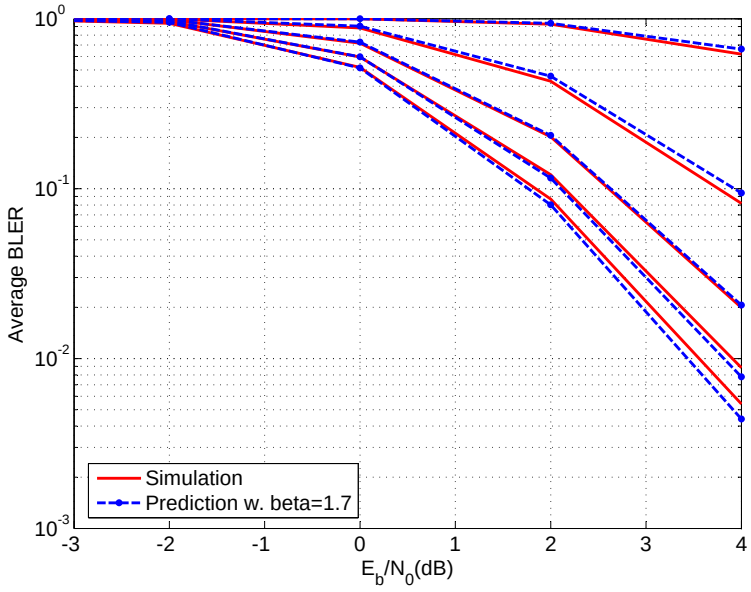

Figure 4.6: Average predicted and simulated BLER vs. SNR (dB) of LAPPR based iterative LMMSE-IC with QPSK-1/2 over CH2

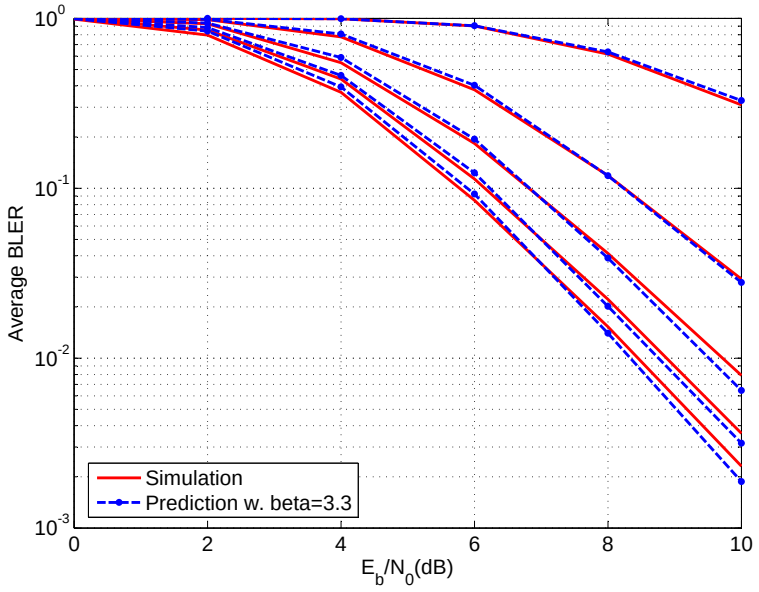

Figure 4.7: Average predicted and simulated BLER vs. SNR (dB) of LAPPR based iterative LMMSE-IC with 16QAM-1/2 over CH2

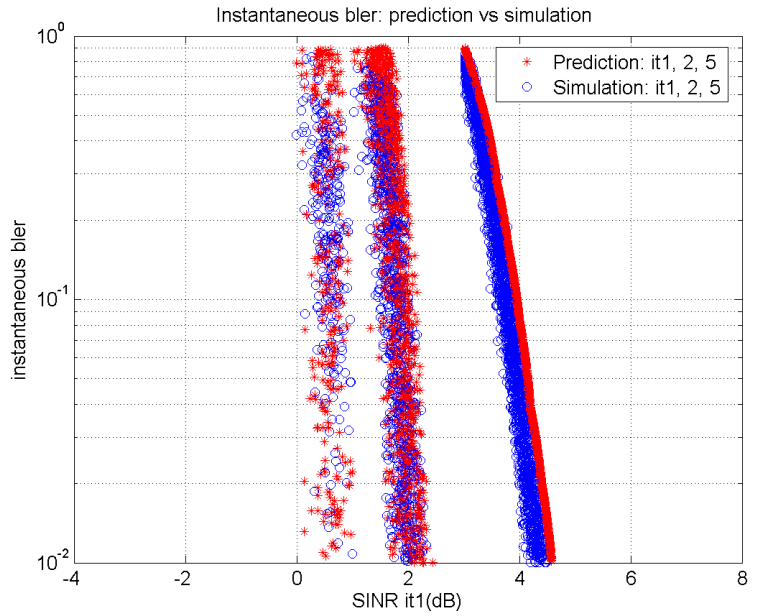

Figure 4.8: Instantaneous predicted and simulated BLER vs. SINR it1(dB) of LAPPR based iterative LMMSE-IC with QPSK-1/2 over CH2

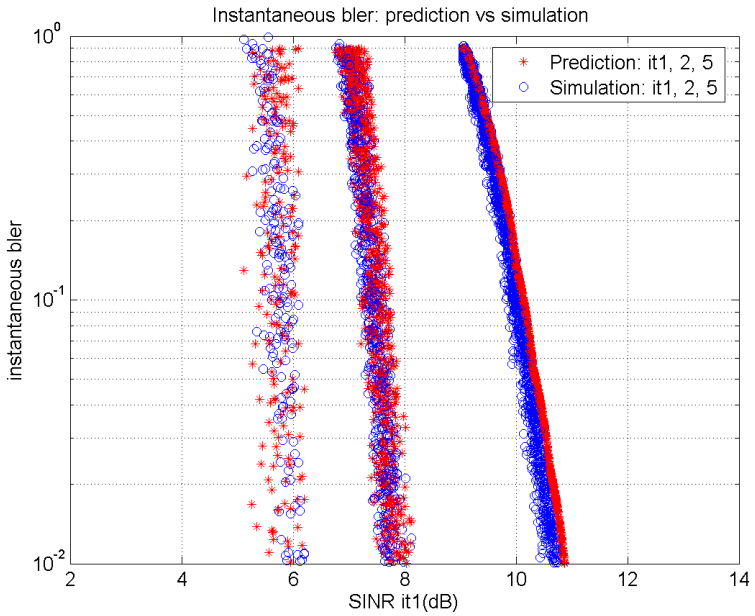

Figure 4.9: Instantaneous predicted and simulated BLER vs. SINR it1(dB) of LAPPR based iterative LMMSE-IC with 16QAM-1/2 over CH2

Chapter 5

Extension to per-antenna turbo coded MIMO systems

5.1 Introduction

In 4G wireless mobile standards (e.g., LTE-A), multiple codewords are allowed to be transmitted. Therefore, PHY-layer abstraction with turbo receivers in independent per-antenna turbo coded MIMO systems are investigated in this chapter.

5.2 System model

We consider a transmission over a MIMO block Rayleigh fading AWGN channel with n_b fading blocks, n_t transmit and n_r receive antennas. Each transmit antenna transmits an independent BICM. No CSI is assumed at the transmitter and perfect CSI is assumed at the receiver. The total number n_s of channel uses available for transmission is fixed and the number of channel uses per fading block is given as $L = n_s/n_b$.

5.2.1 Coding strategy

An MCS indexed by ν_t is a BICM transmitted over the t-th transmit antenna, specified by a turbo code $\mathscr{C}_{\nu_t}$ and a complex constellation $\mathscr{X}_{\nu_t} \subset \mathbb{C}$ of cardinality $2^{q_{\nu_t}}$ and a memoryless labeling rule μ_{ν_t}. The encoding process is detailed for a certain antenna $t \in \{1, \ldots, n_t\}$. The vector of binary data (or information bits) $\mathbf{u}_t$ enters a turbo encoder φ_{ν_t} whose output is the code-

word $\mathbf{c}_t \in \mathscr{C}_{\nu_t}$ of length $n_{c,\nu_t} = n_s q_{\nu_t}$. The codeword bits are interleaved by a random time interleaver π_{ν_t} and reshaped as a collection of integer matrices $\{\mathbf{D}_{b;t}\}_{b=1}^{n_b}$ with $\mathbf{D}_{b;t} \in \mathbb{Z}_{2^{q_{\nu_t}}}^{1\times L}$. Each integer entry can be decomposed into a sequence of q_{ν_t} bits. A Gray mapping μ_{ν_t} transforms each matrix $\mathbf{D}_{b;t}$ into a complex matrix $\mathbf{S}_{b;t} \in \mathscr{X}_{\nu_t}^{1\times L}$. $\mathscr{X}_{\nu_t,j}^{(0)}$ and $\mathscr{X}_{\nu_t,j}^{(1)}$ denote the subsets of points in $\mathscr{X}_{\nu_t}$ whose labels have a 0 or a 1 at position j. With a slight abuse of notation, let $\{d_{b;t,l,j}\}_{j=1}^{q_{\nu_t}}$ denote the set of bits labeling the symbol $s_{b;t,l} \in \mathscr{X}_{\nu_t}$. Let also $\mu_{\nu_t,j}^{-1}(s)$ be the value of the j-th bit in the labeling of any point $s \in \mathscr{X}_{\nu_t}$.

5.2.2 Received signal model

The discrete-time vector $\mathbf{y}_{b;l} \in \mathbb{C}^{n_r}$ received by the destination at b-th fading block and time $l = 1, \ldots, L$, is the same as expressed in (4.1) in chapter 4.

$$\mathbf{y}_{b;l} = \check{\mathbf{H}}_b \mathbf{s}_{b;l} + \mathbf{w}_{b;l} \tag{5.1}$$

where In (5.1) the vectors $\mathbf{s}_{b;l} \in \mathscr{X}_{\nu}^{n_t}$ are i.i.d. random vectors (uniform distribution) with $\mathbb{E}[\mathbf{s}_{b;l}] = \mathbf{0}_{n_t}$ and $\mathbb{E}[\mathbf{s}_{b;l}\mathbf{s}_{b;l}^{\dagger}] = \mathbf{I}_{n_t}$, and the vectors $\mathbf{w}_{b;l} \in \mathbb{C}^{n_r}$ are i.i.d. random vectors, circularly-symmetric Gaussian, with zero-mean and covariance matrix $\sigma_w^2 \mathbf{I}_{n_r}$.

5.2.3 Decoding strategy

The global performance of the turbo receiver depends on the decode ordering. The number of possible decode orderings is $\prod_{t=1}^{n_t} t$. A decode ordering indexed by κ can be seen as a one-to-one correspondence $\{t \to k_{t,\kappa} : t = 1, \ldots, n_t\}$ where t is the antenna index and $k_{t,\kappa}$ is its decode order index. After the n_t-th decode, one global iteration completes. This decode ordering is repeated iteratively. The natural decode ordering is $\{k_{t,1} = t : t = 1, \ldots, n_{t,\theta}\}$.

Furthermore, the turbo decoder is made of *two* BCJR decoders [38] exchanging probabilistic information (log domain). The first BCJR decoder computes the LAPPRs on its own coded bits (information and parity bits) taking into account the available a priori information on systematic information bits stored from an earlier activation (i.e., the most recent LEXTPRs on systematic information bits delivered by the second BCJR decoder). Then the second BCJR decoder is activated and computes the LAPPRs on its

own coded bits (information and parity bits) taking into account the available a priori information transmitted by the first BCJR decoder. The global schedule is described here: First, one global iteration follows the chosen decode ordering. Second, the detection and decoding process at each antenna comprises of one pass of equalizer followed by one pass of first BCJR decoder followed by one pass of second BCJR decoder. Such a global message-passing schedule provides much better global results than the conventional one, i.e., a single pass of joint equalizer followed by an arbitrary number of turbo decoder iterations. The message-passing schedule of natural decode ordering is summarized in Fig. 5.1.

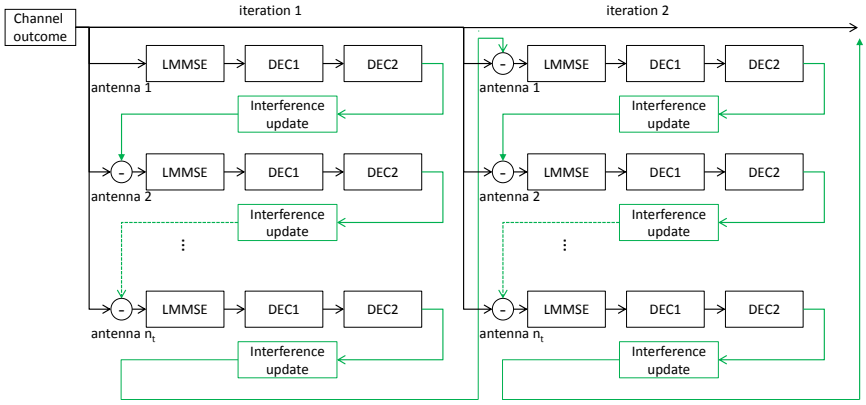

Figure 5.1: Message passing schedule of natural decode ordering

5.3 LMMSE-IC based turbo receivers

Empirical evidence reveals that the LAPPR-based iterative LMMSE-IC algorithm can significantly outperform its LEXTPR-based counterpart for highly loaded multiantenna or multiuser systems. As a consequence, we intentionally focus on this particular class.

For the sake of readability, the detection and decoding process of the t-th antenna (codeword) $t \in \{1, 2, \ldots, n_t\}$ is detailed at a certain global iteration i. This is necessary and sufficient because the detection and decoding process is the same for every antennas. Considering the decode ordering κ, the antenna t' with $k_{t',\kappa} < k_{t,\kappa}$ have already been decoded at the current iteration i and the antenna t' with $k_{t',\kappa} > k_{t,\kappa}$ will be decoded after the t-th

antenna. Therefore, the updated sets of LAPPR on coded bits are $\mathbf{\Lambda}_{D,DEC_t}^{(i-1)}$ and $\{\mathbf{\Lambda}_{D,DEC_{t'}}^{(i_{t'})}\}_{t'=1,t'\neq t}^{n_t}$ where

$$i_{t'} = \begin{cases} i & \text{if } k_{t',\kappa} < k_{t,\kappa} \\ i-1 & \text{if } k_{t',\kappa} > k_{t,\kappa} \end{cases}$$

These sets of LAPPR on coded bits become after interleaving the sets $\mathbf{\Lambda}_{D,LE_t}^{(i-1)}$ and $\{\mathbf{\Lambda}_{D,LE_{t'}}^{(i_{t'})}\}_{t'=1,t'\neq t}^{n_t}$ of all log "a priori" probability ratios on labeling bits used for (soft) interference regeneration and cancellation, although LAPPR contain "observation". Let $\{\Lambda_{D,LE}^{(i-1)}\}_{s_{b;t,l}}$ be the set of all LAPPR on coded bits involved in the labeling of $s_{b;t,l}$ at the current iteration. Let $\{\Lambda_{D,LE}^{(i)}\}_{\mathbf{s}_{b;l}}$ be the set of all LAPPR on coded bits involved in the labeling of $\mathbf{s}_{b;l}$ in the current iteration. Therefore, $\{\Lambda_{D,LE}^{(i)}\}_{\mathbf{s}_{b;l}}$ contains $\left\{\{\Lambda_{D,LE}^{(i-1)}\}_{s_{b;t,l}}, \{\{\Lambda_{D,LE}^{(i_{t'})}\}_{s_{b;t',l}}\}_{t'=1,t'\neq t}^{n_t}\right\}$. Let also $\{\Lambda_{D,LE}^{(i)}\}_{\mathbf{s}_{b;l}\setminus s_{b;t,l}}$ be the set of all LAPPR on coded bits involved in the labeling of $\mathbf{s}_{b;l}$ *except* the coded bits involved in the labeling of $s_{b;t,l}$, i.e., $\{\{\Lambda_{D,LE}^{(i_{t'})}\}_{s_{b;t',l}}\}_{t'=1,t'\neq t}^{n_t}$.

5.3.1 Interference regeneration and cancellation

Prior to LMMSE estimation of the symbol $s_{b;t,l}$, we compute the *conditional* MMSE estimate of the interference, defined as $\breve{\mathbf{y}}_{b;l\setminus t}^{(i)} = \mathbb{E}\left[\mathbf{y}_{b;l}|\{\Lambda_{D,LE}^{(i)}\}_{\mathbf{s}_{b;l}\setminus s_{b;t,l}}\right]$. This computation is intractable for useful signal components and noise samples are of course no more independent conditional on $\{\Lambda_{D,LE}^{(i)}\}_{\mathbf{s}_{b;l}\setminus s_{b;t,l}}$. To solve this issue, we make two symplifying assumptions.

A1 The pdf $p_{\mathbf{s}_{b;l},\mathbf{w}_{b;l}|\{\Lambda_{D,LE}^{(i)}\}_{\mathbf{s}_{b;l}\setminus s_{b;t,l}}}(\mathbf{s}_{b;l},\mathbf{w}_{b;l})$ factorizes as

$$\begin{aligned} &p_{\mathbf{s}_{b;l},\mathbf{w}_{b;l}|\{\Lambda_{D,LE}^{(i)}\}_{\mathbf{s}_{b;l}\setminus s_{b;t,l}}}(\mathbf{s}_{b;l},\mathbf{w}_{b;l}) = \\ &P(s_{b;t,l})p_{\mathbf{w}_{b;l}}(\mathbf{w}_{b;l})\prod_{t'\neq t}P(s_{b;t',l}|\{\Lambda_{D,LE}^{(i_{t'})}\}_{s_{b;t',l}}). \end{aligned} \tag{5.2}$$

A2 The pmf $P(s_{b;t',l}|\{\Lambda_{D,LE}^{(i_{t'})}\}_{s_{b;t',l}})$ in (5.2) is given by

$$P(s_{b;t',l}|\{\Lambda_{D,LE}^{(i_{t'})}\}_{s_{b;t',l}}) \propto e^{\sum_j \mu_{\nu_{t',j}}^{-1}(s_{b;t',l})\Lambda_{D,LE}^{(i_{t'})}(d_{b;t',l,j})}.$$

As a matter of fact, the assumptions (A1) and (A2) never hold even for an ideal interleaver of infinite depth. But we can still force them in all

subsequent derivations. Under (A1), the MMSE estimate of the interference affecting the symbol $s_{b;t,l}$ is given by

$$\tilde{\mathbf{y}}_{b;l\backslash t}^{(i)} = \mathbf{H}_b(\mathbf{I}_{n_t} - \mathbf{e}_t\mathbf{e}_t^\dagger)\mathbf{m}_{b;l}^{(i)} \tag{5.3}$$

where $\mathbf{m}_{b;l}^{(i)}$ is the vector made of all estimates $m_{b;t',l}^{(i_{t'})} = \mathbb{E}\left[s_{b;t',l}|\{\Lambda_{D,LE}^{(i_{t'})}\}_{s_{b;t',l}}\right]$ evaluated under (A2). After IC, the new observed vector is $\mathbf{y}_{b;l} - \tilde{\mathbf{y}}_{b;l\backslash t}^{(i)}$.

5.3.2 LMMSE estimation – unconditional case

The optimization problem to solve can be formulated as follows: Find $\breve{s}_{b;t,l}^{(i)} = \breve{\mathbf{f}}_{b;t}^{(i)^\dagger}(\mathbf{y}_{b;l} - \breve{\mathbf{y}}_{b;l\backslash t}^{(i)})$ minimizing the *unconditional* MSE $\mathbb{E}\left[|\breve{s}_{b;t,l}^{(i)} - s_{b;t,l}|^2\right]$ defined as

$$\mathbb{E}\left[\mathbb{E}\left[|\breve{s}_{b;t,l}^{(i)} - s_{b;t,l}|^2|\{\Lambda_{D,LE}^{(i)}\}_{\mathbf{s}_{b;l}\backslash s_{b;t,l}}\right]\right]. \tag{5.4}$$

The outer expectation in (5.4) renders the (biased) LMMSE filter time-invariant given by $\breve{\mathbf{f}}_{b;t}^{(i)} = \breve{\mathbf{\Xi}}_{b;t}^{(i)^{-1}}\breve{\boldsymbol{\xi}}_{b;t}^{(i)}$ where $\breve{\boldsymbol{\xi}}_{b;t}^{(i)} = \mathbb{E}\left[\breve{\boldsymbol{\xi}}_{b;t,l}^{(i)}\right]$ with

$$\breve{\boldsymbol{\xi}}_{b;t,l}^{(i)} = \mathbb{E}\left[(\mathbf{y}_{b;l} - \breve{\mathbf{y}}_{b;l\backslash t}^{(i)})s_{b;t,l}^*|\{\Lambda_{D,LE}^{(i)}\}_{\mathbf{s}_{b;l}\backslash s_{b;t,l}}\right]$$

and where $\breve{\mathbf{\Xi}}_{b;t}^{(i)} = \mathbb{E}\left[\breve{\mathbf{\Xi}}_{b;t,l}^{(i)}\right]$ with

$$\breve{\mathbf{\Xi}}_{b;t,l}^{(i)} = \mathbb{E}\left[(\mathbf{y}_{b;l} - \breve{\mathbf{y}}_{b;l\backslash t}^{(i)})(\mathbf{y}_{b;l} - \breve{\mathbf{y}}_{b;l\backslash t}^{(i)})^\dagger|\{\Lambda_{D,LE}^{(i)}\}_{\mathbf{s}_{b;l}\backslash s_{b;t,l}}\right].$$

The computation of $\breve{\mathbf{f}}_{b;t}^{(i)}$ is again intractable. However, under (A1), $\breve{\boldsymbol{\xi}}_{b;t}^{(i)}$ and $\breve{\mathbf{\Xi}}_{b;t}^{(i)}$ become $\boldsymbol{\xi}_{b;t}^{(i)} = \mathbf{h}_{b;t} = \mathbf{H}_b\mathbf{e}_t$ and $\mathbf{\Xi}_{b;t}^{(i)} = \mathbf{H}_b\mathbf{V}_{b;\backslash t}^{(i)}\mathbf{H}_b^{(i)^\dagger} + \sigma_w^2\mathbf{I}_{n_r}$ where $\mathbf{V}_{b;\backslash t}^{(i)}$ is the *unconditional* symbol covariance matrix defined as

$$\mathbf{V}_{b;\backslash t}^{(i)} = \mathrm{diag}\{v_{b;1}^{(i_1)}, \ldots, v_{b;t-1}^{(i_{t-1})}, 1, v_{b;t+1}^{(i_{t+1})}, \ldots, v_{b;n_t}^{(i_{n_t})}\}$$

where $\forall t' \neq t$, $v_{b;t'}^{(i_{t'})} = \mathbb{E}\left[v_{b;t',l}^{(i_{t'})}\right]$ with $v_{b;t',l}^{(i_{t'})} = \mathbb{E}\left[|s_{b;t',l} - m_{b;t',l}^{(i_{t'})}|^2 | \{\Lambda_{D,LE}^{(i_{t'})}\}_{s_{b;t',l}}\right]$ evaluated under (A2). Using the matrix inversion lemma, we obtain the filter

$$\mathbf{f}_{b;t}^{(i)} = \frac{1}{1 + \eta_{b;t}^{(i)}(1 - v_{b;t}^{(i-1)})} \mathbf{\Sigma}_b^{(i)^{-1}} \mathbf{h}_{b;t} \tag{5.5}$$

where $\mathbf{\Sigma}_b^{(i)} = \mathbf{H}_b \mathbf{V}_b^{(i)} \mathbf{H}_b^{\dagger} + \sigma_w^2 \mathbf{I}_{n_r}$ and $\eta_{b;t}^{(i)} = \mathbf{h}_{b;t}^{\dagger} \mathbf{\Sigma}_b^{(i)^{-1}} \mathbf{h}_{b;t}$ with

$$\mathbf{V}_b^{(i)} = \mathbf{V}_{b;\backslash t}^{(i)} - (1 - v_{b;t}^{(i-1)}) \mathbf{e}_t \mathbf{e}_t^{\dagger} \tag{5.6}$$

where $v_{b;t}^{(i-1)} = \mathbb{E}\left[v_{b;t,l}^{(i-1)}\right]$ with $v_{b;t,l}^{(i-1)} = \mathbb{E}\left[|s_{b;t,l} - m_{b;t,l}^{(i-1)}|^2 | \{\Lambda_{D,LE}^{(i-1)}\}_{s_{b;t,l}}\right]$ evaluated under (A2). The corresponding estimate $\hat{s}_{b;t,l}^{(i)}$ of $s_{b;t,l}$ can be expressed as

$$\hat{s}_{b;t,l}^{(i)} = \mathbf{f}_{b;t}^{(i)^{\dagger}} (\mathbf{y}_{b;l} - \tilde{\mathbf{y}}_{b;l\backslash t}^{(i)}) = g_{b;t}^{(i)} s_{b;t,l} + \zeta_{b;t,l}^{(i)} \tag{5.7}$$

where $g_{b;t}^{(i)} = \mathbf{f}_{b;t}^{(i)^{\dagger}} \mathbf{h}_{b;t}$ and $\zeta_{b;t,l}^{(i)}$ is the residual interference plus noise term. Clearly, $\zeta_{b;t,l}^{(i)}$ in (5.7) is zero-mean and uncorrelated with the useful signal $s_{b;t,l}$ under (A1), i.e., $\mathbb{E}[s_{b;t,l} \zeta_{b;t,l}^{(i)^*}] = 0$. Under (A1) and (A2) the variance of $\zeta_{b;t,l}^{(i)}$ is $\varsigma_{b;t}^{(i)} = g_{b;t}^{(i)}(1 - g_{b;t}^{(i)})$. Thus, we can define the *unconditional* SINR under (A1) and (A2) as

$$\gamma_{b;t}^{(i)} = \frac{g_{b;t}^{(i)}}{1 - g_{b;t}^{(i)}} = \frac{\eta_{b;t}^{(i)}}{1 - \eta_{b;t}^{(i)} v_{b;t}^{(i-1)}}. \tag{5.8}$$

In practical implementation, we make several assumptions over the covariance matrices $\mathbf{V}_b^{(i)}$.

A3 Due to the particular structure of the MCS, the so-called *equal variance assumption* holds, which states that

$$\mathbf{V}_b^{(i)} = \mathbf{V}^{(i)} = \text{diag}\{v_1^{(i_1)}, \ldots, v_t^{(i-1)}, \ldots, v_{n_t}^{(i_{n_t})}\}, \forall b. \tag{5.9}$$

A4 $v_t^{(i-1)}$ and $\{v_{t'}^{(i_{t'})}\}_{t'=1,t'\neq t}^{n_t}$ can be replaced by their empirical means defined as

$$\begin{aligned}\bar{v}_t^{(i-1)} &= \frac{1}{n_b L}\sum_{b=1}^{n_b}\sum_{l=1}^{L} v_{b;t,l}^{(i-1)},\\ \bar{v}_{t'}^{(i_{t'})} &= \frac{1}{n_b L}\sum_{b=1}^{n_b}\sum_{l=1}^{L} v_{b;t',l}^{(i_{t'})}, \forall t' \neq t.\end{aligned}$$

assuming sufficiently large L. Actually, the ergodic regime assumption (A4) is part of the baseline assumptions of EXIT charts [37]. The assumption (A3) never holds even for an ideal interleaver of infinite depth, but forcing it induces no performance degradation. Finally the covariance matrix becomes

$$\bar{\mathbf{V}}^{(i)} = \mathrm{diag}\{\bar{v}_1^{(i_1)},\ldots,\bar{v}_t^{(i-1)},\ldots,\bar{v}_{n_t}^{(i_{n_t})}\} \tag{5.10}$$

5.3.3 Demapping and decoding

The estimate $\hat{s}_{b;t,l}^{(i)}$ is used as a *decision statistic* to compute the LEXTPR on the q_{ν_t} bits involved in the labeling of $s_{b;t,l}$.

A5 In (5.7), the conditional pdf $p_{\hat{s}_{b;t,l}^{(i)}|s_{b;t,l}}(\hat{s}_{b;t,l}^{(i)})$ is circularly-symmetric complex Gaussian distributed.

Under (A1), (A2) and (A5) the conditional pdf $p_{\hat{s}_{b;t,l}^{(i)}|s_{b;t,l}}(\hat{s}_{b;t,l}^{(i)})$ is $\mathcal{N}_{\mathbb{C}}(g_{b;t}^{(i)}s_{b;t,l},\varsigma_{b;t}^{(i)})$. As a result, under (A1),(A2), and (A5), for the *special case* of Gray labeling, the LEXTPR $\Lambda_{E,DEM}^{(i)}(d_{b;t,l,j})$ on labeling bit $d_{b;t,l,j}$ is expressed as

$$\Lambda_{E,DEM}^{(i)}(d_{b;t,l,j}) = \frac{\sum_{s\in\mathcal{X}_{\nu_t,j}^{(1)}} e^{-|\hat{s}_{b;t,l}^{(i)}-g_{b;t}s|^2/\varsigma_{b;t}^{(i)}}}{\sum_{s\in\mathcal{X}_{\nu_t,j}^{(0)}} e^{-|\hat{s}_{b;t,l}^{(i)}-g_{b;t}s|^2/\varsigma_{b;t}^{(i)}}} \tag{5.11}$$

5.3.4 Message-passing schedule for turbo decoding

The set $\mathbf{\Lambda}_{E,DEM_t}^{(i)}$ of all LEXTPR on labeling bits becomes after deinterleaving the set $\mathbf{\Lambda}_{I,DEC_t}^{(i)}$ of all log intrinsic probability ratios on coded bits used as input for the decoder.

A6 The pdf $p_{\mathbf{\Lambda}^{(i)}_{I,DEC_t}|\mathbf{c}}(\mathbf{\Lambda}^{(i)}_{I,DEC_t})$ factorizes as

$$p_{\mathbf{\Lambda}^{(i)}_{I,DEC_t}|\mathbf{c}_t}(\mathbf{\Lambda}^{(i)}_{I,DEC_t}) = \prod_{n=1}^{n_{c,\nu_t}} p_{\Lambda^{(i)}_{I,DEC}(c_{t,n})|c_{t,n}}(\Lambda^{(i)}_{I,DEC}(c_{t,n}))$$

where $\Lambda^{(i)}_{I,DEC}(c_{t,n})$ is the log intrinsic probability ratio on n-th coded bit $c_{t,n}$ of the t-th codeword. The assumption (A6) allows to simplify the decoding task. It is rightfully confirmed for an interleaver of finite, but large enough, depth. The decoding consists of one pass of first BCJR decoder followed by one pass of second BCJR decoder. This completes the decode task for antenna t.

5.4 PHY-layer abstraction

The global performance evolution analysis should follow the chosen message-passing schedule (Fig. 5.1 exemplifies the natural ordering). The PHY-layer abstraction follows the one described in chapter 4 derived for STBICM transmission. Again, we details the prediction method for the t-th antenna at the iteration i.

5.4.1 Transfer characteristics of LMMSE-IC

The LMMSE-IC part for the t-th antenna ends up with n_b independent parallel channels under (A6). Each of them is modeled as a discrete-input AWGN channel under (A5) whose SNR, given by

$$\gamma^{(i)}_{b;t} = \frac{\eta^{(i)}_{b;t}}{1 - \eta^{(i)}_{b;t}\bar{v}^{(i-1)}_t} \tag{5.12}$$

under (A1)-(A4), turns out to be a function ϕ_t of b, t, $\mathbf{H}_b$, σ^2_w and the input variance $\bar{v}^{(i-1)}_t$. For each such channel, we can compute the AMI $I^{(i)}_{LE_{b;t}}$ between the discrete input $s_{b;t,l} \in \mathscr{X}_{\nu_t}$ and the output $\tilde{s}^{(i)}_{b;t,l} = s_{b;t,l} + \epsilon^{(i)}_{b;t,l}$ with $\epsilon_{b;t,l} \sim \mathcal{N}_{\mathbb{C}}(0, 1/\gamma^{(i)}_{b;t})$. The value of $I^{(i)}_{LE_{b;t}}$ depends on the single parameter

$\gamma_{b;t}^{(i)}$. Let $\bar{I}_{LE_t}^{(i)}$ be the arithmetic mean of the values $\{I_{LE_{b;t}}^{(i)}\}$, i.e.,

$$\bar{I}_{LE_t}^{(i)} = \frac{1}{n_b} \sum_{b=1}^{n_b} I_{LE_{b;t}}^{(i)}. \tag{5.13}$$

The AMI $I_{LE_{b;t}}^{(i)} = \psi_{\nu_t}(\gamma_{b;t}^{(i)})$ is a monotone increasing, thus invertible, function of the SNR, and depends on the MCS index ν_t. It is simulated off-line and stored in a LUT.

5.4.2 Transfer characteristics of joint demapping and decoding

The functional module is MCS-dependent and comprises the following steps: demapping, deinterleaving, turbo decoding (one pass of the first *BCJR decoder* followed by one pass of the second *BCJR decoder*), reinterleaving, and computation of the mean and variance of transmitted symbols based on LAPPR on coded bits (as described before). The algorithm used to generate the different LUTs (BLER $P_{e_t} = F_{JDD_{\nu_t}}(\gamma, I_{A,DEC})$, the variance $\bar{v}_t = G_{JDD_{\nu_t}}(\gamma, I_{A,DEC})$, and the mutual information $I_{E_t} = T_{JDD_{\nu_t}}(\gamma, I_{A,DEC})$) is summarized in Algorithm 5.

5.4.3 Evolution analysis

It remains to relate the output $\bar{I}_{LE_t}^{(i)}$ of the first transfer function (LMMSE-IC) and the input SNR of the second transfer function (joint demapping and decoding) at any iteration. This is done by assuming that $\bar{I}_{LE}^{(i)}$ which measures the information content of knowledge on coded modulated symbols $\{s_{b;t,l}\}$, averaged over all parallel AWGN channels, is equal to the information content of knowledge on coded modulated symbols transmitted over a *single* virtual discrete-input (with values in $\mathscr{X}_{\nu_t}$) AWGN channel with effective SNR $\bar{\gamma}_{LE_t}^{(i)}$ given by

$$\bar{\gamma}_{LE_t}^{(i)} = \psi_{\nu_t}^{-1}(\bar{I}_{LE_t}^{(i)}) = \psi_{\nu_t}^{-1}\left(\frac{1}{n_b} \sum_{b=1}^{n_b} I_{LE_{b;t}}^{(i)}\right). \tag{5.14}$$

This technique inherited from EXIT charts is widely used in practice and often referred to as MIESM. In our framework, it relies on all the defined assumptions (A1)-(A6) or, equivalently, on (A5) and (A6) for the first iteration. The variance $\bar{v}_t^{(i)} = G_{JDD_{\nu_t}}(\bar{\gamma}_{LE}^{(i)}, I_{A,DEC}^{(i)})$ is used in (5.10) under (A4) for other antennas to be detected and decoded. Hence, the evolution of LAPPR-based iterative LMMSE-IC can be tracked through the single scalar parameter $\bar{v}_t^{(i)}$.

5.4.4 Calibration

A major drawback of this performance prediction method is that the assumptions (A1), (A2) and (A3) do not hold for LAPPR-based iterative LMMSE-IC. As explained before in chapter 2 and chapter 4, a simple, yet effective, calibration procedure has been proposed which have the effect to artificially reduce the SINRs that are used in the performance prediction method. Finally, a recapitulative diagram of the method is depicted in Fig. 5.2 for t-th antenna at i-th iteration.

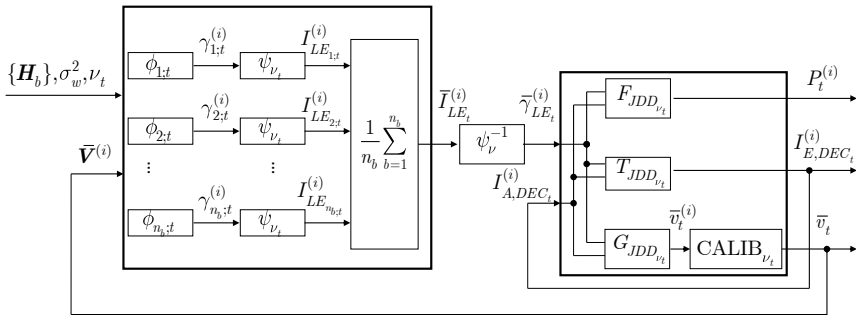

Figure 5.2: Performance prediction method of BICM at antenna t at iteration i

5.5 Numerical results

The proposed physical layer abstraction method is tested over a 2x2 MIMO 4-block flat fading Rayleigh channel. The MCS are built from the LTE turbo-code based on two 8-state rate-1/2 recursive systematic convolutional (RSC) encoders with generator matrix G = [1; g1/g0] where g0 = [1011] and g1 = [1101] and QAM modulations (Gray labeling). LAPPR based iterative

LMMSE-IC is performed at the destination. The natural decode ordering is considered here. The schedule is: one pass of equalizer followed by one pass of first BCJR decoder followed by one pass of second BCJR decoder. This completes one global iteration of the turbo receiver. We witnessed that 5 iterations are generally enough to ensure the convergence in practice.

The average E_b is the same for two antennas. Average simulated and predicted BLER over open-loop MIMO are shown for several SNR. For each SNR, we evaluated the average simulated BLER by Monte Carlo simulation which is stopped after 1000 block errors for both codewords. The predicted BLER is evaluated over 10000 channel realizations. Fig. 5.3 shows the results for two different MCS on two antennas: antenna 1 QPSK-1/2 (prediction with calibration factor 1.7) and antenna 2 16QAM-1/2 (prediction with calibration factor 3.3). Fig. 5.4 shows the results for two identical independent 16QAM-1/2 (prediction with calibration factor 3.3)on two antennas. We observe that the average predicted BLER match exactly the average simulated ones at every iterations.

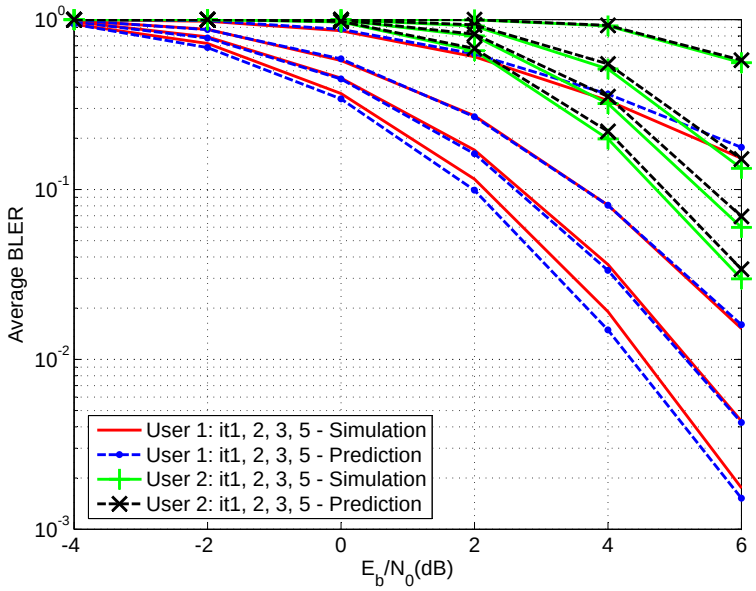

Figure 5.3: Average simulated vs. predicted BLER of LAPPR based iterative LMMSE-IC with QPSK-1/2 at one antenna and 16QAM-1/2 at the other antenna over 2×2 MIMO -4 block fading channel

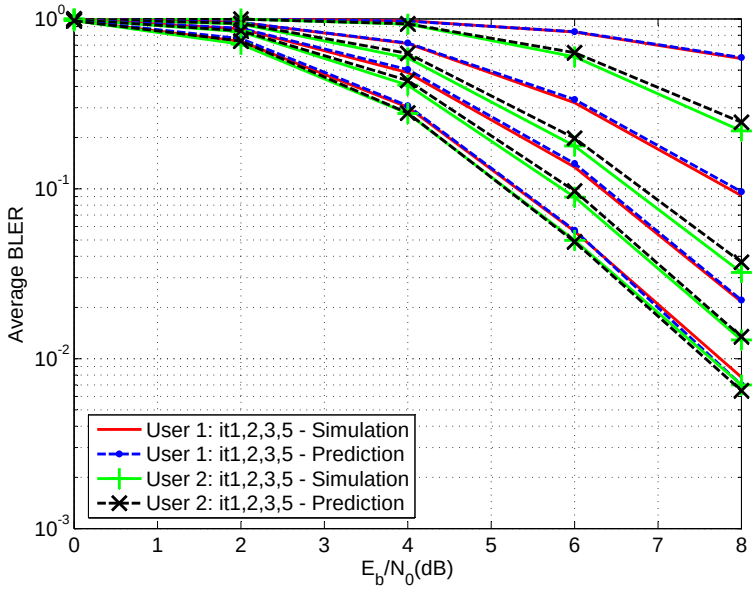

Figure 5.4: Average simulated vs. predicted BLER of LAPPR based iterative LMMSE-IC with two identical independent 16QAM-1/2 on two antennas over 2×2 MIMO -4 block fading channel

5.6 Conclusion

In this chapter, we have investigated the PHY-layer abstractions in independent per-antenna turbo coded MIMO systems with iterative LMMSE-IC receiver. Each antenna transmit an independent BICM. The topic is a generalization of previous chapter 4. The proposed PHY-layer abstractions have been validated by Monte-Carlo simulations with different communication scenarios. The following step is to investigate link adaptation strategies in presence of such receiver and proposed PHY-layer abstractions.

Part II

Link adaptation for closed-loop coded MIMO systems with partial feedback

Chapter 6

Coding across antennas (STBICM)

6.1 Introduction

Cross optimization between PHY and MAC layers, sometimes referred to as cooperative resource allocation, is currently one of the most exciting research topics in the design of MU-MIMO systems. One reason may be that the computational complexity of the problem to solve represents a formidable challenge in terms of mathematical modeling and implementation. In order to build bridges between PHY and MAC layers, it is mandatory that the link-level metrics be accurately modeled and effectively taken into account in higher-level decision-making mechanisms. Only a limited amount of contributions address this issue and, when they do it, most often restrict their study to simple linear receivers (see e.g., [85] and [86]) or, if dealing with more sophisticated non-linear receiver structures, e.g., Cyclic Redundancy Check (CRC) - based SIC [87], idealize some parts of the decoding process, typically assuming continuous-input channels with zero-error Gaussian codebooks, and neglecting error propagation, which leads to inaccurate (i.e., too optimistic) predicted throughputs.

Real systems though deal with discrete-input channels and non-ideal finite-length MCS. Besides, in the light of the substantial improvement they

This chapter is partially presented in the papers accepted to IEEE ICNC'2014, IEEE WIMOB'2013 and a journal paper in preparation

can bring in terms of system throughput or performance compared to conventional receivers (i.e., linear receivers or non-linear SIC receivers), iterative (turbo) LMMSE-IC should become an integral part of the assumptions made on the PHY layer (see e.g., [71] [66] and the references therein). The primarily subject of this chapter is to measure the true impact of this family of iterative "turbo" receivers on the link level performance. The evolution of this family of iterative receiver is analyzed building upon previous work on advanced PHY layer modeling and the calibration enhancement. We show how to incorporate the fine stochastic modeling of such receivers into the joint decision-making mechanisms involved in link adaptation.

6.2 System model

We consider a single-user transmission over a MIMO block Rayleigh fading multipath AWGN channel with n_b fading blocks, n_t transmit and n_r receive antennas. Partial state information is assumed at the transmitter through a low rate feedback. Perfect channel state information is assumed at the receiver. The total number n_s of channel uses available for transmission is fixed and the number of channel uses per fading block is given as $L = n_s/n_b$.

6.2.1 Coding strategy

Under limited feedback, only a finite number of transmission schemes are available at the transmitter side, i.e., a finite set of MCS and a finite set of spatial precoders. Let $\mathcal{M}$ be the set of MCS indices and $\mathcal{P}$ the set of spatial precoders. An MCS indexed by $\nu \in \mathcal{M}$ is a STBICM, specified by a convolutional or turbo code $\mathscr{C}_\nu$ of rate r_ν and a complex constellation $\mathscr{X}_\nu \subset \mathbb{C}$ of cardinality 2^{q_ν} and a memoryless labeling rule μ_ν. We define the rate of the MCS ν as $\rho_\nu = r_\nu q_\nu$ (bits/complex dimension). By convention, MCS are indexed in increasing order of the rates, i.e., the MCS no. 1 has the lowest rate, and the MCS no. $|\mathcal{M}|$ the highest. Antenna selection is used as a simple form of spatial precoding. A spatial precoder indexed by $\theta \in \mathcal{P}$ selects $n_{t,\theta} \leq n_t$ antennas and is specified by a precoding matrix $\mathbf{\Phi}_\theta$. If $\{\delta_1, \ldots, \delta_{n_{t,\theta}}\}$ is the index set of selected antennas, then $\mathbf{\Phi}_\theta = 1/\sqrt{n_{t,\theta}}[\mathbf{e}_{\delta_1}, \ldots, \mathbf{e}_{\delta_{n_{t,\theta}}}]$ where $\mathbf{e}_{\delta_t}$ is the n_t-dimensional vector with 1 at position δ_t and 0 elsewhere. The encoding process for MCS ν and precoder θ is detailed. The vector of binary data (or information bits) $\mathbf{u}$

enters a turbo encoder φ_ν whose output is the codeword $\mathbf{c} \in \mathscr{C}_\nu$ of length $n_{c,\nu,\theta} = n_s n_{t,\theta} q_\nu$. The codeword bits are interleaved by a random space time interleaver $\pi_{\theta,\nu}$ and reshaped as a collection of integer matrices $\{\mathbf{D}_b\}_{b=1}^{n_b}$ with $\mathbf{D}_b \in \mathbb{Z}_{2^{q_\nu}}^{n_{t,\theta} \times L}$. Each integer entry can be decomposed into a sequence of q_ν bits. A Gray mapping μ_ν transforms each matrix $\mathbf{D}_b$ into a complex matrix $\mathbf{S}_b \in \mathscr{X}_\nu^{n_{t,\theta} \times L}$, which is finally precoded as $\mathbf{X}_b = \mathbf{\Phi}_\theta \mathbf{S}_b \in \mathbb{C}^{n_t \times L}$. $\mathscr{X}_{\nu,j}^{(0)}$ and $\mathscr{X}_{\nu,j}^{(1)}$ denote the subsets of points in $\mathscr{X}_\nu$ whose labels have a 0 or a 1 at position j. With a slight abuse of notation, let $\{d_{b;t,l,j}\}_{j=1}^{q_\nu}$ denote the set of bits labeling the symbol $s_{b;t,l} \in \mathscr{X}_\nu$. Let also $\mu_{\nu,j}^{-1}(s)$ be the value of the j-th bit in the labeling of any point $s \in \mathscr{X}_\nu$. STBICM with spatial precoding is depicted in Fig.6.1.

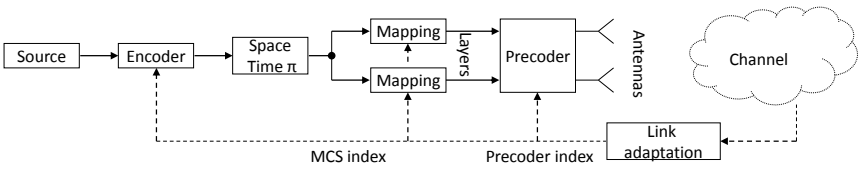

Figure 6.1: Link adaptation – STBICM with spatial precoding (antenna selection)

6.2.2 Received signal model

Transmission occurs over a MIMO block Rayleigh fading multipath AWGN channel. For the b-th fading block, the $n_\tau + 1$ finite-length impulse response (FIR) describes the small-scale multipath fading

$$\mathbf{H}_b(l) = \sum_{\tau=0}^{n_\tau} \mathbf{H}_{b;\tau} \delta(l - \tau). \tag{6.1}$$

Each tap gain $\mathbf{H}_{b;\tau}$ is an $n_r \times n_t$ random matrix whose entries are modeled as i.i.d. circularly-symmetric complex Gaussian random variables with zero-mean and variance $\sigma_{b;\tau}^2$ under the constraint $\sum_{\tau=0}^{n_\tau} \sigma_{b;\tau}^2 = 1$. Let $\check{\mathbf{H}}_{b;\theta}(l)$ be the precoded channel FIR. In $\check{\mathbf{H}}_{b;\theta}(l)$, $\check{\mathbf{H}}_{b;\tau}^{\theta} = \mathbf{H}_{b;\tau} \mathbf{\Phi}_\theta$ denotes the τ-th precoded channel tap. The discrete-time vector $\mathbf{y}_{b;l} \in \mathbb{C}^{n_r}$ received by the

destination at b-th fading block and time $l = 1, \ldots, L$, is expressed as

$$\mathbf{y}_{b;l} = \sum_{\tau=0}^{n_\tau} \check{\mathbf{H}}_{b;\tau}^{\theta} \mathbf{s}_{b;l-\tau} + \mathbf{w}_{b;l} \tag{6.2}$$

with proper boundary conditions. In (6.2), the vectors $\mathbf{s}_{b;l} \in \mathscr{X}_\nu^{n_{t,\theta}}$ are i.i.d. random vectors (uniform distribution) with $\mathbb{E}[\mathbf{s}_{b;l}] = \mathbf{0}_{n_{t,\theta}}$ and $\mathbb{E}[\mathbf{s}_{b;l}\mathbf{s}_{b;l}^\dagger] = \mathbf{I}_{n_{t,\theta}}$, and the vectors $\mathbf{w}_{b;l} \in \mathbb{C}^{n_r}$ are i.i.d. random vectors, circularly-symmetric Gaussian, with zero-mean and covariance matrix $\sigma_w^2 \mathbf{I}_{n_r}$.

6.3 LMMSE-IC based turbo receivers

Empirical evidence reveals that the LAPPR-based iterative LMMSE-IC algorithm can significantly outperform its LEXTPR-based counterpart for highly loaded multiantenna or multiuser systems. As a consequence, we intentionally focus on this particular class.

The LAPPR-based iterative LMMSE-IC receiver architecture under convolutional coded MIMO transmission is described in Fig. 2.3. The different steps of such iterative LMMSE-IC receivers can be found in chapter 2 and are not re-written in this chapter.

The LAPPR-based iterative LMMSE-IC receiver architecture under turbo coded MIMO transmission is described in Fig. 4.1 for the 1-block fading case. The different steps of such iterative LMMSE-IC receivers can be found in chapter 4 and are not re-written in this chapter. For the turbo coded case, the best schedule we have found is the following: one pass of equalizer followed by one pass of first BCJR decoder followed by one pass of second BCJR decoder. This completes one global iteration of the turbo receiver.

6.4 PHY-layer abstraction

The proposed performance prediction method is semi-analytical and relies on ten Brink's stochastic approach of EXIT charts [37] particularly useful in understanding and measuring the dynamics of turbo processing. The PHY-layer abstractions can be found for convolutional coded in chapter 2 (Fig

2.5)and for turbo code case in chapter 4 (Fig 4.2), respectively. There is no need to be repeated in this chapter.

6.5 Link level performance evaluation

Closed-loop link adaptation performs *joint* spatial precoder selection (antenna selection) and MCS selection. It aims at *maximizing* the *average rate* subject to a target BLER constraint assuming LAPPR-based iterative LMMSE-IC at the destination. The number of iterations n_{it} depends on the destination computational capacity.

For a given SNR γ and a given channel outcome $\{\mathbf{H}_b\}$, the optimization problem to solve can be formulated as follows:

$$\begin{array}{ll} \text{Find} & R^\star(\gamma, \{\mathbf{H}_b\}, n_{it}) = \max_{\omega\in\Omega} n_{t,\theta}\rho_\nu \\ \text{subject to} & C_1, C_2 \end{array}$$

where

- $\omega = \{\theta, \nu\}$ is a particular system configuration in Ω, the set of all possible spatial precoder and MCS indices.
- $P_e^{(n_{it})}(\omega)$ is the *predicted* BLER at iteration n_{it} for a given system configuration ω.
- $C1 : n_{t,\theta} \leq \min(n_t, n_r)$
- $C2 : P_e^{(n_{it})}(\omega) \leq \varepsilon$.

In practice, retransmission is activated where one block error is detected. Assuming ARQ Type-I retransmission algorithm and retransmissions within the coherence time of the channel, the *predicted* throughput is defined as

$$T^\star(\gamma, \{\mathbf{H}_b\}, n_{it}) = R^\star(\gamma, \{\mathbf{H}_b\}, n_{it})(1 - P_e^{(n_{it})}(\omega^\star)) \tag{6.3}$$

where $\omega^\star = \{\theta^\star, \nu^\star\} = \arg\max_{\omega\in\Omega} n_{t,\theta}\rho_\nu$. For comparison, the *simulated* BLER $P_{e,sim}^{(n_{it})}(\omega^\star)$ and the *simulated* throughput $T_{sim}^\star(\gamma, \{\mathbf{H}_b\}, n_{it})$ defined as

$$T_{sim}^\star(\gamma, \{\mathbf{H}_b\}, n_{it}) = R^\star(\gamma, \{\mathbf{H}_b\}, n_{it})(1 - P_{e,sim}^{(n_{it})}(\omega^\star)) \tag{6.4}$$

are obtained via Monte Carlo simulation. Then, we evaluate the average predicted rate $\bar{R}^\star(\gamma, n_{it}) = \mathbb{E}[R^\star(\gamma, \{\mathbf{H}_b\}, n_{it})]$, the average predicted throughput $\bar{T}^\star(\gamma, n_{it}) = \mathbb{E}[T^\star(\gamma, \{\mathbf{H}_b\}, n_{it})]$ and the average simulated throughput

$\bar{T}^{\star}_{sim}(\gamma, n_{it}) = \mathbb{E}[T^{\star}_{sim}(\gamma, \{\mathbf{H}_b\}, n_{it})]$ where expectation is w.r.t. $p_{\{\mathbf{H}_b\}}(\{\mathbf{H}_b\})$. An exhaustive search is described in Algorithm 6.

Algorithm 6

Input γ, n_{it}
Init $\bar{R}^{\star} = 0$, $\bar{T}^{\star} = 0$, $\bar{T}^{\star}_{sim} = 0$
for $ch = 1$ to n_{ch} **do**
  Init $R^{\star} = 0$
  Draw channel $\mathbf{H}$
  for $\theta = 1$ to $|\mathcal{P}|$ **do**
    Create (precoded) channel $\boldsymbol{H}_{\theta}$
    for $\nu = 1$ to $|\mathcal{M}|$ **do**
      Compute $R_{\theta,\nu} = n_{t,\theta}\rho_{\nu}$
      if $R_{\theta,\nu} > R^{\star}$ **then**
        Run evolution analysis to get $P_e^{(n_{it})}(\omega)$
        if $P_e^{(n_{it})} \leq \varepsilon$ **then**
          $R^{\star} \leftarrow R_{\theta,\nu}$
        else
          break (save complexity!)
        end if
      end if
    end for
  end for
  $\bar{R}^{\star} \leftarrow \bar{R}^{\star} + R^{\star}$, $\bar{T}^{\star} \leftarrow \bar{T}^{\star} + R^{\star}(1 - P_e^{(n_{it})}(\omega^{\star}))$
  Run Monte Carlo simulation to get $P_{e,sim}^{(n_{it})}(\omega^{\star})$
  $\bar{T}^{\star}_{sim} \leftarrow \bar{T}^{\star}_{sim} + R^{\star}(1 - P_{e,sim}^{(n_{it})}(\omega^{\star}))$
end for
Outputs $\bar{R}^{\star}(\gamma, n_{it}) = \frac{\bar{R}^{\star}}{n_{ch}}$, $\bar{T}^{\star}(\gamma, n_{it}) = \frac{\bar{T}^{\star}}{n_{ch}}$, and $\bar{T}^{\star}_{sim}(\gamma, n_{it}) = \frac{\bar{T}^{\star}_{sim}}{n_{ch}}$

6.6 Numerical results

Multiple channel models are simulated in this section. Therefore, all these channel models are reported in the following Table 6.1.

6.6.1 Convolutionally coded MIMO

The set of MCS constructed out of convolutional code and optimal calibrating factors are reported in Table 6.2. The LUTs of BER, BLER and symbol variance derived from LAPPR on coded bits are plotted in Fig. 6.2, Fig. 6.3

index	MIMO	n_b	n_τ	power profile
CH1	4x4	1	0	$\sigma^2_{1;0} = 1$
CH2	4x4	1	3	$\{\sigma^2_{1;0}, \sigma^2_{1;1}, \sigma^2_{1;2}, \sigma^2_{1;3}\} = \{0.8669, 0.1170, 0.0158, 0.0003\}$
CH3	4x4	4	0	$\sigma^2_{b;0} = 1, \forall b = 1, \ldots, n_b$
CH4	4x4	1	3	$\sigma^2_{1;\tau} = 0.25, \forall \tau = 0, \ldots, n_\tau$

Table 6.1: Set of channel models for numerical simulations

and Fig. 6.4, respectively. They are based on 64-state rate-1/3 or rate-1/2 (punctured) non-recursive non-systematic convolutional (NRNSC) encoders and QAM modulations (Gray labeling). We choose $n_s = 288$.

index ν	type encoder	r_ν	constellation	q_ν	ρ_ν	β_ν
1	NRNSC	1/3	QPSK	2	0.67	1.0
2	NRNSC	1/2	QPSK	2	1.00	1.5
3	NRNSC	2/3	QPSK	2	1.33	2.0
4	NRNSC	3/4	QPSK	2	1.50	2.3
5	NRNSC	5/6	QPSK	2	1.67	2.8
6	NRNSC	1/2	16QAM	4	2.00	2.5
7	NRNSC	2/3	16QAM	4	2.67	4.8
8	NRNSC	3/4	16QAM	4	3.00	6.0
9	NRNSC	5/6	16QAM	4	3.33	6.5
10	NRNSC	2/3	64QAM	6	4.00	8.0
11	NRNSC	3/4	64QAM	6	4.50	9.5
12	NRNSC	5/6	64QAM	6	5.00	10.0

Table 6.2: Set of MCS based on convolutional code and optimal calibrating factors

6.6.1.1 Open-loop MIMO

First, average simulated and predicted BLER are compared over several SNR over CH1 n_s is fixed to 288 which yields $L = 288$. For each SNR, we evaluated the average simulated BLER by Monte Carlo simulation which is stopped after 800 block errors. The predicted BLER is evaluated over 10000 channel outcomes. The simulated and predicted (with calibration factors reported in Table 6.2) results for 16QAM-2/3, 16QAM-5/6, 64QAM-2/3 and 64QAM-5/6 are shown in Fig. 6.5, Fig. 6.6, Fig. 6.7 and Fig. 6.8, respectively. For all MCS, the predicted average BLERs match very well

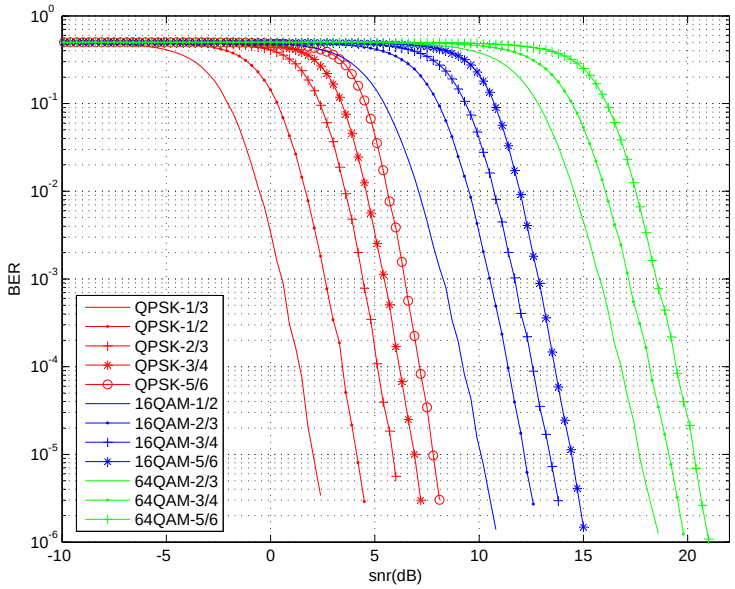

Figure 6.2: LUTs of BER of 12 MCS adapted to 4 transmit antenna

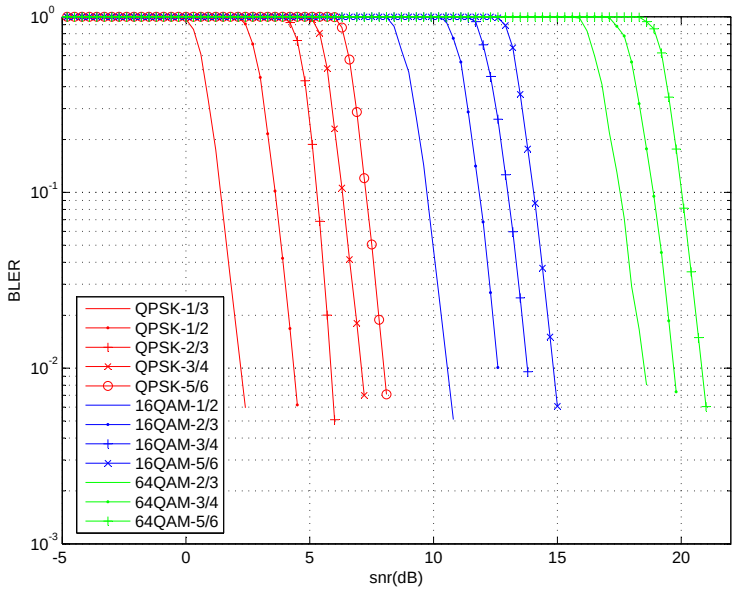

Figure 6.3: LUTs of BLER for 12 MCS adapted to 4 transmit antenna

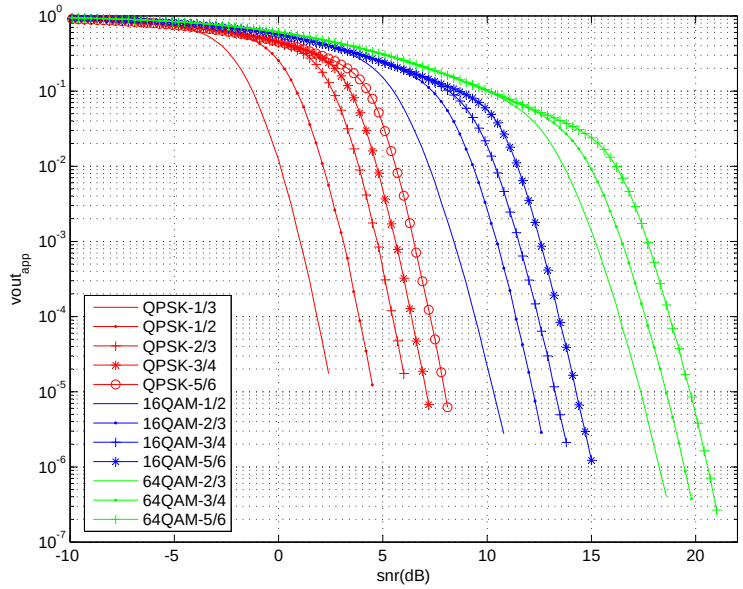

Figure 6.4: LUTs of symbol variance computed from LAPPR on coded bits for 12 MCS adapted to 4 transmit antenna

the simulated ones for each MCS at different iterations which confirm the accuracies and reliabilities of chosen calibration factors per MCS.

6.6.1.2 Closed-loop MIMO

Second, the closed-loop link adaptation procedure is tested for two types of channels: CH1 and CH2 (exponential decreasing ISI power profile) as reported in Table 6.1. The target BLER is $\varepsilon = 10^{-1}$.

Firstly, LAPPR-based iterative LMMSE-IC is performed at the destination. The length of the sliding window (in CH2) is $L_{SW} = 33$ with $L_1 = L_2 = 16$. For each SNR, we evaluated the average predicted and simulated throughputs over $n_{ch} = 1000$ channel outcomes. For each channel outcome, Monte Carlo simulation is stopped after 100 block errors. The results are shown in Fig. 6.9 and Fig. 6.10 for CH1 and CH2, respectively. For CH1, we observe that the average predicted throughput matches exactly the average simulated throughput and increases dramatically as iterations progress. The Genie-aided IC curve corresponds to the ideal case where interference is completely canceled (upper bound). The average rate

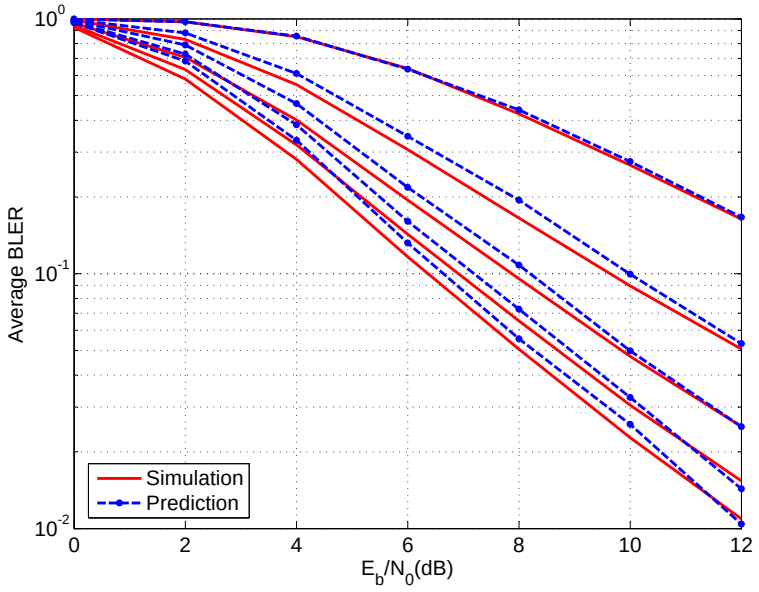

Figure 6.5: Smulated vs. predicted (with calibration) average BLER for 16QAM-2/3 over CH1

at first iteration demonstrates that we should adaptively allocate higher rates (as proposed in this chapter) to exploit the full turbo receiver potential. For CH2, the situation is different. Indeed, the average simulated throughput becomes much worse than the average predicted throughput at the first iteration and high SNR. This may be surprising that the simulated throughput is not monotonically increasing at the first iteration. However, in closed-loop system, good simulated results can be obtained only if the precoder and MCS selections are appropriate, neither too optimist nor too pessimist. After careful examination of all assumptions, the non-validity of (A6-b, chapter 2) in the simulation is identified to be responsible for this phenomenon: The chosen value $n_s = 288$ is too small at this situation for high-order high-rate MCS. Larger interleaver sizes or less residual interference (during the course of iterations) can help to reduce the discrepancy between average predicted and simulated throughputs. This is obviously seen in Fig. 6.10 where the average predicted throughput starts matching very well the average simulated throughput at third and fifth iterations. To resolve the problem of insufficient interleaver size, we keep the $n_s = 288$ for each codeword while 50 codewords are interleaved by a single interleaver

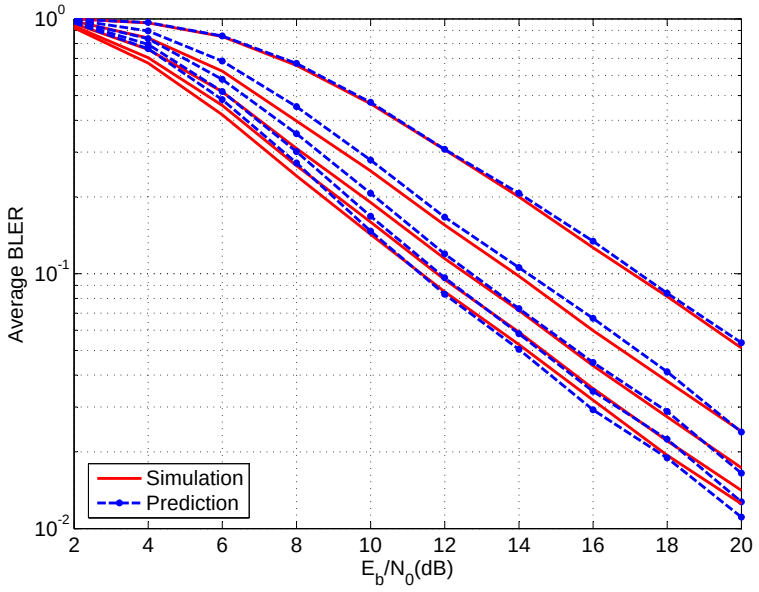

Figure 6.6: Smulated vs. predicted (with calibration) average BLER for 16QAM-5/6 over CH1

with 50 times larger size. The results are potted in Fig. 6.11 where accurate match between the predicted and simulated throughput can be obtained.

We then analyzed LEXTPR-based iterative LMMSE-IC over CH2. The set of MCS, sliding window size, number of channel uses per codeword keep the same. New necessary LUTs are generated for the LEXTPR-based LMMSE-IC. In this case, no calibration is needed since the assumptions (A1-a - A3-a, chapter 2) are valid. In the finite size regime (288 c.u.) the predicted and simulated throughput do not match for all iterations as shown in Fig. 6.12. Indeed, the residual interference after LEXTPR based interference subtraction keeps high having (A6-a, chapter 2) not valid even for the subsequent iterations. This demonstrates the superiority of LAPPR-based iterative LMMSE-IC as shown in Fig. 6.10. For the infinite size regime (50 times larger interleaver size as before), the results are shown in Fig. 6.13 where the predicted throughputs match accurately the simulated throughputs at every iterations (no calibration is applied). Comparing Fig. 6.13 and Fig. 6.11, the performance at the fifth iteration of LEXTPR-based LMMSE-IC is close to the performance at the third iteration of LAPPR-based LMMSE-IC.

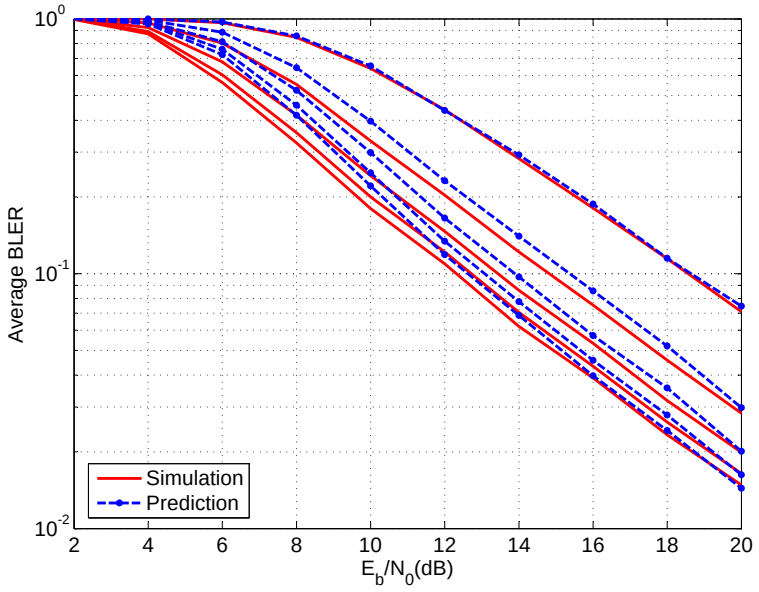

Figure 6.7: Smulated vs. predicted (with calibration) average BLER for 64QAM-2/3 over CH1

6.6.2 Turbo coded MIMO

The set of MCS constructed out of turbo code and optimal calibrating factors are reported in Table 6.3. Turbo codes are based on two 8-state rate-1/2 recursive systematic convolutional (RSC) encoders with generator matrix $\mathbf{G} = [1, g_1/g_0]$ where $g_0 = [1011]$ and $g_1 = [1101]$ and QAM modulations (Gray labeling). LAPPR-based iterative LMMSE-IC is performed at the destination. n_s is fixed to 2040.

6.6.2.1 Open-loop MIMO

First, average simulated and predicted BLER are compared over several SNR over a general CH3 as reported in Table 6.1. n_s is fixed to 2040 which yields $L = 510$. For each SNR, we evaluated the average simulated BLER by Monte Carlo simulation which is stopped after 800 block errors. The predicted BLER is evaluated over 10000 channel outcomes. The simulated and predicted (with calibration factors reported in Table 6.3) results for QPSK-5/6, 16QAM-1/2, 16QAM-2/3 and 16QAM-5/6 are shown in Fig.

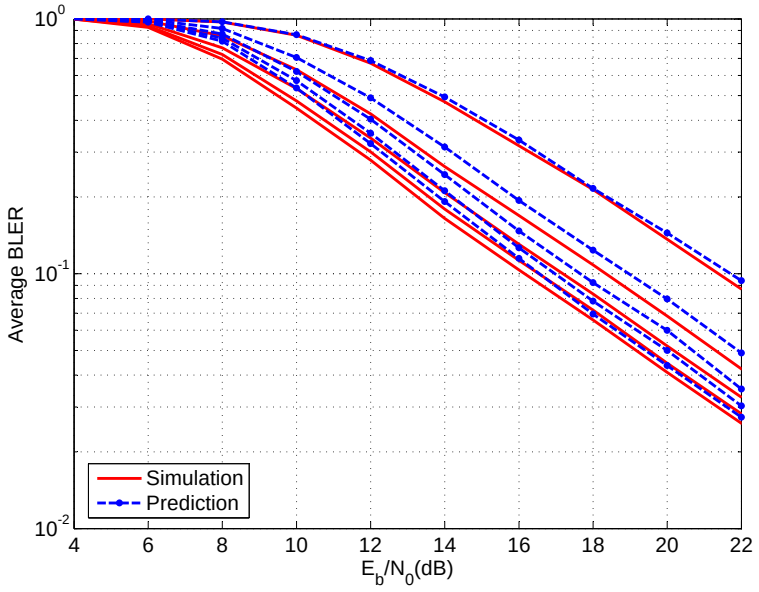

Figure 6.8: Smulated vs. predicted (with calibration) average BLER for 64QAM-5/6 over CH1

index ν	r_ν	constellation	q_ν	ρ_ν	β_ν
1	1/3	QPSK	2	0.67	1.7
2	1/2	QPSK	2	1.00	2.0
3	2/3	QPSK	2	1.33	2.5
4	3/4	QPSK	2	1.50	2.7
5	5/6	QPSK	2	1.67	3.7
6	1/2	16QAM	4	2.00	3.3
7	2/3	16QAM	4	2.67	6.5
8	3/4	16QAM	4	3.00	9.5
9	5/6	16QAM	4	3.33	17.0

Table 6.3: Set of MCS based on turbo code and optimal calibrating factors

6.14, Fig. 6.15, Fig. 6.16 and Fig. 6.17, respectively. For all MCS, the predicted average BLERs match very well the simulated ones for each MCS at different iterations which confirm the accuracies and reliabilities of chosen calibration factors per MCS.

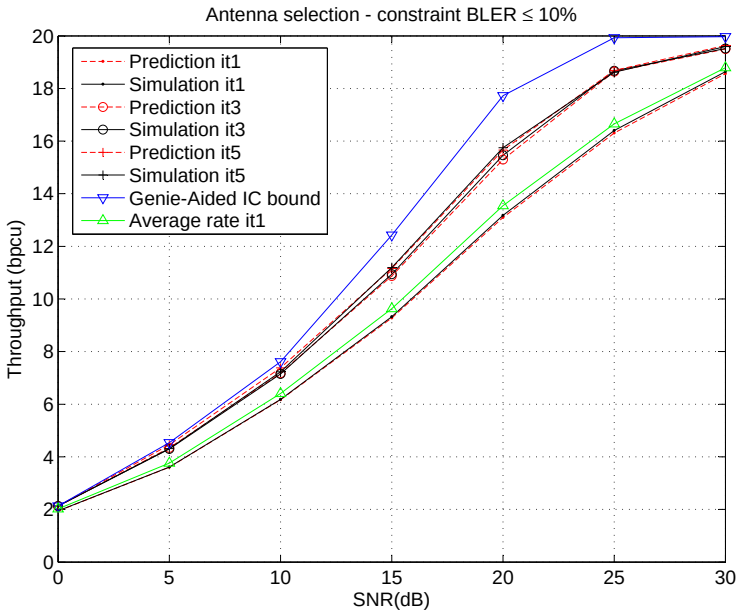

Figure 6.9: Average predicted and simulated throughputs (in bpcu) in closed-loop convolutionally coded MIMO systems vs. SNR (dB) – CH1, LAPPR-based iterative LMMSE-IC

6.6.2.2 Closed-loop MIMO

Second, the closed-loop link adaptation for turbo coded MIMO systems is tested for three types of channels, CH1, CH3 and CH4 as reported in Table 6.1. n_s is fixed to 2040 which yields $L = 2040$ for CH1 and CH4, and $L = 510$ for CH3. The target BLER is $\varepsilon = 10^{-1}$. The set of MCS and optimal calibrating factors are reported in Table 6.3. The maximum number of bits per channel use (bpcu) is 13.33. The length of the sliding window (for CH4) is $L_{SW} = 33$ with $L_1 = L_2 = 16$. For each SNR, we evaluated the average predicted and simulated throughputs over $n_{ch} = 1000$ channel outcomes. For each channel outcome, the Monte Carlo simulation is stopped after 100 block errors. The results for CH1, CH3, and CH4 are shown in Fig. 6.18, Fig. 6.19, and Fig. 6.20, respectively. For all channels, we observe that the average predicted throughputs match perfectly the average simulated ones at every iteration which proves the effectiveness of the performance prediction method. We also note that throughputs increase dramatically as iterations progress.

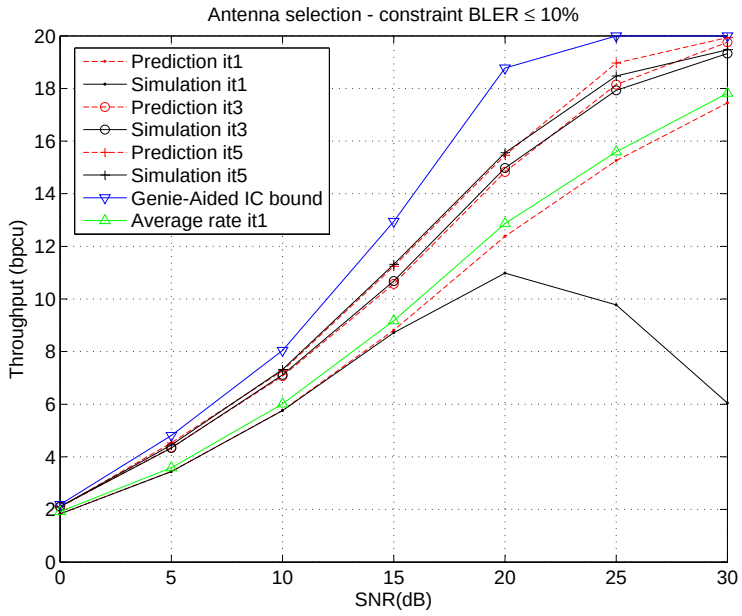

Figure 6.10: Average predicted and simulated throughputs (in bpcu) in closed-loop convolutionally coded MIMO systems vs. SNR (dB) – CH2, LAPPR-based iterative LMMSE-IC

6.7 Conclusion

In this chapter, the problem of link adaptation for closed-loop coded MIMO systems employing LMMSE-IC based turbo receivers has been addressed. For the convolutional coded case, Monte Carlo simulations under limited feedback show a significant gain of around 3 and 4dB compare to the classical LMMSE receiver conditional on a data rate of 12 bits per channel use, for a 4x4 MIMO frequency flat and frequency selective channel, respectively. Moreover, they also confirm that using LAPPR rather than LEXTPR on coded bits for soft interference regeneration and cancellation yields faster convergence of the iterative process and better final performance (both for finite and infinite interleaver length regimes). For the turbo coded case, based on a PHY-layer abstraction of the whole turbo receiver, the link-level predicted and simulated performance for three communication scenarios have been shown.

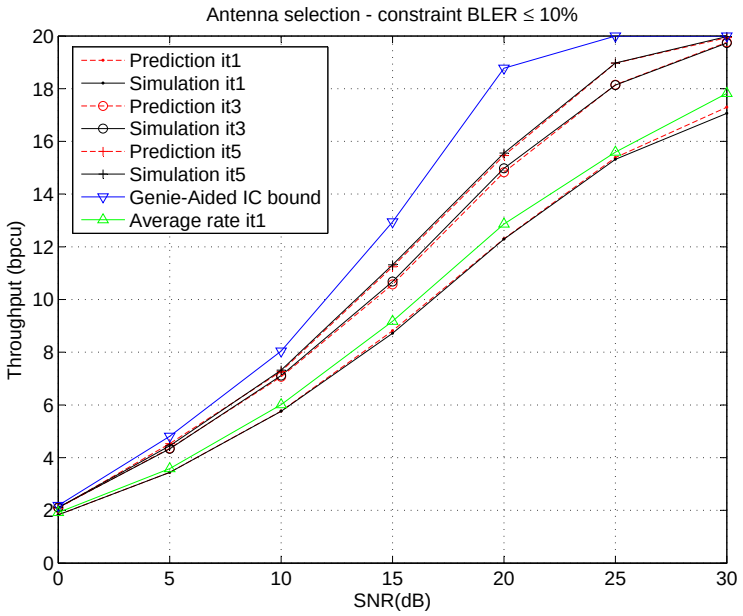

Figure 6.11: Average predicted and simulated throughputs (in bpcu) with 50 times larger interleaver size in closed-loop convolutionally coded MIMO systems vs. SNR (dB) – CH2, LAPPR-based iterative LMMSE-IC

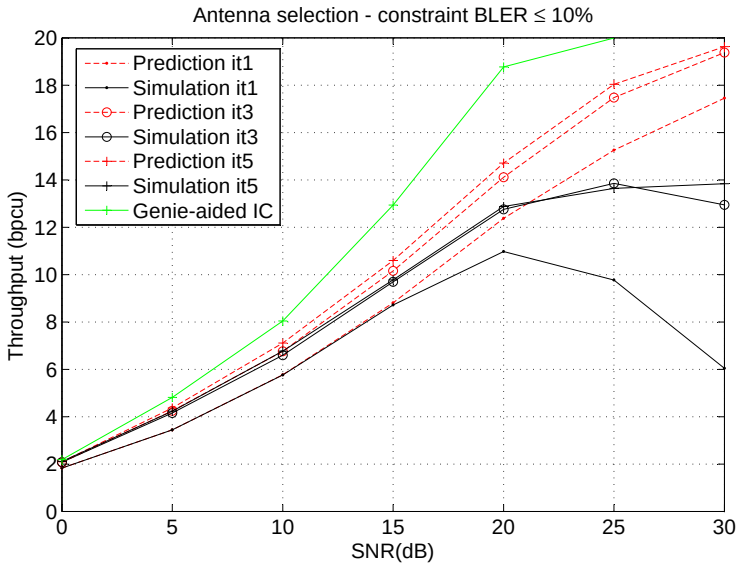

Figure 6.12: Average predicted and simulated throughputs (in bpcu) in closed-loop convolutionally coded MIMO systems vs. SNR (dB) – CH2, LEXTPR-based iterative LMMSE-IC

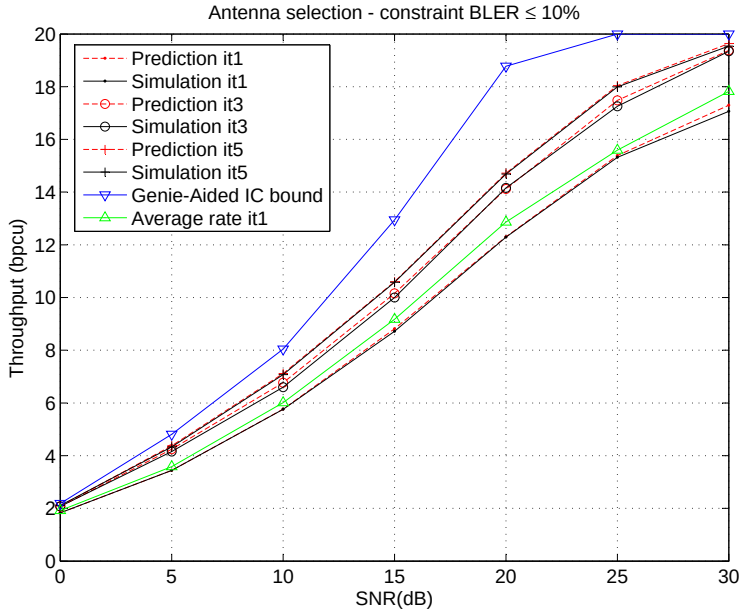

Figure 6.13: Average predicted and simulated throughputs (in bpcu) with 50 times larger interleaver size in closed-loop convolutional coded MIMO systems vs. SNR (dB) – CH2, LEXTPR-based iterative LMMSE-IC

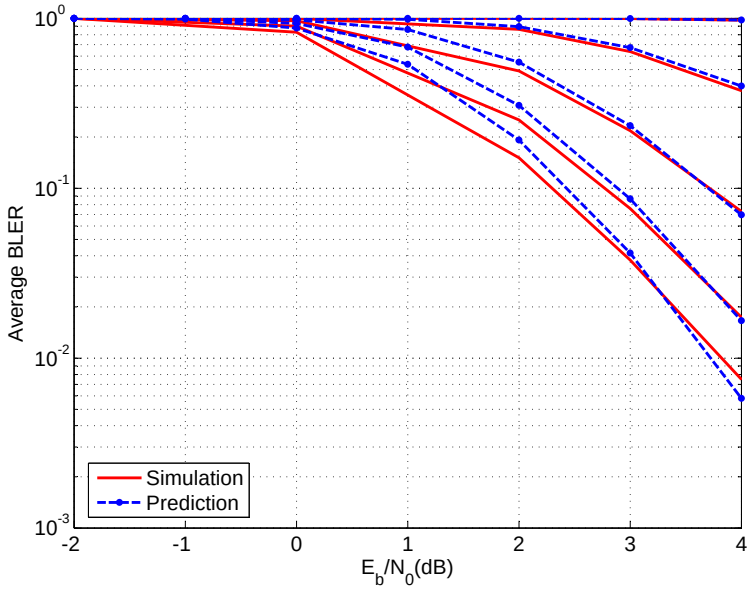

Figure 6.14: Smulated vs. predicted (with calibration) average BLER for QPSK-5/6 over CH3

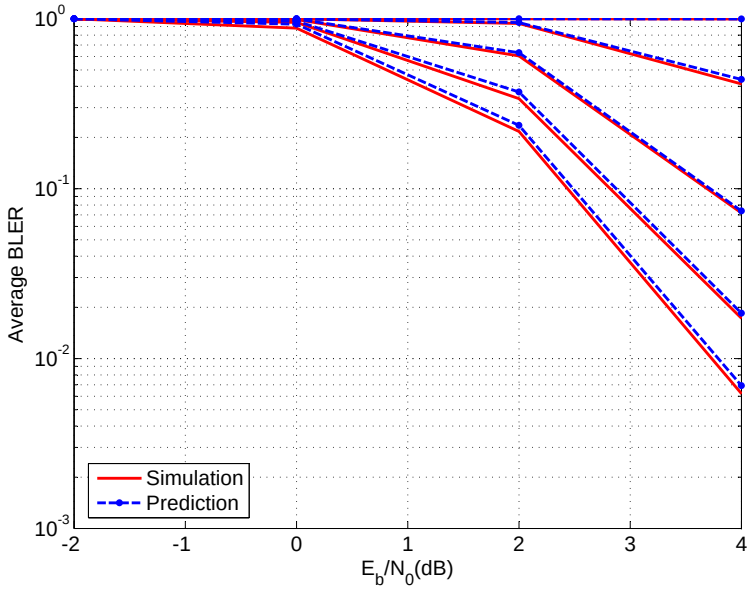

Figure 6.15: Smulated vs. predicted (with calibration) average BLER for 16QAM-1/2 over CH3

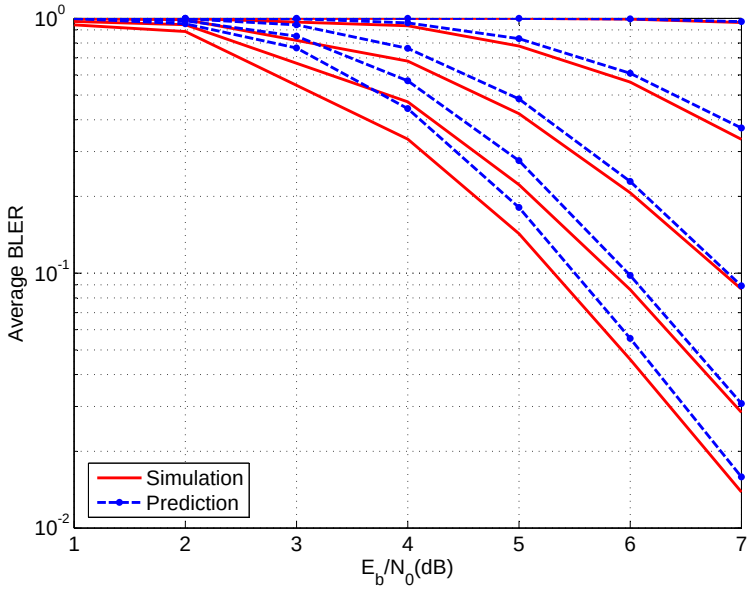

Figure 6.16: Smulated vs. predicted (with calibration) average BLER for 16QAM-2/3 over CH3

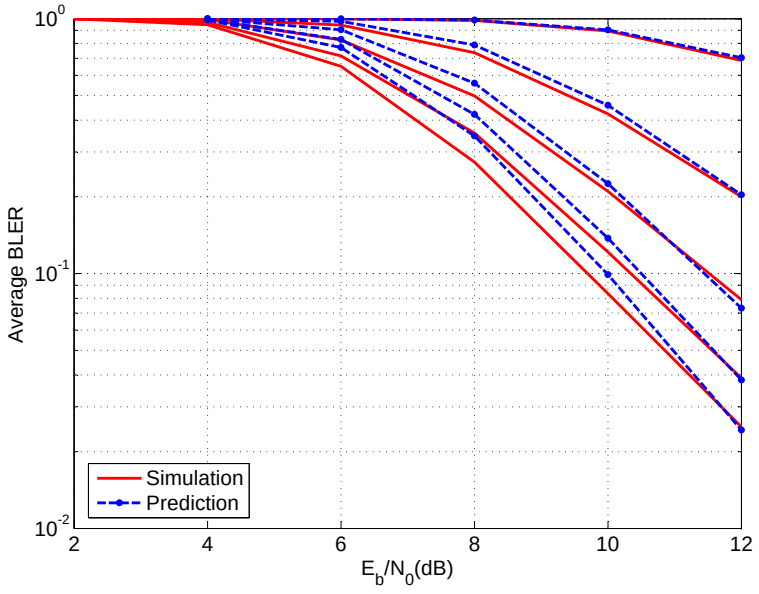

Figure 6.17: Smulated vs. predicted (with calibration) average BLER for 16QAM-5/6 over CH3

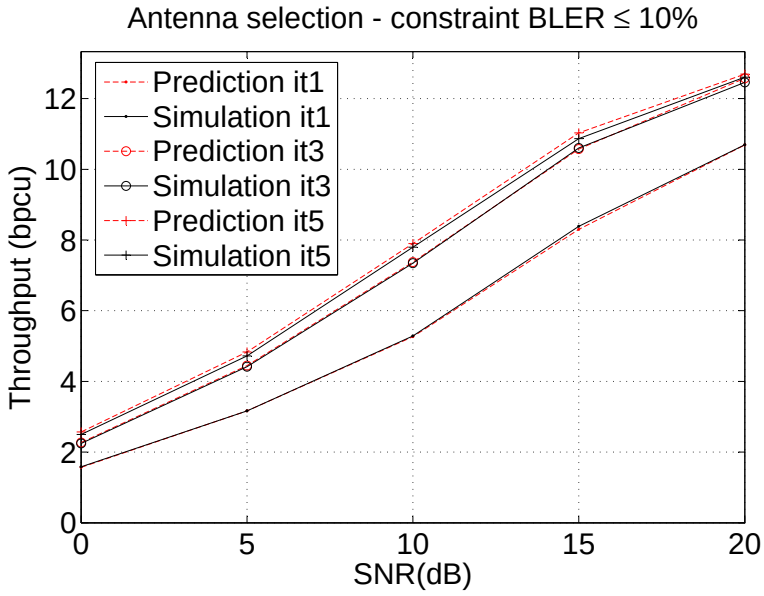

Figure 6.18: Average predicted and simulated throughputs (in bpcu) in closed-loop turbo coded MIMO systems vs. SNR (dB) – CH1, LAPPR-based iterative LMMSE-IC

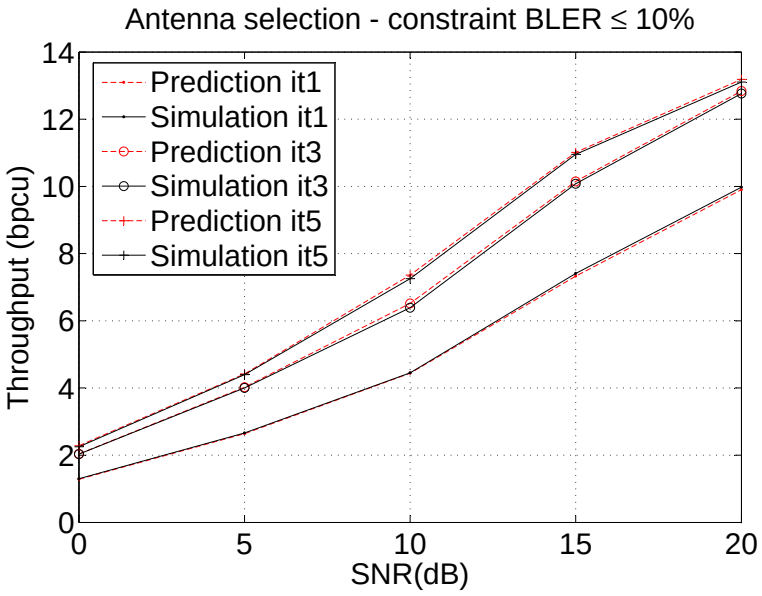

Figure 6.19: Average predicted and simulated throughputs (in bpcu) in closed-loop turbo coded MIMO systems vs. SNR (dB) – CH3, LAPPR-based iterative LMMSE-IC

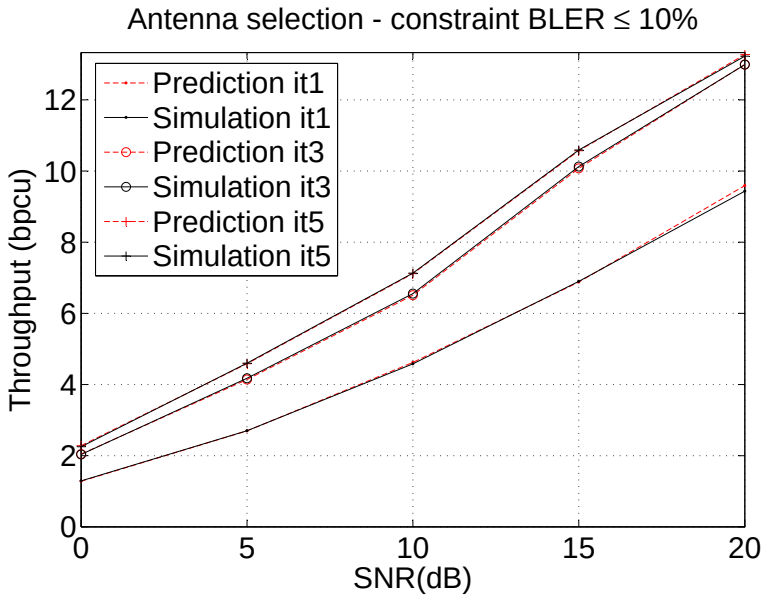

Figure 6.20: Average predicted and simulated throughputs (in bpcu) in closed-loop turbo coded MIMO systems vs. SNR (dB) – CH4, LAPPR-based iterative LMMSE-IC

Chapter 7

Independent coding per antenna (selective PARC)

7.1 Introduction

Employing the proposed PHY-layer abstraction, the link adaptation in closed-loop turbo coded MIMO systems has been firstly investigated in [98] which is limited to STBICM scheme, i.e., single codeword transmission. In 4G wireless mobile standards (e.g., LTE-A), however, multiple codewords are allowed to be transmitted. Therefore, selective PARC [99] with turbo receivers are investigated in this chapter where the best subset of transmit antennas are selected and each antenna transmits an independent MCS constructed out of powerful turbo code. We formulate the task of joint selection of spatial precoder (the best subsets of antennas), decode ordering and per antenna rate as a discrete optimization problem and detail an exhaustive search procedure to accurately predict the average link level performance.

7.2 System model

We consider a transmission over a MIMO block Rayleigh fading AWGN channel with n_b fading blocks, n_t transmit and n_r receive antennas. Each transmit antenna transmits an independent MCS. Partial state information is assumed at the transmitter through a low rate feedback. Perfect channel

This chapter will be partially presented in a conference paper in preparation

state information is assumed at the receiver. The total number n_s of channel uses available for transmission is fixed and the number of channel uses per fading block is given as $L = n_s/n_b$.

7.2.1 Coding strategy

Under limited feedback, only a finite number of transmission schemes are available at the transmitter side, i.e., a finite set of spatial precoders and a finite set of MCS. Let $\mathcal{P}$ be the set of available spatial precoders. Antenna selection is used as a simple form of spatial precoding. A spatial precoder indexed by $\theta \in \mathcal{P}$ selects $n_{t,\theta} \leq n_t$ antennas and is specified by a precoding matrix $\mathbf{\Phi}_\theta$. If $\{\delta_1, \ldots, \delta_{n_{t,\theta}}\}$ is the index set of selected antennas, then $\mathbf{\Phi}_\theta = 1/\sqrt{n_{t,\theta}}[\mathbf{e}_{\delta_1}, \ldots, \mathbf{e}_{\delta_{n_{t,\theta}}}]$ where $\mathbf{e}_{\delta_t}$ is the n_t-dimensional vector with 1 at position δ_t and 0 elsewhere. Let $\mathcal{M}$ be the set of available MCS indices. An MCS indexed by $\nu_t \in \mathcal{M}$ is a BICM transmitted over the t-th transmit antenna, specified by a turbo code $\mathscr{C}_{\nu_t}$ of rate r_{ν_t} and a complex constellation $\mathscr{X}_{\nu_t} \subset \mathbb{C}$ of cardinality $2^{q_{\nu_t}}$ and a memoryless labeling rule μ_{ν_t}. We define the rate of the MCS ν_t as $\rho_{\nu_t} = r_{\nu_t} q_{\nu_t}$ (bits/complex dimension). By convention, MCS are indexed in increasing order of the rates, i.e., the MCS no. 1 has the lowest rate, and the MCS no. $|\mathcal{M}|$ the highest. Under the spatial precoder indexed by θ, there are $|\mathcal{M}|^{n_{t,\theta}}$ MCS combinations to be allocated over $n_{t,\theta}$ antennas. The MCS combination is indexed by χ with possible values among $1, \ldots, |\mathcal{M}|^{n_{t,\theta}}$. By convention, $\chi = 1$ corresponds to the MCS combination $\{\nu_t = 1\}_{t=1}^{n_{t,\theta}}$ and $\chi = |\mathcal{M}|^{n_{t,\theta}}$ corresponds to the MCS combination $\{\nu_t = |\mathcal{M}|\}_{t=1}^{n_{t,\theta}}$. The encoding process under spatial precoder θ is detailed for a certain selected antenna $t \in \{\delta_1, \ldots, \delta_{n_{t,\theta}}\}$. The vector of binary data (or information bits) $\mathbf{u}_t$ enters a turbo encoder φ_{ν_t} whose output is the codeword $\mathbf{c}_t \in \mathscr{C}_{\nu_t}$ of length $n_{c,\nu_t} = n_s q_{\nu_t}$. The codeword bits are interleaved by a random time interleaver π_{ν_t} and reshaped as a collection of integer matrices $\{\mathbf{D}_{b;t}\}_{b=1}^{n_b}$ with $\mathbf{D}_{b;t} \in \mathbb{Z}_{2^{q_{\nu_t}}}^{1\times L}$. Each integer entry can be decomposed into a sequence of q_{ν_t} bits. A Gray mapping μ_{ν_t} transforms each matrix $\mathbf{D}_{b;t}$ into a complex matrix $\mathbf{S}_{b;t} \in \mathscr{X}_{\nu_t}^{1\times L}$. $\mathscr{X}_{\nu_t,j}^{(0)}$ and $\mathscr{X}_{\nu_t,j}^{(1)}$ denote the subsets of points in $\mathscr{X}_{\nu_t}$ whose labels have a 0 or a 1 at position j. With a slight abuse of notation, let $\{d_{b;t,l,j}\}_{j=1}^{q_{\nu_t}}$ denote the set of bits labeling the symbol $s_{b;t,l} \in \mathscr{X}_{\nu_t}$. Let also $\mu_{\nu_t,j}^{-1}(s)$ be the value of the j-th bit in the labeling of any point $s \in \mathscr{X}_{\nu_t}$. Selective PARC with spatial precoding (antenna selection) is depicted in Fig.7.1.

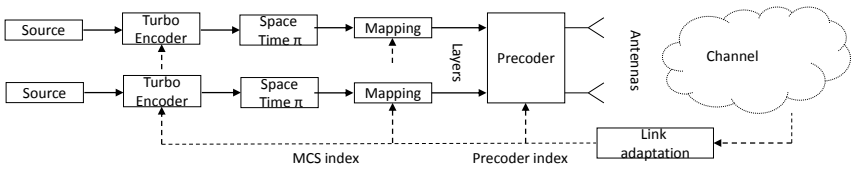

Figure 7.1: Selective PARC with spatial precoding

7.2.2 Received signal model

Let $\check{\mathbf{H}}_b^\theta = \mathbf{H}_b \mathbf{\Phi}_\theta$ denotes the precoded channel for the b-th fading block. The discrete-time vector $\mathbf{y}_{b;l} \in \mathbb{C}^{n_r}$ received by the destination at b-th fading block and time $l = 1, \ldots, L$, is expressed as

$$\mathbf{y}_{b;l} = \check{\mathbf{H}}_b^\theta \mathbf{s}_{b;l} + \mathbf{w}_{b;l} \tag{7.1}$$

In (7.1), the vectors $\mathbf{s}_{b;l} \in \mathscr{X}_\nu^{n_{t,\theta}}$ are i.i.d. random vectors (uniform distribution) with $\mathbb{E}[\mathbf{s}_{b;l}] = \mathbf{0}_{n_{t,\theta}}$ and $\mathbb{E}[\mathbf{s}_{b;l}\mathbf{s}_{b;l}^\dagger] = \mathbf{I}_{n_{t,\theta}}$, and the vectors $\mathbf{w}_{b;l} \in \mathbb{C}^{n_r}$ are i.i.d. random vectors, circularly-symmetric Gaussian, with zero-mean and covariance matrix $\sigma_w^2 \mathbf{I}_{n_r}$.

7.2.3 Decoding strategy

Under spatial precoder indexed by θ, $n_{t,\theta}$ codewords are received. The global performance of the turbo receiver depends on the decode ordering. Let $\mathcal{W}_\theta$ be the set of available decode orderings under spatial precoder θ with $|\mathcal{W}_\theta| = \prod_{t=1}^{n_{t,\theta}} t$. A decode ordering indexed by $\kappa \in \mathcal{W}_\theta$ can be seen as a one-to-one correspondance $\{t \to k_{t,\kappa} : t = 1, \ldots, n_{t,\theta}\}$ where t is the antenna index and $k_{t,\kappa}$ is its decode order index. After the $n_{t,\theta}$-th decode, one global iteration completes. This decode ordering is repeated iteratively. By convention, the decode ordering indexed by 1 correspond to the natural decode ordering $\{k_{t,1} = t : t = 1, \ldots, n_{t,\theta}\}$. This natural ordering may be not the optimal ordering which maximizes the throughput subject to the block error rate constraint.

Furthermore, the turbo decoder is made of *two* BCJR decoders [38] exchanging probabilistic information (log domain). The first BCJR decoder computes the LAPPRs on its own coded bits (information and parity bits)

taking into account the available a priori information on systematic information bits stored from an earlier activation (i.e., the most recent LEXTPRs on systematic information bits delivered by the second BCJR decoder). Then the second BCJR decoder is activated and computes the LAPPRs on its own coded bits (information and parity bits) taking into account the available a priori information transmitted by the first BCJR decoder. The optimal global schedule is described here. First, the best subset of antennas should be selected. Second, one global iteration follows the optimal decode ordering. Third, the detection and decoding process at each antenna comprises of one pass of equalizer followed by one pass of first BCJR decoder followed by one pass of second BCJR decoder. Such a global message-passing schedule provides much better global results than the conventional one, i.e., a single pass of joint equalizer followed by an arbitrary number of turbo decoder iterations. The message-passing schedule without antenna selection considering the natural decode ordering is summarized in Fig. 5.1.

7.3 LMMSE-IC based turbo receivers

Empirical evidence reveals that the LAPPR-based iterative LMMSE-IC algorithm can significantly outperform its LEXTPR-based counterpart for highly loaded multiantenna or multiuser systems. As a consequence, we intentionally focus on this particular class. For each BICM, the different steps comprising the interference regeneration and cancellation, LMMSE estimation, demapping and decoding can be found in chapter 5.

7.4 PHY-layer abstraction

The PHY-layer abstraction follows the one described in in chapter 5. The performance evolution analysis should follow the chosen message-passing schedule (Fig. 5.1 exemplifies the natural ordering). A recapitulative diagram of the method can be found in Fig. 5.2 for t-th antenna at i-th iteration.

7.5 Link level performance evaluation

Selective PARC performs *joint* selection of spatial precoder (the best subset of antennas), decode ordering and MCS combination. It aims at *maximizing* the *average rate* subject to a target BLER constraint assuming LAPPR-based iterative LMMSE-IC at the destination. The number of iterations n_{it} depends on the destination computational capacity.

For a given SNR γ and a given channel outcome $\{\mathbf{H}_b\}$, the optimization problem to solve can be formulated as follows:

$$\begin{array}{ll} \text{Find} & R^\star(\gamma, \{\mathbf{H}_b\}, n_{it}) = \max_{\omega\in\Omega} \sum_{t=1}^{n_{t,\theta}} \rho_{\nu_t} \\ \text{subject to} & C_1, C_2 \end{array}$$

where

- $\omega = \{\theta, \kappa, \chi\}$ is a particular system configuration in Ω, the set of all possible spatial precoder, decode ordering and MCS indices.
- $\{P_t^{(n_{it})}(\omega)\}_{t=1}^{n_{t,\theta}}$ are the *predicted* BLER of all $n_{t,\theta}$ antennas at iteration n_{it} for a given system configuration ω.
- $C1 : n_{t,\theta} \leq \min(n_t, n_r)$.
- $C2 : \{P_t^{(n_{it})}(\omega) \leq \varepsilon\}_{t=1}^{n_{t,\theta}}$.

In practice, retransmission is activated where one block error is detected. Assuming ARQ Type-I retransmission algorithm and retransmissions within the coherence time of the channel, the *predicted* throughput is defined as

$$T^\star(\gamma, \{\mathbf{H}_b\}, n_{it}) = \sum_{t=1}^{n_{t,\theta}} \rho_{\nu_t^\star}(1 - P_t^{(n_{it})}(\omega^\star)) \tag{7.2}$$

where $\omega^\star = \{\theta^\star, \kappa^\star, \chi^\star\}$ is the optimal selection. For comparison, the *simulated* BLER $\{P_{t,sim}^{(n_{it})}(\omega^\star)\}_{t=1}^{n_{t,\theta^\star}}$ and the *simulated* throughput $T_{sim}^\star(\gamma, \{\mathbf{H}_b\}, n_{it})$ defined as

$$T_{sim}^\star(\gamma, \{\mathbf{H}_b\}, n_{it}) = \sum_{t=1}^{n_{t,\theta}} \rho_{\nu_t^\star}(1 - P_{t,simu}^{(n_{it})}(\omega^\star)) \tag{7.3}$$

are obtained via Monte Carlo simulation. Then, we evaluate the average predicted rate $\bar{R}^\star(\gamma, n_{it}) = \mathbb{E}[R^\star(\gamma, \{\mathbf{H}_b\}, n_{it})]$, the average predicted throughput $\bar{T}^\star(\gamma, n_{it}) = \mathbb{E}[T^\star(\gamma, \{\mathbf{H}_b\}, n_{it})]$ and the average simulated throughput $\bar{T}_{sim}^\star(\gamma, n_{it}) = \mathbb{E}[T_{sim}^\star(\gamma, \{\mathbf{H}_b\}, n_{it})]$ where expectation is w.r.t. $p_{\{\mathbf{H}_b\}}(\{\mathbf{H}_b\})$. An exhaustive search procedure is described in Algorithm 7.

Algorithm 7

Input γ, n_{it}
Init $\bar{R}^\star = 0$, $\bar{T}^\star = 0$, $\bar{T}^\star_{sim} = 0$
for $ch = 1$ to n_{ch} **do**
  Init $R^\star = 0$, $T^\star = 0$
  Draw channel $\{\mathbf{H}_b\}$
  for $\theta = 1$ to $|\mathcal{P}|$ **do**
    Create (precoded) channel $\{\check{\mathbf{H}}_{b;\theta}\}$
    for $\kappa = 1$ to $|\mathcal{W}_\theta|$ **do**
      The evolution analysis ordering is fixed by κ.
      for $\chi = 1$ to $|\mathcal{M}|^{n_{t,\theta}}$ **do**
        Compute $R_{\theta,\kappa,\chi} = \sum_{t=1}^{n_{t,\theta}} \rho_{\nu_t}$
        if $R_{\theta,\chi,\kappa} > R^\star$ **then**
          Run evolution analysis to get $\{P_t^{(n_{it})}(\omega)\}_{t=1}^{n_{t,\theta}}$
          if $\{P_t^{(n_{it})} \leq \varepsilon\}_{t=1}^{n_{t,\theta}}$ **then**
            $R^\star \leftarrow R_{\theta,\chi,\kappa}$,
            $T^\star \leftarrow \sum_{t=1}^{n_{t,\theta}} \rho_{\nu_t}(1 - P_t^{(n_{it})}(\omega))$
          else
            break (save complexity!)
          end if
        end if
      end for
    end for
  end for
  $\bar{R}^\star \leftarrow \bar{R}^\star + R^\star$,
  $\bar{T}^\star \leftarrow \bar{T}^\star + T^\star$
  Run Monte Carlo simulation to get $P_{t,sim}^{(n_{it})}(\omega^\star)$
  $\bar{T}^\star_{sim} \leftarrow \bar{T}^\star_{sim} + \sum_{t=1}^{n_{t,\theta^\star}} \rho_{\nu_t^\star}(1 - P_{t,sim}^{(n_{it})}(\omega^\star))$
end for
Outputs $\bar{R}^\star(\gamma, n_{it}) = \frac{\bar{R}^\star}{n_{ch}}$, $\bar{T}^\star(\gamma, n_{it}) = \frac{\bar{T}^\star}{n_{ch}}$, and $\bar{T}^\star_{sim}(\gamma, n_{it}) = \frac{\bar{T}^\star_{sim}}{n_{ch}}$

7.6 Numerical results

A 2×2 MIMO 4-block Rayleigh fading AWGN channel (i.e., $n_b = 4$) is chosen for simulations. n_s is fixed to 4080 which yields $L = 1020$. Turbo codes are based on two 8-state rate-1/2 RSC encoders with generator matrix $\mathbf{G} = [1, g_1/g_0]$ where $g_0 = [1011]$ and $g_1 = [1101]$ and QAM modulations (Gray labeling). LAPPR-based iterative LMMSE-IC is performed at the destination. The target BLER is $\varepsilon = 10^{-1}$. We witnessed that 5 iterations are generally enough to ensure the convergence in practice. The MCS family as well as their associated calibration factor are reported in Table 7.1.

index ν	r_ν	constellation	q_ν	ρ_ν	β_ν
1	1/3	QPSK	2	0.67	1.7
2	1/2	QPSK	2	1.00	2.0
3	2/3	QPSK	2	1.33	2.5
4	3/4	QPSK	2	1.50	2.7
5	5/6	QPSK	2	1.67	3.7
6	1/2	16QAM	4	2.00	3.3
7	2/3	16QAM	4	2.67	6.5
8	3/4	16QAM	4	3.00	9.5
9	5/6	16QAM	4	3.33	17.0
10	2/3	64QAM	4	4.00	12.0
11	3/4	64QAM	4	4.50	22.0
12	5/6	64QAM	4	5.00	34.0

Table 7.1: Set of MCS and optimal calibrating factors

7.6.1 Open-loop MIMO

First, we test open loop spatial multiplexing in which the MCS at every antenna is fixed. The natural decode ordering is considered here. The average E_b is the same for two antennas. Average simulated an predicted BLER over open loop MIMO are shown for several SNR. For each SNR, we evaluated the average simulated BLER by Monte Carlo simulation which is stopped after 1000 block errors for both codewords. The predicted BLER is evaluated over 10000 channel realizations.

The results for two identical independent MCS fixed on two antenna are plotted in Fig 7.2, Fig 7.3, Fig 7.4 and Fig 7.5 for 16QAM-3/4, 64QAM-2/3, 64QAM-3/4 and 64QAM-5/6, respectively. We observe that the average pre-

dicted BLER match exactly the average simulated ones at every iterations which confirm the accuracies and reliabilities of chosen calibration factors per MCS.

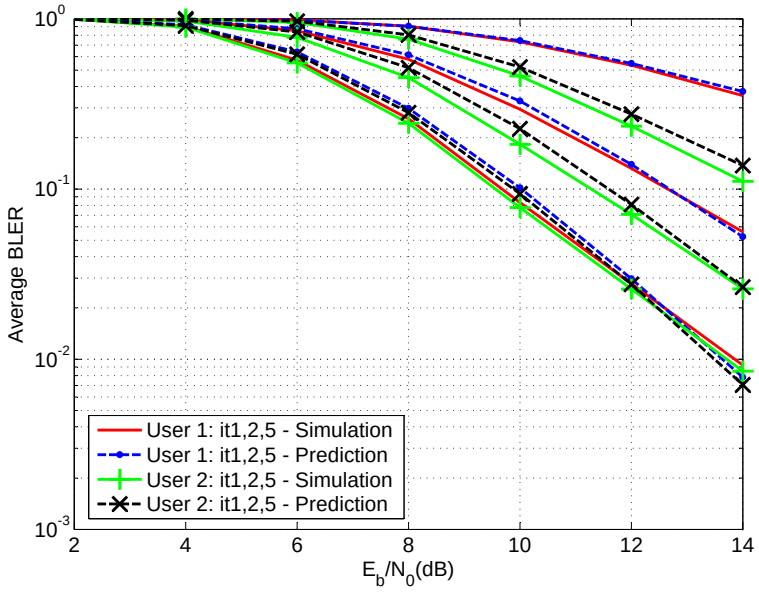

Figure 7.2: Average simulated vs. predicted BLER of LAPPR based iterative LMMSE-IC with two identical independent 16QAM-3/4 on two antennas over 2×2 MIMO -4 block fading channel

7.6.2 Selective PARC

Second, we consider a selective PARC system based on the turbo-encoded family. At each SNR, the average predicted throughput is evaluated over 1000 channel realizations. For each channel realization, Monte Carlo simulation is stopped after 100 block errors. The LMMSE benchmark corresponds to the one pass of joint LMMSE followed by 8 iterations of turbo-decoding. The Genie-Aided bound corresponds to perfect interference cancellation.

7.6.2.1 LAPPR-based iterative LMMSE-IC

The receiver is the described turbo-SIC receiver with one pass of DEC1 followed by one pass of DEC2 in the turbo decoder. The link adaptation

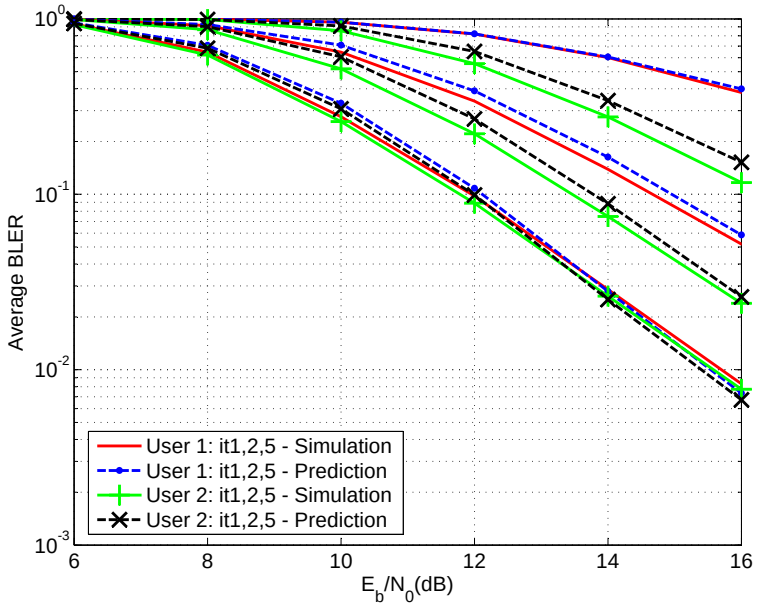

Figure 7.3: Average simulated vs. predicted BLER of LAPPR based iterative LMMSE-IC with two identical independent 64QAM-2/3 on two antennas over 2×2 MIMO -4 block fading channel

algorithm is the one described in Algorithm 7.

The results are plotted in Fig. 7.6. We observe that the predicted throughput match accurately the simulated throughput at every iterations. An exciting gain around 3dB is observed at 8 bpcu between iteration 8 and the LMMSE reference.

7.6.2.2 Non-iterative soft SIC

The receiver is a slightly modified schedule: the non-iterative soft SIC receiver with eight turbo decoding iterations. The link adaptation algorithm is the one described in Algorithm 7. The MCS family as well as their associated calibration factor are the same as reported in Table 7.1. The LUTs of BLER and BER for these MCS with 8 iterations turbo decodings are plotted in Fig. 7.7 and Fig. 7.8, respectively. The results are plotted in Fig. 7.9. We observe that the predicted throughput match accurately the simulated throughput in which an exciting gain is also observed.

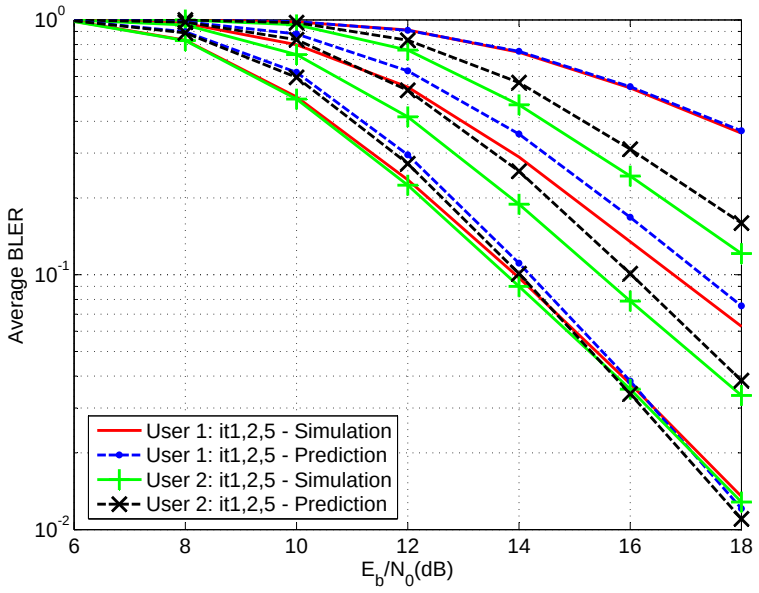

Figure 7.4: Average simulated vs. predicted BLER of LAPPR based iterative LMMSE-IC with two identical independent 64QAM-3/4 on two antennas over 2×2 MIMO -4 block fading channel

7.7 Conclusion

In this chapter, we have investigated the selective PARC in closed-loop MIMO systems with iterative LMMSE-IC (Turbo SIC) receiver and non-iterative soft SIC receiver. Each antenna transmits an independent BICM. The algorithm performs *joint* selection of spatial precoder (the best subset of antennas), decode ordering and MCS combination so as to *maximize* the *average rate* subject to a target BLER constraint. This is enabled by a novel semi-analytical PHY-layer abstraction whose accuracy and robustness are confirmed by the analysis and simulation results. A very exciting gain compare to the conventional LMMSE receiver is observed. Several future research works exist. First, the existing CRC-based SIC receiver will be simulated for comparison soon. Second, selective PARC in closed-loop convolutionally coded MIMO systems are to be tackled combing chapter 5 and chapter 6. Third, the generalization the whole framework of selective PARC to a more generalized MU-MIMO channel system and finally the multi-cell multiuser MIMO systems is necessary.

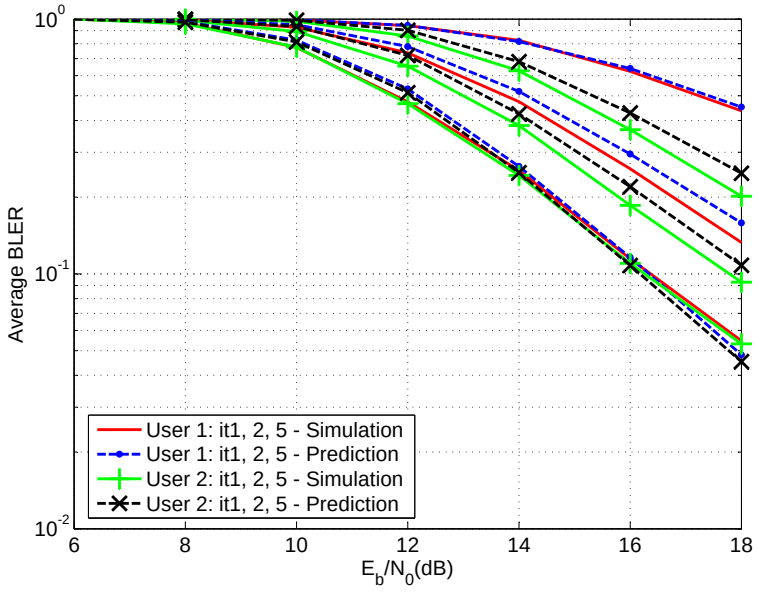

Figure 7.5: Average simulated vs. predicted BLER of LAPPR based iterative LMMSE-IC with two identical independent 64QAM-5/6 on two antennas over 2×2 MIMO -4 block fading channel

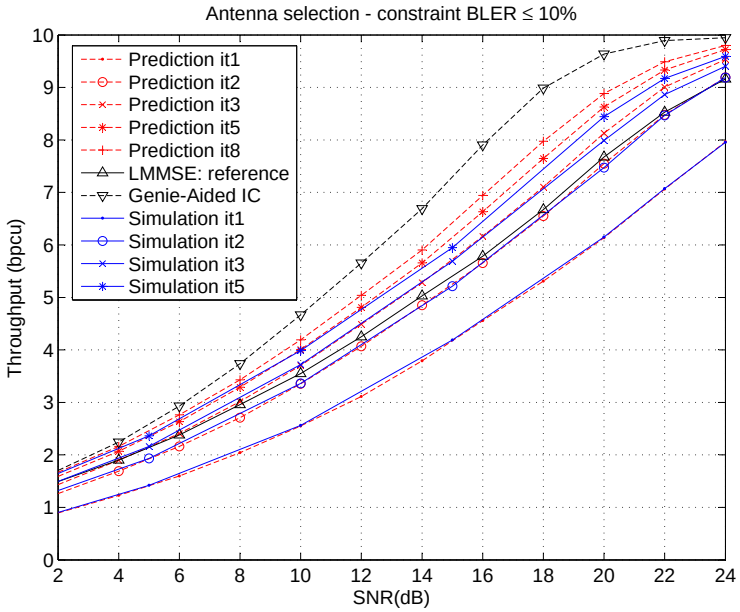

Figure 7.6: Predicted average throughput at iteration 1,2,3,5,8, simulated average throughput at iteration 1,2,3, the LMMSE reference and the Genie-Aided IC bound over 2×2 MIMO -4 block fading channel

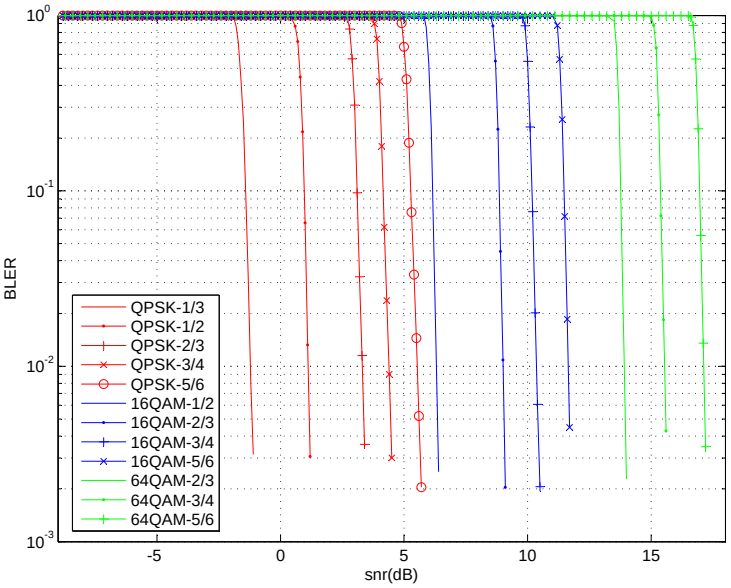

Figure 7.7: BLER LUTs of 12 MCS with 8 iteration turbo decode

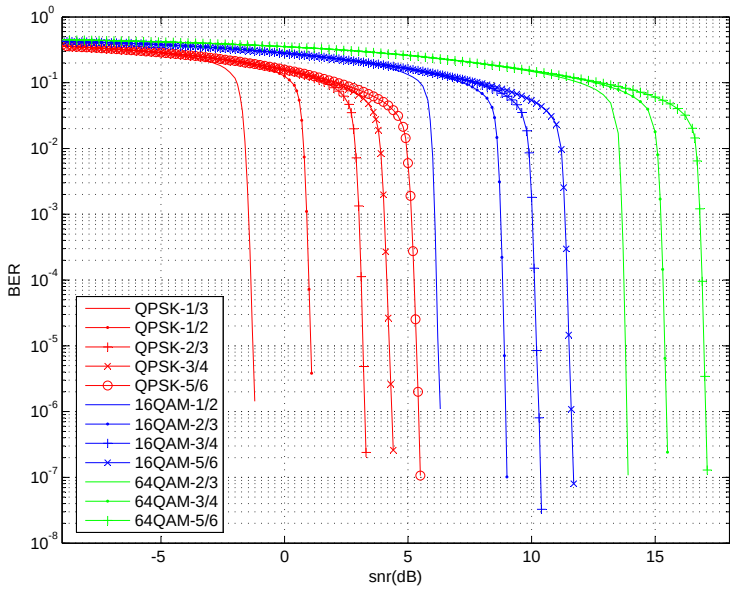

Figure 7.8: BER LUTs of 12 MCS with 8 iteration turbo decode

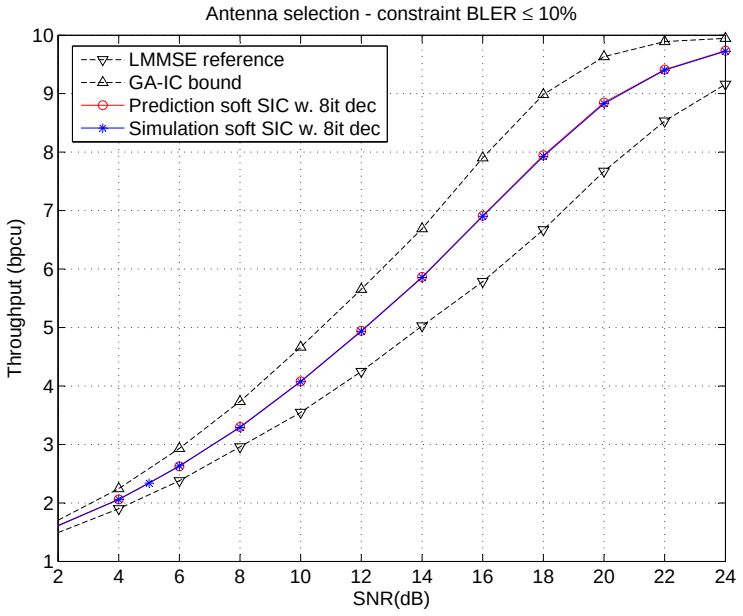

Figure 7.9: Predicted average throughput, simulated average throughput of soft SIC receiver with 8 iteration decode, the LMMSE reference and the Genie-Aided IC bound over 2×2 MIMO -4 block fading channel

Chapter 8

Conclusions

The purpose of the last chapter is to conclude and give perspectives for future research.

8.1 Summary

Multiple antenna technology and advanced turbo receivers have a large potential to increase the spectral efficiency of future wireless communication system. PHY-layer abstractions for a particular class of turbo receivers, i.e., iterative LMMSE-IC algorithms and link adaptation in presence of such advanced receivers are the core contributions of this PHD study.

This PhD study has been able to propose accurate, robust and practical semi-analytical PHY-layer abstractions for MIMO systems employing iterative LMMSE-IC receivers. For this issue, multiple PHY layer fundamental assumptions are investigated, such as the available CSIR, the MCS adopted and the type of LLR on coded bits fed back from the decoder for interference reconstruction and cancellation inside the iterative LMMSE-IC algorithm.

These work could be used as a milestone to design new interference cancellation engines for next-generation wireless networks. Closed-loop link adaptations in MIMO systems based on the proposed PHY-layer abstractions for iterative LMMSE-IC receivers have been tackled. Partial CSI is assumed at the transmitter under limited feedback derived by the PHY-layer abstractions and perfect CSI is assumed at the receiver. Link level predicted and simulated performance are compared in different communication scenarios to measure the true impact on the performance brought by turbo receiver.

- In the second chapter, PHY-layer abstractions have been proposed for convolutionally coded MIMO systems employing iterative LMMSE-IC receiver under perfect CSIR. The PHY layer abstractions are able to analyze and predict the iterative receiver performance per iteration. The underlying assumptions for this family of turbo receiver are clarified after careful examinations. Indeed, under perfect CSIR, while the underlying assumptions hold in practice for LEXTPR-based iterative LMMSE-IC, some of them prove to be approximate (and optimistic) in the second case. To solve this problem, an improved PHY-layer abstraction has been proposed for LAPPR-based iterative LMMSE-IC by introducing a calibration procedure whose efficiency has been validated by Monte-Carlo simulations. These work help to understand thoroughly the turbo receiver's behaviors.

- In the third chapter, PHY-layer abstractions have been proposed for convolutionally coded MIMO systems employing iterative LMMSE-IC receiver under imperfect CSIR. The emphasis is put on the situation when the number of pilot symbols are reduced and we can no longer neglect the channel estimation errors. Under imperfect CSIR, a novel semi-analytical PHY-layer abstraction has been proposed for LEXTPR-based iterative LMMSE-IC detection joint decoding and semi-blind channel estimation by extending the existing approach derived under perfect CSIR. It allows computing the average BLER conditional on an initial pilot assisted channel estimation and long term channel distribution information. It heavily relies on Gaussian approximation on the LMMSE-IC and channel estimation error models whose second order statistics are governed by the SINRs and the channel estimate MSE, respectively. Simulation in the context of SU-MIMO frequency selective transmission, modeled by a discrete input MIMO memoryless block fading Rayleigh channel, demonstrates the validity of the proposed approach.

- In the forth chapter, novel semi-analytical PHY-layer abstractions have been proposed for turbo coded MIMO systems employing iterative LMMSE-IC receiver under perfect CSIR. This works enables the introduction of iterative LMMSE-IC receivers in LTE. A stochastic modeling of the whole turbo receiver based on EXIT charts (and variants) has been proposed and its effectiveness have been demon-

strated through Monte Carlo simulations in a variety of transmission scenarios. As the core of the contribution, it is found that, even in the simplified case of Gray mapping, a bivariate LUT is needed to characterize the evolution of the joint demapper and turbo decoder embedded within the iterative LMMSE-IC. This is in contrast with existing PHY-layer abstraction where simple convolutional codes were considered and univariate LUT sufficient. The approach can be easily extended to other types of compound codes (e.g., serially concatenated codes, LDPC codes). Therefore, the approach may constitute the core of link adaptation and RRM procedures in closed-loop turbo coded MIMO systems employing iterative LMMSE-IC receivers in LTE-A.

- In the fifth chapter, PHY-layer abstractions for a generic per-antenna turbo coded MIMO system employing iterative LMMSE-IC have been proposed. Compare to the third topic of this part, a new degree of freedom is the decode ordering. The global turbo receiver performance depends on the decode ordering which should be taken into account in the PHY-layer abstractions. The proposed PHY-layer abstractions have been validated by Monte-Carlo simulations with different communication scenarios

- In the sixth chapter, the problem of link adaptation in closed-loop coded MIMO systems employing LAPPR- based iterative LMMSE-IC receiver has been tackled. Partial CSI is assumed at the transmitter under limited feedback derived by the PHY-layer abstraction and perfect CSI is assumed at the receiver. Univariate LUTs and associated optimal calibration factors per MCS constructed out of convolutional code are obtained off-line. Bivariate LUTs and associated optimal calibration factors per MCS constructed out of turbo code are obtained off-line. Closed-loop link adaptation performs joint spatial precoder selection (i.e., antenna selection) and MCS selection. It aims to maximize the average rate subject to a target BLER constraint assuming LAPPR-based iterative LMMSE-IC at the destination. For the convolutional coded case, Monte Carlo simulations show a significant gain compare to the classical LMMSE receiver over different channel models. Moreover, they also confirm that using LAPPR rather than LEXTPR on coded bits for soft interference regeneration and cancellation yields faster convergence of the iterative process and better final

performance (both for finite and infinite interleaver length regimes). For the turbo-coded case, based on the proposed PHY-layer abstraction of the whole turbo receiver, we have shown the link-level predicted and simulated performance for three communication scenarios.

- In the seventh chapter, the selective PARC in closed-loop turbo coded MIMO systems with LAPPR-based iterative LMMSE-IC receiver has been investigated. Bivariate LUTs and associated optimal calibration factors per MCS constructed out of turbo code are obtained off-line. The algorithm performs joint selection of spatial precoder (the best subset of antennas), decode ordering and MCS combination so as to maximize the average rate subject to a target BLER constraint. This is enabled by the semi-analytical PHY-layer abstraction proposed before whose accuracy and robustness are confirmed again by the analysis and simulation results. A very exciting gain of iterative LMMSE-IC receiver compared to the conventional LMMSE receiver has been observed.

8.2 Perspectives

Future research topics include several mains aspects.

- More performant iterative receiver: There is still a gap between the performances of iterative LMMSE-IC algorithms and the perfect interference cancellation bound in SU-MIMO communication scenarios. Further improvement of spectral efficiency relies on more powerful receiver such as iterative MAP receiver. We would like to propose an accurate, robust and practical semi-analytical PHY-layer abstraction for iterative MAP receiver, however there are no SINRs to be computed. Inspired by the introduction of a calibration factor (greater than one) over the symbol variance to compensate the assumption inaccuracies for LAPPR-based iterative LMMSE-IC, the iterative MAP algorithm might be approximated by a virtual LEXTPR-based iterative LMMSE-IC compensated by a calibration factor (smaller than one) over the symbol variance. If this ides is validated, we are able to propose a framework of PHY-layer abstractions for turbo receivers.

- More aggressive calibrations in conjunction with Incremental-Redundancy Hybrid Automatic Repeat reQuest (IR-HARQ): The introduced calibration factors for LAPPR-based iterative LMMSE-IC algorithm are obtained by minimizing the sum distance between the simulated and calibrated predicted BLER (or BER) over large number of channel realizations drawn from a generic channel distribution model. In this ways, the obtained calibration factors work well in most of channel realizations. By avoiding to allocate too optimist data rate for bad radio conditions which results in a lot of retransmissions, the usage of calibration factors inevitably sacrifices the data rate over good radio conditions. If we want to adopt more aggressive (smaller) calibration factors to allocate higher rate over good radio conditions, there should exist some mechanisms to compensate the possible allocations of too optimist data rate over bad radio conditions. In this line of thought, there is a need to employ IR- HARQ [88], [89], [90], [91], [92], [93] in the transmission.

- Open-loop link adaptation: The part of FLA in this PhD study is based on ideal instantaneous and perfect feedback and all instantaneous feedbacks can be treated by MAC layer immediately. However, these may be not realistic in practice. For example, the feedbacks become no longer reliable when the UE is moving too fast, or a basestation under heavy load is not able to follow the feedbacks of every UE. In such situations, a better strategy is to perform open-loop link adaptation regardless the instantaneous feedback. Shifting from closed-loop to open-loop link adaptation, the gain brought by iterative receiver compare to conventional linear receiver will increase. Therefore, it is of interest to compare the performance of different types of receiver in the context of open-loop link adaptation.

- More generic channel model: Cross layer optimization has been tackled mainly over SU-MIMO systems. Future topics include uplink and downlink system level performance evaluation, as well as an extension of this work to multicell MIMO. However, we have observed that cross layer optimization starts introducing a very high computational complexity to search the optimal solution as the degree of freedoms increase greatly. Due to the complexity constraint, selected PARC is limited to dual codeword transmission over a 2x2 MIMO block fading

channel model in this PhD study. The following step should be selective PARC for dual codeword transmission over a 4x4 MIMO block fading channel model. Furthermore, a smart exploration of the search space is required to lower the complexity of optimizing all the degree of freedoms: user, antenna, precoding, rate, ordering and eventually the frequency and power. We believe that iterative receivers in conjunction with such advanced LA and RRM mechanisms will increase substantially the system throughputs.

Appendix

The objective of this appendix is to derive the statistics of the biased LMMSE channel estimation error model from the first iteration. For the sake of notation simplicity, we will remove the iteration superscript (i) in the following, since the derivation is the same for all iteration $i \geq 1$

$$\widehat{\mathbf{H}} = \overline{\mathbf{Y}}\mathbf{F} = (\mathbf{H}\overline{\mathbf{S}} + \overline{\mathbf{W}})\mathbf{F} = \mathbf{H}\overline{\mathbf{S}}\mathbf{F} + \overline{\mathbf{W}}\mathbf{F} = \mathbf{H}\mathbf{G} + \mathbf{\Psi}$$

where

$$\mathbf{G} = \overline{\mathbf{S}}(R\sigma_h^2)\mathbf{\Sigma}_{\overline{w}}^{-1}\overline{\mathbf{S}}^{\dagger}\left(\overline{\mathbf{S}}(R\sigma_h^2)\mathbf{\Sigma}_{\overline{w}}^{-1}\overline{\mathbf{S}}^{\dagger} + \mathbf{I}_{n_t}\right)^{-1}. \tag{1}$$

We develop further

$$\overline{\mathbf{S}}(R\sigma_h^2)\mathbf{\Sigma}_{\overline{w}}^{-1}\overline{\mathbf{S}}^{\dagger} \quad = \quad [\mathbf{A}^{ps}, \tilde{\mathbf{S}}](R\sigma_h^2)\mathbf{\Sigma}_{\overline{w}}^{-1}[\mathbf{A}^{ps}, \tilde{\mathbf{S}}]^{\dagger} = \frac{\sigma_h^2}{N_0}\mathbf{A}^{ps}\mathbf{A}^{ps\dagger} + \frac{\sigma_h^2}{N_0 + \triangle N_0}\tilde{\mathbf{S}}\tilde{\mathbf{S}}^{\dagger} \tag{2}$$

It is important to remember here that the MSE estimates $m_{t,l}$ are built from LEXTPR and, thus, Assumption A2 and A3 hold for infinite size interleaver. As a result, for a sufficiently large L_{ds} as well as interleaver size and invoking ergodicity, we have

$$\mathbb{E}\{m_t m_{t'}^{\dagger}\} = L_{ds}\sum_{l=1}^{L_{ds}} m_{t,l}m_{t',l}^{\dagger} = \delta_{t,t'}L_{ds}(\sigma_{ds}^2 - \tilde{v}) \tag{3}$$

where $\delta_{t,t'}$ is equal to 1 iff $t = t'$ or 0 otherwise. From this last observation, we can further simplified (2) as

$$\overline{\mathbf{S}}(R\sigma_h^2)\mathbf{\Sigma}_{\overline{w}}^{-1}\overline{\mathbf{S}}^{\dagger} = L_{ps}\sigma_{ps}^2\frac{\sigma_h^2}{N_0}\mathbf{I}_{n_t} + L_{ds}(\sigma_{ds}^2 - \tilde{v})\frac{\sigma_h^2}{N_0 + \triangle N_0}\mathbf{I}_{n_t}$$

which, finally, yields

$$\mathbf{G} = \frac{L_{ps}\sigma_{ps}^2 + L_{ds}(\sigma_{ds}^2 - \tilde{v})\frac{N_0}{N_0+\triangle N_0}}{L_{ps}\sigma_{ps}^2 + L_{ds}(\sigma_{ds}^2 - \tilde{v})\frac{N_0}{N_0+\triangle N_0} + \frac{N_0}{\sigma_h^2}}\mathbf{I}_{n_t} = g\mathbf{I}_{n_t}. \tag{4}$$

Finally, the channel estimation error model can be expressed as

$$\widehat{\mathbf{H}} = g\mathbf{H} + \boldsymbol{\psi} \tag{5}$$

On the other hand, since the channel estimation is carried out row by row, the second order statistics of $\boldsymbol{\Psi}$ is given by the covariance of one of its row $\boldsymbol{\psi}^r$, i.e.,

$$\boldsymbol{\Sigma}_{\psi^r} = \mathbb{E}\{\boldsymbol{\psi}^{r\dagger}\boldsymbol{\psi}^r\} = \mathbf{F}^\dagger\mathbb{E}\{\overline{\mathbf{w}}^{r\dagger}\overline{\mathbf{w}}^r\}\mathbf{F} = \frac{1}{R}\mathbf{F}^\dagger\boldsymbol{\Sigma}_{\overline{w}}\mathbf{F} = \sigma_\Psi^2\mathbf{I}_{n_t} \tag{6}$$

with

$$\sigma_\Psi^2 = N_0\frac{L_{ps}\sigma_{ps}^2 + L_{ds}(\sigma_{ds}^2 - \tilde{v})\frac{N_0}{N_0+\triangle N_0}}{\left(L_{ps}\sigma_{ps}^2 + L_{ds}(\sigma_{ds}^2 - \tilde{v})\frac{N_0}{N_0+\triangle N_0} + \frac{N_0}{\sigma_h^2}\right)^2}. \tag{7}$$

Bibliography

[1] ITU, "*Global ICT developments*," http://www.itu.int/en/ITU-D/Statistics/Pages/stat/default.aspx, 2013.

[2] D. Tse and P. Viswanath, "*Fundamentals of Wireless Communication*," 2005.

[3] G. Foschini, "*Layered space-time architecture for wireless communication in a fading environment when using multi-element antennas*," *Bell Labs Technical Journal*, vol. 1, no. 2, pp. 41–59, 1996.

[4] A. J. Paulraj, D. A. Gore, R. Nabar, and H. Bölcskei, "*An overview of MIMO communication - A key to gigabit wireless*," in *Proc. IEEE*, vol. 92, no. 2, Feb. 2004, pp. 198–218.

[5] A. J. Paulraj and T. Kailath, "*Increasing capacity in wireless broadcast systems using distributed transmission/directional reception*," in *American patent 5 345 599*, 1994.

[6] I. Telatar, "*Capacity of multi-antenna Gaussian channels*," *Eur. Trans. Tel.*, vol. 10, no. 6, pp. 585–595, Nov./Dec. 1999.

[7] H. Bölcskei, D. Gesbert, and A. J. Paulraj, "*On the capacity of OFDM-based spatial multiplexing systems*," *IEEE Trans. Commun.*, vol. 50, pp. 225–234, Dec. 2002.

[8] "*Physical Channels and Modulation, v8.9*," *3GPP Technical Specification 36.211*, Dec. 2009.

[9] R. van Nee and R. Prasad, "*OFDM for Wireless Multimedia Communications*," 2000.

[10] H. G. Myung, J. Lim, and D. J. Goodman, "*Single Carrier FDMA for Uplink Wireless Transmission*," *IEEE Vehicular Technology Magazine*, vol. 1, no. 3, pp. 30–38, Sep. 2006.

[11] ——, "*PEAK-TO-AVERAGE POWER RATIO OF SINGLE CARRIER FDMA SIGNALS* ," in *Proc. IEEE PIMRC*, Helsinki, Finland, Sep. 2006.

[12] C. Berrou, A. Glavieux, and P. Thitimajshima, "*Near Shannon limit error-correcting coding and decoding*," in *Proc. IEEE ICC'93*, Geneva, Switzerland, May 1993, pp. 1064–1070.

[13] S. Song and Y. Li, "*Cross-Layer Optimization for OFDM Wireless Networks - Part I: Theoretical Framework*," *IEEE Wireless Commun.*, pp. 614–624, Mar. 2005.

[14] ——, "*Cross-layer Optimization for OFDMA Wireless Networks-Part II: Algorithm Development*," *IEEE Wireless Commun.*, vol. 4, pp. 625–634, Mar. 2005.

[15] J. Chuang and N. Sollenberger, "*Beyond 3G: Wideband wireless data access based on OFDM and dynamic packet assignment*," *IEEE Commun. Mag.*, vol. 38, no. 7, pp. 78–87, Jul. 2000.

[16] S. Nanda, K. Balachandran, and S. Kumar, "*Adaptation techniques in wireless packet data services*," *IEEE Commun. Mag.*, vol. 38, no. 1, pp. 54–64, Jan. 2000.

[17] A. J. Goldsmith and S. G. Chua, "*Variable-rate variable-power MQAM for fading channel*," *IEEE Trans. Commun.*, vol. 45, no. 10, pp. 1218–1230, Oct. 1997.

[18] P. Viswanath, D. N. C. Tse, and R. L. Laroia, "*Opportunistic beamforming using dumb antennas*," *IEEE Trans. Inf. Theory*, vol. 48, no. 6, pp. 1277–1294, June 2002.

[19] D. Tse and S. Hanly, "*Multi-access fading channels: Part I: Polymatroid structure, optimal resource allocation and throughput capacities*," *IEEE Trans. Inf. Theory*, vol. 44, no. 7, pp. 2796–2815, Nov. 1998.

[20] L. Li and A. J. Goldsmith, "*Optimal resource allocation for fading broadcast channels- Part I: Ergodic capacity*," *IEEE Trans. Inf. Theory*, vol. 47, no. 3, pp. 1083–1102, Mar. 2001.

[21] C. Y. Wong, R. S. Cheng, K. B. Letaief, and R. D. Murch, "*Multiuser OFDM with adaptive subcarrier, bit, and power allocation*," *IEEE J. Sel. Areas Commun.*, vol. 17, no. 10, pp. 1747–1458, Oct. 1999.

[22] W. Rhee and J. M. Ciofi, "*Increase in capacity of multiuser OFDM system using dynamic subcarrier allocation*," in *Proc. IEEE Vehicular Technology Conf.*, 2000.

[23] L. M. Hoo, B. Halder, J. Tellado, and J. M. Ciofi, "*Multiuser transmit optimization for multicarrier broadcast channels: Asymptotic FDMA capacity region and algorithms*," *IEEE Trans. Commun.*, vol. 52, no. 6, pp. 922–930, Jun. 2004.

[24] S. Hämäläinen, P. Slanina, M. Hartman, A. Lappeteläinen, and H. Holma, "*A novel interface between link and system level simulations*," in *Proc. ACTS Mobile Telecommunications Summit'97*, Aalborg, Denmark, Oct. 1997, pp. 599–604.

[25] R. Knopp and P. A. Humblet, "*Information capacity and power control in single cell multiuser communications*," in *Proc. IEEE ICC'95*, Seattle, WA, Jun. 1995.

[26] V. R. Cadambe and S. A. Jafar, "*Interference Alignment and Spatial Degrees of Freedom for the K User Interference Channel*," in *Proc. IEEE ICC*, Beijing, China, May 2008.

[27] RP-130404, "*Network Assisted Interference Cancellation and Suppression for LTE*," MediaTek, Renesas and Broadcom.

[28] J. Hagenauer, "*The turbo principle: Tutorial introduction and state of the art*," in *Proc. 1st International Symposium on Turbo Codes (ISTC'97)*, Brest, France, Sep. 1997, pp. 1–12.

[29] M. Fu, "*Stochastic analysis of turbo decoding*," *IEEE Trans. Inform. Theory*, vol. 51, no. 1, pp. 81–100, Jan. 2005.

[30] T. Richardson, "*The geometry of turbo-decoding dynamics*," *IEEE Trans. Inf. Theory*, vol. IT-46, no. 1, pp. 9–23, Jan. 2000.

[31] T. Richardson and R. Urbanke, "*The capacity of low-density parity-check codes under message-passing decoding*," *IEEE Trans. Inform. Theory*, vol. 47, no. 2, pp. 599–618, Feb. 2001.

[32] T. Richardson, M. Shokrollahi, and R. Urbanke, "*Design of capacity-approaching irregular low-density parity-check codes*," *IEEE Trans. Inf. Theory*, vol. 47, no. 2, pp. 619–637, Feb. 2001.

[33] F. R. Kschischang, B. J. Frey, and H. A. Loeliger, "*Factor graphs and the sum-product algorithm*," *IEEE Trans. Inf. Theory*, vol. 47, no. 2, pp. 498–519, Feb. 2001.

[34] R. Gallager, "*Low-Density Parity-Check Codes*," 1963.

[35] S. T. Brink, "*Convergence of iterative decoding*," *IEE Electron. Lett.*, vol. 35, pp. 75–80, Jan. 2000.

[36] S. ten Brink, "*Iterative decoding trajectories of parallel concatenated codes*," in *Proc. 3rd International Symposium on Turbo Codes (ISTC'00)*, Münich, Germany, Jan. 2000, pp. 75–80.

[37] ——, "*Convergence behavior of iteratively decoded parallel concatenated codes*," *IEEE Trans. Commun.*, vol. 49, no. 10, pp. 1727–1737, Oct. 2001.

[38] L. Bahl, J. Cocke, F. Jelinek, and J. Raviv, "*Optimal decoding of linear codes for minimizing symbol error rate*," *IEEE Trans. Inf. Theory*, vol. 20, no. 2, pp. 284–287, Mar. 1974.

[39] S. Y. Chung, T. Richardson, and R. Urbanke, "*Gaussian approximation for sum-product decoding of low-density parity-check codes*," in *Proc. IEEE ISIT'00*, Sorento, Italy, Jun. 2000.

[40] ——, "*Analysis of the sum-product decoding of low-density parity-check codes using a Gaussian approximation*," *IEEE Trans. Inf. Theory*, vol. 47, pp. 657–670, Feb. 2001.

[41] H. E. Gamal and A. Hammons, "*Analyzing the turbo decoder using the Gaussian approximation*," *IEEE Trans. Inf. Theory*, vol. 47, no. 2, pp. 671–686, Feb. 2001.

[42] D. Divsalar, S. Dolinar, and F. Pollara, "*Iterative turbo decoder analysis based on density evolution*," *IEEE J. Sel. Areas Commun.*, vol. 19, no. 5, pp. 891–907, May 2001.

[43] P. D. Alexander, A. J. Grant, and M. C. Reed, "*Iterative detection on code-division multiple-access with error-control coding*," *European Trans. Telecommun.*, vol. 9, no. 5, pp. 419–426, Oct. 1998.

[44] J. Boutros and G. Caire, "*Iterative multiuser joint decoding: Unified framework and asymptotic analysis*," *IEEE Trans. Inf. Theory*, vol. 48, no. 7, pp. 1772–1793, Jul. 2002.

[45] M. Tüchler, S. ten Brink, and J. Hagenauer, "*Measures for tracing the convergence of iterative decoding algorithms*," in *Proc. 4th International Symposium on Turbo Codes (ISTC'02)*, Berlin, Germany, Jan. 2002, pp. 53–60.

[46] X. Wang and H. V. Poor, "*Iterative (turbo) soft interference cancellation and decoding for coded CDMA*," *IEEE Trans. Commun.*, vol. 47, no. 7, pp. 1046–1061, Jul. 1999.

[47] H. E. Gamal and E. Geraniotis, "*Iterative multiuser detection for coded CDMA signals in AWGN and fading channels*," *IEEE J. Sel. Areas Commun.*, vol. 18, no. 1, pp. 30–41, Jan. 2000.

[48] G. Caire and R. Müller, "*The optimal received power distribution of IC-based iterative multiuser joint decoders*," in *Proc. 39th Annual Allerton Conf. on Communications, Control and Computing*, Monticello, USA, Oct. 2001.

[49] M. Tüchler, R. Koetter, and A. Singer, "*Turbo equalization: Principles and new results*," *IEEE Trans. Commun.*, vol. 50, no. 5, pp. 754–767, May 2002.

[50] N. Elhelw, C. Hermosilla, and L. Szczecinski, "*Analytical evaluation of turbo multiuser detection algorithms*," in *Proc. Canadian Conf. on Electrical and Computer Engineering*, vol. 3, Montreal, Canada, May 2004, pp. 1405–1408.

[51] C. Hermosilla and L. Szczecinski, "*Performance evaluation of linear turbo receivers using analytical EXIT functions*," in *Proc. IEEE PIMRC'04*, vol. 2, Barcelona, Spain, Sep. 2004, pp. 1307–1311.

[52] ——, "*Performance evaluation of linear turbo receivers using analytical extrinsic information transfer functions*," *EURASIP Journal on Applied Signal Processing*, vol. 6, pp. 892–905, 2005.

[53] K. Narayanan, X. Wang, and G. Yue, "*Estimating the PDF of the SIC-MMSE equalizer output and its applications in designing LDPC codes with turbo-equalization*," *IEEE Trans. Wireless Commun.*, vol. 4, no. 1, pp. 278–287, Jan. 2005.

[54] K. Kansanen and T. Matsumoto, "*An Analytical Method for MMSE MIMO Turbo Equalizer EXIT Chart Computation*," *IEEE Trans. Wireless Commun.*, vol. 6, no. 1, pp. 59–63, Jan. 2007.

[55] V. Ramon, C. Herzet, and L. Vandendorpe, "*A semi-analytical method for predicting the performance and convergence behavior of a multiuser turbo-equalizer/demapper*," *IEEE Trans. Signal Process.*, vol. 55, no. 3, pp. 1104–1117, Mar. 2007.

[56] X. Yuan, Q. Guo, X. Wang, and L. Ping, "*Evolution analysis of low-cost iterative equalization in coded linear systems with cyclic prefixes*," *IEEE J. Sel. Areas Commun.*, vol. 26, no. 2, pp. 301–310, Feb. 2008.

[57] L. Ping, J. Tong, X. Yuan, and Q. Guo, "*Performance analysis of multi-ary systems with iterative linear minimum-mean-square-error detection*," in *Proc. 5th International Symposium on Turbo Codes (ISTC'08)*, Lausanne, Switzerland, Sep. 2008, pp. 192–197.

[58] M. Moher, "*An iterative multiuser detection decoder for near-capacity communications*," *IEEE Trans. Commun.*, vol. 46, no. 7, pp. 870–880, Jul. 1998.

[59] R. Knopp and P. Humblet, "*On coding for block fading channels*," *IEEE Trans. Inf. Theory*, vol. 46, no. 1, pp. 189–205, Jan. 2000.

[60] J. Cheng, "*Coding performance of various type-I HARQ schemes with BICM*," in *Proc. IEEE ISIT'04*, Chicago, USA, Jun./Jul. 2004, pp. 319–319.

[61] K. Brueninghaus, D. Astely, T. Sälzer, S. Visuri, A. Alexiou, S. Karger, and G. A. Seraji, "*Link performance models for system level simulations of broadband radio access systems*," in *Proc. IEEE PIMRC'05*, vol. 4, Berlin, Germany, Sep. 2005, pp. 2306–2311.

[62] L. Wan, S. Tsai, and M. Almgren, "*A fading-insensitive performance metric for a unified link quality model*," in *Proc. IEEE WCNC'06*, vol. 4, Las Vegas, USA, Apr. 2006, pp. 2110–2114.

[63] S. Stiglmayr, M. Bossert, and E. Costa, "*Adaptive coding and modulation in OFDM systems using BICM and rate-compatible punctured codes*," in *Proc. European Wireless Conference*, Paris, France, Apr. 2007.

[64] N. Network, "*OFDM Exponential Effective SIR Mapping Validation, EESM simulation results*," in *3GPP, Tech. Rep. R1- 040089*, Jan. 2004.

[65] G. Caire, G. Taricco, and E. Biglieri, "*Bit-interleaved coded modulation*," *IEEE Trans. Inf. Theory*, vol. 44, no. 3, pp. 927–946, may 1998.

[66] R. Visoz, A. O. Berthet, and M. Lalam, "*Semi-Analytical Performance Prediction Methods for Iterative MMSE-IC Multiuser MIMO Joint Decoding*," *IEEE Trans. Commun.*, vol. 58, no. 9, pp. 2576–2589, Sep. 2010.

[67] M. Tüchler, A. Singer, and R. Koetter, "*Minimum mean squared error equalization using a priori information*," *IEEE Trans. Signal Process.*, vol. 50, no. 3, pp. 673–683, Mar. 2002.

[68] S. ten Brink, J. Speidel, and R.-H. Yan, "*Iterative demapping and decoding for multilevel modulation*," in *Proc. IEEE GLOBECOM'98*, Sydney, Australia, Nov. 1998, pp. 579–584.

[69] U. Wachsmann, R. F. H. Fisher, and J. B. Huber, "*Multilevel codes: Theoretical concepts and practical design rules*," *IEEE Trans. Inf. Theory*, vol. 45, no. 5, pp. 1361–1391, Jul. 1999.

[70] M. Isaka and H. Imai, "*On the iterative decoding of multilevel codes*," *IEEE J. Sel. Areas Commun.*, vol. 19, no. 5, pp. 935–943, May 2001.

[71] R. Visoz, A. O. Berthet, and M. Lalam, "*A novel fast semi-analytical performance prediction method for iterative MMSE-IC multiuser MIMO joint decoding*," in *Proc. IEEE GLOBECOM'08*, New Orleans, USA, Nov./Dec. 2008, pp. 1–5.

[72] S. ten Brink, "*Convergence of multi-dimensional iterative decoding schemes*," in *Proc. IEEE ACSSC'01*, Pacific Grove, USA, Nov. 2001.

[73] S. ten Brink, G. Kramer, and A. Ashikhmin, "*Design of low-density parity-check codes for modulation and detection*," *IEEE Trans. Commu.*, vol. 52, no. 4, pp. 670–678, Apr. 2004.

[74] F. Brannstrom, L. Rasmussen, and A. Grant, "*Convergence analysis and optimal scheduling for multiple concatenated codes*," *IEEE Trans. Inform. Theory*, vol. 51, pp. 3354–3364, Sep. 2005.

[75] G. Taricco and E. Biglieri, "*Space-Time Decoding With Imperfect Channel Estimation*," *IEEE Trans. Wireless Commun.*, pp. 1536–1276, Jul. 2005.

[76] P. Piantanida, S. Sadough, and P. Duhamel, "*On the outage capacity of a practical decoder using channel estimation accuracy*," in *Proc. IEEE International Symposium on Information Theory*, Nice, France, Jun. 2007, pp. 2281–2285.

[77] ——, "*On the Outage Capacity of a Practical Decoder Accounting for Channel Estimation Inaccuracies*," *IEEE Trans. Commun.*, vol. 57, no. 5, pp. 1341 –1350, May 2009.

[78] P. Ha and B. Honary, "*Improved blind turbo detector*," in *Proc. IEEE VTC'00*, vol. 2, Tokyo, Japan, May 2000, pp. 1196–1199.

[79] A. O. Berthet, B. Ünal, and R. Visoz, "*On Iterative Decoding of Trellis-Encoded Signals over Multipath Rayleigh Fading Channels*," *IEEE J. Sel. Areas Commun., Special Issue on Turbo-Principle II*, vol. 19, no. 9, pp. 1729–1743, Sep. 2001.

[80] M. Nicoli, S. Ferrara, and U. Spagnolini, "*Soft-Iterative Channel Estimation: Methods and Performance Analysis*," *IEEE Trans. Signal Process.*, vol. 50, pp. 2993–3006, May 2007.

[81] A. O. Berthet, R. Visoz, and S. Chtourou, "*Efficient MMSE-based Turbo-Decoding of Space-Time BICM over MIMO Block Fading ISI Channel with Imperfect CSIR*," in *Proc. IEEE PIMRC'04*, Barcelona, Spain, Sep. 2004, pp. 2621–2626.

[82] S.Buzzi, M. Lops, and S. Sardellitti, "*Performance of Iterative Data Detection and Channel Estimation for Single-Antenna and Multiple-Antennas Wireless Communications*," *IEEE Trans. Veh. Technol.*, jul. 2004.

[83] M. A. Khalighi, J. J. Boutros, and J. F. Hélard, "*Data-aided Channel Estimation for Turbo-PIC MIMO Detectors*," *IEEE Commun. Lett.*, pp. 350–352, Jun. 2006.

[84] A. R. N. Sellami and I. Fijalkow, "*The impact of both a priori information and channel estimation errors on the MAP equalizer performance*," *IEEE Trans. Signal Process.*, vol. 54, no. 7, pp. 2716–2724, Jul. 2006.

[85] R. Heath and D. Love, "*Multimode antenna selection for spatial multiplexing systems with linear receivers*," *IEEE Trans. Sig. Proc.*, vol. 53, no. 8, pp. 3042–3056, Aug. 2005.

[86] G. F. E. Ohlmer, "*Link adaptation in linearly precoded closed-loop MIMO-OFDM systems with linear receivers*," in *Proc. IEEE ICC'09*, Dresden, Germany, Jun. 2009.

[87] T. G. K.M. Varanasi, "*Optimum decision feedback multiuser equalization with successive decoding achieves the total capacity of the Gaussian multiple access channel*," in *Proc. Asilomar Conf.*, Pacific Grove, CA, USA, Nov. 1997.

[88] J. Hagenauer, "*Rate-Compatible Punctured Convolutional Codes (RCPC Codes) and their Applications*," *IEEE Trans. Communication*, vol. 36, no. 4, pp. 389 – 400, Apr. 1988.

[89] D. J. Costello, J. Hagenauer, H. Imai, and S. B. Wicker, "*Applications of Error-Control Coding*," *IEEE Trans. Information Theory*, vol. 44, no. 6, pp. 2531 – 2560, Oct. 1998.

[90] K. Narayanan and G. L. Stüber, "*A Novel ARQ Technique using the Turbo Coding Principle*," *IEEE COMMUNICATIONS LETTERS*, vol. 1, no. 4, pp. 49 – 51, Mar. 1997.

[91] A. S. Barbulescu and S. S. Pietrobon, "*Rate compatible turbo codes*," *Electronics Letters*, vol. 31, no. 7, pp. 535 – 536, Mar. 1995.

[92] J. Hamorsky, U. Wachsmanny, J. B. Huber, and A. Cizmar, "*Hybrid Automatic Repeat Request Scheme with Turbo Codes*," in *Proc. 1997 Int. Symp. on Turbo Codes*, Brest, France, Sept. 1997, pp. 247–250.

[93] D. N. Rowitch and L. B. Milstein, "*On the performance of Hybrid FEC/ARQ Systems Using Rate Compatible Punctured Turbo (RCPT) Codes*," *IEEE Trans. Communication*, vol. 48, no. 6, pp. 948 – 959, Jun. 2000.

[94] M. Witzke, S. Baro, F. Schreckenbach, and J. Hagenauer, "*Iterative Detection of MIMO Signals with Linear Detectors*," in *Proc. Annual Asilomar Conference on Signals, Systems, and Computers*, California, USA, Nov. 2002, pp. 289–293.

[95] J. Wolfmann, "*Almost Perfect Autocorrelation Sequences*," *IEEE Trans. Inf. Theory*, vol. 38, no. 4, pp. 1412–1418, 1992.

[96] S. M. Lopez, F. Diehm, R. Visoz, and B. Ning, "*Measurement and prediction of Turbo-SIC receiver performance for LTE*," in *Proc. IEEE VTC Fall'2012*, Québec City, Canada, Sep. 2012.

[97] B. Ning, R. Visoz, and A. Berthet, "*Extrinsic versus a posteriori probability based iterative LMMSE-IC algorithms for coded MIMO communications: Performance and analysis* ," in *Proc. IEEE ISWCS'12*, Paris, France, Aug. 2012.

[98] ——, "*A Novel Link Adaptation Scheme for Closed-Loop Turbo Coded MIMO Systems with LMMSE-IC based Turbo Equalization*," in *Proc. IEEE WIMOB'13*, Lyon, France, Oct. 2013.

[99] S. Grant, J.-F. Cheng, L. Krasny, K. Molnar, and Y.-P. Wang, "*Per-antenna-rate-control (PARC) in frequency selective fading with SIC-GRAKE receiver*," in *Proc. (IEEE VTC-Fall'04)*, Los Angeles, US, Sep. 2004.